DISSERTATION

Titel der Dissertation

“Continuous and Pulsed
Cavity Quantum Optomechanics”

Verfasser

Michael R. Vanner

angestrebter akademischer Grad

Doktor der Naturwissenschaften (Dr.rer.nat.)

Wien, 2013

Studienkennzahl lt. Studienblatt:	A 091 411
Dissertationsgebiet lt. Studienblatt:	Physik
Betreuer:	Univ.-Prof. Dr. Markus Aspelmeyer

Contents

Abstract 1

Zusammenfassung 3

1 Introduction 5
  1.1 Optomechanics and Radiation Pressure 5
    1.1.1 Some History and Motivation of Quantum Optomechanics 6
    1.1.2 The Cavity Optomechanical System 8
    1.1.3 System Dynamics 9
  1.2 This Thesis 11
    1.2.1 Three Temporal Interaction Regimes 13
    1.2.2 List of Publications 14
    1.2.3 How This Thesis May Be Read 15

2 Sideband Cooling of Mechanical Motion 17

3 Optomechanical Normal Mode Splitting 27

4 Geometry Dependent Mechanical Clamping Losses 37

5 A Toolset for Quantum Optomechanical Phonon Control 55

6 Pulsed Quantum Optomechanics 65

7 Experimental Pulsed Quantum Optomechanics 73

8 Enhanced Strength Displacement Squared Measurement 87

9 A Scheme to Probe Planck-Scale Modifications to the Canonical Commutation Relation 97

10 Optically Induced Mechanical Non-Linearity 109

Conclusions 123

Acknowledgments 125

Bibliography 127

Curriculum Vitae 137

Abstract

The field of cavity quantum optomechanics is now established as one of the newest branches of quantum optics. Utilising electromagnetic radiation circulating inside an optical resonator, the research field exploits optical forces for the precise control and high precision measurement of the motion of micro- and nano-fabricated mechanical oscillators. With a broad scope, the field has significant potential to contribute to applied science, e.g. by improving weak force sensing or the development of hybrid-quantum-system quantum-information applications, and fundamental science, e.g. by ultimately probing the existence of gravitationally induced wavefunction collapse or other quantum gravitational phenomena.

The research summarised in this cumulative dissertation was conducted over a period of approximately five years (March 2008 to January 2013), and made both theoretical and experimental developments towards the preparation of a non-classical motional state of a mechanical resonator. The main optomechanical system studied here is a deformable Fabry-Pérot cavity that has one large rigid input mirror, and a second mechanically compliant micro-scale back mirror, which can move simply under the reflection of light.

During the first two years, this research concentrated on experiments with a continuous interaction between an optical field and a mechanical element. We made improvements to cooling the mechanical thermal motion of a high quality factor mechanical oscillator by combining cryogenics and laser sideband cooling; and we also performed the first experimental demonstration of normal mode splitting between the cavity field and the mechanical motion, which emerges given sufficiently strong coupling. A complementary line of research also performed during this time was to study mechanical geometry dependent clamping losses, i.e. how the shape and vibrational profile of a mechanical resonator affects the mechanical quality factor by unwanted phonon coupling into the surrounding thermal bath.

In the latter three years, this research changed course from a continuous interaction and pioneered the regime of *pulsed quantum optomechanics*. As is detailed below, a pulsed interaction that is much shorter in duration than a mechanical period provides a number of opportunities that are not available with a continuous interaction. These include a mechanical position measurement precision that can surpass the standard quantum limit, and the ability to perform optomechanical experiments that investigate dynamics rather than the steady-state, to list two primary advantages. We theoretically developed the framework to conditionally prepare a

squeezed state of mechanical motion using a pulsed measurement, and, importantly, proposed a technique for motional quantum state tomography. These concepts were then experimentally implemented, where the position uncertainty was reduced to less than 20 pm in addition to performing full motional state tomography. A further theoretical work in this direction was to exploit the optical nonlinearity of the optomechanical interaction to allow for strong mechanical displacement squared measurements.

Using a time-domain approach also allows one to develop experimental protocols comprising several (coherent) pulsed interactions. Within this research, two protocols utilising a sequence of four pulsed optomechanical interactions were developed. Both protocols exploit a geometric phase, i.e. a phase resulting from a closed loop in phase space, albeit for quite different purposes. Our first scheme is an experimental proposal to probe quantum gravity using the tools of quantum optomechanics. The scheme uses a geometric phase imparted to the light after the four interactions to infer the mechanical commutation relation between the position and momentum. In various models of quantum gravity, including string theory for example, this commutation relation is modified to accommodate a minimum length scale in the universe. The second proposal, where the roles of light and the mechanical oscillator are reversed, uses a closed loop in optical phase space to impart a nonlinear, i.e. state dependent, phase shift onto the mechanical resonator for deterministic quantum state engineering.

Finally, an additional theoretical project was completed during the final year of this research that explored the regime between a continuous and a pulsed interaction. This project developed the theoretical framework to manipulate a mechanical resonator at the single phonon level by introducing a tool that can perform a controllably weighted superposition of phonon addition, subtraction and the identity operation. Our framework is applicable to other physical systems, such as trapped ions and spin ensembles, and can be used to perform arbitrary quantum state engineering and for mechanical resonator based quantum information applications.

Zusammenfassung

Das Feld der Resonator-Quanten-Optomechanik ist heute einer der neuesten etablierten Zweige der Quantenoptik. Die Nutzung von elektromagnetischer Strahlung, die in einem optischen Resonator zirkuliert, erlaubt die Strahlungsdruck Interaktion für hochpräzise Messung und präzise Kontrolle der Bewegung von mikro- und nano-fabrizierten mechanischen Resonatoren zu nutzen. Das Feld hat eine weite Bandbreite, und damit signifikantes Potential angewandte Forschung, so wie zB. hoch-sensitiven Kraftsensoren oder die Entwicklung von hybriden Quantensystemen für Anwendungen in der Quanteninformation, und fundamentale Forschung, zB um die Existenz von Schwerkraft-induziertem Kollaps der Wellenfunktion oder anderen Quanten-Schwerkraft Phänomenen, voranzutreiben.

Die Forschung, die in dieser Kumulative Dissertation zusammengefasst ist, wurde über eine Periode von fünf Jahren (März 2008 bis Jänner 2013) durchgeführt, und beinhaltet sowohl theoretische als auch experimentelle Fortschritte zur Herstellung von nicht-klassischen Bewegungszuständen von mechanischen Resonatoren. Das opto-mechanische System das die Grundlage dieser darstellt ist ein verformbarer Fabry-Pérot Resonator mit einem fixen Spiegel, und einem zweiten, mechanisch verformbaren mikro-Skalen Spiegel, der auf eingestrahltes Licht reagiert.

Die Forschung der ersten zwei Jahren war auf Experimente mit kontinuierlicher Interaktion zwischen optischen Feldern und einem mechanischen Element fokussiert. Wir haben Tieftemperatur mit Laser Seitenband Kühlung kombiniert um die Kühlung der mechanisch-thermischen Bewegung eines mechanischen Resonators mit hohem Qualitätsfaktor zu verbessern. Ebenso haben wir zum ersten Mal Normalmodentrennung zwischen dem Resonator Feld und der mechanischen Bewegung experimentell demonstriert, ein Effekt der bei ausreichend starker Kopplung entsteht. Komplementär dazu haben wir in dieser Zeit mechanische, Geometrie abhängige Klemmungsverluste untersucht, d.h. den Einfluss von Form und dem Vibrationsprofil von mechanischen Resonatoren auf ihren Qualitätsfaktor durch ungewollte Phononen Kopplung mit dem thermischen Umgebungsbad.

In den folgenden drei Jahren vollzogen wir einen Kurswechsel von kontinuierlichen Interaktionen hin zu Pionierarbeit im Bereich der *gepulsten Optomechanik*. Gepulste Interaktion auf Zeitskalen unterhalb der mechanischen Schwingungsperioden öffnen eine Anzahl an neuen Möglichkeiten die im kontinuierlichen Regime nicht zur Verfügung stehen. Diese beinhalten, unter anderem, die zwei beträchtlichen Vorteile, mechanische Positionsmessungen mit Präzision jenseits des Standard Quantenlim-

its, und die Fähigkeit, opto-mechanische Experimente durchzuführen, die Dynamik anstatt nur stationäres Verhalten untersuchen. Wir haben theoretische Grundlagen entwickelt die es erlauben gequetschte Zustände mechanischer Bewegung durch gepulste Messungen herzustellen, und eine Methode für die Tomographie von beweglichen Zuständen vorgestellt. Diese Methoden wurden von uns experimentell implementiert, mit dem Resultat dass ein neuer Rekord für die Quetschung von thermischen Rauschen mit einer Reduktion in der Unsicherheit von Positionsmessungen unterhalb von 20 pm unter gleichzeitiger Bewegungszustands Tomographie erreicht wurde. Weitere theoretische Arbeit in diese Richtung nutzte die Nichtlinearität der opto-mechanischen Interaktion für starke quadratische Positionsmessungen.

Das Studium der Zeitdomäne hat uns erlaubt experimentelle Protokolle zu entwickeln die aus mehreren (kohärenten) gepulsten Interaktionen bestehen. Im speziellen haben wir zwei Protokolle entwickelt die eine Sequenz von vier gepulsten opto-mechanischen Interaktionen ausnützen. Beide Protokolle beruhen auf einer geometrischen Phase, d.h. einer Phase die aus einer geschlossenen Kurve im Phasenraum entsteht, allerdings für unterschiedliche Zielsetzung. Das erste Schema ist ein experimenteller Vorschlag um Quantenschwerkraft mit den Werkzeugen der Quanten Optomechanik zu testen. Das Schema erlaubt es, vom der geometrischen Phase, die Licht nach vier Wechselwirkungen erfährt, auf die mechanische Kommutator Relation von Position und Impuls zurückzuschließen. In verschiedenen Modellen der Quantenschwerkraft, zB der Stringtheorie, wird diese Relation modifiziert um eine minimale Längenskala des Universums zu beinhalten. Unser zweiter Vorschlag, in dem die Rolle des Lichts und des mechanischen Resonators vertauscht sind, nutzt eine geschlossene Kurve im optischen Phasenraum um einen nichtlinearen, d.h. zustandsabhängigen, Phasenschub in dem mechanischen Resonator zu induzieren und dadurch deterministische Kontrolle des Quantenzustands zu ermöglichen.

Ein weiteres theoretisches Projekt, das im letzten Jahr dieser Arbeit fertiggestellt wurde, befasste sich mit der Domäne zwischen einer kontinuierlichen und gepulsten Interaktion. Wir entwickelten theoretische Grundlagen um einen mechanischen Resonator im Einzel-phonon Bereich zu manipulieren, durch eine Methode die kontrollierte, gewichtete Überlagerungen von Phononen Addition, Subtraktion, und der Identitätsoperation erlaubt. Unsere Resultate können generell Anwendungen für Quanteninformationsprotokolle die auf mechanischen Resonatoren beruhen finden, und im speziellen benutzt werden um beliebige Quantenzustände herzustellen, und weiters auf andere Systeme so wie zB in Fallen gefangenen Ionen und Spinensembles angewendet werden.

1 Introduction

1.1 Optomechanics and Radiation Pressure

Radiation pressure – the force per unit area exerted by electromagnetic radiation on a surface – is the term that refers to a broad class of forces, e.g. optical gradient forces, the force due to the reflection or absorption of light, and even radiometric (light induced thermal) forces. It was realized in the early 17th century that optical radiation could exert such forces by Kepler who (correctly) believed that radiation pressure from solar radiation played a role in comet tail formation. More than a century later in 1871 Maxwell provided a rigorous theoretical description of radiation pressure due to the reflection of light, which was experimentally observed by Nichols and Hull [1, 2] and Lebedev [3] in the early 1900s. Shortly after these experiments came the dawn of relativity and quantum mechanics and research on, or utilizing, radiation pressure did not actively continue until the late 1960s. At that time, radiation pressure became one of the key tools of atomic, molecular and optical (AMO) physics for the trapping and cooling of atoms and particles [4, 5, 6].

With the exception of chapter 10, the research in this thesis utilizes radiation pressure from the reflection of light. The key to understanding the origin of a force from a reflection is that light itself carries momentum. A pulse of light with energy E carries momentum E/c, where c is the speed of light in vacuum, and a reflection, due to conservation of momentum, will transfer $2E/c$ momentum to the surface. The force, or momentum transfer per unit time, is then $F = 2P/c$, where P is the optical power. Note that the radiation pressure force is halved for the case of absorption of the light by the surface.

Radiation pressure is the central interaction in the field of optomechanics, which uses light to measure and manipulate the motion of mechanical objects. The basic optomechanical system has a mechanical element that has been engineered to be sufficiently low mass and compliant to move even under the feeble force of radiation pressure. As radiation pressure is such a weak force optomechanical setups often employ an optical resonator to enhance the radiation pressure force. A typical and conceptually simple configuration is a Fabry-Pérot cavity that has one massive rigid mirror and one end mirror that is small and vibrates in a (typically harmonic) potential. Such a system is of considerable practical interest because the mechanical oscillator is susceptible to weak external forces that can be measured with high precision via the optical readout. Moreover, and of particular interest of this thesis, such a system offers an attractive experimental route to prepare and investigate quantum mechanical behavior of the motion of the macroscopic mechanical resonator. In such a regime, i.e. *quantum optomechanics*, the quantum noise on the intensity of light causes a significant change to the mechanical resonator's momentum. In this regime, the momentum carried by each photon will transfer momentum $2\hbar k = 2\hbar\omega/c$.

1.1.1 Some History and Motivation of Quantum Optomechanics

The field of quantum optomechanics has a history about half as long as quantum mechanics itself, i.e. four to five decades. For much of that time, research on optomechanics came under numerous different guises and it was only quite recently that such research became a field in its own right. It is not the purpose of this cumulative dissertation to provide a thorough review of the developments of the field and the reader is instead directed to the review articles, Refs. [7, 8, 9, 10, 11, 12].

The main line of research from which quantum optomechanics emerged is gravitational wave detection via optical interferometry [13, 14]. There, the stochastic back-action forces imparted to the interferometer mirrors by the reflected optical fields placed a limit (the standard quantum limit) on the sensitivity of the device and a quantum mechanical treatment of the radiation pressure interaction between the optical field and the motion of the mirrors was important [15]. Much of the discussion and thoughts of that time on the quantum optical aspects of radiation pressure can be found in the collection of conference contributions in Ref. [16]. A particularly important development of that time was that methods were conceived to circumvent the standard quantum limit, which gave rise to the concepts of back-action evading or quantum non-demolition (QND) measurements [17]. The QND concept now plays a key role throughout all of quantum optics. Both the standard quantum limit and the concept of QND measurement were developed by V. B. Braginsky [18] and undoubtedly Braginsky is the father of optomechanics. His book 'Quantum measurement' [19] has perhaps had the strongest influence on the field and despite being published in 1995 'Quantum measurement' still serves to describe many of optomechanics' main current research directions.

Another line of research that contributed to the birth of quantum optomechanics is nonlinear optics. The field of nonlinear optics is primarily concerned with the development and study of materials or systems that permit an optical field to interact with itself or other optical fields. In most cases the influence of light on a material is very weak and it is challenging to find a system that exhibits a sufficiently strong non-linearity to allow light-light interaction at low optical intensities. An optomechanical cavity, due to its length dependence on the optical intracavity intensity, has now become a prime example of a nonlinear optical system. For a fixed laser frequency incident upon an optomechanical cavity, the amount of light entering the cavity depends upon the cavity length, and in turn the cavity length depends upon the optical intensity. This type of radiation pressure induced (Kerr) nonlinearity was observed in an early and elegant experiment by Dorsel and colleagues [20]. In their experiment a laser field with a fixed frequency was incident upon a Fabry-Pérot cavity with one large rigid mirror and a smaller low mass suspended mirror. By slowly scanning the incident optical intensity initially from a low power to a higher power and then back down, Dorsel *et al.* observed a sudden jump in the transmitted intensity with a hysteresis cycle that demonstrated bistability in the optomechanical system – a characteristic feature of Kerr media. Following this experiment it was considered by Mancini and Tombesi [21] and Fabre *et al.* [22] that for incident intensity levels close to bistability the nonlinearity can be utilised to squeeze the quantum fluctuations of the optical field. Such ponderomotive squeezing, i.e. optical squeezing resulting from a radiation pressure interaction, was recently experimentally observed with an optomechanical system of trapped cold atoms inside an optical cavity [23, 24, 25]. A potential application of such ponderomotive squeezing is that it can provide low frequency squeezing (below 1 kHz) with a spectrum well suited for injection into gravitational wave detectors [26, 27, 28].

In present day quantum optomechanics, research focus has broadened and considerable efforts are now made towards the preparation of non-classical motion of the mechanical element itself. Many of the quantum-state-engineering techniques now being employed build upon methods previously developed in cavity quantum electrodynamics [29], spin ensemble [30], trapped ion [31], and quantum optical experiments [32]. However, there are directions in quantum optomechanics that are distinctly different from established quantum optics research programs. An early notable theoretical proposal for quantum state preparation of mechanical motion using a quantum state of light and radiation pressure is that by Bose, Jacobs, and Knight [33, 34], where an optical field inside an optomechanical cavity is prepared in a quantum superposition of the vacuum and a single photon. The radiation pressure interaction between this non-classical optical field and the mechanical resonator generates a light-mechanical resonator 'Schrödinger's-cat-like' entangled state, which can be used to investigate mechanisms of quantum decoherence. Another notable work is that by Mancini, Manko, and Tombesi [35] who also considered preparing 'Schrödinger's-cat-like' states between light and the motion of a mechanical element. Building upon these ideas Marshall *et al.* [36] and Armour *et al.* [37] developed schemes to probe such entanglement in optomechanics and electromechanics, respectively. Experiments that realize these proposals will be able to probe so called 'collapse models' of the wavefunction [38, 39, 40, 41] that consider modifications to quantum dynamics for macroscopic systems that result in a degradation of large spatial superposition states. Other notable works include schemes for teleportation from an optical field to mechanical motion [42] and entanglement between two mechanical elements [43, 44, 45]. Recently the author, together with colleagues M. Aspelmeyer and M. S. Kim, proposed a technique to allow manipulation of mechanical motion at the single phonon level that can be used for arbitrary quantum state preparation and quantum information applications [46]. At the time of writing this thesis it is certainly an exciting time in the field of quantum optomechanics. The first signs of quantum motion of mechanical resonators have been observed [47, 48, 49] and there are still numerous intriguing questions to answer both theoretically and experimentally.

1.1.2 The Cavity Optomechanical System

A cavity optomechanical system is shown schematically in Fig. 1.1. The system consists of a large rigid mirror and a smaller mechanically compliant mirror that is able to move under the influence of radiation pressure. Such a deformable Fabry-Pérot cavity is a common configuration for optomechanics experiments and also serves to provide a conceptually simple picture to understand and model most cavity optomechanical systems. In this thesis, and in the majority of cavity optomechanical schemes, just a single optical longitudinal mode of the cavity, here described by field operator a where $[a, a^\dagger] = 1$, is excited. The cavity has a mean length L and hence a mean resonance frequency $\langle\omega_c\rangle = \pi c n/L$, where n is the longitudinal mode number. The cavity is driven by an external field in a coherent state, which may be detuned from the cavity resonance frequency, through the larger rigid cavity mirror. This mirror has a lower reflectivity than the mechanical mirror that allows the light to enter and exit through this mirror with minimal transmission through the mechanical mirror, i.e. the cavity is ‘single-sided’. The mechanical mirror is harmonically bound with angular frequency ω_M. An important property of the mechanical oscillator is its quality factor $Q = \omega_M/\gamma_M$, where γ_M is the mechanical amplitude decay rate. When the mechanical oscillator moves away from the equilibrium position $x_M = 0$ this causes a time-dependent modulation to the cavity resonance frequency, i.e.

$$\omega_c(x_M) = \frac{\pi c n}{L} \frac{1}{1 + x_M/L} \simeq \langle\omega_c\rangle(1 - x_M/L). \tag{1.1}$$

This expression is a convenient point to determine the quantized Hamiltonian for the optomechanical system. The form of the optomechanical Hamiltonian has been known in the quantum optics community for quite some time and an early publication that explicitly utilizes the Hamiltonian is the work by Pace, Collett, and Walls [50]. A more rigorous analysis and derivation of the optomechanical Hamiltonian can be found in the work of Law [51]. First the mechanical position is quantized, i.e

$$\langle\omega_c\rangle(1 - x_M/L) \rightarrow \langle\omega_c\rangle \left(1 - \frac{x_0}{L}(b + b^\dagger)\right), \tag{1.2}$$

where the mechanical field operator b with commutation relation $[b, b^\dagger] = 1$ has been introduced to describe the center of mass motion; $x_0 = \sqrt{\hbar/2m\omega_M}$ is the standard deviation of the mechanical ground-state width; and m is the mechanical effective mass. To arrive at the full Hamiltonian we then consider the sum of the mechanical energy, the mechanical position dependent energy of the intracavity optical field, and the external drive. In a frame rotating at the drive frequency the Hamiltonian is then

$$\frac{H}{\hbar} = \omega_M b^\dagger b + \Delta a^\dagger a - g_0 a^\dagger a(b + b^\dagger) + i\mathcal{E}(a^\dagger - a), \tag{1.3}$$

where Δ is the detuning between the external drive and the mean cavity resonance frequency and $\mathcal{E}$ quantifies the drive strength where the phase of the drive was chosen to give a real intracavity amplitude. An important parameter introduced here is the optomechanical coupling rate $g_0 = \langle\omega_c\rangle x_0/L$, which quantifies the rate at which the mechanical oscillator is displaced per photon, and concurrently, the rate at which the light accumulates a phase shift for a given mechanical displacement.

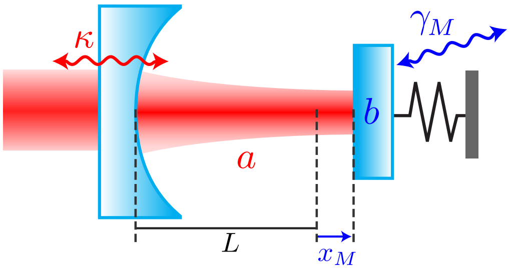

Figure 1.1: Schematic for a cavity optomechanical system. The mechanical oscillator, which forms one end mirror of a Fabry-Pérot cavity with mean length L, is described by field operator b, elongates the cavity by displacement x_M, and has an amplitude decay rate γ_M. The intracavity field is described by field operator a and has an amplitude decay rate of κ.

1.1.3 System Dynamics

Before proceeding to discuss the equations of motion that describe the dynamics and stochastic processes of such an optomechanical system it is instructive to connect the above Hamiltonian description to the classical radiation pressure force described in section 1.1. Applying Hamilton's equations to the interaction term the force is

$$F = -\frac{\partial H_{int}}{\partial x} = \frac{\hbar\langle\omega_c\rangle a^\dagger a}{L}. \tag{1.4}$$

As the optical power inside the cavity is enhanced in proportion to the cavity finesse $\mathcal{F} = \pi c/2L\kappa$, where κ is the optical amplitude decay rate, the force is then written as

$$F = \frac{2\hbar\langle\omega_c\rangle a^\dagger a \mathcal{F}\kappa}{\pi c} = \frac{2P_{cav}}{c}, \tag{1.5}$$

where the intracavity power P_{cav} has been introduced.

Returning now to the quantised Hamiltonian (1.3) we can write the stochastic differential equations of motion that describe the time evolution of the optical field inside the cavity and the mechanical field operator, i.e. the Langevin equations

$$\begin{aligned} \frac{\mathrm{d}a}{\mathrm{d}t} &= -i\left(\Delta - g_0(b + b^\dagger)\right)a + \mathcal{E} - \kappa a + \sqrt{2\kappa}a_{in}, \\ \frac{\mathrm{d}b}{\mathrm{d}t} &= -i\omega_M b + ig_0 a^\dagger a - \gamma_M b + \sqrt{2\gamma_M}b_{in}, \end{aligned} \tag{1.6}$$

where the noise operators a_{in} and b_{in} have been introduced. These noise operators describe any classical, e.g. thermal, noise if present and the ubiquitous quantum noise that is present in all quantum systems and is responsible to maintain the commutation relations. (An excellent text that greatly assisted the research in this thesis is *Quantum Noise* by Gardiner and Zoller [52].) Firstly, it should be noted that these are coupled equations, i.e. a depends on b and vice-versa, and secondly, the equation for a is non-linear, i.e. the optical dynamics depend upon the optical intensity and not the amplitude. For these two reasons, most works in the field of optomechanics linearise these equations, see Refs. [53, 54] and chapters 5, 6, 2, and 3, for more detail. By contrast, in chapter 8 this linearisation approximation is not made and the optical non-linearity is exploited to yield a route for a strong measurement of the mechanical position squared.

The mechanical resonator when in thermal equilibrium with its surrounding environment at temperature T has a mean thermal occupation described by Bose statistics

$$\bar{n} = \frac{1}{\exp(\hbar\omega_M/k_B T) - 1} \simeq \frac{k_B T}{\hbar\omega_M}, \tag{1.7}$$

where the approximation made on the right is accurate for large thermal occupation, i.e. $\bar{n} \gg 1$. It should also be noted that a particular form of mechanical bath coupling is assumed in (1.6) where the noise affects the position and momentum equally. The noise has zero mean, i.e. $\langle b_{in}\rangle = \langle b_{in}^\dagger\rangle = 0$ and for high Q mechanical oscillators it is delta correlated, i.e. the noise is white

$$\left\langle b_{in}^\dagger(t) b_{in}(t')\right\rangle = \bar{n}\delta(t - t') \quad \text{and} \quad \left\langle b_{in}(t) b_{in}^\dagger(t')\right\rangle = (\bar{n} + 1)\delta(t - t'). \tag{1.8}$$

Similarly, the optical input vacuum noise has zero mean and is delta correlated, however, has zero thermal occupation so $\langle a_{in}^\dagger(t) a_{in}(t')\rangle = 0$ and $\langle a_{in}(t) a_{in}^\dagger(t')\rangle = \delta(t - t')$.

Finally, to obtain the output optical field as it decays out of the cavity, as is required to determine the field at an external detector, one applies the input-output relation

$$a_{out} = \sqrt{2\kappa}a - a_{in}. \tag{1.9}$$

While the system and dynamics may be concisely summarized in these two subsections all the diversity and richness of the field of optomechanics stems from these equations and small variations thereof.

1.2 This Thesis

To summarize the direction of this research with a single sentence: This thesis worked, both experimentally and theoretically, towards the preparation and state reconstruction of non-classical motional states of a macroscopic mechanical resonator to experimentally investigate quantum decoherence, develop quantum information and quantum-physics-enhanced sensing technologies, and ultimately experimentally probe potential quantum gravitational phenomena.

In the first two years of this research, from the beginning of 2008, we focussed on a continuous interaction between the optical field and the mechanical element. During this period we further developed cooling of mechanical motion by simultaneously employing cryogenic and laser cooling techniques, see chapter 2. Furthermore, by using large amplitude optical driving fields we were able to observe normal-mode splitting between the intracavity field and the harmonic mechanical motion. These experimental efforts built upon prior work performed by Gigan, Böhm, *et al.* [55] and many of the technical details are outlined in Hannes Böhm's thesis [56]. For further details and discussion, in particular on the improvements to the mechanical resonators and the optical setup used for the cooling and strong coupling, see the thesis of Simon Gröblacher [57].

Monitoring the position of a mechanical resonator continuously is fundamentally limited to a measurement precision set by the standard quantum limit. This limit to the precision of position read-out needs to be surpassed in order to resolve features in the mechanical position probability distribution smaller than the ground state extension, which is important for quantum state reconstruction. An experimental technique able to perform quantum state reconstruction of the mechanical motional state is yet to be realized and developing such a technique was a primary goal of this thesis. To this end, in late 2008 we considered a pulsed optomechanical interaction of duration much shorter than a mechanical period to surpass the standard quantum limit. Such an interaction was first considered in the seminal works by Braginsky [58, 19] for an improved force detection scheme. We utilized the pulsed interactions to develop a fully quantum mechanical protocol for the preparation of squeezed states of motion via measurement and, importantly, for quantum state tomography by measurement of all the mechanical quadratures. In this theoretical proposal, discussed in chapter 6, we use an initial pulse for mechanical state preparation and then a second pulse made at a later time for mechanical state reconstruction. Prior to this proposal being published we began implementing this technique in the laboratory and a proof-of-concept experiment, using a relatively low frequency mechanical cantilever, was completed at the end of 2012. Details of this experiment are provided in chapter 7. This theoretical proposal and experimental implementation form the primary project of this thesis.

In parallel to work on the experiment, further exploration down this path with short optical pulses led to novel schemes to prepare quantum states of motion of the mechanical element. In particular, chapter 8 discusses a scheme to perform a measurement of the square of the mechanical position, which can be used to generate position superposition states via measurement. Other techniques using a dispersive interaction were known at the time to perform such measurements, however, the approach offered here provides a significantly stronger measurement strength and is therefore considerably more feasible to implement experimentally. Furthermore, the mechanical state tomography mentioned above can be readily implemented in this scheme and thus a complete framework for quantum state preparation and reconstruction can be implemented.

Using a pulsed approach not only has the advantage that the standard quantum limit can be surpassed it also allows one to consider various protocols involving more than one pulse in time. Our first idea in this direction was to use a sequence of four optomechanical interactions separated by quarter periods of mechanical motion to probe the canonical commutator between the mechanical position and momentum, see chapter 9. Our primary motivation to experimentally investigate the mechanical commutation relation is that numerous models of quantum gravity predict the existence of a minimum length, of order of the Planck length, and thus a modification to the Heisenberg uncertainty relation. By inferring the value of the canonical commutator using this four pulsed scheme one may then, given an experimental precision, detect or place limits on such a potential quantum gravitational modification to regular quantum mechanics. The other idea in this direction was to again use a sequence of four optomechanical interactions, however, displace the optical field between the interactions in a closed loop in phase space. In this manner the mechanical oscillator gains a state dependent phase shift and can be used for unconditional quantum state preparation, see chapter 10.

There is a third regime for the optomechanical interaction time-scale that is between the continuous interaction, which looks at the steady-state of the system, and the short pulsed case, which probes and manipulates the mechanical dynamics. This third case uses optical pulses that are much longer than the mechanical period, which allows optical sidebands to be generated due to the modulation from the mechanical motion but can still be used in multi-pulse time-based protocols. In mid 2008 we conceived a scheme that uses single photon detection on the optical sidebands to perform phonon addition or subtraction. Later we further developed this to allow for a controllable coherent superposition of these two operations and used this to form a continuous-variable quantum state orthogonalizer that may have future applications in quantum information and quantum state engineering. See chapter 5 for details. These three regimes of interaction time-scales are compared in the section below.

1.2.1 Three Temporal Interaction Regimes

To clarify and contrast the three temporal interaction regimes interactions explored in this thesis, Fig. 1.2 provides a comparison.

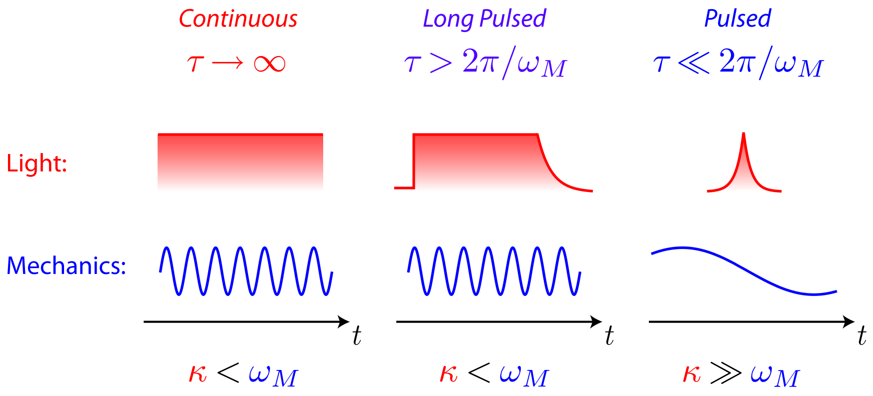

Figure 1.2: The three temporal interaction regimes explored in this thesis. In order of increasing interaction time τ (left to right) there is the continuous regime, the long pulsed regime, and the pulsed regime, respectively. The optical drive amplitude is compared to the mechanical oscillation period. In the continuous regime the interaction occurs for many mechanical periods and the steady state is analyzed. In the long pulsed interaction regime the optomechanical interaction again proceeds for many periods, so that the optical sidebands are generated by the modulation provided by the motion of the mechanics, however, the light may be switched on and off so that the state of the mechanics immediately after the interaction can be analyzed. In the pulsed regime the interaction is much faster than a mechanical period and the mechanical position is essentially a constant during the interaction. No optical sidebands are produced in this regime.

As will be detailed in the publications included in the chapters below, in the continuous and long pulsed regime one typically detunes the optical drive by one mechanical frequency away from cavity resonance. Provided that the cavity amplitude decay rate κ is much smaller than the mechanical frequency ω_M the drive then creates a sideband at the cavity resonance frequency only, i.e. the sideband at $2\omega_M$ away from resonance is suppressed and the situation is accurately described using a rotating-wave-approximation. In this regime, when the incident drive has a frequency lower than the cavity resonance an optomechanical beam-splitter interaction occurs, i.e. $H_{int} \propto ab^\dagger + a^\dagger b$, and when the drive has a higher frequency the two-mode-squeezing interaction occurs, i.e. $H_{int} \propto ab + a^\dagger b^\dagger$.

By contrast, in the pulsed regime, as there is no interplay between mechanical evolution and the radiation pressure interaction, regardless of the detuning the interaction is always $H_{int} \propto a^\dagger a X_M$, which may be linearised to $H_{int} \propto X_L X_M$, where X_L describes the optical amplitude quadrature.

1.2.2 List of Publications

The following is a list of publications in chronological order resulting from the research performed during this thesis. A complete list of publications by the author may be found in the curriculum vitae provided at the end of this thesis.

1. **Demonstration of an ultracold micro-optomechanical oscillator in a cryogenic cavity**
   Simon Gröblacher, Jared B. Hertzberg, **Michael R. Vanner**, Garrett D. Cole, Sylvain Gigan, Keith C. Schwab, and Markus Aspelmeyer
   Nature Physics **5**, 485 (2009)

2. **Observation of strong coupling between a micromechanical resonator and an optical cavity field**
   Simon Gröblacher, Klemens Hammerer, **Michael R. Vanner**, and Markus Aspelmeyer
   Nature **460**, 724 (2009)

3. **Phonon-tunnelling dissipation in mechanical resonators**
   Garrett D. Cole, Ignacio Wilson-Rae, Katharina Werbach, **Michael R. Vanner**, and Markus Aspelmeyer
   Nature Communications **2**, 231 (2011)

4. **Pulsed Quantum Optomechanics**
   M. R. Vanner, I. Pikovski, G. D. Cole, M. S. Kim, C. Brukner, K. Hammerer, G. J. Milburn, and M. Aspelmeyer
   Proc. Natl. Acad. Sci. USA **108**, 16182 (2011)

5. **Selective Linear or Quadratic Optomechanical Coupling via Measurement**
   Michael R. Vanner
   Phys. Rev. X **1**, 021011 (2011)

6. **Probing Planck-scale physics with quantum optics**
   Igor Pikovski, **Michael R. Vanner**, Markus Aspelmeyer, Myungshik Kim, and Caslav Brukner
   Nature Physics **8**, 393 (2012)

7. **Quantum State Orthogonalization and a Toolset for Quantum Optomechanical Phonon Control**
   M. R. Vanner, M. Aspelmeyer, and M. S. Kim
   Phys. Rev. Lett. **110**, 010504 (2013)

8. **Quantum state preparation of a mechanical resonator using an optomechanical geometric phase**
   K. E. Khosla, **M. R. Vanner**, W. P. Bowen, and G. J. Milburn
   New J. Phys. **15**, 043025 (2013)

9. **Cooling-by-measurement and mechanical state tomography via pulsed optomechanics**
   M. R. Vanner, J. Hofer, G. D. Cole, and M. Aspelmeyer
   Nature Communications **4**, 2295 (2013)

1.2.3 How This Thesis May Be Read

After reading this introduction there are various ways to navigate the following chapters. Each subsequent chapter in this cumulative dissertation provides a project synopsis and the published journal article. Each chapter could be read independently, however, in Fig. 1.3 a reading guide is given, as some chapters build upon and follow naturally from earlier chapters.

Although not shown in Fig. 1.3 there are, of course, connections between all of the three temporal interaction regimes; ‘Continuous’, ‘Long Pulsed’, and ‘Pulsed’, and it has been insightful to compare these three regimes, which is discussed in the publications in chapters 5, 6 and 7.

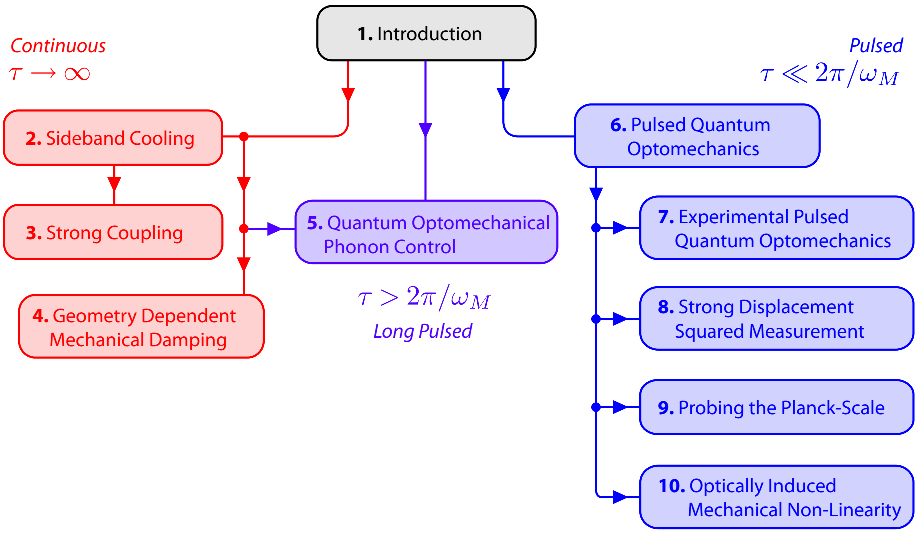
Continuous
$\tau \to \infty$
1. Introduction
Pulsed
$\tau \ll 2\pi/\omega_M$
2. Sideband Cooling
3. Strong Coupling
4. Geometry Dependent Mechanical Damping
5. Quantum Optomechanical Phonon Control
$\tau > 2\pi/\omega_M$
Long Pulsed
6. Pulsed Quantum Optomechanics
7. Experimental Pulsed Quantum Optomechanics
8. Strong Displacement Squared Measurement
9. Probing the Planck-Scale
10. Optically Induced Mechanical Non-Linearity

Figure 1.3: How this thesis may be read. Lines with arrows indicate recommended routes. The three temporal interaction regimes; 'Continuous', 'Long Pulsed', and 'Pulsed' are shown from left to right, respectively, where the optomechanical interaction time-scale τ is compared to the mechanical period of motion $2\pi/\omega_M$.

2 Sideband Cooling of Mechanical Motion

For quantum state preparation of the motion of a mechanical oscillator it is important that the oscillator have a low entropy initial state so that any non-classical motion is not ‘washed away’ by the thermal or incoherent contribution. To this end, a significant amount of research is spent on developing and improving techniques to cool the motion to low thermal occupation.

Sideband or laser cooling is now a well established approach to achieve such low entropy states and has been successfully demonstrated in a number of physical systems. The approach is implemented by injecting electromagnetic radiation with a detuning below the cavity resonance frequency so that the radiation scattered by the motion of the mechanical system is preferentially scattered into a higher frequency sideband. Scattering radiation into a higher frequency mode requires energy, which in this case, is obtained from the mechanical motion itself due to conservation of momentum. Experimentally such cooling will be seen as an increase in the mechanical damping and importantly a reduced noise power, i.e. the integral over all frequency components of the noise power spectrum. For a narrow linewidth cavity, i.e. $\kappa \ll \omega_M$ the optimum detuning is approximately equal to the mechanical frequency and we can then understand this type of cooling as a result of the beam-splitter interaction resulting in a partial state transfer from the low entropy optical field onto the mechanical resonator.

This technique was first experimentally demonstrated by Braginsky in 1970 [59] to cool the motion of a mechanical oscillator and it is closely related to the independently studied cooling of the motion of trapped ions [60]. Following these experiments, modern cavity optomechanics based laser cooling experiments were initiated by Refs. [61, 55, 62].

The contribution covered in this thesis [63] combined a number of technical improvements that resulted in cooling a MHz scale mechanical resonator to a final thermal occupation of $\bar{n} \simeq 30$, which set the state-of-the-art at the time. We implemented a two-field experiment with a weak ‘signal’ kept on resonance with the cavity for mechanical position monitoring via optical homodyne interferometry and a stronger ‘cooling’ field with an intensity and detuning that could be controlled independently from the signal field. A second improvement was to employ high mechanical Q oscillators comprising a thin mechanically compliant silicon-nitride base with a high reflectivity dielectric mirror. My specific contributions to this interdisciplinary team project were: align and optimize the homodyne interferometers; develop the calibration procedure; work together on the experimental runs for data collection; and write the software for and together complete the data analysis.

After this work performed in 2008/2009, the thermal ground state, i.e. $\bar{n} < 1$, has now quite recently been observed in both electro-mechanical [47, 64] and opto-mechanical [65] systems, marking a convenient starting point for experiments towards the observation of non-classical mechanical motion.

nature physics

LETTERS

PUBLISHED ONLINE: 7 JUNE 2009 DOI: 10.1038/NPHYS1301

Demonstration of an ultracold micro-optomechanical oscillator in a cryogenic cavity

Simon Gröblacher[1,2], Jared B. Hertzberg[3,4], Michael R. Vanner[1,2], Garrett D. Cole[1,5], Sylvain Gigan[6], K. C. Schwab[3]* and Markus Aspelmeyer[1†]

Preparing and manipulating quantum states of mechanical resonators is a highly interdisciplinary undertaking that now receives enormous interest for its far-reaching potential in fundamental and applied science[1,2]. Up to now, only nanoscale mechanical devices achieved operation close to the quantum regime[3,4]. We report a new micro-optomechanical resonator that is laser cooled to a level of 30 thermal quanta. This is equivalent to the best nanomechanical devices, however, with a mass more than four orders of magnitude larger (43 ng versus 1 pg) and at more than two orders of magnitude higher environment temperature (5 K versus 30 mK). Despite the large laser-added cooling factor of 4,000 and the cryogenic environment, our cooling performance is not limited by residual absorption effects. These results pave the way for the preparation of 100-μm scale objects in the quantum regime. Possible applications range from quantum-limited optomechanical sensing devices to macroscopic tests of quantum physics[5,6].

Recently, the combination of high-finesse optical cavities with mechanical resonators has opened up new possibilities for preparing and detecting mechanical systems close to—and even in—the quantum regime by using well-established methods of quantum optics. Most prominently, the mechanism of efficient laser cooling has been demonstrated[7–13] and has been shown to be capable, in principle, of reaching the quantum ground state[14–16]. A particularly intriguing feature of this approach is that it can be applied to mechanical objects of almost arbitrary size, from the nanoscale in microwave strip-line cavities[13] up to the centimetre scale in gravitational-wave interferometers[11]. In addition, whereas quantum-limited readout is still a challenging development step for non-optical schemes[3,17,18], optical readout techniques at the quantum limit are readily available[19].

Approaching and eventually entering the quantum regime of mechanical resonators through optomechanical interactions essentially requires the following three conditions to be fulfilled: (1) sideband-resolved operation; that is, the cavity amplitude decay rate κ has to be small with respect to the mechanical frequency ω_m; (2) both ultralow noise and low absorption of the optical cavity field (phase noise at the mechanical frequency can act as a finite-temperature thermal reservoir and absorption can increase the mode temperature and even diminish the cavity performance in the case of superconducting cavities); and (3) sufficiently small coupling of the mechanical resonator to the thermal environment; that is, low environment temperature T and large mechanical quality factor Q (the thermal coupling rate is given by $k_B T/\hbar Q$, where k_B is the Boltzmann constant and $\hbar$ is the reduced Planck constant). So far, no experiment has demonstrated all three requirements simultaneously. Criterion (1) has been achieved[10,13,20]; however, the performance was limited in one case by laser phase noise[10] and in the other cases by absorption in the cavity[13,20]. Other, independent, experiments have implemented only criterion (2)[11,12,19,21]. Finally, criterion (3) has been realized in several cryogenic experiments[4,13,21,22], however not in combination with both (1) and (2).

We have designed a novel micro-optomechanical device that enables us to meet all requirements at the same time. Specifically, we have fabricated a Si_3N_4 micromechanical resonator that carries a high-reflectivity, ultralow-loss Bragg mirror (Fig. 1a), which serves as the end mirror of a Fabry–Pérot cavity. We designed the system to exhibit a fundamental mechanical mode at relatively high frequency (of the order of 1 MHz; Fig. 1b) such that sideband-resolved operation (criterion (1)) can be achieved already with a medium-finesse cavity. Criterion (2) can first be fulfilled because our solid-state pump laser used for optical cooling exhibits low phase noise (laser linewidth below 1 kHz). Second, absorption in the Bragg mirror is sufficiently low to prevent residual heating in the mechanical structure. Absorption levels as low as 10^{-6} have been reported for similar Bragg mirrors[23] and recent measurements suggest even lower values of 4×10^{-7} for the specific coatings used in this experiment (R. Lalezari, private communication). In addition, although absorption in Si_3N_4 is comparable to silicon, the transmission mismatch of the two cavity mirrors (~10:1) and the resulting low transmission through the Bragg mirror prevents residual heating of the resonator as has been observed for cryogenically cooled silicon cantilevers[24]. Finally, criterion (3) requires low temperature and high mechanical quality. The mechanical properties of our design are dominated by the Si_3N_4, which is known to exhibit superior performance in particular at low temperatures, where Q-factors beyond 10^6 have been observed at millikelvin temperatures[25].

We operate our device, a 100 μm × 50 μm × 1 μm microresonator, in a cryogenic ^4He environment at 10^{-7} mbar and in direct contact with the cryostat cold finger. To measure the mechanical displacement, the frequency of a 7 μW continuous-wave Nd:YAG laser is locked close to resonance of the cryogenic Fabry–Pérot cavity (length $L \approx 25$ mm), which consists of a fixed macroscopic mirror and the moving micromechanical mirror. The optical

---

[1] Institute for Quantum Optics and Quantum Information (IQOQI), Austrian Academy of Sciences, Boltzmanngasse 3, A-1090 Vienna, Austria, [2] Faculty of Physics, University of Vienna, Boltzmanngasse 5, A-1090 Vienna, Austria, [3] Department of Physics, Cornell University, Ithaca, New York 14853, USA, [4] Department of Physics, University of Maryland, College Park, Maryland 20742, USA, [5] The Center for Micro- and Nanostructures (ZMNS), Vienna University of Technology, Floragasse 7, A-1040 Vienna, Austria, [6] Laboratoire Photon et Matière, Ecole Superieure de Physique et de Chimie Industrielles, CNRS-UPRA0005, 10 rue Vauquelin, 75005 Paris, France. *Permanent address: Department of Applied Physics, Caltech, Pasadena, California 91125, USA. †e-mail: markus.aspelmeyer@quantum.at.

© 2009 Macmillan Publishers Limited. All rights reserved.

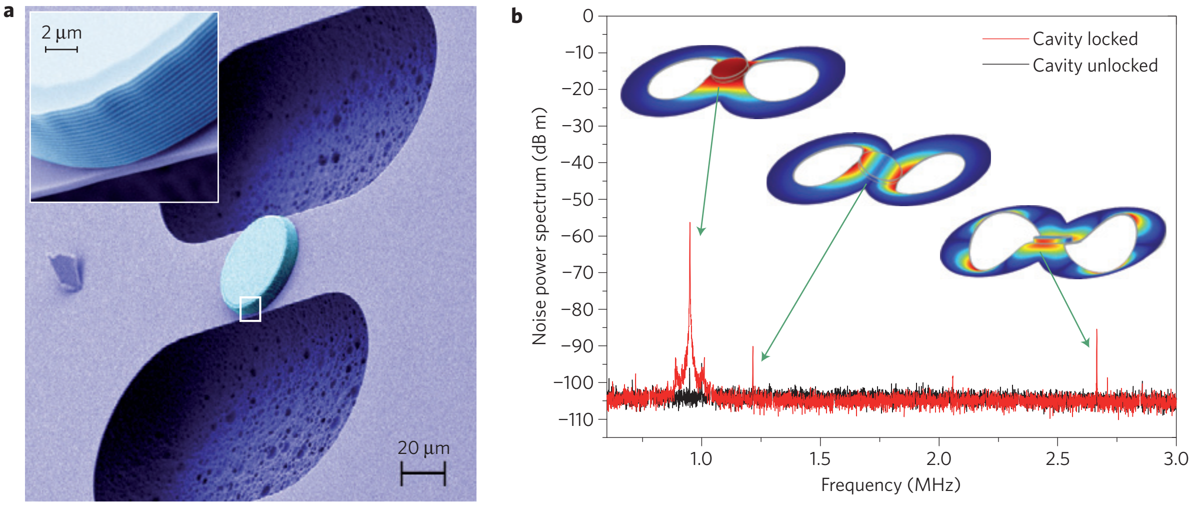

Figure 1 | High-quality micro-optomechanical resonator. a, Scanning electron micrograph of the basic mechanical system, which is formed by a doubly clamped Si_3N_4 beam. A circular, high-reflectivity Bragg mirror is used as the end mirror of a Fabry–Pérot cavity. The Bragg mirror is made of low-absorption, alternating dielectric stacks of Ta_2O_5/SiO_2. The magnified section in the inset shows the stacking sequence. **b**, Micromechanical displacement spectra shown as noise power spectra of the readout-beam phase quadrature for a locked and an unlocked cavity. The fundamental mode at $\omega_m = 2\pi \times 945$ kHz and all higher mechanical modes are identified by finite element simulation. For the cases that involve large Bragg mirror displacements, we provide the simulated mode profile.

cavity of finesse $F \approx 3{,}900$ achieves moderate sideband resolution ($\kappa \approx 0.8\omega_m$), which in principle would allow cooling to a final occupation number $\langle n \rangle_{\min} = (\kappa^2/4\omega_m^2) \approx 0.16$, that is, well into the quantum ground state[14,15]. The experimentally achievable temperature is obtained as the equilibrium state of two competing processes, namely the laser cooling rate and the coupling rate to the thermal (cryogenic) environment. In essence, laser cooling is driven (in the ideal resolved-sideband limit and at detuning $\Delta = \omega_m$) at a rate $\Gamma \approx G^2/(2\kappa)$ (G is the effective optomechanical coupling rate, as defined in ref. 16), whereas mechanical relaxation to the thermal environment at temperature T takes place at a rate $(k_B T/\hbar Q)$. The final achievable mechanical occupation number is therefore, to first order, given by $n_f \approx (1/\Gamma) \times (k_B T/\hbar Q)$. A more accurate derivation taking into account effects of non-ideal sideband resolution can be found, for example, in refs 14–16, 26. Our experimental parameters limit the minimum achievable mode temperature to approximately 1 mK ($n_f \approx 30$). The fact that we can observe this value in the experiment (see below) shows that other residual heating effects are negligible. The micromechanical flexural motion modulates the cavity-field phase quadrature, which is measured by optical homodyning. For $Q \gg 1$ its noise power spectrum (NPS) is a direct measure of the mechanical position spectrum $S_q(\omega)$, as described in ref. 16. We observe a minimum noise floor of 2.6×10^{-17} m Hz$^{-0.5}$, which is a factor of 4 above the achievable quantum (shot-noise) limit, when taking into account the finite cavity linewidth, the cavity losses and the non-perfect mode-matching, and due to the residual amplitude noise of the pump laser at the sideband frequency of our mechanical mode. We observe the fundamental mechanical mode at $\omega_m = 2\pi \times 945$ kHz with an effective mass $m_{\mathrm{eff}} = 43 \pm 2$ ng and a quality factor $Q \approx 30{,}000$ at 5.3 K ($Q \approx 5{,}000$ at 300 K). These values are consistent with independent estimates based on finite-element method simulations yielding $\omega_m = 2\pi \times 945$ kHz and $m_{\mathrm{eff}} = 53 \pm 5$ ng (see Supplementary Information).

Optomechanical laser cooling requires driving of the cavity with a red-detuned (that is, off-resonant), optical field[6–13]. We achieve this by coupling a second laser beam—detuned by Δ in frequency but orthogonal in polarization—into the same spatial cavity mode (Fig. 2a). Birefringence of the cavity material leads to both an optical path length difference for the two cavity modes (resulting in an 800 kHz frequency difference of the cavity peak positions) and a polarization rotation of the outgoing fields. We compensate both effects by an offset in Δ and by extra linear optical phase retarders, respectively. A change in detuning Δ modifies the mechanical rigidity and results in both an optical spring effect ($\omega_{\mathrm{eff}}(\Delta)$) and damping ($\gamma_{\mathrm{eff}}(\Delta)$), which is directly extracted by fitting the NPS using the expressions from ref. 16. Figure 2b shows the predicted behaviour for several powers of the red-detuned beam. The low-power curve at 140 μW is used to determine both the effective mass of the mechanical mode, m_{eff}, and the cavity finesse, F. For higher powers and detunings closer to cavity resonance, the onset of cavity instability prevents a stable lock (see, for example, ref. 16). All experimental data are in agreement with theory and hence in accordance with pure radiation-pressure effects[15].

The effective mode temperature is obtained through the equipartition theorem. For our experimental parameter regime, $Q \gg 1$ and $\langle n \rangle \gg 0.5$, the integrated NPS is also a direct measure of the mean mechanical mode energy and hence, through the equipartition theorem, of its effective temperature through $T_{\mathrm{eff}} = (m_{\mathrm{eff}}\,\omega_{\mathrm{eff}}^2/k_B)\int_{-\infty}^{+\infty} \mathrm{NPS}(\omega)\,d\omega$. Note that, for the case of strong optomechanical coupling, normal-mode splitting can occur and has to be taken into account when evaluating the mode temperature[27]. In our present case, this effect is negligible because of the large cavity decay rate κ. The amplitude of the NPS is calibrated by comparing the mechanical NPS with the NPS of a known frequency modulation applied to the laser (see, for example, ref. 28). For a cold-finger temperature of 5.3 K, we obtain a mode temperature $T = 2.3$ K, which is consistent with an expected moderate cooling due to slightly off-resonant locking of the Fabry–Pérot cavity (by less than 3% of the cavity intensity linewidth). The locking point is deliberately chosen to be on the cooling side to avoid unwanted parametric mechanical instabilities. The mean thermal occupancy was calculated according to $\langle n \rangle = k_B T_{\mathrm{eff}}/\hbar\omega_{\mathrm{eff}}$. We note, however, that Bose–Einstein statistics will have a dominant role as one approaches the quantum ground state.

Figure 3a shows mechanical noise power spectra with the cooling beam switched off and with maximum cooling beam pump power at 7 mW. For a detuning $\Delta \approx \omega_m$, we demonstrate laser cooling to a mean thermal occupation of 32 ± 4 quanta, which is more than 2 orders of magnitude lower than previously reported values for optomechanical devices[10] and is comparable to the lowest

© 2009 Macmillan Publishers Limited. All rights reserved.

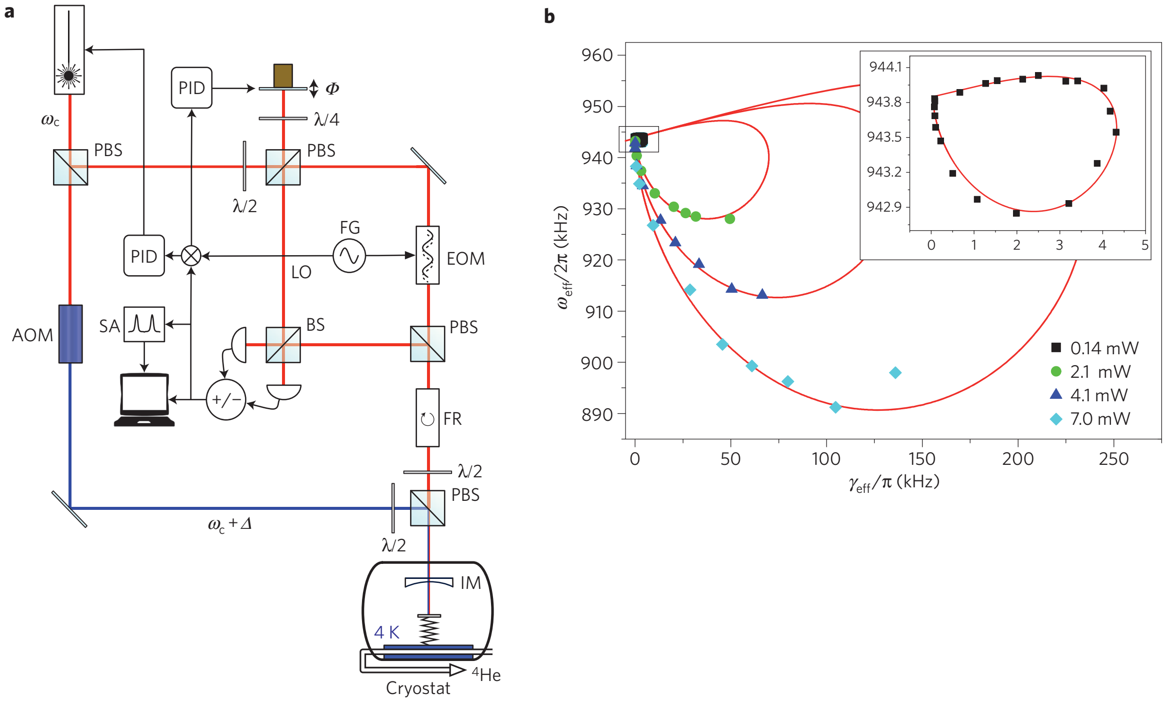

Figure 2 | Experimental set-up and characterization of optomechanical radiation-pressure interaction. a, The laser is split at a polarizing beamsplitter (PBS) into a weak locking field (red) tuned near cavity resonance ω_c and the cooling field (blue) tuned off-resonant with an acousto-optical modulator (AOM) to $\omega_c + \Delta \approx \omega_c - \omega_m$. An electro-optical modulator (EOM) in the weak field is used to generate a Pound–Drever–Hall error signal for cavity locking. The beams are recombined on a PBS into the same spatial mode at orthogonal polarization before they enter the cavity comprising an input mirror (IM) and the micro-mechanical mirror. The phase quadrature of the locking beam is measured in a homodyne detection scheme (BS: beamsplitter; LO: local oscillator; Φ: local oscillator phase; SA: spectrum analyser). Φ is stabilized in a separate proportional–integral–derivative controller (PID). A combination of a Faraday rotator (FR) and a half-wave plate (λ/2) separates the reflected from the original signal. **b**, The effective frequency ω_{eff} and damping γ_{eff} of the micro-mechanical motion for different detuning and power settings. All power levels follow the theoretical predictions for pure radiation-pressure interaction. The symbols are experimental data, and the solid lines are simulations based on ref. 16. The inset shows the data set taken at 140 μW optical power.

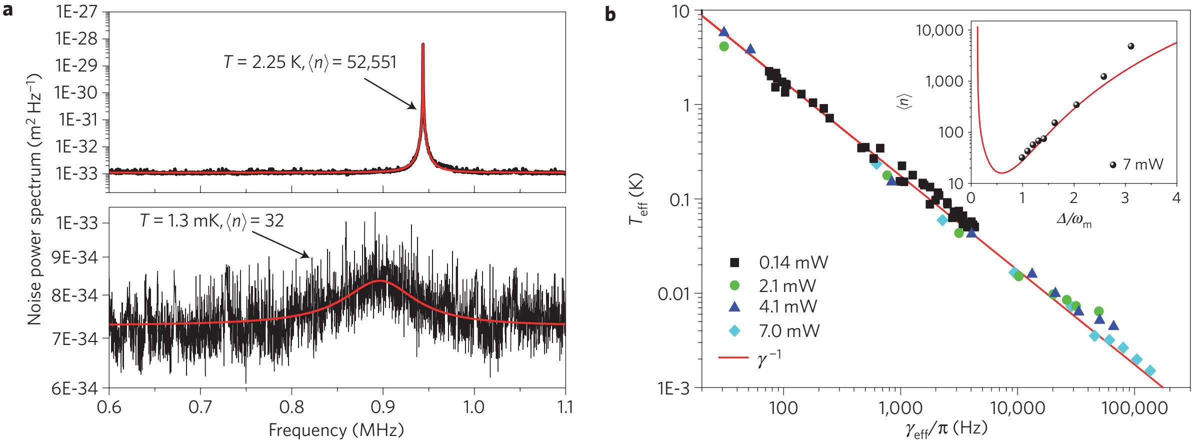

Figure 3 | Optomechanical laser cooling inside a cryogenic cavity. a, Calibrated noise power spectra for the fundamental mechanical mode at 5.3 K environmental temperature with small cavity cooling (top) and at maximum cooling (bottom). The thermal energy is reduced from ≈53,000 quanta at 7 μW laser power to 32 ± 4 quanta at 7 mW. The vertical axes in both plots are logarithmic. The change in the technical noise floor is due to different locking levels of the local oscillator phase Φ in the homodyne detection. **b**, Plot of the calibrated effective temperature T_{eff} versus the observed damping γ_{eff} for various power and detuning values of the cooling beam. No deviations from the theoretically expected power-law dependence (red solid line) can be observed. The inset shows the mean thermal occupation $\langle n \rangle$ as a function of detuning for maximal laser power. Cavity instability prevents detunings arbitrarily close to resonance. The red solid curve is a simulation based on ref. 16 that uses only experimentally obtained parameters.

reported temperature of 25 quanta for nano-electromechanical systems[4] (NEMS). In contrast to previous experiments[10,13], the achieved cooling performance is not limited by optical absorption or residual phase noise, but follows exactly the theoretically predicted behaviour (Fig. 3b). This agrees with the expected device performance: a fraction of approximately 10^{-6} of the intra-cavity power is absorbed by the Bragg mirror (~13 μW at maximum cooling) and a maximum of 1% of the transmitted power is absorbed by the Si_3N_4 beam[29] (~14 μW at maximum cooling and taking into account the impedance mismatch of the cavity mirrors).

© 2009 Macmillan Publishers Limited. All rights reserved.

The cryogenic cooling power of the cryostat used is orders of magnitude larger than the maximum heat load expected on the micromechanical structures. The absence of absorption can also be seen from the inferred mode temperature T_{eff}, which decreases with the mechanical damping rate γ_{eff} in strict accordance with the power law $T_{\mathrm{eff}} \propto \gamma_{\mathrm{eff}}^{-1}$. This relation follows immediately from the simple expression for the mechanical occupation n_{f} given above ($n_{\mathrm{f}} \propto \Gamma^{-1}$) and from the fact that the laser cooling rate Γ is to first approximation equivalent to the effective mechanical damping γ_{eff}, at least for all data points of our experiment. Both heating and the onset of normal-mode splitting for strong coupling[27] would result in a deviation of this behaviour.

The remaining obstacle that prohibits us from reaching the quantum ground state is the intrinsic phonon coupling to the thermal environment at rate $k_{\mathrm{B}}T/\hbar Q \approx 1.4 \times 10^7$ Hz. By reducing the reservoir temperature to that of NEMS experiments (20 mK), this coupling will significantly reduce, not only owing to the lower bath temperature but also because Si_3N_4 resonators markedly improve in mechanical Q with decreasing temperature. For example, thermal heating rates as low as 3×10^3 Hz have been observed for Si_3N_4 at 300 mK (ref. 25), which would place our effective mode temperature already well into the quantum ground state using otherwise unchanged parameters.

In summary, we have demonstrated optical cooling of the fundamental mode of a 100 μm scale mechanical resonator in a cryogenic cavity to a thermal occupation of only 32 ± 4 quanta. This is comparable to the performance of state-of-the-art NEMS devices. In contrast to previous approaches, the large laser cooling rates attained are no longer limited by residual absorption or phase-noise effects. This is achieved by a new micro-optomechanical resonator design with exceptionally low intrinsic optical absorption and both high optical and mechanical quality. This leaves the reduction of the thermal coupling, for example, by further decreasing the environment temperature to those available in conventional ^{3}He cryostats, as the only remaining hurdle to prepare the mechanical quantum ground state. Our approach hence establishes a feasible route towards the quantum regime of massive micromechanical systems.

Methods

Micro-mirror fabrication. Our micro-mechanical oscillator is made of 1-μm-thick low-stress Si_3N_4 deposited on a Si substrate and coated through ion beam sputtering with a high-reflectivity Bragg mirror. Standard photolithography and plasma etching is used for forming, in subsequent steps, the mirror pad and the micro-mechanical resonator, which is finally released from the Si substrate in a XeF_2 atmosphere. The mirror stack, designed and deposited by ATFilms, comprises 36 alternating layers of Ta_2O_5 and SiO_2 with an overall nominal reflectivity of 99.991% at 1,064 nm. The measured finesse of 3,900 is consistent with an input coupler reflectivity of 99.91% and with extra diffraction losses due to a finite size of the cavity beam waist.

Received 5 March 2009; accepted 1 May 2009;
published online 7 June 2009

References

1. Schwab, K. C. & Roukes, M. L. Putting mechanics into quantum mechanics. *Phys. Today* **58**, 36–42 (2005).
2. Aspelmeyer, M. & Schwab, K. C. (eds) Mechanical systems at the quantum limit. *New J. Phys.* **10**, 095001 (2008).
3. LaHaye, M., Buu, O., Camarota, B. & Schwab, K. C. Approaching the quantum limit of a nanomechanical resonator. *Science* **304**, 74–77 (2004).
4. Naik, A. *et al.* Cooling a nanomechanical resonator with quantum backaction. *Nature* **443**, 193–196 (2006).
5. Marshall, W., Simon, C., Penrose, R. & Bouwmeester, D. Towards quantum superpositions of a mirror. *Phys. Rev. Lett.* **91**, 130401 (2003).
6. Vitali, D. *et al.* Optomechanical entanglement between a movable mirror and a cavity field. *Phys. Rev. Lett.* **98**, 030405 (2007).
7. Metzger, C. H. & Karrai, K. Cavity cooling of a microlever. *Nature* **432**, 1002–1005 (2004).
8. Gigan, S. *et al.* Self-cooling of a micromirror by radiation pressure. *Nature* **444**, 67–71 (2006).
9. Arcizet, O., Cohadon, P.-F., Briant, T., Pinard, M. & Heidmann, A. Radiation-pressure cooling and micromechanical instability of a micromirror. *Nature* **444**, 71–75 (2006).
10. Schliesser, A., Rivière, R., Anetsberger, G., Arcizet, O. & Kippenberg, T. J. Resolved-sideband cooling of a micromechanical oscillator. *Nature Phys.* **4**, 415–419 (2007).
11. Corbitt, T. *et al.* An all-optical trap for a gram-scale mirror. *Phys. Rev. Lett.* **98**, 150802 (2007).
12. Thompson, J. D. *et al.* Strong dispersive coupling of a high-finesse cavity to a micromechanical membrane. *Nature* **452**, 72–75 (2008).
13. Teufel, J. D., Harlow, J. W., Regal, C. A. & Lehnert, K. W. Dynamical backaction of microwave fields on a nanomechanical oscillator. *Phys. Rev. Lett.* **101**, 197203 (2008).
14. Wilson-Rae, I., Nooshi, N., Zwerger, W. & Kippenberg, T. J. Theory of ground state cooling of a mechanical oscillator using dynamical backaction. *Phys. Rev. Lett.* **99**, 093901 (2007).
15. Marquardt, F., Chen, J. P., Clerk, A. A. & Girvin, S. M. Quantum theory of cavity-assisted sideband cooling of mechanical motion. *Phys. Rev. Lett.* **99**, 093902 (2007).
16. Genes, C., Vitali, D., Tombesi, P., Gigan, S. & Aspelmeyer, M. Ground-state cooling of a micromechanical oscillator: Comparing cold damping and cavity-assisted cooling schemes. *Phys. Rev. A* **77**, 033804 (2008).
17. Regal, C. A., Teufel, J. D. & Lehnert, K. W. Measuring nanomechanical motion with a microwave cavity interferometer. *Nature Phys.* **4**, 555–560 (2008).
18. Poggio, M. *et al.* An off-board quantum point contact as a sensitive detector of cantilever motion. *Nature Phys.* **4**, 635–638 (2008).
19. Arcizet, O. *et al.* High-sensitivity optical monitoring of a micromechanical resonator with a quantum-limited optomechanical sensor. *Phys. Rev. Lett.* **97**, 133601 (2006).
20. Cole, G. D., Gröblacher, S., Gugler, K., Gigan, S. & Aspelmeyer, M. Monocrystalline AlGaAs heterostructures for high-reflectivity high-*Q* micromechanical resonators in the MHz regime. *Appl. Phys. Lett.* **92**, 261108 (2008).
21. Gröblacher, S., Gigan, S., Böhm, H. R., Zeilinger, A. & Aspelmeyer, M. Radiation-pressure self-cooling of a micromirror in a cryogenic environment. *Eur. Phys. Lett.* **81**, 54003 (2008).
22. Poggio, M., Degen, C. L., Mamin, H. J. & Rugar, D. Feedback cooling of a cantilever's fundamental mode below 5 mK. *Phys. Rev. Lett.* **99**, 017201 (2007).
23. Rempe, G., Thompson, R. J., Kimble, H. J. & Lalezari, R. Measurement of ultralow losses in an optical interferometer. *Opt. Lett.* **17**, 363–365 (1996).
24. Bleszynski-Jayich, A. C., Shanks, W. E. & Harris, J. G. E. Noise thermometry and electron thermometry of a sample-on-cantilever system below 1 K. *Appl. Phys. Lett.* **92**, 013123 (2008).
25. Zwickl, B. M. *et al.* High quality mechanical and optical properties of commercial silicon nitride membranes. *Appl. Phys. Lett.* **92**, 103125 (2008).
26. Wilson Rae, I., Nooshi, N., Dobrindt, J., Kippenberg, T. J. & Zwerger, W. Cavity-assisted backaction cooling of mechanical resonators. *New J. Phys.* **10**, 095007 (2008).
27. Dobrindt, J. M., Wilson-Rae, I. & Kippenberg, T. J. Optomechanical normal-mode splitting. *Phys. Rev. Lett.* **101**, 263602 (2008).
28. Pinard, M., Hadjar, Y. & Heidmann, A. Effective mass in quantum effects of radiation pressure. *Eur. Phys. J. D* **7**, 107–116 (1997).
29. Edward, D., Palik, E. D. & Ghosh, G. (eds) *Handbook of Optical Constants of Solids* (Academic, 1998).

Acknowledgements

We thank R. Lalezari (ATFilms) and M. Metzler, R. Ilic and M. Skvarla (CNF) and F. Blaser, T. Corbitt and W. Lang for discussion and support. We acknowledge support by the Austrian Science Fund FWF (Projects P19539, L426, START), by the European Commission (Projects MINOS, IQOS) and by the Foundational Questions Institute fqxi.org (Grants RFP2-08-03, RFP2-08-27). Part of this work was carried out at the Cornell NanoScale Facility, a member of the National Nanotechnology Infrastructure Network, which is supported by the National Science Foundation (Grant ECS-0335765). S.Gr. is a recipient of a DOC-fellowship of the Austrian Academy of Sciences and G.D.C. of a Marie Curie Fellowship of the European Commission. S.Gr. and M.R.V. are members of the FWF doctoral program Complex Quantum Systems (W1210).

Author contributions

All authors have made a significant contribution to the concept, design, execution or interpretation of the presented work.

Additional information

Supplementary information accompanies this paper on www.nature.com/naturephysics. Reprints and permissions information is available online at http://npg.nature.com/reprintsandpermissions. Correspondence and requests for materials should be addressed to M.A.

© 2009 Macmillan Publishers Limited. All rights reserved.

nature physics

SUPPLEMENTARY INFORMATION

DOI: 10.1038/NPHYS1301

Demonstration of an ultracold micro-optomechanical oscillator in a cryogenic cavity

Simon Gröblacher[1,2], Jared B. Hertzberg[3,4], Michael R. Vanner[1,2], Garrett D. Cole[1], Sylvain Gigan[5], K. C. Schwab[3] & Markus Aspelmeyer[1]

SUPPLEMENTARY INFORMATION

Effective Mass

We have estimated the effective mass of the fundamental mode of our micromechanical structure using both analytic models and FEM analysis. The experimentally observed value of 43 ± 2 ng agrees to within 10% with the estimated value of 53 ± 5 ng.

The total mass of the dielectric Bragg mirror (radius $R \approx 24.5 \pm 0.5\ \mu\text{m}$) made of 36 alternating layers of Ta_2O_5 ($\rho \approx 8200\ \text{kg/m}^3$, $t = 126.4\ \text{nm}$) and SiO_2 ($\rho = 2200\ \text{kg/m}^3$, $t = 179.6\ \text{nm}$) is 45 ± 5 ng, not taking into account the lateral etch and tapering of the mirror pad. The large error stems from the uncertainty in the exact value of the Ta_2O_5 density, which can vary between 6800 and 8300 kg/m^3. The mass of the Si_3N_4 resonator ($\rho = 3000\ \text{kg/m}^3$, approximate dimensions of $100 \times 50 \times 1\ \mu\text{m}^3$) is approx. 11 ng, resulting in a maximum total mass of 56 ± 5 ng for the full optomechanical device.

The mode mass, i.e. the actual mass contributing to the motion of the Si_3N_4 resonator fundamental mode, is approx. 74% of the total mass of the Si_3N_4 resonator (see any standard literature on elasticity theory, for example [S1]). This would result in a total mode mass of the optomechanical resonator (Si_3N_4 beam plus micromirror) of approx. 53 ± 5 ng. However, because of the flat-top mode shape of our actual device (see the FEM simulation shown in

---

[1] Institute for Quantum Optics and Quantum Information (IQOQI), Austrian Academy of Sciences, Boltzmanngasse 3, A-1090 Vienna, Austria

[2] Faculty of Physics, University of Vienna, Boltzmanngasse 5, A-1090 Vienna, Austria

[3] Department of Physics, Cornell University, Ithaca, NY 14853, USA

[4] Department of Physics, University of Maryland, College Park, MD 20742, USA

[5] Laboratoire Photon et Matière, Ecole Superieure de Physique et de Chimie Industrielles,CNRS-UPRA0005, 10 rue Vauquelin, 75005 Paris, France

Figure S1), this value is only a conservative lower bound. A more realistic value that takes into account the actual mode shape can be obtained directly from FEM simulation and is approx. 56 ± 5 ng (see below).

Finally, to calculate the effective mass one has to take into account the mode overlap between the mechanical resonator mode and the mode of the optical probe beam (for a detailed analysis on the calculation of the effective mass see for example [S2]). Based on the experimentally obtained optical finesse, which is limited by intensity losses due to a finite mirror size, we can provide an upper bound on the cavity beam waist at the micromirror position of 8 ± 2 µm. If we assume a mechanical mode shape of an ideal doubly-clamped beam of dimensions $100 \times 50 \times 1\ \mu\text{m}^3$ we would calculate an effective mass (see e.g. [S2,S3]) of 50 ± 5 ng, Again, the actual flat-top mode shape of our device results in a decreased mean square displacement (by approx. 6%) compared to the ideal doubly-clamped beam. Taking this into account yields a final effective mass of 53 ± 5 ng, which agrees to within 10% with the experimentally observed value of 43 ± 2 ng.

The abovementioned FEM simulations make use of the exact geometry and material data for our resonator. The main idea is to impose a force on the structure and have the FEM simulation calculate the deflection. Using Hooke's law one can then extract the spring constant k of the device. The mode mass can be extracted by using $\omega_m = \sqrt{k/m_{\text{mode}}}$. For our specific device the FEM solver provides us with a spring constant of 2196 N/m and a fundamental mode at $\omega_m = 2\pi \times 945$ kHz, which results in $m_{\text{mode}} = 57 \pm 5$ ng.

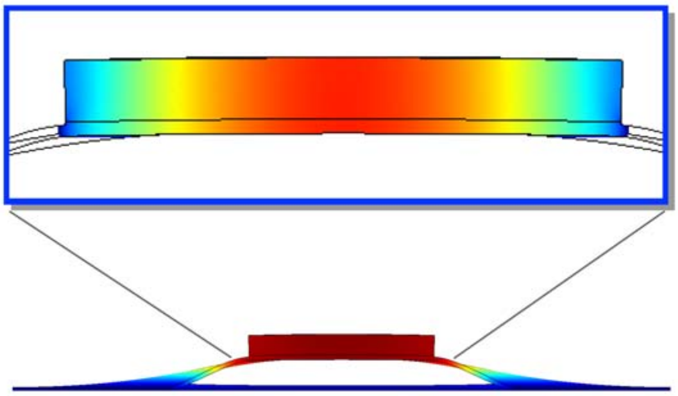

Figure S1: *FEM simulation of our optomechanical device. Shown is the side-view of the fundamental resonance mode at its maximum displacement (below). The cylindrical mirror pad on top of the Si_3N_4 beam induces a flat-top mode shape (inset).*

Error Analysis

The error associated with the noise power spectra peak areas, which provide the mechanical mean square displacement, can be estimated as follows: Assuming that the NPS comprises a sequence of N independent data points (x_i, y_i) (with $i = 1 \ldots N$) with measurement uncertainty $(\delta x_i, \delta y_i)$ one can calculate the area underneath the NPS by Riemann integration as $A = \sum_{i=1}^{N-1} (x_{i+1} - x_i) y_i$ with an uncertainty $\delta A = \sqrt{\sum_{i=1}^{N-1} (x_{i+1} - x_i)^2 (\delta y_i)^2}$, which is obtained by Gaussian error propagation and neglecting the uncertainty in x. The strongly cooled NPS shown in Figure 3a is given by a data set of $N = 5000$ points with $x_{i+1} - x_i = 100$ Hz and with $\delta y_i \approx 1 \times 10^{-34}$ m^2 Hz^{-1} for all i. We obtain $A = 3.780 \times 10^{-28}$ m^2 (by numerically integrating the data set), δA ≈ $\sqrt{N} \times 100$ Hz $\times 1 \times 10^{-34}$ m^2 Hz^{-1} $= 7.1 \times 10^{-31}$ m^2 and an integrated noise floor of $N \times 100$ Hz $\times 7.3 \times 10^{-34}$ m^2 Hz^{-1} $= 3.65 \times 10^{-28}$ m^2. This results in an integrated “real thermal noise” of $(3.78 - 3.65) \times 10^{-28}$ m^2 $= 1.3 \times 10^{-29}$ m^2 with an overall error of approx. $\sqrt{2} \times 7.3 \times 10^{-31}$ m^2 $\approx 1 \times 10^{-30}$ m^2, i.e. with an error of approx. 8%. The SNR of our measurement is therefore sufficient to support our result of $\langle n \rangle = 32$ and accounts for an uncertainty of $\delta \langle n \rangle = \pm 1.5$.

Other possible sources of experimental uncertainty are: an uncertainty related to the absolute displacement amplitude calibration (amounting to approx. 12% relative uncertainty), an uncertainty related to determining the mechanical resonance frequency (known up to an error of approx. 5%) and an uncertainty related to the absolute power calibration of the intracavity optical pump field (known up to an error of approx. 10%). These additional experimental uncertainties add up to an overall error of approx. 25%. All errors are conservatively estimated and finally result in $\langle n \rangle = 32 \pm 4$.

Shot-Noise

The noise floor of our measurement is limited by optical shot-noise. The corresponding displacement noise can be calculated according to [S4] as

$$\delta x_{Shot} = \frac{\lambda}{16F\sqrt{\frac{P\lambda}{hc}}} \cdot \sqrt{1+\left(\frac{\omega_m}{\kappa}\right)^2} \cdot \sqrt{\frac{T+l}{T}} \cdot \sqrt{\frac{P}{P_{MM}}} \; .$$

Our experimental parameters (finesse $F = 3900$, input power $P = 14$ µW, $\lambda = 1064$ nm, $\omega_m = 2\pi \times 945$ kHz, $\kappa = 2\pi \times 770$ kHz, input coupler transmission $T = 900$ ppm, overall intra-cavity losses $l = 620$ ppm, optical input power (corrected for imperfect mode-matching) $P_{MM} = 7$ µW) result in a minimal noise-floor of $\delta x_{Shot} = 6 \times 10^{-18}$ m Hz$^{-0.5}$.

[S1] D. A. Harrington and M. L. Roukes, Caltech Technical Rep. No. CMP-106 (1994).

[S2] M. Pinard, M. Y. Hadjar, and A. Heidmann, Effective mass in quantum effects of radiation pressure, *Eur. Phys. J. D* **7**, 107-116 (1999).

[S3] S. Gigan et al., Self-cooling of a micromirror by radiation pressure, *Nature* **444**, 67-71 (2006).

[S4] T. Briant, Caractérisation du couplage optomécanique entre la lumière et un miroir: bruit thermique et effets quantiques, PhD thesis, l'Université Paris VI (2003).

3 Optomechanical Normal Mode Splitting

An important line of research in quantum optics is the development of the ability to coherently exchange quantum states from one system to another. A prominent application of this research is quantum memory [66] where a a travelling light field, which carries the quantum information to be stored, interacts with a stationary quantum system and coherently transfers its quantum state onto the stationary system for later retrieval. In order for such a transfer to occur, the coherent or reversible dynamics must proceed faster than any of the irreversible dynamics, e.g. damping and decoherence. This parameter regime has been explored in the cavity quantum electrodynamics community [67, 68] for light interacting with atoms inside a cavity and is now of vital importance for the research in that field.

A key step towards meeting this goal in optomechanical systems is to achieve normal mode splitting [69, 70], i.e. a splitting of the mechanical noise power spectrum due to the emergence of hybrid light-mechanical modes brought about by their mutual interaction. This is observable when $g = g_0\alpha > \kappa, \gamma_M$, i.e. the coupling is larger than the optical and mechanical damping rates, and the situation then resembles two coupled masses on springs. When the central spring that couples the two masses is sufficiently stiff the motion of each mass strongly influences the other mass and they will then tend to move either in phase or out of phase – the two normal modes of the system.

As a natural extension to our sideband cooling work, we used the same experimental setup to observe optomechanical normal mode splitting [71]. We implemented some key changes to our setup, however, that allowed us to enter the required parameter regime. Foremost, improvements were made to the cavity that increased the finesse from approximately 4 000, which was used for our sideband cooling work, to 14 000. These challenging improvements were implemented by the excellent work of Simon Gröblacher that reduced the amplitude decay rate from $\kappa/2\pi \simeq 770$ kHz to $\kappa/2\pi \simeq 214$ kHz. My specific contribution in the laboratory remained largely the same as our sideband cooling project. I worked in the lab to align a second homodyne interferometer to measure the stronger cooling beam in addition to the signal beam. (It was realized during our theoretical modeling of the experiment that better performance could be attained by measuring this stronger field.) In addition, I worked together to complete the data analysis and played an active role in understanding the theory of this phenomena and gauging the experimental feasibility in the early stages of planning the experiment.

Following this experiment, which to the best of our knowledge is the first demonstration of optomechanical normal-mode splitting, this parameter regime has been attained for electro-mechanics [72] and has also been attained in an optomechanical system with simultaneous low thermal excitation showing signs of coherent coupling between the light and a mechanical resonator [73].

nature
Vol 460|6 August 2009|doi:10.1038/nature08171

LETTERS

Observation of strong coupling between a micromechanical resonator and an optical cavity field

Simon Gröblacher[1,2], Klemens Hammerer[3,4], Michael R. Vanner[1,2] & Markus Aspelmeyer[1]

Achieving coherent quantum control over massive mechanical resonators is a current research goal. Nano- and micromechanical devices can be coupled to a variety of systems, for example to single electrons by electrostatic[1,2] or magnetic coupling[3,4], and to photons by radiation pressure[5–9] or optical dipole forces[10,11]. So far, all such experiments have operated in a regime of weak coupling, in which reversible energy exchange between the mechanical device and its coupled partner is suppressed by fast decoherence of the individual systems to their local environments. Controlled quantum experiments are in principle not possible in such a regime, but instead require strong coupling. So far, this has been demonstrated only between microscopic quantum systems, such as atoms and photons (in the context of cavity quantum electrodynamics[12]) or solid state qubits and photons[13,14]. Strong coupling is an essential requirement for the preparation of mechanical quantum states, such as squeezed or entangled states[15–18], and also for using mechanical resonators in the context of quantum information processing, for example, as quantum transducers. Here we report the observation of optomechanical normal mode splitting[19,20], which provides unambiguous evidence for strong coupling of cavity photons to a mechanical resonator. This paves the way towards full quantum optical control of nano- and micromechanical devices.

A common feature of all coupled quantum systems is that their dynamics are dominated by the competition between the joint coupling rate and the rates at which the coupled systems decohere into their local environments. Only for sufficiently strong coupling can the effects of decoherence be overcome. This so-called 'strong coupling regime' is, in all cases, indispensable for the experimental investigation of a manifold of quantum phenomena. Nano- and micro-optomechanical oscillators are currently emerging as a new 'textbook' example for coupled quantum systems. In this case, a single electromagnetic field mode is coupled to a (nano- or micrometre sized) mechanical oscillator. In analogy to cavity quantum electrodynamics (cQED), one can identify strong coupling as the regime where the coupling rate g exceeds both the cavity amplitude decay rate κ and the mechanical damping rate γ_m—as required, for example, in refs 15–17. Another class of proposals requires the weaker condition of 'large cooperativity', that is, $g > \sqrt{\kappa\gamma_m}$ (refs 18, 21). Strong coupling, ideally in combination with the preparation of zero entropy initial states (for example, by ground-state cooling of the mechanical resonator), is essential to obtain (quantum) control over this new domain of quantum physics. Whereas ground state preparation is a goal of continuing research (in which much progress has been made, in particular by using optical laser cooling techniques[22]), here we demonstrate strong optomechanical coupling using state-of-the-art micromechanical resonators.

Consider the canonical situation in which a mechanical resonator is coupled to the electromagnetic field of a high-finesse cavity via momentum transfer of the cavity photons (Fig. 1). The system naturally comprises two coupled oscillators: the electromagnetic field at cavity frequency ω_c (typically of the order of 10^{15} Hz) and the mechanical resonator at frequency ω_m ($\sim 10^7$ Hz). At first sight, the large discrepancy in the oscillator frequencies seems to inhibit any coupling; it is, however, alleviated by the fact that the cavity is driven by a laser field at frequency ω_L, which effectively creates an optical oscillator at frequency $\Delta = \omega_c - \omega_L - \delta_{rp}$ (in a reference frame rotating at ω_L; δ_{rp} is the mean shift of the cavity frequency due to radiation pressure). Each of the two oscillators decoheres into its local environment: the optical field at the cavity amplitude decay rate κ and the mechanics at the damping rate γ_m. Entering the desired strong coupling regime requires a coupling rate $g \gtrsim \kappa, \gamma_m$.

The fundamental optomechanical radiation-pressure interaction $H_{int} = -\hbar g_0 n_c X_m$ couples the cavity photon number n_c to the position X_m of the mechanics ($\hbar$ is $h/2\pi$, where h is Planck's constant). On the single-photon level, this interaction provides an intrinsically nonlinear coupling, where the coupling rate $g_0 = \frac{\omega_c}{L}\sqrt{\frac{\hbar}{m\omega_m}}$ (L, cavity length; m, effective mass) describes the effect of a single photon on the optomechanical cavity. In all currently available optomechanical systems, however, g_0 is well below 100 Hz. Because the corresponding cavity decay rates are typically much larger than 10 kHz, the effect is too small to exploit the strong coupling regime on the single-photon level. For our experiment $g_0 = 2\pi \times 2.7$ Hz, which is smaller than both κ ($2\pi \times 215$ kHz) and γ_m ($2\pi \times 140$ Hz). To circumvent this limitation, we use a strong optical driving field ($\lambda = 1{,}064$ nm), which shifts the optomechanical steady state by means of radiation pressure from vacuum to a mean cavity amplitude α (mean cavity photon number $\langle n_c\rangle = \alpha^2$) and from zero displacement to a mean mechanical displacement β. The resulting effective interaction is obtained by standard mean-field expansion, and resembles two harmonic oscillators that are coupled linearly in their optical and mechanical position quadratures $X_c = (a_c + a_c^\dagger)$ and $X_m = (a_m + a_m^\dagger)$, respectively. This strongly driven optomechanical system is then described by equation (1) (see Supplementary Information):

$$H = \frac{\hbar\Delta}{2}\left(X_c^2 + P_c^2\right) + \frac{\hbar\omega_m}{2}\left(X_m^2 + P_m^2\right) - \hbar g X_c X_m \qquad (1)$$

The effective coupling strength $g = g_0\alpha$ is now enhanced by a factor of $\alpha = \sqrt{\langle n_c\rangle}$. Note that this enhancement comes at the cost of losing the nonlinear character of the interaction. Although there exist proposals that do require strong nonlinear coupling at the single-photon level[16], the majority of schemes for quantum optomechanical state manipulation work well within the regime of linear albeit strong coupling. They rely on the fact that linear interactions allow for protocols such as quantum state transfer and readout[23], generation of entanglement[15,17], conditional preparation of states via projective measurements on

---

[1]Institute for Quantum Optics and Quantum Information (IQOQI), Austrian Academy of Sciences, Boltzmanngasse 3, A-1090 Vienna, Austria. [2]Faculty of Physics, University of Vienna, Strudlhofgasse 4, A-1090 Vienna, Austria. [3]Institute for Quantum Optics and Quantum Information (IQOQI), Austrian Academy of Sciences, Technikerstraße 21a, A-6020 Innsbruck, Austria. [4]Institute for Theoretical Physics, University of Innsbruck, Technikerstrasse 25, A-6020 Innsbruck, Austria.

©2009 Macmillan Publishers Limited. All rights reserved

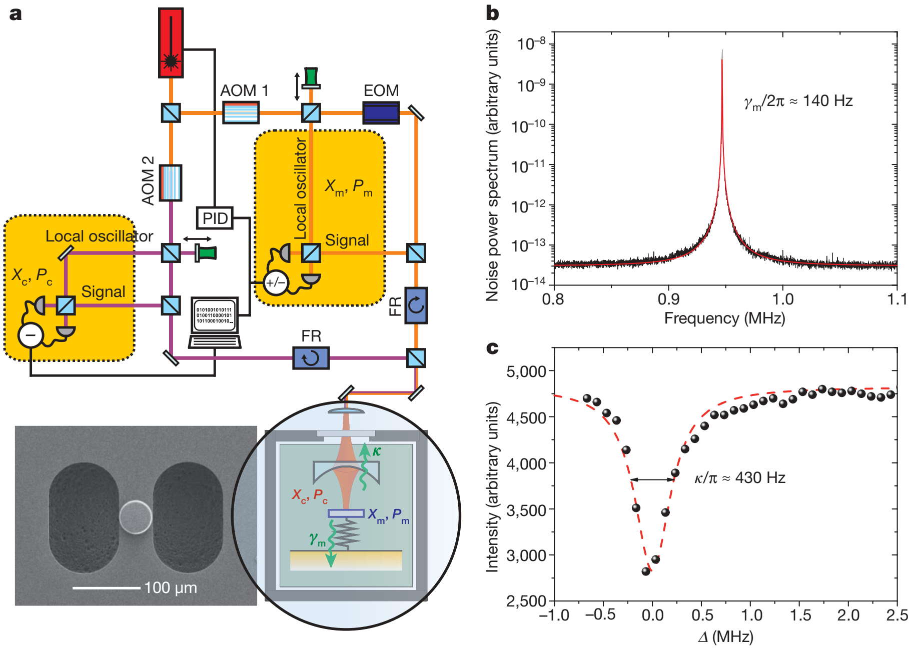

Figure 1 | Experimental set-up and characterization of the uncoupled mechanical and optical oscillator. **a**, Our micromechanical resonator with a high-reflectivity mirror pad ($R > 0.99991$) that forms the end-face of a 25-mm-long Fabry–Pérot cavity (magnified view circled, bottom right). A strong continuous-wave Nd:YAG laser is used to drive the optomechanical system (purple beam). By splitting off a faint part (15 μW) of the drive laser, the laser frequency is actively locked to the Fabry–Pérot cavity frequency (orange beam). Locking is achieved by phase-modulation (electro-optical modulator, EOM) and by obtaining a Pound-Drever-Hall error signal required for feedback with a proportional–integral–derivative controller (PID). Acousto-optical modulators (AOM) control the relative frequency detuning Δ and thus allow for off-resonant driving of the cavity. Data presented here have been taken by varying the detuning Δ and the power of the drive beam. Both beams are coupled to the Fabry–Pérot cavity via the same spatial mode but orthogonal in polarization. The measured cavity linewidth (full-width at half-maximum, FWHM) $2\kappa \approx 2\pi \times 430$ kHz corresponds to an optical finesse $F \approx 14{,}000$. The fundamental mechanical mode of the microresonator at $\omega_m = 2\pi \times 947$ kHz has a natural linewidth (FWHM) of $\gamma_m \approx 2\pi \times 140$ Hz (mechanical quality factor $Q \approx 6{,}700$) at room temperature. With $\kappa/\omega_m \approx 0.2$, these parameters place us well into the resolved sideband regime $\kappa/\omega_m \ll 1$. The effective mass of 145 ng was obtained by direct fitting of the optomechanical response at low driving powers. After interaction with the optomechanical system, both (drive and lock) beams are separated by a polarizing beamsplitter and Faraday rotators (FR) and are each independently measured by optical homodyning (Supplementary Information). Each homodyne phase can be either scanned or locked to a fixed value by actuating a piezo-driven mirror. **b**, Mechanical noise power spectrum obtained by homodyne detection of the lock beam. Red line, fit to the data assuming an ideal harmonic oscillator in thermal equilibrium. **c**, Intensity of the drive beam that is reflected off the Fabry–Pérot cavity when scanning its detuning Δ, which provides direct access to the cavity transfer function. Dashed red line, Lorentzian fit to the data.

light[18,21], and so on, a fact which is well established in the fields of quantum optics and quantum information. In our experiment, by using external optical pump powers of up to 11 mW, we are able to achieve an increase in coupling by more than five orders of magnitude, sufficient to reach the desired strong coupling regime.

An unambiguous signature of strongly coupled systems is the occurrence of normal mode splitting, a phenomenon known to both classical and quantum physics. In the simplest case, two independent harmonic oscillators coupled via an additional joint spring will behave as a pair of uncoupled oscillators—so-called normal modes—with shifted resonance frequencies compared to the individual resonators. For the particular case of resonators with equal bare frequencies, a sufficiently strong coupling will introduce a spectral splitting of the two normal modes that is of the order of the coupling strength g. Normal mode splitting has been observed in a number of realizations of cQED, where it is also known as Rabi-splitting, with photons coupled either to atoms[24,25,26], to excitons in semiconductor structures[27,28,29] or to Cooper pair box qubits in circuit QED[14]. In case of the strongly driven optomechanical system described by equation (1), the normal modes occur at frequencies $\omega_\pm^2 = \frac{1}{2}\left(\Delta^2 + \omega_m^2 \pm \sqrt{(\Delta^2 - \omega_m^2)^2 + 4g^2\omega_m\Delta}\right)$ and exhibit a splitting of $\omega_+ - \omega_- \approx g$. In the given simple expression for normal mode frequencies, cavity decay and mechanical damping are neglected. A more careful analysis is carried out in the Supplementary Information, and shows that normal mode splitting occurs only above a threshold $g \gtrsim \kappa$ (refs 19, 20) for our damped optomechanical system. The Hamiltonian can be re-written in terms of the normal modes and one obtains:

$$H = \frac{\hbar\omega_+}{2}\left(X_+^2 + P_+^2\right) + \frac{\hbar\omega_-}{2}\left(X_-^2 + P_-^2\right) \qquad (2)$$

For the resonant case $\Delta = \omega_m$, equation (2) describes two uncoupled oscillators with position and momentum quadratures $X_\pm = \sqrt{\frac{\omega_m \pm g}{2\omega_m}}(X_c \pm X_m)$ and $P_\pm = \sqrt{\frac{\omega_m}{2(\omega_m \pm g)}}(P_c \pm P_m)$. These new dynamical variables cannot be ascribed to either the cavity field or the mechanical resonator, but are true hybrid optomechanical degrees of freedom. The overall system energy spectrum $E_{m,n}$ is therefore given by the sum of the energies of the two normal modes, that is, $E_{m,n} = \hbar(m\omega_+ + n\omega_-)$. The degeneracy of the uncoupled energy levels is lifted, and normal mode splitting of adjacent levels occurs with a separation that is equivalent to the coupling strength g. In the presence of decoherence, the spectral lines are broadened to a width of $(\kappa + \gamma_m)$ and the splitting can therefore only be resolved for $g \gtrsim \kappa, \gamma_m$, that is, for strong coupling.

We observe normal mode splitting via direct spectroscopy of the optical field emitted by the cavity. Emission of a cavity photon can in general be understood as a transition between dressed states of the optomechanical system, that is, between mechanical states that are dressed by the cavity radiation field. The structure of the optomechanical interaction only allows for transitions that lower or raise the total number of normal mode excitations by one (see Supplementary Information). Photons emitted from the cavity therefore

©2009 Macmillan Publishers Limited. All rights reserved

have to lie at sidebands equal to the dressed state frequencies $\omega_{\pm}$ relative to the incoming laser photons of frequency ω_L, that is, they have to be emitted at sideband frequencies $\omega_L \pm \omega_+$ or $\omega_L \pm \omega_-$. Homodyne detection provides us with direct access to the optical sideband spectrum, which is presented in Fig. 2a for the resonant case $\Delta \approx \omega_m$. For small optical pump power, that is, in the regime of weak coupling, the splitting cannot be resolved and one obtains the well-known situation of resolved sideband laser cooling, in which Stokes and anti-Stokes photons are emitted at one specific sideband frequency. The splitting becomes clearly visible at larger pump powers, which is unambiguous evidence for entering the strong coupling regime. Indeed, at a maximum optical driving power of ~11 mW, we obtain a coupling strength $g = 2\pi \times 325$ kHz, which is larger than both $\kappa = 2\pi \times 215$ kHz and $\gamma_m = 2\pi \times 140$ Hz and which corresponds to the magnitude of the level crossing shown in Fig. 2b. As is expected, for detunings Δ off resonance, the normal mode frequencies approach the values of the uncoupled system.

These characteristics of our strongly driven optomechanical system are reminiscent of a strongly driven two-level atom, and indeed a strong and instructive analogy exists. If an atom is pumped by a strong laser field, optical transitions can only occur between dressed atomic states, that is, atomic states 'dressed' by the interaction with the laser field. For strong driving, any Rabi splitting that is induced by strong coupling is effectively of order $G_0\sqrt{\langle n_L\rangle}$ (n_L, mean number of laser photons; G_0, electric dipole coupling) and one therefore obtains an equally spaced level splitting, fully analogous to the coupled optomechanical spectrum. From this point of view, the optomechanical modes can be interpreted in a dressed state approach as excitations of mechanical states that are dressed by the cavity radiation field. The origin of the sideband doublet as observed in the output field of the strongly driven optomechanical cavity corresponds to the resonance fluorescence spectrum of a strongly driven atom, in which strong coupling gives rise to the two side-peaks in the so-called Mollow triplet. It is interesting to note that the analogy even holds for the single-photon regime, in which both systems are close to their quantum ground state. For both cases (that is, the atom–cavity system and the cavity–optomechanical system), a sufficiently strong single-photon interaction g_0 would allow one to obtain the well-known vacuum Rabi splitting as well as state-dependent level spacing, which is due to intrinsic nonlinearities in the coupling.

We should stress that normal mode splitting alone does not establish a proof for coherent dynamics, that is, for quantum interference effects. With the present experimental parameters, such effects are washed out by thermal decoherence and normal mode splitting has a classical explanation in the framework of linear dispersion theory[30]. Still, the demonstration of normal mode splitting is a necessary condition for future quantum experiments.

We finally comment on the prospects for mechanical quantum state manipulation in the regime of strong coupling. One important additional requirement in most proposed schemes is the initialization of the mechanical device close to its quantum ground state. Recent theoretical results show that both ground state laser cooling and strong coupling can be achieved simultaneously, provided that the conditions $\frac{k_B T}{\hbar Q} \ll \kappa \ll \omega_m$ are fulfilled[20,22]. Thus, in addition to operating in the resolved sideband regime, a thermal decoherence rate that is small compared to the cavity decay rate is required. Cryogenic experiments have demonstrated thermal decoherence rates as low as 20 kHz for nanomechanical resonators for a 20 mK environment temperature[9]. For our experiment, temperatures below 300 mK would be sufficient to combine strong coupling with ground state cooling.

We have demonstrated strong coupling of a micromechanical resonator to an optical cavity field. This regime is a necessary precondition to obtaining quantum control of mechanical systems.

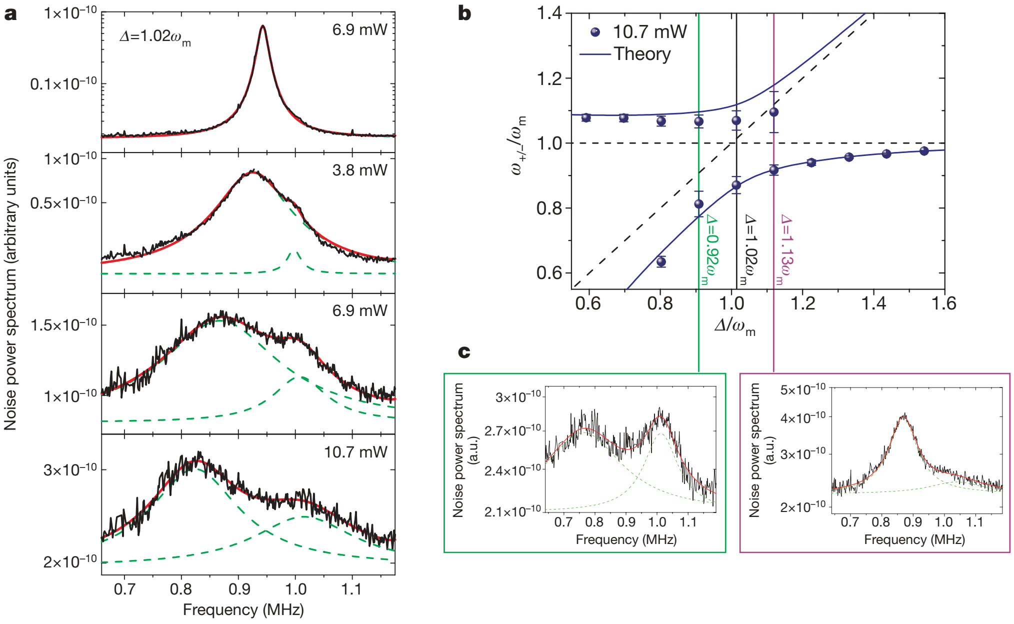

Figure 2 | Optomechanical normal mode splitting and avoided crossing in the normal-mode frequency spectrum. a, Emission spectra of the driven optomechanical cavity, obtained from sideband homodyne detection on the strong driving field after its interaction with the optomechanical system (see Supplementary Information). The power levels from top to bottom (0.6, 3.8, 6.9, 10.7 mW) correspond to an increasing coupling strength of $g = 78$, 192, 260 and 325 kHz ($g = 0.4$, 0.9, 1.2, 1.5 κ). All measurements are performed close to resonance ($\Delta = 1.02\,\omega_m$). For strong driving powers a splitting of the cavity emission occurs, corresponding to the normal mode frequencies of true hybrid optomechanical degrees of freedom. This normal mode splitting is an unambiguous signature of the strong coupling regime. All plots are shown on a logarithmic scale. Green dashed lines are fits to the data assuming two independent Lorentzian curves, red solid lines are the sum signal of these two fits. **b**, Normal mode frequencies obtained from the fits to the spectra as a function of detuning Δ. For far off-resonant driving, the normal modes approach the limiting case of two uncoupled systems. Dashed lines indicate the frequencies of the uncoupled optical (diagonal) and mechanical (horizontal) resonator, respectively. At resonance, normal mode splitting prevents a frequency degeneracy, which results in the shown avoided level crossing. Error bars, s.d. Solid lines are simulations (see Supplementary Information). For larger detuning values, the second normal mode peak could no longer be fitted owing to a nearby torsional mechanical mode. **c**, Normal mode spectra measured off resonance.

©2009 Macmillan Publishers Limited. All rights reserved

Together with the availability of high-quality mechanical resonators operated at low temperatures, which minimizes thermal decoherence of the mechanics, strong optomechanical coupling provides the basis for full photonic quantum control of massive mechanical resonators. We suggest that future developments will eventually also allow strong coupling to be achieved in the nonlinear regime, that is, at the single-photon level[11,16], to exploit optomechanical vacuum Rabi splitting.

Received 4 February; accepted 26 May 2009.

1. Naik, A. *et al.* Cooling a nanomechanical resonator with quantum back-action. *Nature* **443,** 193–196 (2006).
2. Cleland, A. N., Aldridge, J. S., Driscoll, D. C. & Gossard, A. C. Nanomechanical displacement sensing using a quantum point contact. *Appl. Phys. Lett.* **81,** 1699–1701 (2002).
3. Rugar, D., Budakian, R., Mamin, H. J. & Chui, B. W. Single spin detection by magnetic resonance force microscopy. *Nature* **430,** 329–332 (2004).
4. Rabl, P. *et al.* Strong magnetic coupling between an electronic spin qubit and a mechanical resonator. *Phys. Rev. B* **79,** 041302(R) (2009).
5. Kippenberg, T. J., Rokhsari, H., Carmon, T., Scherer, A. & Vahala, K. J. Analysis of radiation-pressure induced mechanical oscillation of an optical microcavity. *Phys. Rev. Lett.* **95,** 033901 (2005).
6. Gigan, S. *et al.* Self-cooling of a micromirror by radiation pressure. *Nature* **444,** 67–71 (2006).
7. Arcizet, O., Cohadon, P.-F., Briant, T., Pinard, M. & Heidmann, A. Radiation-pressure cooling and micromechanical instability of a micromirror. *Nature* **444,** 71–75 (2006).
8. Thompson, J. D. *et al.* Strong dispersive coupling of a high-finesse cavity to a micromechanical membrane. *Nature* **452,** 72–75 (2008).
9. Regal, C. A., Teufel, J. D. & Lehnert, K. W. Measuring nanomechanical motion with a microwave cavity interferometer. *Nature Phys.* **4,** 555–560 (2008).
10. Eichenfield, M., Michael, C. P., Perahia, R. & Painter, O. Actuation of micro-optomechanical systems via cavity-enhanced optical dipole forces. *Nature Photon.* **1,** 416–422 (2007).
11. Li, M. *et al.* Harnessing optical forces in integrated photonic circuits. *Nature* **456,** 480–484 (2008).
12. Walther, H., Varcoe, B. T. H., Englert, B.-G. & Becker, T. Cavity quantum electrodynamics. *Rep. Prog. Phys.* **69,** 1325–1382 (2006).
13. Khitrova, G., Gibbs, H. M., Kira, M., Koch, S. W. & Scherer, A. Vacuum Rabi splitting in semiconductors. *Nature Phys.* **2,** 81–90 (2006).
14. Wallraff, A. *et al.* Strong coupling of a single photon to a superconducting qubit using circuit quantum electrodynamics. *Nature* **431,** 162–167 (2004).
15. Bose, S., Jacobs, K. & Knight, P. L. Preparation of nonclassical states in cavities with a moving mirror. *Phys. Rev. A* **56,** 4175–4186 (1997).
16. Marshall, W., Simon, C., Penrose, R. & Bouwmeester, D. Towards quantum superpositions of a mirror. *Phys. Rev. Lett.* **91,** 130401 (2003).
17. Vitali, D. *et al.* Optomechanical entanglement between a movable mirror and a cavity field. *Phys. Rev. Lett.* **98,** 030405 (2007).
18. Clerk, A. A., Marquardt, F. & Jacobs, K. Back-action evasion and squeezing of a mechanical resonator using a cavity detector. *N. J. Phys.* **10,** 095010 (2008).
19. Marquardt, F., Chen, J. P., Clerk, A. A. & Girvin, S. M. Quantum theory of cavity-assisted sideband cooling of mechanical motion. *Phys. Rev. Lett.* **99,** 093902 (2007).
20. Dobrindt, J. M., Wilson-Rae, I. & Kippenberg, T. J. Parametric normal-mode splitting in cavity optomechanics. *Phys. Rev. Lett.* **101,** 263602 (2008).
21. Hammerer, K., Aspelmeyer, M., Polzik, E. & Zoller, P. Establishing Einstein-Podolsky-Rosen channels between nanomechanics and atomic ensembles. *Phys. Rev. Lett.* **102,** 020501 (2009).
22. Wilson Rae, I., Nooshi, N., Dobrindt, J., Kippenberg, T. J. & Zwerger, W. Cavity-assisted backaction cooling of mechanical resonators. *N. J. Phys.* **10,** 095007 (2008).
23. Zhang, J., Peng, K. & Braunstein, S. L. Quantum-state transfer from light to macroscopic oscillators. *Phys. Rev. A* **68,** 013808 (2003).
24. Thompson, R. J., Rempe, G. & Kimble, H. J. Observation of normal-mode splitting for an atom in an optical cavity. *Phys. Rev. Lett.* **68,** 1132–1135 (1992).
25. Colombe, Y. *et al.* Strong atom–field coupling for Bose–Einstein condensates in an optical cavity on a chip. *Nature* **450,** 272–276 (2007).
26. Aoki, T. *et al.* Observation of strong coupling between one atom and a monolithic microresonator. *Nature* **443,** 671–674 (2006).
27. Reithmaier, J. P. *et al.* Strong coupling in a single quantum dot–semiconductor microcavity system. *Nature* **432,** 197–200 (2004).
28. Weisbuch, C., Nishioka, M., Ishikawa, A. & Arakawa, Y. Observation of the coupled exciton-photon mode splitting in a semiconductor quantum microcavity. *Phys. Rev. Lett.* **69,** 3314–3317 (1992).
29. Yoshie, T. *et al.* Vacuum Rabi splitting with a single quantum dot in a photonic crystal nanocavity. *Nature* **432,** 200–203 (2004).
30. Zhu, Y. *et al.* Vacuum Rabi splitting as a feature of linear-dispersion theory: analysis and experimental observations. *Phys. Rev. Lett.* **64,** 2499–2502 (1990).

Supplementary Information is linked to the online version of the paper at www.nature.com/nature.

Acknowledgements We are grateful to T. Corbitt, C. Genes, S. Goßler, P. K. Lam, G. Milburn, P. Rabl and P. Zoller for discussions. We also thank M. Metzler, R. Ilic and M. Skvarla (CNF), and K. C. Schwab and J. Hertzberg, for microfabrication support, and R. Blach for technical support. We acknowledge financial support from the Austrian Science Fund FWF, the European Commission and the Foundational Questions Institute. S.G. is a recipient of a DOC fellowship of the Austrian Academy of Sciences; S.G. and M.R.V. are members of the FWF doctoral programme Complex Quantum Systems (CoQuS).

Author Contributions All authors have made a significant contribution to the concept, design, execution or interpretation of the presented work.

Author Information Reprints and permissions information is available at www.nature.com/reprints. Correspondence and requests for materials should be addressed to M.A. (markus.aspelmeyer@quantum.at).

©2009 Macmillan Publishers Limited. All rights reserved

I. NORMAL MODE FREQUENCIES AND DAMPING RATES

As shown in [1–3] the linearized Hamiltonian for a driven cavity mode coupled via radiation pressure to a harmonically bound mirror is

$$H = \frac{\hbar\Delta}{2}(X_c^2 + P_c^2) + \frac{\hbar\omega_m}{2}(X_m^2 + P_m^2) - \hbar g X_c X_m \tag{S1}$$

with an opto-mechanical coupling rate $g = g_0\alpha = \frac{2}{L}\sqrt{\frac{P\kappa\omega_c}{m\omega_m(\kappa^2+\Delta^2)}}$ (following [3]) for an input power P of the driving laser (L, ω_c and κ are cavity length, resonance and amplitude decay rate respectively, m the effective mass of the mechanical oscillator). For a two-sided cavity with decay rate κ through the input-coupler and $\bar{\kappa}$ through the oscillating mirror, this formula generalizes to $g = \frac{2}{L}\sqrt{\frac{P\kappa\omega_c}{m\omega_m((\kappa+\bar{\kappa})^2+\Delta^2)}}$.

It is convenient to define $\vec{R}^T = (X_c, P_c, X_m, P_m)$ and express the Hamiltonian as $H = \frac{\hbar}{2}\vec{R}^T M \vec{R}$ where

$$M = \begin{pmatrix} \Delta & 0 & g & 0 \\ 0 & \Delta & 0 & 0 \\ g & 0 & \omega_m & 0 \\ 0 & 0 & 0 & \omega_m \end{pmatrix}.$$

The transformation to normal modes $\vec{R}^{\mathrm{NM}} = (X_+, P_+, X_-, P_-)$ is achieved with a linear transformation $\vec{R}^{\mathrm{NM}} = S\vec{R}$, where S fulfills $M = S^T \mathrm{diag}(\omega_+, \omega_+, \omega_-, \omega_-) S$ and is symplectic, i.e. it obeys $J = SJS^T$ where

$$J = \begin{pmatrix} 0 & 1 & 0 & 0 \\ -1 & 0 & 0 & 0 \\ 0 & 0 & 0 & 1 \\ 0 & 0 & -1 & 0 \end{pmatrix}.$$

The latter property guarantees that canonical commutation relations are conserved, i.e. $[\vec{R}_i, \vec{R}_j] = [\vec{R}_i^{\mathrm{NM}}, \vec{R}_j^{\mathrm{NM}}] = iJ_{ij}$. The explicit form of S can in principle be determined, but is quite involved and does not give much insight. As will become clear in a moment, the normal mode frequencies $\omega_\pm$ can be easily calculated without constructing S and are given by

$$\omega_\pm^2 = \frac{1}{2}\left(\Delta^2 + \omega_m^2 \pm \sqrt{(\Delta^2 - \omega_m^2)^2 + 4g^2\omega_m\Delta}\right). \tag{S2}$$

The canonical operators evolve according to

$$\begin{aligned} \dot{\vec{R}}(t) &= i[H, \vec{R}(t)] - D\vec{R}(t) - \sqrt{2D}\vec{R}_{\mathrm{in}}(t) \\ &= (JM - D)\vec{R}(t) - \sqrt{2D}\vec{R}_{\mathrm{in}}(t), \end{aligned} \tag{S3}$$

where we included damping of the cavity field and the mechanical resonator with $D = \mathrm{diag}(\kappa, \kappa, \gamma_m^0, \gamma_m^0)$ and Langevin forces $\vec{R}_{\mathrm{in}}(t) = (x_{\mathrm{in}}, p_{\mathrm{in}}, f_{X_m}, f_{P_m})$. For white vacuum noise input to the cavity and a thermal white noise bath coupling to the mechanical system, all first moments vanish $\langle\vec{R}(t)\rangle \equiv 0$ and the only non-zero two time correlation functions are

$$\begin{aligned} \langle x_{\mathrm{in}}(t)x_{\mathrm{in}}(t')\rangle &= \langle p_{\mathrm{in}}(t)p_{\mathrm{in}}(t')\rangle = \frac{1}{2}\delta(t-t'), \\ \langle f_{X_m}(t)f_{X_m}(t')\rangle &= \langle f_{P_m}(t)f_{P_m}(t')\rangle = \left(\bar{n} + \frac{1}{2}\right)\delta(t-t'), \end{aligned} \tag{S4}$$

where $\bar{n} \simeq \frac{kT}{\hbar\omega_m}$.

From Eq. (S3) it is clear that eigenfrequencies and effective damping rates of the system are given by, respectively, the imaginary and real parts of the eigenvalues of $i(JM - D)$. The eigenvalues occur in complex conjugate pairs and the imaginary parts of the ones in the upper half plane determine eigenfrequencies. For the undamped system, $D = 0$, the eigenvalues are purely complex and one arrives at expression (S2) for the normal mode frequencies. For the damped system, $D \neq 0$, the eigenvalues of $i(JM - D)$ will in general be complex and thus determine normal mode frequencies $\omega_\pm$ and effective damping rates $\gamma_\pm$ of normal modes, as exemplified in Fig. S1. The theoretical values of the normal mode frequencies $\omega_\pm$ in Fig. 2a of the main text were as well determined in this way. While normal mode splitting (NMS) occurs for any non-zero coupling g in an undamped system, a threshold of $g \gtrsim \kappa$ has to be surpassed to observe NMS [2, 4]. Effective damping rates behave complementary and merge above the same threshold. Comparison of the normal mode damping rates $\gamma_\pm$ to the effective mechanical damping rate $\gamma_m = \gamma_m^0 + \frac{2g^2\kappa\Delta\omega_m}{[\kappa^2+(\Delta-\omega_m)^2][\kappa^2+(\Delta+\omega_m)^2]}$, as derived in the theory for cavity-assisted cooling [1, 3], shows that the condition for resolving the normal mode peaks is $g \gg \kappa, \gamma_m$.

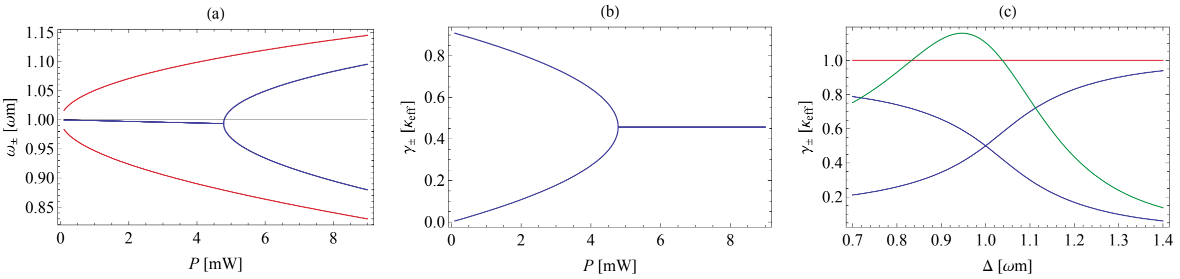

FIG. S1: (a) Normal mode frequencies $\omega_\pm$ for undamped system (red) and damped system (blue) for varying power of driving laser. (b) Same for effective normal mode damping $\gamma_\pm$. (c) Effective damping rates of normal modes (blue), cavity amplitude decay rate κ (red) and effective mechanical decay rate γ_m (green) for varying detuning. Not shown is the natural mechanical damping rate as $\gamma_m^0/\kappa \simeq 10^{-3}$. Parameters are as in the main text, $\omega_m = 2\pi \times 947$ kHz, $\gamma_m^0 = 2\pi \times 140$ Hz, $m = 145$ ng, $L = 2.5$ cm, $\omega_c = 1.77 \times 10^{15}$ Hz, $\kappa = 2\pi \times 172$ kHz and $\bar{\kappa} = 2\pi \times 43$ kHz. In (a) and (b) $\Delta = \omega_m$ and in (c) $P = 10.7$ mW.

II. CAVITY EMISSION SPECTRUM

A. Dressed States and Exact Diagonalization

In terms of normal mode operators the linearized Hamiltonian (S1) is given by $H = \frac{\hbar\omega_+}{2}(X_+^2 + P_+^2) + \frac{\hbar\omega_-}{2}(X_-^2 + P_-^2)$. It can be expressed also in terms of creation and annihilation operators $a_\pm = (X_\pm + iP_\pm)/\sqrt{2}$ as $H = \hbar\omega_+\left(a_+^\dagger a_+ + \frac{1}{2}\right) + \hbar\omega_-\left(a_-^\dagger a_- + \frac{1}{2}\right)$. The Eigenstates and -energies are thus $H|n,m\rangle = E_{n,m}|n,m\rangle$, where

$$|n,m\rangle = \frac{1}{\sqrt{n!m!}}(a_+^\dagger)^n(a_-^\dagger)^m|0,0\rangle,$$
$$E_{n,m} = \hbar\omega_+(n+\frac{1}{2}) + \hbar\omega_-(m+\frac{1}{2}).$$

Emission of a cavity photon is in general accompanied by a transition of the opto-mechanical system from one eigenstate to another by changing a single excitation, $|n,m\rangle \leftrightarrow |n-1,m\rangle$ and $|n,m\rangle \leftrightarrow |n,m-1\rangle$. The energy splitting between these states is $E_{n,m} - E_{n-1,m} = \hbar\omega_+$ and $E_{n,m} - E_{n,m-1} = \hbar\omega_-$ respectively. Photons emitted from the cavity have to carry away this energy excess/deficiency relative to the incoming laser photons of frequency ω_L, i.e. they have to have frequencies $\omega_L \pm \omega_+$ or $\omega_L \pm \omega_-$. Transitions between the dressed opto-mechanical states and the associated emission dublett is illustrated in Fig. S2.

In order to compare the low-energy part of the opto-mechanical spectrum to the one of the Jaynes Cummings system, as shown in Fig. 2 of the main text, we give here the exact eigenstates and -values of the non-linear radiation pressure Hamiltonian

$$H = \hbar\omega_m a_m^\dagger a_m + \hbar\Delta a_c^\dagger a_c - \hbar g_0 a_m^\dagger a_m(a_c + a_c^\dagger).$$

It is straight forward to check that $H|\psi_{k,n}\rangle = E_{k,n}|\psi_{k,n}\rangle$ with

$$|\psi_{k,n}\rangle = \exp\left[\frac{g_0 n}{\omega_m}(a_m - a_m^\dagger)\right]|k\rangle_m|n\rangle_c,$$
$$E_{k,n} = \hbar\left(\omega_m k + \Delta n + \frac{g_0^2}{\omega_m}n^2\right).$$

That is, the eigenstates are shifted Fock states of the uncoupled system and the energy spectrum is anharmonic with a *quadratic* dependence in the photon number. The "opto-mechanical Rabbi splitting" is thus $\frac{g_0^2}{\omega_m}$, see also Fig. S2.

B. Emission Power Spectrum

The power spectral density of light emitted by the cavity is explicitly determined as follows: In frequency space $[\vec{R}(\omega) = \int d\omega \vec{R}(t)\exp(i\omega t)/\sqrt{2\pi}]$ the steady state solutions to the equations of motion (S3) are

$$\vec{R}(\omega) = \frac{1}{i\omega + JM - D}\sqrt{2D}\vec{R}_{\rm in}(\omega). \qquad \text{(S5)}$$

With the quantum optical cavity input-output relations it follows that

$$\vec{R}_{\rm out}(\omega) = \sqrt{2D}\vec{R}(\omega) + \vec{R}_{\rm in}(\omega)$$
$$= \left(\sqrt{2D}\frac{1}{i\omega + JM - D}\sqrt{2D} + 1\right)\vec{R}_{\rm in}(\omega),$$

where $\vec{R}_{\rm out}(\omega) = (x_{\rm out}, p_{\rm out}, f_{X_m,{\rm out}}, f_{P_m,{\rm out}})$. $(x_{\rm out}, p_{\rm out})$ are quadratures for the cavity output field which are subject to homodyne detection. In order to calculate their stationary properties we formally introduce also "phononic output fields" $f_{X_m,{\rm out}}, f_{P_m,{\rm out}})$. The spectral correlation functions can be collected in a Hermitean spectral 4 × 4 correlation matrix $\gamma_{ij}^{\rm out}(\omega,\omega') = \langle(\vec{R}_{\rm out}(\omega'))_i(\vec{R}_{\rm out}(\omega))_j\rangle$. Straight forward

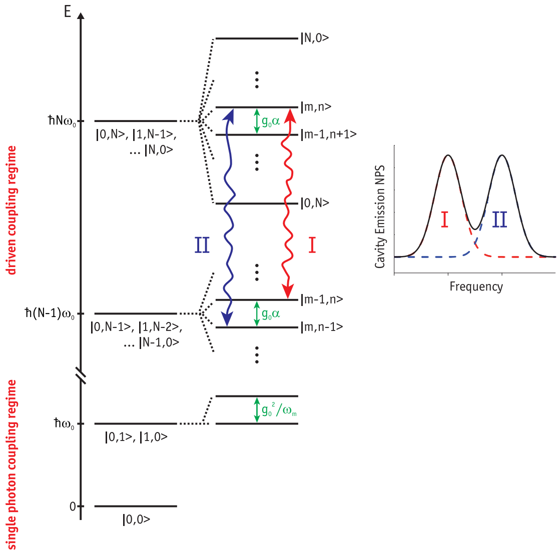

FIG. S2: Energy spectrum of a driven opto-mechanical cavity. For a degenerate, uncoupled system (left), $\omega_m = \Delta$, $g_0 = 0$, the spectrum consists of equidistant multipletts of energy $\hbar N \omega_m$ and degeneracy N ($\hbar$: Planck's constant; N: number of excitations; ω_m: mechanical resonance frequency). For a coupled system (right), $g_0 \neq 0$, the degeneracy is broken. In the strongly driven regime, where the cavity is in a coherent state with mean number of photons $\langle n_c \rangle$, the levels in each N-multiplett split up by $g = g_0\sqrt{\langle n_c \rangle}$ into dressed states $|m,n\rangle$ with $m + n = N$. Emission of a cavity photon is accompanied only by transitions $|m,n\rangle \leftrightarrow |m-1,n\rangle$ or $|m,n\rangle \leftrightarrow |m,n-1\rangle$ between dressed states. Accordingly, emitted photons have to lie at sideband-frequencies $\omega_L + \omega_\pm$. This gives rise to a doublet structure in the sideband spectrum (bottom) with a splitting $\omega_+ - \omega_- \approx g$. The observed normal-mode splitting is shown in Figure 2 of the main text. In the single photon coupling regime, the fundamentally anharmonic nature of the spectrum becomes important, with a splitting between dressed states scaling like $\frac{g_0^2 n_c^2}{\omega_m}$ (shown is the "opto-mechanical vacuum Rabi-splitting" for $n_c = 1$). In the present experiment we cannot access this nonlinear regime, which would require a large single photon coupling $g_0 \gg \kappa, \gamma_m$.

calculation yields $\gamma^{\mathrm{out}}(\omega,\omega') = \delta(\omega+\omega')\Gamma(\omega)$ where

$$\Gamma(\omega) = \left(\sqrt{2D}\frac{1}{i\omega + JM - D}\sqrt{2D} + 1\right) N \times \left(\sqrt{2D}\frac{1}{-i\omega + JM - D}\sqrt{2D} + 1\right)^T$$

and $N = \mathrm{diag}\left(\frac{1}{2}, \frac{1}{2}, \bar{n}+\frac{1}{2}, \bar{n}+\frac{1}{2}\right)$. If losses through the second mirror with amplitude decay rate $\bar{\kappa}$ are taken into account, the last expression generalizes to

$$\begin{aligned}\Gamma(\omega) = &\left(\sqrt{2D}\frac{1}{i\omega + JM - D - \bar{D}}\sqrt{2D} + 1\right) N \\ &\times \left(\sqrt{2D}\frac{1}{-i\omega + JM - D - \bar{D}}\sqrt{2D} + 1\right)^T \\ &+ \left(\sqrt{2D}\frac{1}{i\omega + JM - D - \bar{D}}\sqrt{2\bar{D}}\right) \bar{N} \\ &\times \left(\sqrt{2\bar{D}}\frac{1}{-i\omega + JM - D - \bar{D}}\sqrt{2D}\right)^T, \qquad \text{(S6)}\end{aligned}$$

where $\bar{D} = \mathrm{diag}(\bar{\kappa}, \bar{\kappa}, 0, 0)$ and $\bar{N} = \mathrm{diag}(\frac{1}{2}, \frac{1}{2}, 0, 0)$.

Finally, the spectral density $S(\omega)$ is defined as $S(\omega)\delta(\omega+\omega') = \langle a^\dagger_{\mathrm{out}}(\omega') a_{\mathrm{out}}(\omega)\rangle$ where the amplitude operator for the cavity output field is $a_{\mathrm{out}}(\omega) = (x_{\mathrm{out}}(\omega) + i p_{\mathrm{out}}(\omega))\sqrt{2}$. It follows from the definition of the spectral correlation matrix given above that

$$S(\omega) = \frac{1}{2}\left[\Gamma_{11}(\omega) + \Gamma_{22}(\omega) + i(\Gamma_{12}(\omega) - \Gamma_{21}(\omega))\right].$$

This expression gives the spectral density of sideband modes at a frequency $\omega_L + \omega$. In homodyne detection of sideband modes we do not distinguish sideband frequencies $\omega_L \pm \omega$ and extract only the overall noise power spectrum at a sideband frequency $|\omega|$, which is given by $S_{NPS}(\omega) = \sqrt{S(\omega)^2 + S(-\omega)^2}$ and shown in Fig. S3. The simple consideration in terms of dressed state transitions as given above shows good agreement with the exact calculated positions of spectral peaks, which are in turn in excellent agreement with measured data presented already in Fig. 2b of the main text.

III. HOMODYNE DETECTION OF OPTICAL AND MECHANICAL QUADRATURES

We obtain the generalized optical and mechanical quadratures X_c and X_m via two independent, simultaneous optical homodyne measurements. Homodyne detection requires the mixing of a strong local oscillator field with the signal beam at a symmetric beamsplitter and a balanced photodetection at the beamsplitter output ports. The difference photocurrent then provides a direct measure of the generalized quadrature $X(\phi,t) = a(t)e^{i\phi} + a^\dagger(t)e^{-i\phi}$ of an optical beam (ϕ: local oscillator phase), where $X(\phi=0,t)$ and $X(\phi=\frac{\pi}{2},t)$ are the well-known amplitude and phase quadratures, respectively. To measure X_c, homodyning was performed on the driving beam after its interaction with the cavity. The second homodyning measures the locking beam after its resonant interaction with the cavity. Because of the weak interaction (we choose the power of the lock beam such that $g \ll \kappa$) the cavity field phase quadrature adiabatically follows the evolution of the mechanics and hence provides direct access to X_m. The local oscillator phase in the homodyne measurement of the locking

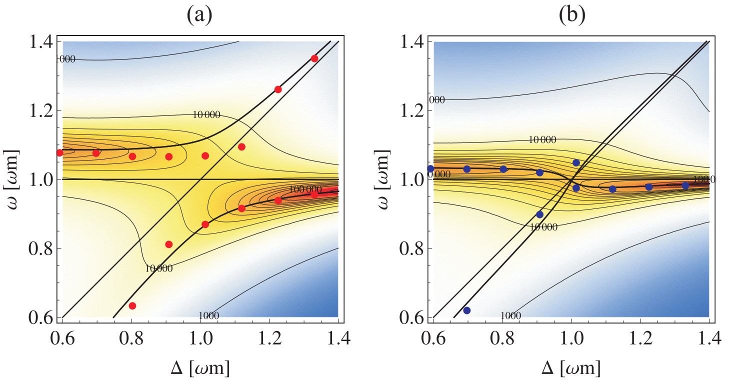

FIG. S3: (a) Emission spectrum $S_{NPS}(\omega)$ of opto-mechanical system for varying detuning (colors refer to a logarithmic scale of arbitrary units). Peak positions are well described by the normal mode eigenfrequencies $\omega_{\pm}$ (black lines). For comparison we reproduce also the measured data of presented in Fig. 3b of the main text. Parameters are as in S1, the input input power was $P = 10.7$ mW. Expression (S6) was used to evaluate the spectrum with a cavity decay rate through the input-coupler $\kappa = 2\pi \times 172$ kHz and at rate $\bar{\kappa} = 2\pi \times 43$ kHz through the oscillating mirror. (b) Same for a power value $P = 3.8$ mW just below threshold for normal mode splitting, cf. Fig. S1a.

field was always actively stabilized to detect the locking beam phase quadrature. Each of the two difference photocurrents was recorded independently by a high-speed analogue-to-digital converter (14 bit, 10 MSample sec^{-1}). The mechanical and optical noise power spectra from Figures 1b and 2a, respectively, were directly inferred from these recorded time traces. In that case, the local oscillator phase of the drive field was locked to a fixed value.

---

[1] I. Wilson-Rae, N. Nooshi, W. Zwerger, T. J. Kippenberg, Phys. Rev. Lett. **99**, 093901 (2007)
[2] F. Marquardt, J. P. Chen, A. A. Clerk, S. M. Girvin, Phys. Rev. Lett. **99**, 093902 (2007)
[3] C. Genes, D. Vitali, P. Tombesi, S. Gigan, M. Aspelmeyer, Phys. Rev. A **77**, 033804 (2008)
[4] J. M. Dobrindt, I. Wilson-Rae, T. J. Kippenberg, Phys. Rev. Lett. **101**, 263602 (2008)
[5] *Gradshteyn and Ryzhik's Table of Integrals, Series, and Products*, Alan Jeffrey and Daniel Zwillinger (eds.), Seventh edition, Academic Press (2007)
[6] V. Giovannetti, D. Vitali, Phys. Rev. A **63**, 023812 (2001)
[7] C.W. Gardiner, P. Zoller, *Quantum Noise*, Springer Series in Synergetics (2004)

4 Geometry Dependent Mechanical Clamping Losses

In both optomechanics experiments and applications employing mechanical oscillators the mechanical quality factor Q is often a primary performance limitation. For instance, fundamental physics experiments that aim to explore non-classical properties of mechanical motion must minimize decoherence by sufficiently isolating the mechanical oscillator from the surrounding environment. This requires $\bar{n}/Q \ll 1$, where $\bar{n}$ is the thermal occupation of the oscillator when in thermal equilibrium, and thus higher quality factors are desired. As a second prominent example, the sensitivity of mechanical oscillator based force sensors improves with an increasing mechanical quality factor. Because of this there is currently a significant amount of physics and engineering based research spent on improving the quality factor of mechanical resonators.

The mechanical quality factor in any given implementation is determined by a number of physical mechanisms, e.g. material losses, thermoelastic damping, and viscous damping from any surrounding gas or fluid. Each of these mechanisms will independently increase the damping rate and hence the overall quality factor is determined via

$$\frac{1}{Q} = \frac{1}{Q_1} + \frac{1}{Q_2} + \frac{1}{Q_3} + \ldots\ , \tag{4.1}$$

where the subscripts label each damping mechanism.

In this work [74] we experimentally studied mechanical clamping losses [75], otherwise known as phonon tunneling, where damping occurs due to the mechanical resonator coupling to the surrounding support or substrate. This damping mechanism is strongly dependent on the shape of the mechanical resonator that determines the profile of each particular mechanical flexural mode. Because of this geometry dependence careful design and fabrication can thus minimize this deleterious damping mechanism. To this end, we studied the change in mechanical Q for a controlled change in its geometry and developed a numerical solver to estimate the clamping loss contribution for a given geometry. My specific contribution to this project was to design and build a fiber based optical setup to probe the mechanical motion. The fiber based interferometer proved to have excellent phase stability and mechanical position sensitivity that the design developed for this work was used again, with modifications, to implement the pulsed optomechanics experiment discussed in chapter 7.

nature COMMUNICATIONS

OPEN

ARTICLE

Received 6 Aug 2010 | Accepted 26 Jan 2011 | Published 8 Mar 2011

DOI: 10.1038/ncomms1212

Phonon-tunnelling dissipation in mechanical resonators

Garrett D. Cole[1,*], Ignacio Wilson-Rae[2,*], Katharina Werbach[1], Michael R. Vanner[1] & Markus Aspelmeyer[1]

Microscale and nanoscale mechanical resonators have recently emerged as ubiquitous devices for use in advanced technological applications, for example, in mobile communications and inertial sensors, and as novel tools for fundamental scientific endeavours. Their performance is in many cases limited by the deleterious effects of mechanical damping. In this study, we report a significant advancement towards understanding and controlling support-induced losses in generic mechanical resonators. We begin by introducing an efficient numerical solver, based on the 'phonon-tunnelling' approach, capable of predicting the design-limited damping of high-quality mechanical resonators. Further, through careful device engineering, we isolate support-induced losses and perform a rigorous experimental test of the strong geometric dependence of this loss mechanism. Our results are in excellent agreement with the theory, demonstrating the predictive power of our approach. In combination with recent progress on complementary dissipation mechanisms, our phonon-tunnelling solver represents a major step towards accurate prediction of the mechanical quality factor.

---

[1] Vienna Center for Quantum Science and Technology (VCQ), Faculty of Physics, University of Vienna, Boltzmanngasse 5, Vienna A-1090, Austria.
[2] Technische Universität München, Garching 85748, Germany. *These authors contributed equally to this work. Correspondence and requests for materials should be addressed to G.D.C. (email: garrett.cole@univie.ac.at) and to I.W.R. (email: ignacio.wilson-rae@ph.tum.de).

© 2011 Macmillan Publishers Limited. All rights reserved.

Mechanical coupling of a suspended structure to its supports is a fundamental energy loss mechanism in micromechanical and nanomechanical resonators[1]. Referred to variously as clamping[2] or anchor loss[3], this process remains significant even in devices fabricated from high-quality materials operated in vacuum and at cryogenic temperatures, and is in fact unavoidable in any non-levitating system. Although much progress has been made towards the understanding of mechanical dissipation at the microscale and nanoscale[2,4], obtaining reliable predictions for the fundamental design-limited quality factor, Q, remains a major challenge while direct experimental tests are scarce[5–7]. At the same time, the implementation of high-quality micromechanical and nanomechanical systems is becoming increasingly important for numerous advanced technological applications in sensing and metrology, with select examples including wireless filters[3,8], on-chip clocks[9], microscopy[10–13] and molecular-scale mass sensing[14,15], and recently for a new generation of macroscopic quantum experiments that involve mesoscopic mechanical structures[16–23]. Here, we introduce a finite-element-enabled numerical solver for calculating the support-induced losses of a broad range of low-loss mechanical resonators. We demonstrate the efficacy of this approach via comparison with experimental results from microfabricated devices engineered to isolate support-induced losses by allowing for a significant variation in geometry, while keeping other resonator characteristics approximately constant. The efficiency of our solver results from the use of a perturbative scheme that exploits the smallness of the contact area, specifically the recently introduced 'phonon-tunnelling' approach[24]. This results in a significant simplification over previous approaches and paves the way for CAD-based predictive design of low-loss mechanical resonators.

The origins of mechanical damping in microscale and nanoscale systems have been the subject of numerous studies during the last decades, and several relevant mechanisms for the decay of acoustic mechanical excitations, that is, phonons, have been investigated[2,4]. These include: (i) fundamental anharmonic effects such as phonon–phonon interactions[4,25], thermoelastic damping (TED)[4,25–28] and the Akhiezer effect[4,25]; (ii) viscous or fluidic damping involving interactions with the surrounding atmosphere or the compression of thin fluidic layers[29–31]; (iii) material losses driven by the relaxation of intrinsic or extrinsic defects in the bulk or surface of the resonator[32–37] for which the most commonly studied model is an environment of two-level fluctuators[38,39] and (iv) support-induced losses, that is, the dissipation induced by the unavoidable coupling of the resonator to the substrate[3,7,8,40,41], which corresponds to the radiation of elastic waves into the supports[5,6,24,42–44]. This last mechanism poses a fundamental limit, as vibrations of the substrate will always be present.

These various dissipation processes add incoherently such that the reciprocals of the corresponding Q-values satisfy $1/Q_{\mathrm{tot}} = \Sigma_i 1/Q_i$, where i labels the different mechanisms. Thus, in a realistic setting, care must be taken to isolate the contribution under scrutiny. In contrast to all other damping mechanisms (i–iii), which exhibit various dependencies with external physical variables such as pressure and temperature, support-induced dissipation is a temperature- and scale-independent phenomenon with a strong geometric character that is present in any suspended structure. Moreover, its scale independence implies that the same analysis can be applied to both microscale and nanoscale devices. We exploit this geometric character to isolate the support-induced contribution and obtain a direct experimental test of phonon-tunnelling dissipation.

The numerical solver we introduce provides a new technique to efficiently model support-induced losses for a broad class of mechanical structures. Previous approaches have relied on either the direct solution of an elastic wave radiation problem involving the substrate[6,7,42–44] or the simulation of a perfectly absorbing artificial boundary[5,41], with systematic tests as a function of geometry limited to a few specific cases[5–7]. In contrast, our technique represents a substantial simplification in that it reduces the problem to the calculation of a perfectly decoupled resonator mode together with free elastic wave propagation through the substrate in the absence of the suspended structure. A key feature of our method is to combine a standard finite-element method (FEM) calculation of the resonator mode together with the use of an extended contact at the support. This allows us to treat complex geometries, taking proper account of interference effects between the radiated waves.

In summary, we develop and test an efficient method for calculating the clamping loss of high-Q mechanical resonators. Our analysis includes a thorough experimental verification of this theoretical framework by employing resonators that are specifically designed to isolate the clamping-loss contribution to the total dissipation $1/Q$. The measured damping in these structures matches the theoretical predictions and demonstrates in a direct manner the strong geometric character of this fundamental dissipation channel.

Results

Phonon-tunnelling approach. In analogy to radiation tunnelling in photonics and electron tunnelling in low-dimensional structures, we adopt a 'phonon tunnelling' picture to describe the support-induced losses[24]. In this picture, the mechanical resonance of interest, characterized by frequency ω_R, is regarded as a phonon cavity that is weakly coupled to the exterior by a hopping process, whereby the elastic energy leaks out of the resonator through the narrow contact areas from which it is suspended. Within this framework, one can start from the harmonic Hamiltonian associated with the elastic scattering eigenmodes of the entire structure, including the substrate, and derive a quantum model for the Brownian motion experienced by each resonance of the suspended structure.

The corresponding weak tunnel couplings can be obtained to lowest order in the small parameter $k_R d$, where $1/k_R$ is the characteristic length scale over which the resonator mode varies appreciably and d is the characteristic dimension of the contact area S from which the resonator is suspended. For typical structures that exhibit high-Q mechanical resonances, $k_R d \ll 1$ is comfortably satisfied. This justifies the weak coupling approximation and leads to a general expression for the associated dissipation $1/Q$ in terms of the 'overlaps' between the scattering modes and the resonator mode. In the limit $d \to 0$, the leading contribution is obtained by replacing the scattering modes by the free (unperturbed) modes of the supports, which yields[24]

$$\frac{1}{Q} = \frac{\pi}{2\rho_s\rho_R\omega_R^3}\int_q\left|\int_S d\bar{S}\cdot\left(\sigma_q^{(0)}\cdot\bar{u}'_R - \sigma'_R\cdot\bar{u}_q^{(0)}\right)\right|^2 \times\delta[\omega_R - \omega(q)]. \qquad (1)$$

Here, σ'_R and $\bar{u}'_R$ are the stress and displacement fields associated with the normalized resonator mode, $\sigma_q^{(0)}$ and $\bar{u}_q^{(0)}$ are the analogous fields for the continuum of support modes labelled by q (eigenfrequencies $\omega(q)$), and ρ_s and ρ_R are, respectively, the densities of the substrate and resonator materials. The resonator mode should satisfy either (i) free or (ii) clamped boundary conditions at the contact area, S, depending on the behaviour of the eigenmode when S is small, whereas the unperturbed support modes should satisfy the converse. These homogeneous boundary conditions correspond, respectively, to $d\bar{S}\cdot\sigma'_R = 0$ and $\bar{u}'_R = 0$ so that only one of the two terms in the surface integral is finite. In general, the decomposition between 'resonator volume' and 'supports' consistent with the weak coupling condition need not be unique. Examples of case (i) are pedestal geometries, such as microspheres, microdisks or microtoroids, when the pedestal is included in the support[24]. It is worth noting that for these geometries, if the pedestal is assumed

© 2011 Macmillan Publishers Limited. All rights reserved.

to have perfect impedance match with the substrate, equation (1) leads to a particularly simple result for the Q of an axially symmetric resonance[7,24], which has been verified in ref. 7 for the radial breathing mode of microtoroid structures. On the other hand, examples of case (ii) include the planar structures investigated here, when the resonator volume consists of the portion of the structure that is free-standing.

A rigorous derivation of equation (1) is given in ref. 24. Alternatively, if one uses a decomposition of the displacement field in terms of the unperturbed support modes and the discrete modes of the resonator volume, equation (1) follows simply from applying Fermi's Golden rule to phonon decay, with the interaction Hamiltonian between the resonator volume (labelled $<$) and the surrounding supports (labelled $>$) given by $\int_S \mathrm{d}\bar{S}\cdot\sigma_{>}\cdot\bar{u}_{<}$ for case (i) and $-\int_S \mathrm{d}\bar{S}\cdot\sigma_{<}\cdot\bar{u}_{>}$ for case (ii). Within this framework, it is straightforward to realize that the validity of equation (1) is more general than the condition $k_\mathrm{R}d \ll 1$ and will also apply to any resonance, for which the support-induced frequency shift is small compared with the relevant mode spacing (that is, the free spectral range at the corresponding resonant frequency) so that the weak coupling assumption is warranted. For our case, the use of this master formula is completely equivalent to previous intuitive approaches based on forcing the substrate with the stress source generated by the resonator mode[6,42–44], as can be shown rigorously by using—for the elastic Green's function of the substrate—a spectral decomposition in terms of its free modes. In the presence of mode coupling[5,7] not induced by disorder, our treatment remains valid provided that the mode mixing is not dominated by support-induced interactions, which includes the case where it is accounted for by FEM assuming perfect clamping and excludes cases where symmetry breaking induced by the support is relevant. Finally, one should note that in the weak-coupling regime, it is straightforward to incorporate mode coupling not accounted for by the FEM into our phonon-tunnelling formalism.

Q-solver. Though the aforementioned framework is completely general, to investigate the predictive power of our approach, we focus specifically on the flexural modes of a symmetric plate geometry of thickness t that is inscribed in a circle of radius R, with the contact area S corresponding to the outer rim of an idealized circular undercut (undercut distance of L_und). To calculate the theoretical Q-values of such devices via equation (1), we have developed a numerical solution technique that determines the normalized resonator eigenmode and eigenfrequency via FEM (with $\bar{u}_\mathrm{R} = 0$ at S) and is based on a decomposition into cylindrical modes for the support, which is approximated by the substrate modelled as an isotropic elastic half-space. The latter approximation is expected to be quantitatively precise for the low-lying flexural resonances when the underetched gap between the suspended structure and the substrate satisfies $h < R$ (where h is the gap height), and the largest resonant wavelength for elastic wave propagation in the substrate is smaller than the relevant length scales characterizing the mounting of the sample (see below). The aforementioned weak-coupling condition, $k_\mathrm{R}d \ll 1$, follows in this case from $t \ll R$. From equation (1), exploiting the fact that the eigenmodes of an elastic half-space are given by straightforward analytical expressions[45], we obtain (see Methods section for details of this derivation)

$$\frac{1}{Q} = \frac{\pi}{2\rho_\mathrm{s}\rho_\mathrm{R}\omega_\mathrm{R}} \sum_{n,\gamma} \frac{|f_{z,n}|^2}{c_\gamma^3} \tilde{u}_{n,\gamma}(\omega_\mathrm{R} R / c_\gamma, \nu_\mathrm{s}). \qquad (2)$$

Here, we introduce the dimensionless functions $\tilde{u}_{n,\gamma\neq s}(\tilde{q},\nu_\mathrm{s}) = 2\pi\int_0^{\pi/2} \mathrm{d}\theta \sin\theta \, |u^{(0)}_{\bar{q},\gamma;z}(0,\nu_\mathrm{s})|^2 \, J_n^2(\tilde{q}\sin\theta)$, $\tilde{u}_{n,s}(\tilde{q},\nu_\mathrm{s}) = 2\pi \, |u^{(0)}_{\bar{q},s;z}(0,\nu_\mathrm{s})|^2 \, J_n^2(\tilde{q})$ and the linear stress Fourier components $f_{z,n} = \int_S \mathrm{d}\bar{S}\cdot\sigma'_\mathrm{R}\cdot\hat{z}\mathrm{e}^{in\phi}$ with $n = 0, \pm 1, \pm 2, \ldots$. The different types of relevant plane-wave modes $\bar{u}^{(0)}_{\bar{q},\gamma}(\bar{r},\nu_\mathrm{s})$ of the half-space[45] (that is, longitudinal (l), transverse vertical (t) and surface acoustic waves (s) given that transverse horizontal waves do not contribute) are labelled by $\gamma = l, t, s$ with c_γ, the corresponding speed of sound—as determined by the density ρ_s, Poisson ratio ν_s and Young's modulus E_s of the substrate. We adopt spherical coordinates for the incident wave vector $\bar{q}$ with polar angle θ and cylindrical coordinates for the position $\bar{r}$. The squared displacements $|u^{(0)}_{\bar{q},\gamma;z}(0,\nu_\mathrm{s})|^2$ are given by analytical expressions, that only depend on γ, $\cos\theta$ and ν_s[24,45], which lead to straightforward integrals for the functions $\tilde{u}_{n,\gamma\neq s}(\tilde{q},\nu_\mathrm{s})$ detailed in the Methods section.

If one considers low frequency modes that are symmetric with respect to both the $x-z$ and $y-z$ planes so that $f_{z,0} \neq 0$ and $\omega_\mathrm{R} \ll c_\gamma/R$ $\forall\gamma$, one can approximate the series in equation (2) by the $n = 0$ term with the $\tilde{u}_{n,\gamma}$ evaluated at $\tilde{q} = 0$. For a Poisson ratio $\nu_\mathrm{s} = 1/3$, this yields the following approximation

$$Q \approx 1.8 \frac{\rho_\mathrm{R}\omega_\mathrm{R}E_\mathrm{s}^{3/2}}{\sqrt{\rho_\mathrm{s}}\,|f_{z,0}|^2}, \qquad (3)$$

where $f_{z,0}$ corresponds to the total force applied on the contact area S. For the typical micromechanical resonators analysed here (see below), this approximation deviates from equation (2) by 20%. Finally, we highlight that it is straightforward to generalize the above to in-plane modes and the rim need not be continuous, as in cases where the resonator volume makes contact with the support at a disjoint set of small areas (for example, a bridge geometry with no undercut).

Free–free design. To experimentally verify our solver, we have developed 'free–free' micromechanical resonators consisting of a central plate (resonator) of length L and width w suspended by four auxiliary beams as depicted in Figure 1a. These structures are etched from a high-reflectivity monocrystalline distributed Bragg reflector (DBR)—as described in the Methods section, suited for Fabry–Perot-based optomechanical systems[46]. The devices used in this study constitute a variant of the previously demonstrated free–free flexural design in which auxiliary beams with widths $w_\mathrm{s} \ll w$ and lengths $L_\mathrm{s} = \lambda_\mathrm{t}/4$ (where λ_t is the resonant wavelength for the propagation of torsional waves) placed at the nodes of the central resonator mode provide noise filters to suppress support-induced losses[3]. A major drawback with the $\lambda_\mathrm{t}/4$-beam design is that the resulting auxiliary beam length can be excessive. In fact for the eigenfrequencies investigated in this work, the corresponding beam length (>400 µm at 1.7 MHz) leads to proliferation of low-frequency flexural resonances that compromise the stability of the optical cavity and render mode identification difficult. We circumvent this issue by utilizing instead a reduced length $L_\mathrm{s} \ll \lambda_\mathrm{t}/4$ chosen to avoid spectral overlap between the free–free resonance and flexural resonances of the auxiliary beams.

The free–free design provides an ideal platform to isolate and measure phonon tunnelling dissipation: first, by altering the attachment position of the auxiliary beams, this design allows for a significant variation of geometry, while approximately preserving the frequencies and effective surface-to-volume ratios of the resonators. As these characteristics are kept constant, one can rule out the influence of additional damping mechanisms (specifically those driven by internal losses and surface effects) on the variation in Q and hence isolate support-induced losses in the measured devices. Second, the free–free resonators provide an intuitive illustration of the strong geometric character of the support-induced dissipation. Heuristically, the clamping loss will be proportional to the elastic energy radiated through the auxiliary beams, which should approximately scale as the squared deflection of their contacts with the central resonator (see Fig. 1b,c). Thus, varying the contact position

© 2011 Macmillan Publishers Limited. All rights reserved.

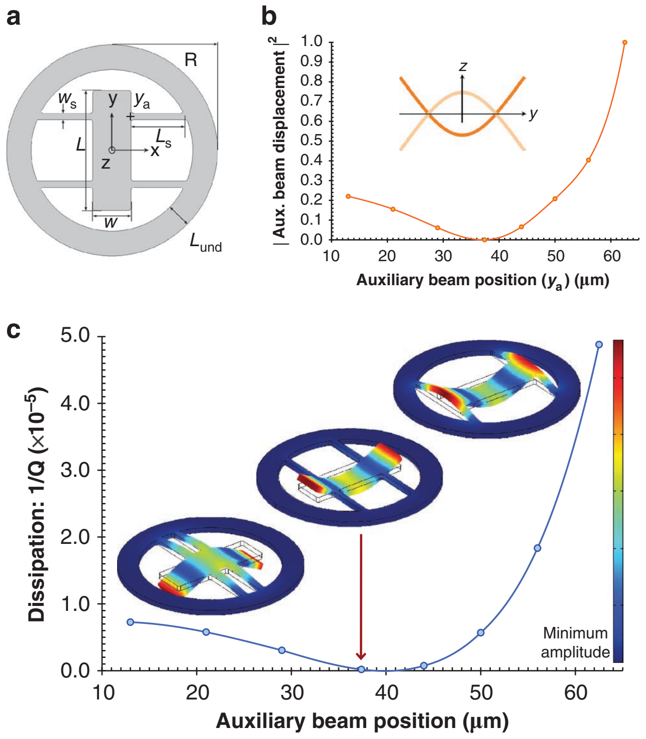

Figure 1 | Mapping out phonon-tunnelling dissipation in a free-free resonator. (**a**) Schematic diagram of the resonator geometry. (**b**) Normalized squared centre of mass displacement of a single auxiliary-beam central-resonator contact calculated via FEM (the inset shows the profile of the free–free mode as approximated by Euler–Bernoulli theory). (**c**) Simulated dissipation (see equation (2)) as a function of the auxiliary beam's *y*-coordinate (y_a). Values corresponding to eight discrete geometries were calculated here with $t=6.67\,\mu m$, $w_s=7\,\mu m$, $w=42\,\mu m$, $L=132\,\mu m$, $R=116\,\mu m$ and $L_{und}=27\,\mu m$—the line is simply a guide for the eye. The FEM-calculated mode shapes correspond to the three extreme examples of the resonator design, from left to right: auxiliary beams near the resonator centre ($y_a=13\,\mu m$), beams near the ideal nodal position ($y_a=37.4\,\mu m$) and beams attached at the ends ($y_a=62.5\,\mu m$). The theoretical clamping loss limit $1/Q_{th}$ for nodal positioning is always finite with the geometry closest to this position (indicated by the arrow) yielding $1/Q_{th}\approx 2\times 10^{-7}$.

of the auxiliary beams results in a characteristic modulation of the damping rate, which approximately maps out the central resonator mode shape (Fig. 1b). As expected, the minimum-loss design corresponds to the geometry in which the auxiliary beams are attached at the nodes of the fundamental resonance of the central resonator. It is interesting to note that the theoretical clamping loss limit $1/Q_{th}$ for nodal positioning is always finite as described in Figure 1c. In turn, for generic placement away from the nodal points, one obtains for the improvement in Q with respect to the clamped–clamped configuration the heuristic relation $Q_{f-f}/Q_{c-c}\sim(w/2w_s)^2$, which assumes that ω_R and the effective mass m_R are the same for both configurations and ω_R lies away from the flexural resonances of the auxilliary beams. This figure of merit can be derived from equation (3), if one uses the approximate scalings $|f_{z,0}|_{c-c}\sim E_R t^3 w k_R^3\sqrt{\rho_R/m_R}/6$ and $|f_{z,0}|_{f-f}\sim E_R t^3 w_s k_R^3\sqrt{\rho_R/m_R}/3$, which follow from neglecting the undercut, using thin-plate elasticity, and exploiting the fact that $w_s\ll L$ to analyse the elastic wave propagation in the auxilliary beams[24].

Measured dissipation. To identify the mechanical modes of our microfabricated resonators (see Figure 2a for an example of a completed device), we compare the optically measured resonator frequencies, as a function of the auxiliary beam position, with the theoretical eigenfrequency variation. The simulated values are generated using the geometric parameters determined via careful analysis of the completed resonators (see Supplementary Method). As can be seen in Figure 2b, in addition to the symmetric free–free resonance, there is also an antisymmetric eigenmode with comparable frequency. We observe no mode coupling between these resonances, which is consistent with the specific mirror symmetries of the structure. The frequencies are accurately reproduced by the FEM simulation, if we allow for frequency offsets that are solely dependent on the mode parity (262 kHz offset for the free–free mode and 89 kHz offset for the antisymmetric mode). We attribute these shifts to a material-related dissipation mechanism involving both surface and bulk contributions (see Supplementary Method for further details).

All dissipation measurements have been performed at high vacuum (10^{-7} mbar) and at cryogenic temperatures (20 K) to suppress fluidic and thermoelastic damping in the devices (Fig. 2c,d). Under these conditions, we record quality factors spanning 1.4×10^4 to 5.1×10^4, with the minimum Q corresponding to the free–free mode of devices with an auxiliary position of 62.5 μm and $R=116\,\mu m$, and with the maximum Q to the geometry closest to nodal positioning (37.4 μm) for the same radius and type of mode (see Fig. 3). For the symmetric mode, we readily observe the expected characteristic modulation in Q as a function of the placement of the auxiliary beams with a relative variation of $\Delta Q_{exp}/Q_{exp}\sim 260\%$ (~80%) for $R=116\,\mu m$ ($R=131\,\mu m$). At the same time, the use of the free–free geometry ensures that the frequency variation is kept small, with a range of $\Delta f/f\sim 20\%$ (~10%). In contrast, the Q-values for the antisymmetric mode are nearly constant with $Q\approx 2.1\times10^4$ (Fig. 3c). This is expected as the theoretical support-induced loss for this mode is negligible. Additionally, as this resonance involves mainly deformations of the auxiliary beams, its dissipation is not correlated with the mode shapes of the central resonator. The damping of this mode is instead dominated by other sources of dissipation, most likely by the material-related losses that are also responsible for the frequency shifts. Thus, we obtain an independent corroboration that the characteristic Q-variation observed for the free–free mode is indeed induced by the modification of the geometry rather than by the small frequency variation present in the devices.

Discussion

To quantitatively compare the measurements with our numerical predictions, two issues must be considered: (i) our model only captures support-induced losses, although other loss mechanisms may still contribute to the overall damping in the devices and (ii) the parameters for the half-space model of the substrate must be properly chosen. Consideration (i) together with the fact that we have designed sets of resonators for which the frequencies and effective surface-to-volume ratios are kept approximately constant implies that any additional damping mechanism that is relevant at low temperatures and high vacuum, but is insensitive to the variation in geometry, should contribute a constant offset $1/Q_*$ in the measured dissipation $1/Q_{tot}$. Consideration (ii) is non-trivial given the long-wavelength nature of the elastic waves radiated into the substrate. For an average resonator frequency of 2.12 MHz, estimates of the maximum wavelength for the freely propagating elastic waves yield a value of 2.5 mm, which largely exceeds the wafer thickness (300 ± 25 μm). Thus, the mechanical material parameters for the substrate should be determined by the properties of the underlying stage and positioning mechanism in the cryostat rather than those of the chip itself. Hence, we assume for the half-space the mechanical properties of polycrystalline commercially pure (grade 2) titanium (see the caption of Figure 3 for more details), of which the bulk of the structure beneath the resonator consists. Taking all of this into account, the theory shows remarkable agreement with the measured dissipation (as shown in Fig 3). It is important to note that

© 2011 Macmillan Publishers Limited. All rights reserved.

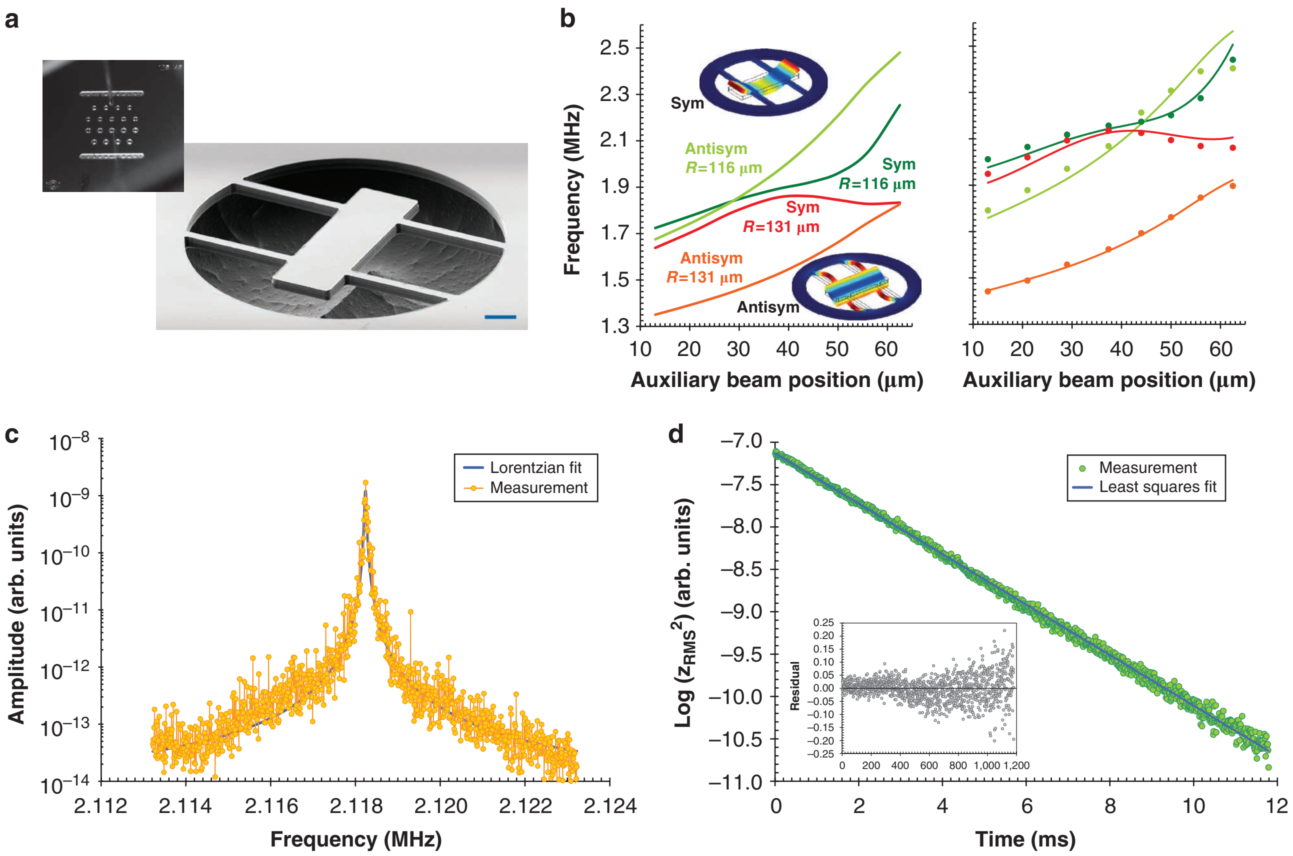

Figure 2 | Characterization of the completed free–free resonators. (**a**) Optical micrograph of the 5×5 mm chip containing the batch-fabricated microresonators as well as an electron micrograph highlighting a single suspended structure; the scale bar in this image is 20 μm. (**b**) Simulated (left) and measured (right) eigenfrequencies as a function of the auxiliary beam *y*-coordinate. The measured values (discrete points) show excellent agreement with the simulated data set, albeit with a slight offset dependent on the parity of the mode. The fitting lines in the right plot correspond to a mean frequency offset of 262 kHz for the symmetric (sym) free–free modes and 89 kHz for the neighbouring antisymmetric (antisym) modes (inset images show the FEM-derived mode shapes). Lower panels—examples of the fitting techniques utilized for *Q*-value extraction including: (**c**) Lorentzian fitting of the free–free resonance (captured on a spectrum analyser) for a device with $R=116\,\mu$m and $y_a=29\,\mu$m resulting in $Q=4.5\times10^4$ and (**d**) ringdown fitting of the same device using linear regression of the natural log of the mean square of the free-ringdown signal captured single-shot with a high-speed oscilloscope yielding $Q=4.46\times10^4$. The inset includes the residuals to the linear fit showing an excellent agreement with the expected exponential decay.

the only free parameter used in the model of the free–free mode is a constant offset of $1/Q_*=2.41\times10^{-5}$. Although the exact nature of the corresponding dissipation mechanism is currently unknown, we assume that it arises from material losses in the resonator epi-structure.

It should be noted that most commercially viable resonators operate in a regime where TED dominates, and in some instances, intuitive understandings of the support-induced damping[3,8,40] have allowed for its suppression below other limiting damping mechanisms. Nonetheless, if current efforts to minimize TED in such structures at room temperature are successful[28], support-induced losses may pose the next challenge for maximizing *Q*. On the other hand, in fundamental research thrusts employing high vacuum and cryogenic systems, support-induced losses can become a dominant factor[7,41]. For example, the free–free designs explored here provide a route to minimize support-induced losses for application in optomechanical experiments utilizing the micromechanical resonator as an end mirror in a high-finesse Fabry–Perot cavity[46]. To gauge the relevance of our 'free–free' micromirror design in this context, it is instructive to compare the fundamental limit at nodal positioning $Q_{th}\approx5\times10^6$ and the maximum measured *Q*-value of 5.1×10^4 with the corresponding results for the fundamental flexural mode of a clamped bridge of comparable dimensions. In fact, for the typical dimensions considered, as required for integration in a high-performance Fabry–Pérot cavity, we obtain a theoretical limit $Q_{c-c}\sim10^3$ in line with previous measurements on monocrystalline DBR optomechanical structures[47].

Given the scale-independent nature of support-induced losses, our solver can be applied equally well to nanoscale mechanical devices. We find that for a recent demonstration of a nanomechanical doubly clamped beam coupled to a superconducting qubit at milliKelvin temperatures[48], the measured values for the resonator's maximum *Q* ($\approx6\times10^4$) can be understood solely via the phonon-tunnelling loss model (beam geometry of 0.3×0.18×6 μm; M. LaHaye, private communication), which predicts a *Q*-value of 5.4×10^4, in excellent agreement with the experimental value. In addition, the phonon-tunnelling framework is also applicable to prestressed nanoresonators such as Si_3N_4 strings[34] or membranes and has recently been experimentally verified for the latter[49].

In conclusion, we have developed an efficient FEM-enabled numerical method for predicting the support-induced dissipation in microscale and nanoscale mechanical resonators. In combination with existing models for other relevant damping channels (for example, fluidic and TED[27,28]), our 'phonon-tunnelling' solver makes further strides towards accurate prediction of *Q*. Furthermore, we provide a stringent experimental test of the corresponding theory using resonators engineered to isolate support-induced losses. Our results unambiguously demonstrate that phonon-tunnelling plays a significant

© 2011 Macmillan Publishers Limited. All rights reserved.

role in the mechanical dissipation of these devices and illustrate the strong geometric character of this fundamental damping mechanism. Finally, we note that as the weak-coupling approximation underlying our treatment is more general than the condition of small contact area, our numerical solver can in principle be extended to other relevant scenarios such as phononic-band-gap structures[41].

Methods

Numerical calculation of *Q*-values. To derive equation (2) from equation (1), we adopt for the free elastic half-space[45], modelling the decoupled support, a decomposition into eigenmodes $\bar{u}^{(0)}_{q,\theta,n,\gamma}(\bar{r})$ (with $n=0, \pm1, \pm2, \ldots$) that have axial symmetry with respect to z (see Fig. 1). These are related to the plane wave eigenmodes $\bar{u}^{(0)}_{\bar{q},\gamma}(\bar{r})$ by

$$\bar{u}^{(0)}_{q,\theta,n,\gamma}(\bar{r})=\frac{(-i)^n}{\sqrt{2\pi}}\int_{-\pi}^{\pi}\mathrm{d}\varphi\,\mathrm{e}^{in\varphi}\bar{u}^{(0)}_{\bar{q}(q,\theta,\varphi),\gamma}(\bar{r}) \tag{4}$$

where we adopt spherical coordinates for the incident wavevector $\bar{q}(q,\theta,\varphi)=q(\sin\theta\cos\varphi,\sin\theta\sin\varphi,\cos\theta)$ ($\theta=\pi/2$ for $\gamma=s$ and $\theta\leq\pi/2$ otherwise). We note that for the suspended plate geometry considered, the appropriate resonator mode satisfies $\bar{u}'_{\mathrm{R}}=0$ at the contact S so that we need to evaluate the second term in equation (1).

The thin-plate condition $t\ll R$ directly allows us, given the flexural nature of the modes of interest, to neglect stresses at S that are parallel to the substrate, with the possible exception of bending-moment contributions[45]—this also applies if there are small transverse dimensions comparable to t. However, the bending-moment contributions also become negligible in the limit $t/R\rightarrow0$, as can be shown by using: (i) that, given $\omega_{\mathrm{R}}\ll c_\gamma/R\ \forall\gamma$, we can Taylor expand $\bar{u}^{(0)}_{q,\theta,n,\gamma}(\bar{r})$ at the origin in the integral over S, (ii) that we can assume relevant stresses to be concentrated around the ends of the auxiliary beams so that the bending moments at S are mostly oriented along y, (iii) the reflection symmetries with respect to the $y-z$ (operator $\hat{R}_x$) and $x-z$ (operator $\hat{R}_y$) planes and (iv) that, barring interference effects, these bending-moment contributions are at most of relative order[24] $k_{\mathrm{R}}t$—here $k_{\mathrm{R}}=(12\rho_{\mathrm{R}}/E_{\mathrm{R}})^{1/4}\sqrt{\omega_{\mathrm{R}}/t}$ is the resonant wavevector for the propagation of flexural waves. Thus, we find that for all mode types other than $-+$ (antisymmetric (symmetric) with respect to $\hat{R}_x$ ($\hat{R}_y$)), the correction associated to neglecting the bending moments scales as $\Delta Q/Q\sim(k_{\mathrm{R}}t)^2$, whereas for $-+$ modes, it scales as $\Delta Q/Q\sim(k_{\mathrm{R}}t)$ (note that $L\sim R$). In turn, we find that the relative error in using equation (1), arising from the weak-coupling approximation, scales in this case as $\Delta Q/Q\sim|\Delta\omega_{\mathrm{R}}|/\omega_{\mathrm{R}}\sim|\Delta_I(\omega_{\mathrm{R}})|/2\omega_{\mathrm{R}}\sim(k_{\mathrm{R}}t)^3$, where the phonon-tunnelling-induced frequency shift $\Delta\omega_{\mathrm{R}}$ is approximated by $\Delta_I(\omega_{\mathrm{R}})/2\approx-(1/\pi)\int_0^\infty \mathrm{d}\omega I(\omega)/\omega$ where $I(\omega)$ is the environmental spectrum[24].

Hence, we can assume $\mathrm{d}\bar{S}\cdot\sigma'_{\mathrm{R}}\parallel\hat{z}$ and neglect the variation of $\bar{u}^{(0)}_{q,\theta,n,\gamma}(\bar{r})$ across the thickness t (that is, the z-dependence at S), so that the support modes only enter into equation (1) through $u^{(0)}_{q,\theta,n,\gamma;z}(\bar{r})|_{z=0}$. To determine the latter, we adopt cylindrical coordinates $\bar{r}=(r\cos\phi,r\sin\phi,z)$, exploit that reflection at the free surface preserves the tangential component of the wavevector implying

$$u^{(0)}_{\bar{q}(q,\theta,\varphi),\gamma;z}(\bar{r})\Big|_{z=0}=u^{(0)}_{\bar{q}(q,\theta,\varphi),\gamma;z}(0)e^{irq\sin\theta\cos(\phi-\varphi)}, \tag{5}$$

and use the Bessel integral

$$J_n(x)=\frac{1}{2\pi}\int_{-\pi}^{\pi}\mathrm{d}\phi\,\mathrm{e}^{-i(n\phi-x\sin\phi)}. \tag{6}$$

Thus from equations (4–6), we obtain

$$\begin{aligned}u^{(0)}_{q,\theta,n,\gamma;z}(\bar{r})|_{z=0}&=\frac{(-i)^n}{\sqrt{2\pi}}u^{(0)}_{\bar{q}(q,\theta,\varphi),\gamma;z}(0)\int_{-\pi}^{\pi}\mathrm{e}^{\mathrm{i}[n\varphi+rq\sin\theta\cos(\phi-\varphi)]}\mathrm{d}\varphi\\&=\sqrt{2\pi}u^{(0)}_{\bar{q}(q,\theta,\varphi),\gamma;z}(0)J_n(rq\sin\theta)\mathrm{e}^{in\phi},\end{aligned} \tag{7}$$

where we have also used that $u^{(0)}_{\bar{q}(q,\theta,\varphi),\gamma;z}(0)$ is independent of φ. Subsequently, substitution of equation (7) into equation (1) leads to equation (2) after using that here

$$\int_q\rightarrow\sum_{n,\gamma}\int_0^\infty\mathrm{d}q\,q^{d_\gamma-1}\left[\left(1-\delta_{\gamma s}\right)\int_0^{\pi/2}\mathrm{d}\theta\sin\theta+\delta_{\gamma s}\right]$$

where d_γ is the dimensionality (that is, $d_\gamma=3$ for $\gamma\neq s$ and $d_\gamma=2$ for $\gamma=s$), performing the substitution $\omega=c_\gamma q$ (for each γ), and integrating over ω. Finally, substitution of the explicit expressions for the plane wave eigenmodes $\bar{u}^{(0)}_{\bar{q},\gamma}(\bar{r})$ (see for example

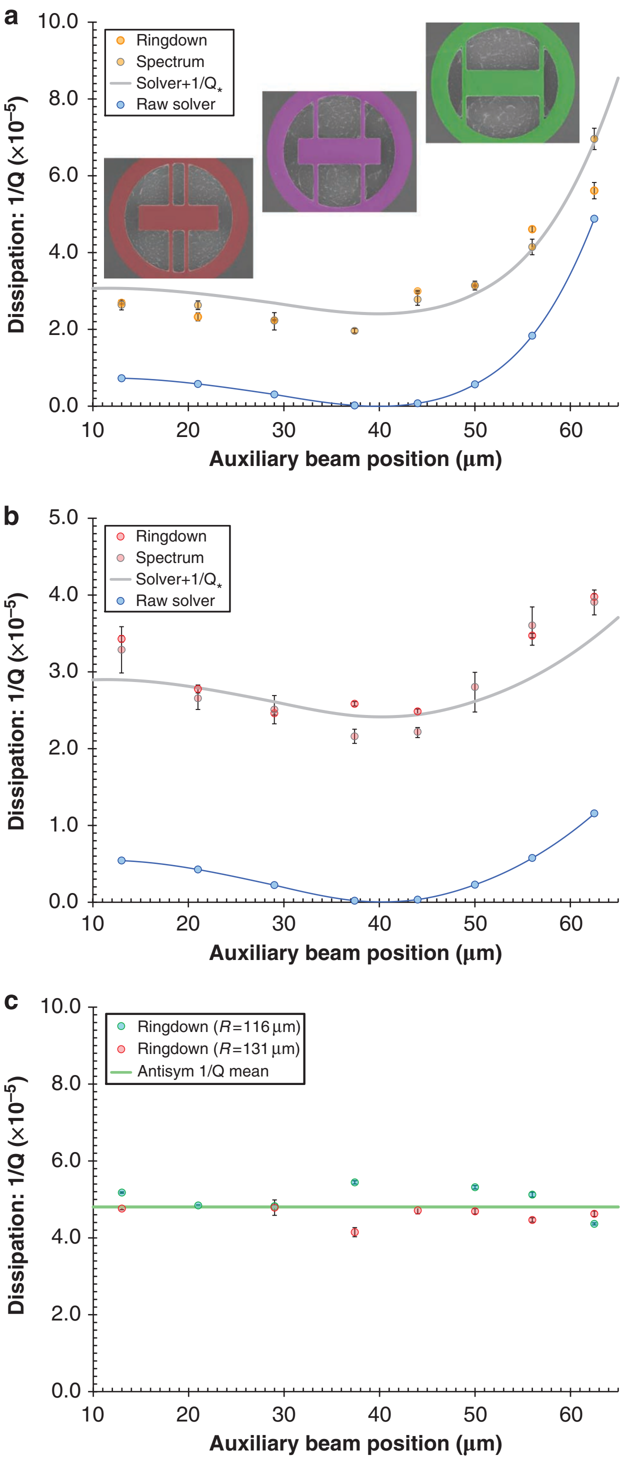

Figure 3 | Compiled dissipation results displaying excellent agreement between the theory and experiment. (**a**,**b**) Comparison of experimental measurements at $T=20$ K, with theoretical dissipation values for the free-free mode of resonators with measured central dimensions of 132×42 μm and radius $R=116$ μm and $R=131$ μm, respectively. Panel (**a**) includes SEM images of the three extreme designs (for R=116 μm) with overlaid CAD models of the resonator geometry. Both ringdown and spectrally-derived data are included, with values averaged over two nominally identical chips (error bars denote a confidence interval of 99%). We include both raw simulated data as well as fitted data (continuous lines are a guide to the eye) incorporating a constant offset $1/Q_*=2.41\times10^{-5}$. For the effective substrate, we utilize the mechanical properties of Ti, which is the main constituent of the positioning system on which the chips are mounted ($\rho=4{,}540$ kg m^{-3}, $E_s=116$ GPa and $\nu_s=0.34$). (**c**) Measured dissipation for the antisymmetric (antisym) mode of the same structures exhibiting a lack of geometric dependence.

© 2011 Macmillan Publishers Limited. All rights reserved.

Appendix A in ref. 24) and $\nu=\cos\theta$ into the definition of $\tilde{u}_{n,\gamma}(\tilde{q},\nu_s)$ allows us to obtain:

$$\begin{aligned}
\tilde{u}_{n,l}(\tilde{q},\nu_s) &= \frac{1}{\pi^2}\int_0^1 d\nu \frac{(1-2\alpha+2\alpha\nu^2)^2\nu^2 J_n^2(\tilde{q}\sqrt{1-\nu^2})}{\left[4\alpha^{3/2}\sqrt{1-\alpha+\alpha\nu^2}(1-\nu^2)\nu+(1-2\alpha+2\alpha\nu^2)^2\right]^2}\Bigg|_{\alpha=\alpha[\nu_s]} \\
\tilde{u}_{n,t}(\tilde{q},\nu_s) &= \frac{4}{\pi^2}\left\{\int_0^{\sqrt{1-\alpha}} d\nu \frac{(1-\alpha-\nu^2)(1-\nu^2)\nu^2 J_n^2(\tilde{q}\sqrt{1-\nu^2})}{16(1-\alpha-\nu^2)(1-\nu^2)^2\nu^2+(2\nu^2-1)^4}\right. \\
&\quad \left.+\int_{\sqrt{1-\alpha}}^1 d\nu \frac{(\alpha-1+\nu^2)(1-\nu^2)\nu^2 J_n^2(\tilde{q}\sqrt{1-\nu^2})}{\left[4\sqrt{\alpha-1+\nu^2}(1-\nu^2)\nu+(2\nu^2-1)^2\right]^2}\right\}\Bigg|_{\alpha=\alpha[\nu_s]} \qquad (8) \\
\tilde{u}_{n,s}(\tilde{q},\nu_s) &= \frac{C^2(\alpha)}{\pi}\left[\sqrt{1-\alpha\xi^2(\alpha)}-\frac{1-\xi^2(\alpha)/2}{\sqrt{1-\xi^2(\alpha)}}\right]^2 J_n^2(\tilde{q})\Bigg|_{\alpha=\alpha[\nu_s]}
\end{aligned}$$

where we use the ratio $\alpha\equiv(c_t/c_l)^2=(1-2\nu_s)/2(1-\nu_s)$ for the supports' material (ν_s is the corresponding Poisson ratio). In turn, $\xi(\alpha)$ is the ratio of the propagation velocity of surface waves to c_t, which is always less than unity[45], and

$$\begin{aligned}
C(\alpha) = &\left\{\frac{2-\xi^2(\alpha)}{\left[1-\xi^2(\alpha)\right]^{3/2}}\left[\xi^4(\alpha)/4+\xi^2(\alpha)-1\right]\right. \\
&\left.+\frac{2-\alpha\xi^2(\alpha)}{\sqrt{1-\alpha\xi^2(\alpha)}}\right\}^{-1/2}. \qquad (9)
\end{aligned}$$

The sum in equation (2) can be reduced to a sum over $n\geq 0$ by noting that $J_{-n}(x)=(-1)^n J_n(x)$ and that as the resonator mode is real, the linear stress Fourier components satisfy $f_{z,-n}=f_{z,n}^{*}$. Furthermore, the length of the central resonator L is comparable to the radius R, and we focus on low-lying resonances of the suspended structure so that the aforementioned condition $\omega_R \ll c_\gamma/R\ \forall\gamma$ is always satisfied. This implies $|\Sigma_\gamma \tilde{u}_{m,\gamma}/\Sigma_\gamma \tilde{u}_{n,\gamma}| \ll 1$ for $m>n$ and $\Sigma_\gamma \tilde{u}_{n,\gamma}\neq 0$, which can be understood by considering the behaviour of the Bessel functions for small arguments. Thus, we find that in equation (2), the sum over the index n is dominated by the first non-vanishing term as determined by the reflection symmetries $\hat{R}_x,\hat{R}_y$. The latter also imply ($n=0, 1, 2, \ldots$):

$$\begin{aligned}
f_{z,2n}^{++} &= R\int_{-\pi}^{\pi} d\phi \int_{-t/2}^{t/2} dz\, \hat{r}\cdot\sigma_R^{++}(\bar{r})\cdot\hat{z}\cos 2n\phi, \\
f_{z,2n+1}^{+-} &= R\int_{-\pi}^{\pi} d\phi \int_{-t/2}^{t/2} dz\, \hat{r}\cdot\sigma_R^{+-}(\bar{r})\cdot\hat{z}\sin(2n+1)\phi, \\
f_{z,2n+1}^{-+} &= R\int_{-\pi}^{\pi} d\phi \int_{-t/2}^{t/2} dz\, \hat{r}\cdot\sigma_R^{-+}(\bar{r})\cdot\hat{z}\cos(2n+1)\phi, \\
f_{z,2n}^{--} &= R\int_{-\pi}^{\pi} d\phi \int_{-t/2}^{t/2} dz\, \hat{r}\cdot\sigma_R^{--}(\bar{r})\cdot\hat{z}\sin 2n\phi, \qquad (10) \\
f_{z,2n+1}^{++} &= f_{z,2n}^{+-} = f_{z,2n}^{-+} = f_{z,2n+1}^{--} = 0;
\end{aligned}$$

where the resonator mode of type α,β satisfies $\hat{R}_x\sigma_R^{\alpha,\beta}=\alpha\sigma_R^{\alpha,\beta}$ and $\hat{R}_y\sigma_R^{\alpha,\beta}=\beta\sigma_R^{\alpha,\beta}$. To efficiently extract the above from the FEM simulation, we convert them into volume integrals using an adequate Gaussian weight so that, for example, for a fully symmetric mode, we have

$$f_{z,2n}^{++} = \lim_{a_\star\to 0}\frac{2}{\sqrt{\pi}a_\star}\int_V dr^3 e^{-\left(\frac{r-R}{a_\star}\right)^2}\hat{r}\cdot\sigma_R'(\bar{r})\cdot\hat{z}\cos 2n\phi, \qquad (11)$$

where we again use cylindrical coordinates and V denotes the resonator volume. In addition, we exploit that the reflection symmetries naturally allow to perform the FEM simulation on a single quadrant. Thus, numerical evaluation can be conveniently performed using a fixed $a_\star$ and a mesh size M such that $(V/4M)^{1/3} < a_\star \ll t$. We have checked the convergence and estimate the numerical error to be of order 5%.

Numerical simulations of the resonator mode are performed with the aid of COMSOL multiphysics. Accurate three-dimensional CAD models representing the resonator geometry are generated using Solidworks (matched with high-quality scanning electron microscope images as described in Supplementary Method), and the bidirectional interface between the two programs is exploited to perform a parametric sweep of the auxiliary beam contact position for determining the pertinent information about the relevant mode, namely its eigenfrequency, linear stress Fourier components $f_{z,n}$ and normalization constant. In this instance, a single CAD file is used with a global variable incorporated to control the lateral position of the auxiliary beams with respect to the centre of the central resonator. We use for the mechanical properties of our single-crystal resonators an anisotropic material model incorporating the elastic stiffness matrix for the epitaxial structure as obtained from a weighted average between the relative content of GaAs and AlAs (46.37% GaAs/53.63% AlAs). The corresponding parameters are: $C_{11}=119.6$ GPa, $C_{12}=55.5$ GPa, $C_{44}=59.1$ GPa and $\rho_R=4{,}483$ kg m^{-3}. The resonator axes are aligned along ⟨100⟩ (zinc-blende structure). Note that we ignore the 6° misorientation of the germanium substrate, as we have checked that it has a negligible impact (error of 0.3%) on the simulated frequency response of the resonators. Finally, as a non-trivial check, we have applied our numerical method to bridge geometries with no undercut for which a simple analytic expression is valid in the limit of large aspect ratio (see Supplementary Method).

Epitaxial material structure and resonator fabrication procedure. The layer structure for our high reflectivity resonators consists of 40.5 periods of alternating quarter-wave GaAs (high index) and AlAs (low index) grown lattice-matched to an off-cut monocrystalline germanium substrate. The ideal total thickness of the heterostructure is 6,857.6 nm, with individual layer thicknesses of 77.6 and 91.9 nm for the GaAs and AlAs, respectively, yielding a nominal peak reflectivity at 1,064 nm, as with our previous optomechanics experiments[47]. With this design, the germanium substrate enables the use of a high-selectivity gas-phase etching procedure, based on the noble-gas halide XeF$_2$, to rapidly and selectively undercut the underlying germanium substrate. Thus, we realize a free-standing epitaxial Bragg mirror via a simple and fast-turnaround fabrication procedure. The details of both the epitaxial material design and microfabrication procedure are covered in ref. 50.

Measurement technique. To characterize the frequency response of our microresonators, we utilize a custom-built optical fibre interferometer featuring a continuous flow ^{4}He cryostat as the sample chamber[51]. High-sensitivity displacement resolution is achieved in this system via optical homodyne interferometry. Cryogenic testing of these devices is necessitated because of the limitations imposed by TED at room temperature. Estimation of the magnitude of TED is possible using the analytical and finite element models developed previously[26–28], which predict a Q-value of ~4,000 for the current DBR composition and thickness at 1.8 MHz and 300 K—consistent with performed measurements. To avoid TED, our cryostat enables interrogation down to 20 K (resulting in an estimated TED limited Q of 9.9×10^8); the minimum temperature is currently limited by the large view-port above the sample stage. Additionally, this system is capable of vacuum levels down to 2.5×10^{-7} mbar at cryogenic temperatures, removing any additional damping induced by fluidic or squeeze film effects[29–31]. The eigenmodes of the resonator are excited by driving a high-frequency (10 MHz) piezo disc soldered to a copper stage in thermal contact with the cold finger. For spectral characterization, the piezo disc is driven with white noise and the resonator frequency response is recorded on a spectrum analyser. For the free-ringdown measurements, the decay of a resonantly excited device is recorded in a single shot on a high-speed oscilloscope (see Supplementary Method for further details).

References

1. Craighead, H. G. Nanoelectromechanical systems. *Science* **290,** 1532–1535 (2000).
2. Ekinci, K. L. & Roukes, M. L. Nanoelectromechanical systems. *Rev. Sci. Instrum.* **76,** 061101 (2005).
3. Wang, K., Wong, A.- C. & Nguyen, C. T.- C. VHF free-free beam high-Q micromechanical resonators. *J. Microelectromech. Syst.* **9,** 347–360 (2000).
4. Cleland, A. N. *Foundations of Nanomechanics* (Springer, 2003).
5. Bindel, D. S. & Govindjee, S. Elastic PMLs for resonator anchor loss simulation. *Int. J. Numer. Methods Eng.* **64,** 789–818 (2005).
6. Judge, J. A., Photiadis, D. M., Vignola, J. F., Houston, B. H. & Jarzynski, J. Attachment loss of micromechanical and nanomechanical resonators in the limits of thick and thin support structures. *J. Appl. Phys.* **101,** 013521 (2007).
7. Anetsberger, G., Riviere, R., Schliesser, A., Arcizet, O. & Kippenberg, T. J. Ultralow-dissipation optomechanical resonators on a chip. *Nature Photonics* **2,** 627–633 (2008).
8. Clark, J., Hsu, W.- T., Abdelmoneum, M. & Nguyen, C.- C. High-Q UHF micromechanical radial-contour mode disk resonators. *J. Microelectromech. Syst.* **14,** 1298–1310 (2005).
9. Lutz, M. *et al.* MEMS oscillators for high volume commercial applications. in *Proc. Transducers, Solid-State Sensors, Actuators and Microsyst* (2007). 14th Int. Conf.
10. Sidles, J. A. *et al.* Magnetic resonance force microscopy. *Rev. Mod. Phys.* **67,** 249–265 (1995).
11. Rugar, D., Budakian, R., Mamin, H. J. & Chui, B. W. Single spin detection by magnetic resonance force microscopy. *Nature* **430,** 329–332 (2004).
12. Degen, C. L., Poggio, M., Mamin, H. J., Rettner, C. T. & Rugar, D. Nanoscale magnetic resonance imaging. *Proc. Natl Acad. Sci. USA* **106,** 1313–1317 (2009).
13. Li, M., Tang, H. X. & Roukes, M. L. Ultra-sensitive nems-based cantilevers for sensing, scanned probe and very high-frequency applications. *Nat. Nanotechnol.* **2,** 114–120 (2007).
14. Jensen, K., Kim, K. & Zettl, A. An atomic-resolution nanomechanical mass sensor. *Nat. Nanotechnol.* **3,** 533–537 (2008).
15. Naik, A. K., Hanay, M. S., Hiebert, W. K., Feng, X. L. & Roukes, M. L. Towards single-molecule nanomechanical mass spectrometry. *Nat. Nanotechnol.* **4,** 445–450 (2009).

© 2011 Macmillan Publishers Limited. All rights reserved.

16. Armour, A. D., Blencowe, M. P. & Schwab, K. C. Entanglement and decoherence of a micromechanical resonator via coupling to a cooper-pair box. *Phys. Rev. Lett.* **88,** 148301 (2002).
17. Marshall, W., Simon, C., Penrose, R. & Bouwmeester, D. Towards quantum superpositions of a mirror. *Phys. Rev. Lett.* **91,** 130401 (2003).
18. Blencowe, M. Quantum electromechanical systems. *Phys. Rep.* **395,** 159–222 (2004).
19. Schwab, K. C. & Roukes, M. L. Putting mechanics into quantum mechanics. *Phys. Today* **58,** 36–42 (2005).
20. Kippenberg, T. J. & Vahala, K. J. Cavity optomechanics: back-action at the mesoscale. *Science* **321,** 1172–1176 (2008).
21. Aspelmeyer, M. & Zeilinger, A. A quantum renaissance. *Phys. World* **21,** 22–28 (2008).
22. Aspelmeyer, M. & Schwab, K. Focus on mechanical systems at the quantum limit. *New J. Phys.* **10,** 095001 (2008).
23. O'Connell, A. D. *et al.* Quantum ground state and single-phonon control of a mechanical resonator. *Nature* **464,** 697–703 (2010).
24. Wilson-Rae, I. Intrinsic dissipation in nanomechanical resonators due to phonon tunneling. *Phys. Rev. B* **77,** 245418 (2008).
25. Kiselev, A. A. & Iafrate, G. J. Phonon dynamics and phonon assisted losses in Euler-Bernoulli nanobeams. *Phys. Rev. B* **77,** 205436 (2008).
26. Zener, C. Internal friction in solids. I. Theory of internal friction in reeds. *Phys. Rev.* **52,** 230–235 (1937).
27. Lifshitz, R. & Roukes, M. L. Thermoelastic damping in micro- and nanomechanical systems. *Phys. Rev. B* **61,** 5600–5609 (2000).
28. Duwel, A., Candler, R. N., Kenny, T. W. & Varghese, M. Engineering MEMS resonators with low thermoelastic damping. *J. Microelectromech. Syst.* **15,** 1437–1445 (2006).
29. Vignola, J. F. *et al.* Effect of viscous loss on mechanical resonators designed for mass detection. *Appl. Phys. Lett.* **88,** 041921 (2006).
30. Karabacak, D. M., Yakhot, V. & Ekinci, K. L. High-frequency nanofluidics: an experimental study using nanomechanical resonators. *Phys. Rev. Lett.* **98,** 254505 (2007).
31. Verbridge, S. S., Craighead, H. G. & Parpia, J. M. A megahertz nanomechanical resonator with room temperature quality factor over a million. *Appl. Phys. Lett.* **92,** 013112 (2008).
32. Yasumura, K. *et al.* Quality factors in micron- and submicron-thick cantilevers. *J. Microelectromech. Syst.* **9,** 117–125 (2000).
33. Mohanty, P. *et al.* Intrinsic dissipation in high-frequency micromechanical resonators. *Phys. Rev. B* **66,** 085416 (2002).
34. Verbridge, S. S. *et al.* High quality factor resonance at room temperature with nanostrings under high tensile stress. *J. Appl. Phys.* **99,** 124304 (2006).
35. Southworth, D. R. *et al.* Stress and silicon nitride: a crack in the universal dissipation of glasses. *Phys. Rev. Lett.* **102,** 225503 (2009).
36. Venkatesan, A. *et al.* Dissipation due to tunneling two-level systems in gold nanomechanical resonators. *Phys. Rev. B* **81,** 073410 (2010).
37. Unterreithmeier, Q. P., Faust, T. & Kotthaus, J. P. Damping of nanomechanical resonators. *Phys. Rev. Lett.* **105,** 027205 (2010).
38. Seoánez, C., Guinea, F. & Castro Neto, A. H. Surface dissipation in nanoelectromechanical systems: unified description with the standard tunneling model and effects of metallic electrodes. *Phys. Rev. B* **77,** 125107 (2008).
39. Remus, L. G., Blencowe, M. P. & Tanaka, Y. Damping and decoherence of a nanomechanical resonator due to a few two-level systems. *Phys. Rev. B* **80,** 174103 (2009).
40. Mattila, T. *et al.* A 12 MHz micromechanical bulk acoustic mode oscillator. *Sens. Actuators A Phys.* **101,** 1–9 (2002).
41. Eichenfield, M., Chan, J., Camacho, R. M., Vahala, K. J. & Painter, O. Optomechanical crystals. *Nature* **462,** 78–82 (2009).
42. Cross, M. C. & Lifshitz, R. Elastic wave transmission at an abrupt junction in a thin plate with application to heat transport and vibrations in mesoscopic systems. *Phys. Rev. B* **64,** 085324 (2001).
43. Park, Y.- H. & Park, K. C. High-fidelity modeling of MEMS resonators-part I: anchor loss mechanisms through substrate. *J. Microelectromech. Syst.* **13,** 238–247 (2004).
44. Photiadis, D. M. & Judge, J. A. Attachment losses of high Q oscillators. *Appl. Phys. Lett.* **85,** 482–484 (2004).
45. Graff, K. F. *Wave Motion in Elastic Solids* (Dover, 1991).
46. Gröblacher, S. *et al.* Demonstration of an ultracold micro-optomechanical oscillator in a cryogenic cavity. *Nat. Phys.* **5,** 485–488 (2009).
47. Cole, G. D., Gröblacher, S., Gugler, K., Gigan, S. & Aspelmeyer, M. Monocrystalline Al(x)Ga(1-x)As heterostructures for high-reflectivity high-q micromechanical resonators in the megahertz regime. *Appl. Phys. Lett.* **92,** 261108 (2008).
48. LaHaye, M. D., Suh, J., Echternach, P. M., Schwab, K. C. & Roukes, M. L. Nanomechanical measurements of a superconducting qubit. *Nature* **459,** 960–964 (2009).
49. Wilson-Rae, I. *et al.* High-Q nanomechanics via destructive interference of elastic waves. *Phys. Rev. Lett.* **106,** 047205 (2011).
50. Cole, G. D., Bai, Y., Aspelmeyer, M. & Fitzgerald, E. A. Free-standing Al(x)Ga(1-x)As heterostructures by gas-phase etching of germanium. *Appl. Phys. Lett.* **96,** 261102 (2010).
51. Cole, G. D. *et al.* Megahertz monocrystalline optomechanical resonators with minimal dissipation in *Proc. IEEE Micro Electro Mechanical Syst.* 847–850 (2010). 23rd Int. Conf.

Acknowledgments

G.D.C. is a recipient of a Marie Curie Fellowship of the European Commission (EC). Additional financial support is provided by the EC (projects MINOS, IQOS, QESSENCE), the Austrian Science Fund (projects START, L426 and SFB FoQuS) and the European Research Council (ERC StG QOM). Microfabrication was carried out at the Zentrum für Mikro- und Nanostrukturen (ZMNS) of the Technische Universität Wien, while the heterostructure was grown by Yu Bai at MIT. G.D.C. gratefully acknowledges Stephan Puchegger and Markus Schinnerl for assistance with scanning electron microscopy and focused ion beam milling. I.W.R. acknowledges financial support via the Nanosystems Initiative Munich, K.W. via the Austrian Research Promotion Agency (FFG) and M.R.V. via the FWF Doctoral Programme (CoQuS).

Author contributions

G.D.C. and I.W.R. designed the experiment (with the use of the free–free design suggested by I.W.R.) and developed the numerical solver. G.D.C. fabricated the microresonators. M.R.V. and G.D.C. designed and constructed the cryogenic optical-fiber interferometer. K.W. and G.D.C. measured the resonator frequency response and extracted the dissipation values. M.A. supervised the research effort. All authors contributed to the writing of the manuscript.

Additional information

Supplementary Information accompanies this paper at http://www.nature.com/naturecommunications

Competing financial interests: The authors declare no competing financial interests.

Reprints and permission information is available online at http://npg.nature.com/reprintsandpermissions/

How to cite this article: Cole, G. D. *et al.* Phonon-tunnelling dissipation in mechanical resonators. *Nat. Commun.* 2:231 doi: 10.1038/ncomms1212 (2011).

License: This work is licensed under a Creative Commons Attribution-NonCommercial-Share Alike 3.0 Unported License. To view a copy of this license, visit http://creativecommons.org/licenses/by-nc-sa/3.0/

© 2011 **Macmillan Publishers Limited. All rights reserved.**

SUPPLEMENTARY INFORMATION — Phonon-tunneling dissipation in mechanical resonators

Garrett D. Cole,[1,*] Ignacio Wilson-Rae,[2,†] Katharina Werbach,[1] Michael R. Vanner,[1] and Markus Aspelmeyer[1]

[1] *Vienna Center for Quantum Science and Technology (VCQ),*
Faculty of Physics, University of Vienna,
Boltzmanngasse 5, A-1090 Vienna, Austria.

[2] *Technische Universität München, 85748 Garching, Germany.*

(Dated: February 14, 2011)

Supplementary Figures

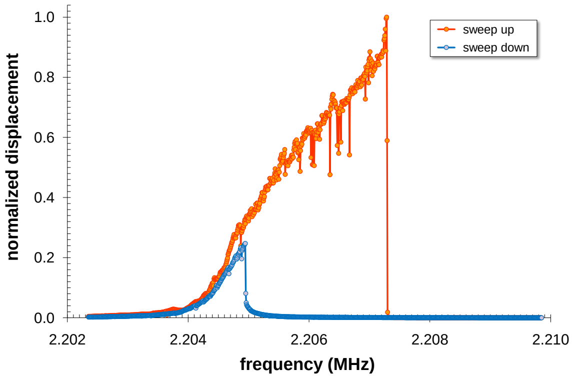

Supplementary Figure S1. Measured bistable driven response of the antisymmetric mode – For large drive amplitudes the expected hysteresis is observed. The red points are recorded for an increasing frequency of the drive (sweep up), while the blue dataset is generated with a decreasing frequency (sweep down). The significant nonlinearity present in this mode helps to distinguish it from the free-free resonance.

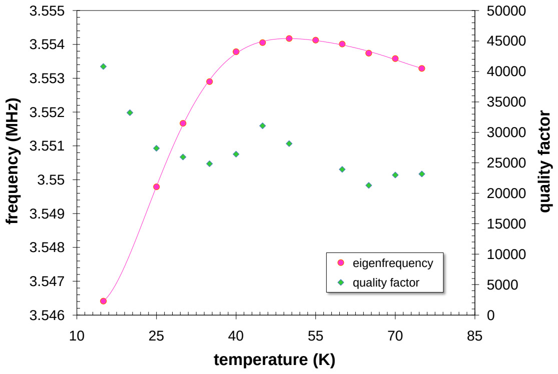

Supplementary Figure S2. Temperature dependence of the resonant frequency and Q-value for the symmetric (free-free) mode – Measurements were performed on a representative resonator fabricated from the AlGaAs-on-Ge materials system with auxiliary beams near the ideal nodal positions for the fundamental flexural mode of the central plate. The curve shown for the resonant frequency is simply a guide for the eye.

Supplementary Methods

A: Numerical verification with bridge geometries

Our generic symmetric inscribed structure includes the particular case of bridge geometries with no undercut for which a simple variant of the method used in Ref. [24] allows us to obtain an analytical approximation for the Q-value of the fundamental mode Q_{c-c} valid for $3\pi\mathsf{t}/2L \ll 1$. Our scenario differs from the one considered in Ref. [24] in two ways: (i) there is now a single half-space support instead of two and (ii) its free surface is oriented parallel to the beam's axis instead of perpendicular to it. Thus, for the fundamental flexural mode as the resonant wavelength in the support is much larger than the bridge length L, to lowest order in $(\mathsf{t}/L)^2$ the stresses at both clamping points add coherently so that the overall effect of (i) is to double the dissipation. In turn (ii) implies that the roles of the dimensionless displacements for compression and bending are interchanged so that the dissipation of the vertical bending modes are further corrected by a factor of $\tilde{u}_c/\tilde{u}_v$. Thus if we consider that the support and resonator are made of the same material characterized by a Poisson ratio $\nu = 1/3$ we obtain

$$Q_{c-c} = \frac{0.92\, L^5}{\pi^4 \mathsf{w}\mathsf{t}^4}\,. \tag{S1}$$

Hence as a non-trivial check we have applied our numerical method to the fundamental mode of clamped-clamped square beam monolithic geometries with no undercut, $\nu = 1/3$, and aspect ratios L/t ranging from 15 to 40 and compared the results with those corresponding to Eq. (S1). We find a discrepancy ϵ that decreases monotonically from 20% to 4% which is consistent with the rough heuristic estimate $\epsilon \sim 3\pi\mathsf{t}/2L$.

B: Analysis of Completed Devices

The resonator layout we have designed features 16 devices on chip, each with identical central resonator dimensions (nominally $130 \times 40\,\mu\mathrm{m}^2$). The 16 devices are divided into two sub-units featuring different outer radii (116 um and 131 um respectively), which are included in order to probe the effects of the auxiliary beam length on the dissipation. Finally, each of the two subsets contains 8 variations of the auxiliary beam contact position, varying from the center to the extreme outer edge of the central beam, with a single design chosen to match the theoretically calculated node position (auxiliary beam positions of 13, 21, 29, 37.4, 44, 50, 56, and finally, 62.5 μm). To ensure a thorough investigation of each geometry, two separate but nominally identical chips are measured.

Central to this study is an accurate determination of the geometric properties of the optomechanical resonators. Thus, we employ a variety of analytical techniques for the characterization of these devices as detailed below. We find that the actual thickness of the DBR is 6.67 μm, the central resonator dimensions are enlarged by 1 μm at each free edge as compared with the nominal design values, and finally, L_{und} is destructively measured post characterization and found to be on average 27 μm. In turn the microfabrication procedure detailed Ref. [50] entails $h \sim L_{\mathrm{und}}$.

Thickness: In order to accurately determine the physical thickness of the resonators, we rely on measurements of the DBR reflectance spectrum. This procedure begins by recording the reflectance of the mirror stack (on wafer) as a function of wavelength via spectrophotometry. A transmission matrix model is then used to fit the measured high-reflectivity stop-band; the individual layer thicknesses are adjusted assuming constant (fixed percentage) growth errors for the constituent films. Note that the wavelength of peak reflectivity of the mirror is highly sensitive to variations in layer thickness. In fact for this structure, a 1 nm variation in the individual layer thickness shifts the wavelength of peak reflectivity by approximately 10 nm. Relying on accurate knowledge of the room temperature refractive index of the binary films, we realize a minimum wavelength resolution of ±1nm; thus, the thickness accuracy is better than 20 nm for the DBR. From this analysis we have determined that the actual thickness of the DBR is slightly shorter than desired at 6.67μm with a peak on-wafer reflectance near 1060 nm at room temperature (ideal target thickness of 6.86μm, corresponding to a peak wavelength of 1078 nm at 300 K). The thickness is further verified by scanning probe measurement of the DBR following the anisotropic etch of the epitaxial layers. The profilometer provides an upper limit to the DBR thickness, as additional etching arising from surface sputtering of the Ge substrate is unavoidable. These measurements yield a conservative thickness estimate between 6.7μm and 6.8μm, verifying the more accurate spectrophotometer derived value.

Resonator Dimensions: The lateral dimensions of the resonators are determined by obtaining high resolution micrographs of each individual structure in a field emission scanning electron microscope (Zeiss Gemini). Image analysis shows that the lateral dimensions of the resonators have expanded by $+1\,\mu$m on each edge, with the following results: reducing the nominal external support diameter by $2 \pm 0.3\,\mu$m, increasing the auxiliary beam width from $5\,\mu$m to $7 \pm 0.3\,\mu$m, and increasing the overall lateral dimensions of the resonator by $2\,\mu$m to $132 \pm 0.3\,\mu$m and $42 \pm 0.3\,\mu$m. Additionally, a combination of process non-idealities (non-optimized exposure or development times) during lithography result in the formation of a 3-μm-radius fillet of at each corner of the device. These results are fed back into the CAD model of the resonator in order to generate the true resonator geometry for simulation. An overlay of the simulated resonator geometry and micrographs obtained via scanning electron microscopy can be seen in Fig. 3(a). Note that the resonators used in this study were not subject to potentially damaging energetic processes beyond the required plasma etching, including both SEM and FIB (as described below), until all dissipation measurements had been completed.

Undercut: In order to perform measurements of the support undercut distance, a dual beam SEM/FIB (Zeiss Gemini) is utilized to mill a window through the DBR and expose the underlying germanium. Because the GaAs/AlAs heterostructure is opaque to visible light, it is not possible to simply view the undercut distance with an optical microscope. This method allows for an accurate determination of the lateral etch distance below the supports. Image analysis yields an average distance of 27 μm for the structures. Note that multiple chips of identical geometry were released simultaneously in a single process run, in order to ensure repeatability in the resonator dimensions. Selected measurements across the chip verify that the undercut length is constant for the resonators studied here (measured values fall between 26.5 and $28.2\,\mu$m).

C: Q-value and frequency measurements

We utilize two options for driving and characterizing the resonance of interest: (i) by applying broadband white noise to the piezo disc for extraction of the mechanical frequency spectrum (simultaneously driving all modes within the system bandwidth), and (ii) by exciting a desired mode resonantly with a sinusoidal voltage input, abruptly shutting off the drive, and then recording the free-ringdown of the structure. In the first method, Q is extracted by measuring the width of the resonance of interest, while in the latter, the single-shot amplitude decay time of the ringing structure provides the damping rate of the resonator.

For data analysis, we employ a combination of spectral fitting with a Lorentzian function, with linear-regression-based fitting of a decaying exponential in the case of the ringdown data. The envelope of the raw ringdown signal is created by first squaring the dataset (in order to utilize both the positive and negative components of the decaying sinusoid) and then averaging over a 10-20 period window (it is important to note that a typical ringdown dataset contains more than 1.5×10^3 periods of oscillation). Finally, to linearize the data, we simply take the natural logarithm of the mean-squared amplitude. In contrast to the single-shot ringdown datasets, the spectral measurements require multiple averages for a clean signal (typically $\sim 50 - 100$). The Lorentzian fit parameters include the amplitude, center frequency, and full width at half maximum (FWHM), with the latter two used for calculating Q from their ratio. The fast Fourier transform (FFT) of the ringdown signal can also be used to determine the eigenfrequency, while the $1/e$ decay time τ allows for the extraction of the resonator quality factor via the relation $\tau = Q/\pi f$.

Mode identification is realized by comparing the resonator frequency response as a function of geometry with the simulated eigenfrequency values. The modes are further distinguished by the relative geometric-induced nonlinearity at resonance. The desired free-free mode remains linear to the limits of our piezoelectric-based inertial drive. On the other hand, the neighboring anti-symmetric mode exhibits a significant hardening spring Duffing response and can readily be driven into a bistable regime as shown in Supplementary Figure S1. Care is taken to drive this mode below the threshold for bistability to avoid complications in dissipation extraction. This marked difference in the responses of these two types of modes is consistent with their free-free versus clamped-clamped nature[4].

To each dissipation mechanism there is an associated dispersive effect induced by the interactions with the corresponding environment that shifts the resonant frequencies. For a given resonance (ω_R) this shift can be positive or negative depending on whether the environmental spectrum is dominated, respectively, by modes with frequencies lower or higher than ω_R. In turn, the two types of modes have markedly different surface-to-volume ratios, larger for the antisymmetric resonance and smaller for the symmetric one; exhibit a positive shift which is substantially larger for the symmetric mode, and a "background" dissipation that is larger for the antisymmetric one (cf. Fig. 3). These facts can be reconciled by assuming that two materials-related dissipation mechanisms contribute to the "background": a bulk one leading to an overall positive shift which is the same for both types of modes, and a surface one leading to a smaller negative shift that naturally scales as the surface-to-volume ratio. In turn, theoretical estimates for the phonon-tunneling induced shift yield a negligible *negative* shift that should also follow the mode profile leading to a significant modulation that is not observed. Likewise, mode coupling between the different resonators would also be incompatible with a constant shift.

Currently, the nature of the background dissipation mechanism in these resonators is unknown. It is important to point out that these devices are grown using a heteroepitaxial materials platform: in this implementation the GaAs/AlAs DBR is grown on an off-cut germanium substrate[50]. The advantage of the germanium substrate is that it significantly simplifies processing (enabling the use of a gas-phase release process via XeF_2), resulting in an extremely high yield and excellent geometric control — ideal characteristics for our dissipation study. Unfortunately, as discussed in Ref. [50], the materials quality is compromised in this implementation due to the slight lattice mismatch between Ge and GaAs/AlAs. Here misfit dislocations and residual anti-phase boundaries in the bulk of the resonator lead not only to a reduced surface quality (with an RMS roughness value exceeding 30Å), but also an enhanced background dissipation level. In comparison, we have fabricated nominally identical resonators (i.e. utilizing the same lithographic mask) from a homoepitaxial AlGaAs Bragg stack grown on a binary GaAs substrate[51]. The improved surface roughness measured for this structure ($\sim$ 6Å) points towards a significantly reduced defect density; this is also supported by the increased maximum quality factor, Q, which is measured to be $> 8 \times 10^4$ at cryogenic temperatures[51].

We have additionally investigated the temperature dependence of the quality factor, albeit over a limited range. As mentioned in the Methods Section, at room temperature thermoelastic (TED) damping limits the achievable Q to $< 10^4$. In Supplementary Figure S2 we include the temperature dependence of Q in the range $20-80$ K for a resonator dominated by the background dissipation given that the auxiliary beams are placed near the nodal positions. By 80 K, the theoretical TED limited Q exceeds 5×10^5, at this point the device becomes limited by the aforementioned background damping channel. As the temperature decreases, the device exhibits a reduced dissipation with a local maximum in Q near 50 K, potentially corresponding to the zero-crossing of the thermal expansion in GaAs as previously observed in Ref. [52].The large viewport in our cryostat as well as the thermally-insulating piezoelectric disc, limit the minimum realizable temperature to $\sim$ 15 K. It appears that with further cooling it would be possible to realize even higher quality factors.

Supplementary References

[52] Okamoto, Hajime, Ito, Daisuke, Onomitsu, Koji & Yamaguchi, Hiroshi Thermoelastic damping in GaAs microme-chanical resonators. In *Pys. Stat. Sol.* C, 5, 2920-2922 (2008). 34th Int. Symp. on Compound Semiconductors.

---

[*] garrett.cole@univie.ac.at

[†] ignacio.wilson-rae@ph.tum.de

G.D.C and I.W.R. contributed equally to this work.

5 A Toolset for Quantum Optomechanical Phonon Control

In this work [46] we introduced a method to control the motion of a mechanical resonator at the single phonon level. Specifically, we theoretically developed a technique to allow for an arbitrary superposition of phonon subtraction, addition, and the identity operation, which provides considerable versatility for mechanical non-Gaussian quantum state engineering and continuous variable quantum information applications. Utilising this tool, we introduced the concept of a *quantum state orthogonalizer* $\Upsilon_\perp$ that generates a state that is orthogonal to the input state, i.e. $\langle\psi|\Upsilon_\perp|\psi\rangle = 0$.

Experimentally, quanta subtraction and addition processes have been used to great success on traveling light fields, with leading examples being superposition state preparation via photon subtraction from squeezed vacuum [76, 77] and non-classical state preparation by photon addition [78]. Also, optical phonon addition and subtraction has recently been experimentally performed to a bulk lattice vibrational mode in diamond [48, 49]. Our theoretical proposal brings these operations to the field of quantum cavity optomechanics. Applying such operations to a stationary mechanical system has the advantage that one can more easily repeat the process to coherently and controllably perform multi-quanta operations. Using this fact, our work also introduced a protocol how to transform a known initial pure state into any other desired target pure state, i.e. *quantum state transformation*.

My specific contributions to this project were: in late 2008, during discussion with Markus Aspelmeyer in Vienna, I conceived how to perform phonon addition and subtraction; then during discussion with Myungshik Kim at Imperial College London we realized that these operations can be performed in a coherent superposition and Myungshik had the insight that such a superposition could be used for quantum state orthogonalization; I later conceived the arbitrary quantum state transformation protocol; and I played the leading role performing the calculations, preparing the manuscript, and working through the peer review process.

This work uses the long pulse interaction regime and thus, although this project was completed during the latter stages of my PhD, this chapter bridges the continuous and pulsed regimes, see Fig. 1.2.

PRL 110, 010504 (2013) PHYSICAL REVIEW LETTERS week ending 4 JANUARY 2013

Quantum State Orthogonalization and a Toolset for Quantum Optomechanical Phonon Control

M. R. Vanner,[1] M. Aspelmeyer,[1] and M. S. Kim[2]
[1]*Vienna Center for Quantum Science and Technology (VCQ) and Faculty of Physics, University of Vienna, Boltzmanngasse 5, A-1090 Vienna, Austria*
[2]*QOLS, Blackett Laboratory, Imperial College London, London SW7 2AZ, United Kingdom*
(Received 16 March 2012; published 3 January 2013)

We introduce a method that can orthogonalize any pure continuous variable quantum state, i.e., generate a state $|\psi_\perp\rangle$ from $|\psi\rangle$ where $\langle\psi|\psi_\perp\rangle = 0$, which does not require significant *a priori* knowledge of the input state. We illustrate how to achieve orthogonalization using the Jaynes-Cummings or beamsplitter interaction, which permits realization in a number of physical systems. Furthermore, we demonstrate how to orthogonalize the motional state of a mechanical oscillator in a cavity optomechanics context by developing a set of coherent phonon level operations. As the mechanical oscillator is a stationary system, such operations can be performed at multiple times providing considerable versatility for quantum state engineering applications. Utilizing this, we additionally introduce a method how to transform any known pure state into any desired target state.

DOI: 10.1103/PhysRevLett.110.010504 PACS numbers: 03.67.−a, 03.65.Ta, 42.50.Ct, 42.50.Dv

A qubit basis formed by a pair of orthogonal quantum states is central to quantum information processing. Currently there is considerable effort towards implementing quantum information processing with two-level systems. For such systems, an intriguing and fundamental fact is that quantum mechanics prohibits the construction of a universal-NOT gate that would produce an orthogonal qubit from any input qubit [1]. This quantum mechanical property is closely related to the quantum no-cloning theorem [2]; however, faithful cloning can be achieved probabilistically provided that the set of input states is linearly independent [3]. Similarly, using such an input set of states, it is possible to construct a probabilistic NOT operation for qubits [4]. A qubit basis may, however, also be formed using two orthogonal continuous variable states. Thus far, efforts to construct such a basis have mainly concentrated on using a superposition of coherent states [5]. Also, recently a qubit basis was realized using photon subtraction from squeezed vacuum [6].

In this Letter, we introduce a method for quantum state orthogonalization for continuous variable quantum systems. Notably, the method only requires knowing the angle ϑ made by the state's mean amplitude $\langle b\rangle = |\langle b\rangle|e^{i\vartheta}$, where b is the annihilation operator, and hence the scheme is magnitude independent. Furthermore, our method is readily extended to generate an arbitrary superposition of the initial state and an orthogonal counterpart to allow the encoding of quantum information. The orthogonalizer $\Upsilon_\perp \propto be^{-i\phi} + b^\dagger e^{i\phi}$ is formed by a linear superposition of the bosonic annihilation and creation operators, and generates a state orthogonal to any pure state $|\psi\rangle$, i.e., $\langle\psi|\Upsilon_\perp|\psi\rangle = 0$, when $\phi = \vartheta + \pi/2$. Thus, $\Upsilon_\perp$ is a quadrature operator that is perpendicular to ϑ [7].

The orthogonalizer can be realized with interactions that are available in many physical systems; e.g., to realize $\Upsilon_\perp$ in cavity quantum electrodynamics [8,9], one prepares an input qubit in the state $A|g\rangle + B|e\rangle$ which then weakly interacts via the Jaynes-Cummings Hamiltonian $H/\hbar = -i\Omega(b\sigma_+ - b^\dagger\sigma_-)$, where Ω is the coupling rate and $\sigma_{+,-}$ are the raising and lowering operators. A controllably weighted superposition of addition and subtraction is achieved by projective measurement of the qubit onto $B^*|g\rangle - A^*|e\rangle$ following the interaction. The measurement operator is then $\Upsilon_{\mathrm{QED}} = (\langle g|B - \langle e|A)[1 - \Omega\tau(b\sigma_+ - b^\dagger\sigma_-)](A|g\rangle + B|e\rangle) = \Omega\tau(A^2 b + B^2 b^\dagger)$, see Fig. 1(a). With this interaction, optical [8] or microwave [9] fields in a cavity, or the motional state of trapped ions [10] can be orthogonalized by appropriately setting A and B. Similarly, a pure state of a traveling optical field can be orthogonalized by interaction on a beam splitter and then measurement of an optical qubit comprising a superposition of zero and one photons [11], see Fig. 1(b). As these interactions are common throughout quantum optics, adaptations of this orthogonalization protocol to other physical systems can be readily achieved. Moreover, a different scheme to perform a superposition of photon subtraction and addition was recently proposed [12], which could also be used to realize state orthogonalization.

The tools we introduce for orthogonalization can also be utilized for quantum state engineering applications. Currently, single quanta manipulation techniques performed on traveling light fields [13] have prepared superposition states via photon subtraction [14], observed the bosonic commutation relation [15], and engineered arbitrary quantum states up to the two-photon level [16].

Published by the American Physical Society under the terms of the Creative Commons Attribution 3.0 License. Further distribution of this work must maintain attribution to the author(s) and the published article's title, journal citation, and DOI.

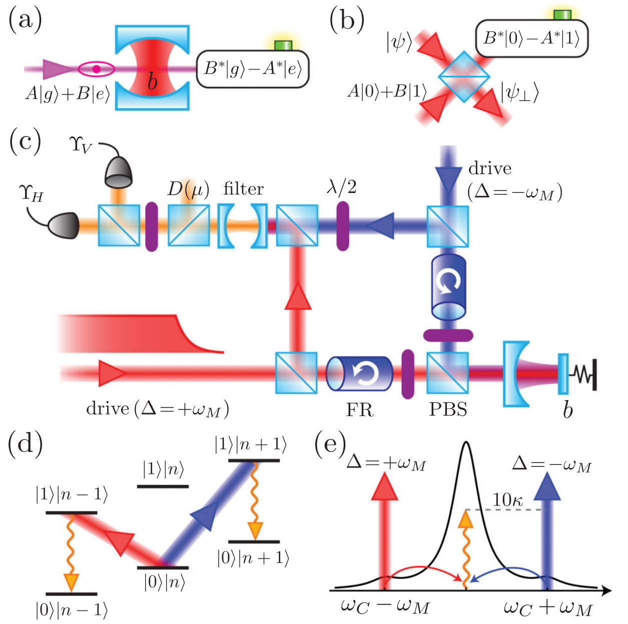

FIG. 1 (color). A continuous variable pure state can be orthogonalized by coupling with a qubit via the Jaynes-Cummings (a) or the beamsplitter (b) interaction and then measurement of the qubit. Alternatively, simultaneously using the beamsplitter and two-mode-squeezing interactions can be used for state orthogonalization. This can be realized with cavity optomechanics to coherently manipulate the quantum state of motion of a mechanical oscillator (c). (PBS, polarizing beam splitter; FR, Faraday rotator). One of the drive fields is blue detuned and gives rise to a phonon-number-increasing process, whereas the other is red detuned and gives rise to a phonon-number-reducing process. This is shown in (d); a truncated energy level diagram of the optomechanical system where the left kets describe the intracavity photon number and the right kets describe the mechanical phonon number. Each drive generates a sideband at cavity resonance, which is shown in (e), an example optomechanical spectrum. Thus, after erasure of the polarization information, photon detection at the cavity resonance frequency causes the mechanical element to undergo a coherent superposition of phonon addition and subtraction.

Much progress has also been made for arbitrary quantum state preparation of the motion of trapped ions and microwave field states [17]. As mechanical elements are now also considered for quantum applications, experimental tools are required for the coherent manipulation of phononic modes. Examples of progress in this direction are the observation of low thermal excitation [18–20], steps towards single-phonon manipulation by coupling to a superconducting phase qubit [18], strong coupling [21], and mechanical mode thermometry via sideband asymmetry [22]. Also, recently the lattice vibrations of two diamonds were entangled by coherently distributing one quanta across the two vibrational modes [23].

Coherent phonon manipulation.—In this section we demonstrate how to perform an arbitrary coherent superposition of phonon subtraction, addition, and the identity operation to a mechanical oscillator using cavity optomechanics. The prototypical optomechanical system is a Fabry-Perot cavity where one of the mirrors is sufficiently compliant that the reflection of light can modify the mirror momentum via radiation pressure. Concurrently, the motion of the moving mirror modulates the optical phase and generates sidebands. To realize phonon subtraction (addition) one can optically drive an optomechanical cavity at the red (blue) sideband, and then perform single photon detection on the field scattered onto cavity resonance. Provided that the sidebands are well resolved and the optical phase shifts are small allowing linearization, the red-detuned drive gives rise to a beamsplitter interaction and the blue-detuned drive gives rise to a two-mode-squeezing interaction. This linearization procedure was discussed for optomechanics in Ref. [24], where quantum state transfer between light and mechanics was proposed. Drive on the blue sideband has also been considered for continuous-variable teleportation from light to the mechanics [25]. Some other applications utilizing these sidebands are reviewed in Ref. [26].

Our proposed setup for coherent phonon control uses two orthogonally polarized optical fields to interact with the mechanical resonator, see Fig. 1(c). We consider a pulsed protocol where the conditional mechanical state following the pulsed interaction and measurement is determined. The optomechanical Hamiltonian [27] for the two independent optical modes in the optical rotating frame at the drive frequencies is

$$\frac{H}{\hbar} = \omega_M b^\dagger b + \sum_i [\Delta_i a_i^\dagger a_i - g_0 a_i^\dagger a_i (b + b^\dagger)] + \frac{H_d}{\hbar}, \qquad (1)$$

where $H_d/\hbar = \sum_i \sqrt{2\kappa N_i}(\mathcal{E}_i^* a_i + \mathcal{E}_i a_i^\dagger)$ is the drive term, the subscripts label the two orthogonally polarized modes $i \in \{h, v\}$, and a (b) is the cavity (mechanical) annihilation operator. (ω_M mechanical angular frequency; Δ optical detuning; g_0 optomechanical coupling rate; κ cavity amplitude decay rate; N photon number per pulse; $\mathcal{E}$ drive amplitude, where $\int dt|\mathcal{E}|^2 = 1$.) Neglecting mechanical damping and input noise, as the interaction time can be made shorter than the decoherence time scale, we compute the dynamics in a similar manner to Ref. [24]. The mechanical evolution is computed via the Hamiltonian, and the cavity field is computed via the Langevin equation $\dot{a}_i = -ia_i[\Delta_i - g_0(b + b^\dagger)] + \sqrt{2\kappa}(a_{\text{in},i} - i\sqrt{N_i}\mathcal{E}_i) - \kappa a_i$, where a_{in} is the optical input noise. We enter a displaced frame to follow the mean of the operators, i.e., $a_i \to \sqrt{N_i}\alpha_i + a_i$ and $b \to \beta + b$. Provided that the intracavity intensity varies much slower than the mechanical frequency, the mechanical mean amplitude is $\beta \simeq \frac{g_0}{\omega_M}\sum_i N_i|\alpha_i|^2$. This displacement, due to the optical steady state intensity, shifts the mean cavity length. Introducing $\Delta_i' = \Delta_i - 2g_0\beta$, the intracavity amplitude is $\alpha_i \simeq -i\sqrt{2\kappa}\mathcal{E}_i/(i\Delta_i' + \kappa)$, where it has been assumed that $\mathcal{E}$ varies much slower than κ. In the proceeding discussion this change to the detuning is neglected as the effect is small and can be readily compensated by frequency stabilization and/or appropriate predetuning. We turn now to the noise operators, and for brevity discuss the dynamics for a single drive frequency. We enter the mechanical and optical rotating frames via $a \rightarrow a e^{-i\Delta t}$ and $b \rightarrow b e^{-i\omega_M t}$, respectively. Assuming $\kappa \ll \omega_M$, we make the rotating-wave approximation and obtain $\dot{a} = i g_0 \sqrt{N} \alpha b^{(,\dagger)} + \sqrt{2\kappa} a_{\rm in} - \kappa a$ and $\dot{b} = i g_0 \sqrt{N} \alpha^{(*,)} a^{(,\dagger)}$, where the brackets in the superscripts are used to describe the two detunings we consider ($\Delta = +\omega_M$, $\Delta = -\omega_M$), respectively. For $g_0\sqrt{N}\alpha \ll \kappa$, we use the adiabatic solution $a \simeq i \frac{g_0}{\kappa} \sqrt{N} \alpha b^{(,\dagger)} + \zeta$, where $\zeta(t) = \sqrt{2\kappa} \int_{-\infty}^{t} dt' e^{-\kappa(t-t')} a_{\rm in}(t')$. The photon number scattered by the optomechanical interaction is $n = \int_0^\tau dt a_{\rm out}^\dagger a_{\rm out}$, which has been approximated to include detection up to the drive duration $\tau \gg \kappa^{-1}$, and $a_{\rm out} = \sqrt{2\kappa} a - a_{\rm in}$ is the cavity output. For the h polarization driving the beamsplitter interaction ($\Delta = +\omega_M$), $\langle n_h \rangle = (1 - e^{-2G_h\tau}) \langle b_0^\dagger b_0 \rangle$, where $G_i = \frac{g_0^2}{\kappa} N_i |\alpha_i|^2$ and b_0 is the mechanical field operator at the beginning of the interaction, time $t = 0$. For the v polarization ($\Delta = -\omega_M$), which drives the two-mode-squeezing interaction $\langle n_v \rangle = (e^{2G_v\tau} - 1) \times \langle b_0 b_0^\dagger \rangle$. We now consider weak drive such that the probability of more than one quanta being scattered is negligible. In this case, from the scattered photon number expectations, we introduce an effective beamsplitter parameter $\frac{\theta}{2} = \sqrt{2G_h\tau}$ and an effective squeezing parameter $r = \sqrt{2G_v\tau}$ [28], and we describe the interaction using the effective unitary $U_{\rm eff} = 1 + (\frac{\theta}{2} a_h^\dagger b e^{-i\phi} - r a_v^\dagger b^\dagger e^{i\varphi} - {\rm H.c.})$ [29]. Here, ϕ and φ are the beamsplitter and two-mode-squeezer phases, respectively, which can be controlled via the phase of the drives. The fields at cavity resonance generated via $U_{\rm eff}$ are spatially combined and filtered from the drive fields. Next, to control the weighting of identity in the operation, a weak displacement of amplitude μ is performed [30]. Doing this to the h polarization, $U_{\rm eff} \rightarrow 1 + (\frac{\theta}{2} a_h^\dagger b e^{-i\phi} - r a_v^\dagger b^\dagger e^{i\varphi} + \mu a_h^\dagger - {\rm H.c.})$. At this point the polarization of a scattered photon reveals how the phonon number changed. The field then passes through a wave plate that performs $a_h \rightarrow \frac{1}{\sqrt{2}}(a_h + a_v)$ and $a_v \rightarrow \frac{1}{\sqrt{2}}(a_v - a_h)$, and is then incident upon a polarizing beam splitter to conceal this information and allow for a quantum superposition. Conditioned on an h photon detection, the resulting mechanical state is $\rho_M^{\rm out} = \Upsilon_h \rho_M^{\rm in} \Upsilon_h^\dagger / \Pr(h)$, where $\Pr(h) = {\rm Tr}_M(\Upsilon_h^\dagger \Upsilon_h \rho_M)$ is the probability of photon detection and

$$\Upsilon_h = \frac{1}{\sqrt{2}} \left(\frac{\theta}{2} b e^{-i\phi} + r b^\dagger e^{i\varphi} + \mu\right). \tag{2}$$

A v photon detection gives a measurement operator of the same form, however, with a π phase shift on the identity.

Applications.—Υ_h provides a method to prepare and manipulate quantum coherence between the mechanical energy levels. Setting $\mu = 0$, $\frac{\theta}{2} = r$, and $\phi = \varphi = \vartheta + \pi/2$ we obtain the *quantum state orthogonalizer* $\Upsilon_\perp = r[b e^{-i(\vartheta + \pi/2)} + b^\dagger e^{i(\vartheta+\pi/2)}]/\sqrt{2} = r P_M^{(\vartheta)}$. This quadrature is depicted in Fig. 2 as is its action on a displaced squeezed state. Such orthogonalization is heralded by the detection of a single photon that occurs with probability $\Pr(h) = r^2 \langle (P_M^{(\vartheta)})^2 \rangle$, which is greater than zero for all physical states [31]. We also note here that for states with zero phase space mean, i.e., $\langle \psi | b | \psi \rangle = \langle \psi | b^\dagger | \psi \rangle = 0$, one can see that quanta subtraction or addition to the state $|\psi\rangle$ yields a state which is orthogonal to $|\psi\rangle$. Addition alone can orthogonalize all such states with a heralding probability of $r^2(\langle b^\dagger b \rangle + 1)/2$, whereas subtraction alone has a heralding probability of $(\frac{\theta}{2})^2 \langle b^\dagger b \rangle / 2$. We thus further note that the operations $b - \beta$ and $b^\dagger - \beta^*$ can orthogonalize all pure states with $\langle b \rangle = \beta$. These operations may be simpler to experimentally implement; however, they are less versatile, as complete information of the state's mean is required as opposed to the partial knowledge required by $\Upsilon_\perp$. Returning to Eq. (2), one can now form a superposition of orthogonalization and identity $\Upsilon_h = \mu/\sqrt{2} + \Upsilon_\perp$ to prepare a superposition of the initial state and an orthogonal state, i.e., a qubit, see Fig. 2(d).

A mechanical resonator is a stationary system that allows Υ_h to be conveniently performed at multiple times. Moreover, as the superposition weightings can be changed between applications, this provides considerable versatility for quantum state engineering and quantum control protocols. For instance, one could realize the protocol by Dakna *et al.* [32] to synthesize an arbitrary mechanical motional state. As another application, here we show that with N applications of Υ_h, one can transform the state $|\psi\rangle = \sum_n^N \psi_n |n\rangle$ into any target state $|\phi\rangle = \sum_n^N \phi_n |n\rangle$, i.e., *arbitrary quantum state transformation*. Our method uses only the subtraction and identity components of Υ_h [33] and proceeds in a manner similar to Ref. [32] and generalizes the scheme presented in Ref. [34]. Specifically, by applying $\Phi = \prod_{j=1}^N (\mu_j + \nu_j b)/\sqrt{2} = \sum_{i=0}^N C_i b^i$, where $\nu = \frac{\theta}{2} e^{-i\phi}$, to the state $|\psi\rangle$ one can obtain $|\phi\rangle$ provided that the set of coefficients C_i is such that $\sum_{i=0}^{N-n} C_i \psi_{i+n} \sqrt{(i+n)!/n!} = \phi_n$. Determining C_i can be readily achieved via matrix inversion, and a solution exists

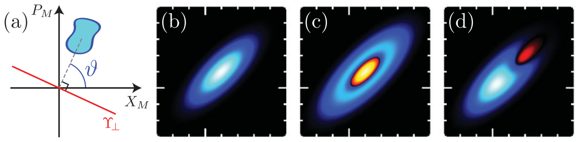

FIG. 2 (color). An equally weighted superposition of quanta addition and subtraction can orthogonalize any pure quantum state. (a) The orthogonalizer $\Upsilon_\perp$ is a quadrature perpendicular to the angle ϑ made by the input state's mean in phase space. The Wigner function (blue-cyan, positive; red-yellow, negative; larger ticks mark the origin and they increment by unity) of a displaced squeezed state (b), which has been orthogonalized (c). A superposition of an initial state with an orthogonal state may be prepared to create a qubit from any initial pure state. In (d) such a superposition is shown by action with $\Upsilon_\perp + |\mu| e^{-i\pi/2}/\sqrt{2}$, where $|\mu| = r$.

provided that $\psi_N \neq 0$ [29]. For the initial state having $\langle b \rangle = 0$, the probability of successful quantum state transformation is $\prod_{i=1}^{N}[(\frac{\theta}{2})_i^2 \langle b^\dagger b \rangle_i + |\mu_i|^2]/2$, where $\langle b^\dagger b \rangle_i$ is the phonon number expectation prior to the ith pulse. This probability may seem low; however, the experiment can readily be performed with a megahertz repetition rate using a ~100 MHz mechanical oscillator, and thus a practical number of heralding events can be attained in a reasonable time. Also, if the target state has a larger (smaller) dimension than the initial state, one can apply creation (annihilation) as many times as necessary in order to make the dimensions the same prior to using Φ.

An experimental approach.—There are numerous realizations of optomechanical systems and much progress has been made that can be built upon; the most pertinent being Refs. [23,35] where phonon addition and subtraction were realized as separate operations. Combining these operations into a coherent superposition can be achieved with the setup in Fig. 1(c). Here we present an alternative route to fulfill the requirements of our proposed scheme using a mechanical element with a bulk-acoustic-wave vibration that forms an end mirror of a Fabry-Perot cavity [36]. This configuration has the advantage that the cavity decay can be controlled independently of the mechanical properties, and such vibrational modes offer high mechanical resonance frequencies [37]. Moreover, simultaneous high reflectivity and high mechanical quality can be realized with multilayer crystalline reflectors [38]. A 40 μm diameter and several micrometer thick mirror has a mechanical resonance $\omega_M/2\pi = 200$ MHz with a 20 ng effective mass. With a finesse of 5×10^4, to achieve resolved sideband operation, i.e., $\omega_M/\kappa = 10$, a 75 μm cavity length can be used. For a drive laser with wavelength 1064 nm and a pulse duration of 100 mechanical periods, an optical power during the pulse of 1.3 mW is needed to achieve $r^2 = 0.01$. During the interaction the mechanical resonator also interacts with its thermal environment. To neglect the effects of environmental coupling we require that $\xi = (\bar{n}/Q)(\tau\omega_M/2\pi) \ll 1$, where $\bar{n}$ is the mechanical phonon occupation in thermal equilibrium and Q is the mechanical quality factor. For $Q = 10^5$ and a 100 mK bath, which can be readily achieved using dilution refrigeration, $\xi \simeq 10^{-2}$. Following the interaction the sideband needs to be separated from the drive field(s) prior to photon detection. For higher mechanical frequencies the filtering requirements simplify. However, it is possible to achieve sufficient filtering even for a 200 MHz mechanical frequency using an optical displacement and spectral filtering [39]. Realizing the displacement with optical fiber-based components, which provide excellent spatial mode matching, one can achieve an interferometric visibility of 99.99% that suppresses the drive by 10^4. The remaining drive can be further reduced by filtering with a cavity that has the same resonance frequency as the optomechanical cavity. To achieve a drive transmission 10^2 times smaller than sideband transmission, a filter cavity amplitude decay rate of 2 kHz is required [40]. We would also like to emphasize that our scheme is robust against optical loss, and inefficient detection as an optomechanically scattered photon that goes undetected does not trigger Υ_h; hence, the primary effect of loss is to merely reduce the heralding probability [41]. To characterize the mechanical motional state, as the parameter regime considered here is suited for the beamsplitter interaction, quantum state transfer of the mechanical motional state to the light [24,42] can be performed followed by optical homodyne tomography. This interaction following action(s) with Υ_h to the stationary mechanical element, also provides a route to prepare optical continuous variable qubits or to synthesize arbitrary quantum states of a traveling optical field.

Conclusions.—A superposition of quanta addition and subtraction can orthogonalize any pure continuous-variable quantum state with known angle made by the mean of the state's amplitude in phase space. Such a superposition in combination with a controllable amount of the identity operation provides extensive control for quantum state engineering and quantum information applications. For stationary systems it is convenient to apply this tool multiple times, which we have utilized to illustrate how to perform arbitrary quantum state transformation. As the interactions we have used are available in many of the facets of quantum optics [43], the tools we introduce can be realized in numerous physical systems.

We thank G. D. Cole, S. G. Hofer, and K. Hammerer for useful discussion. M. R. V. received support from a DOC fellowship of the Austrian Academy of Sciences and gratefully acknowledges the Royal Society. We thank support provided by the European Commission (Q-ESSENCE), the European Research Council (ERC QOM), the Austrian Science Fund (FWF) (START, SFB FOQUS), the Foundational Questions Institute, the John Templeton Foundation, and the Qatar National Research Fund (Grant No. NPRP 4-554-1-084).

---

[1] H. Bechmann-Pasquinucci and N. Gisin, Phys. Rev. A **59**, 4238 (1999); V. Bužek, M. Hillery, and R. F. Werner, Phys. Rev. A **60**, R2626 (1999); F. De Martini, V. Bužek, F. Sciarrino, and C. Sias, Nature (London) **419**, 815 (2002).
[2] V. Scarani, S. Iblisdir, N. Gisin, and A. Acin, Rev. Mod. Phys. **77**, 1225 (2005).
[3] L.-M. Duan and G.-C. Guo, Phys. Rev. Lett. **80**, 4999 (1998).
[4] F. Yan, T. Gao, and Z. Yan, arXiv:1203.0350.
[5] H. Jeong and M. S. Kim, Phys. Rev. A **65**, 042305 (2002).
[6] J. S. Neergaard-Nielsen, M. Takeuchi, K. Wakui, H. Takahashi, K. Hayasaka, M. Takeoka, and M. Sasaki, Phys. Rev. Lett. **105**, 053602 (2010).
[7] It is interesting to note that this method may also be adapted to spin-1/2 systems using a superposition of the raising and lowering operators; however, in this case one

requires knowledge of the phase between the two spin states thus rendering orthogonalization trivial.

[8] H. J. Kimble, Phys. Scr. **T76**, 127 (1998).

[9] J. M. Raimond, M. Brune, and S. Haroche, Rev. Mod. Phys. **73**, 565 (2001).

[10] D. Leibfried, R. Blatt, C. Monroe, and D. Wineland, Rev. Mod. Phys. **75**, 281 (2003).

[11] For an experiment that has generated such optical qubits and performed similar measurements, see, e.g., S. A. Babichev, J. Ries, and A. I. Lvovsky, Europhys. Lett. **64**, 1 (2003).

[12] S.-Y. Lee and H. Nha, Phys. Rev. A **82**, 053812 (2010).

[13] M. S. Kim, J. Phys. B **41**, 133001 (2008).

[14] A. Ourjoumtsev, R. Tualle-Brouri, J. Laurat, and P. Grangier, Science **312**, 83 (2006); J. S. Neergaard-Nielsen, B. Nielsen, C. Hettich, K. Mølmer, and E. Polzik, Phys. Rev. Lett. **97**, 083604 (2006); H. M. Chrzanowski, J. Bernu, B. Sparkes, B. Hage, A. Lund, T. Ralph, P. Lam, and T. Symul, Phys. Rev. A **84**, 050302 (R) (2011).

[15] V. Parigi, A. Zavatta, M. Kim, and M. Bellini, Science **317**, 1890 (2007); A. Zavatta, V. Parigi, M. S. Kim, H. Jeong, and M. Bellini, Phys. Rev. Lett. **103**, 140406 (2009).

[16] E. Bimbard, N. Jain, A. MacRae, and A. I. Lvovsky, Nat. Photonics **4**, 243 (2010).

[17] A. Ben-Kish *et al.*, Phys. Rev. Lett. **90**, 037902 (2003); M. Hofheinz, *et al.*, Nature (London) **459**, 546 (2009).

[18] A. D. O'Connell *et al.*, Nature (London) **464**, 697 (2010).

[19] J. D. Teufel, T. Donner, D. Li, J. W. Harlow, M. S. Allman, K. Cicak, A. J. Sirois, J. D. Whittaker, K. W. Lehnert, and R. W. Simmonds, Nature (London) **475**, 359 (2011).

[20] J. Chan, T. P. Mayer Alegre, A. H. Safavi-Naeini, J. T. Hill, A. Krause, S. Gröblacher, M. Aspelmeyer, and O. Painter, Nature (London) **478**, 89 (2011).

[21] S. Gröblacher, K. Hammerer, M. R. Vanner, and M. Aspelmeyer, Nature (London) **460**, 724 (2009); J. D. Teufel, D. Li, M. S. Allman, K. Cicak, A. J. Sirois, J. D. Whittaker, and R. W. Simmonds, Nature (London) **471**, 204 (2011); E. Verhagen, S. Deléglise, S. Weis, A. Schliesser, and T. J. Kippenberg, Nature (London) **482**, 63 (2012).

[22] A. H. Safavi-Naeini, J. Chan, J. Hill, T. Alegre, A. Krause, and O. Painter, Phys. Rev. Lett. **108**, 033602 (2012).

[23] K. C. Lee *et al.*, Science **334**, 1253 (2011).

[24] J. Zhang, K. Peng, and S. L. Braunstein, Phys. Rev. A **68**, 013808 (2003).

[25] S. Mancini, D. Vitali, and P. Tombesi, Phys. Rev. Lett. **90**, 137901 (2003); O. Romero-Isart, A. Pflanzer, M. Juan, R. Quidant, N. Kiesel, M. Aspelmeyer, and J. Cirac, Phys. Rev. A **83**, 013803 (2011); S. G. Hofer, W. Wieczorek, M. Aspelmeyer, and K. Hammerer, Phys. Rev. A **84**, 052327 (2011).

[26] T. J. Kippenberg and K. J. Vahala, Science **321**, 1172 (2008); F. Marquardt and S. M. Girvin, Physics **2**, 40 (2009); M. Aspelmeyer, S. Gröblacher, K. Hammerer, and N. Kiesel, J. Opt. Soc. Am. B **27**, A189 (2010).

[27] C. K. Law, Phys. Rev. A **51**, 2537 (1995).

[28] See, e.g., M. O. Scully and M. S. Zubairy, *Quantum Optics* (Cambridge University Press, Cambridge, England, 1997).

[29] See Supplemental Material at http://link.aps.org/supplemental/10.1103/PhysRevLett.110.010504 for further discussion on the effective unitary and arbitrary quantum state transformation.

[30] We remark here that one could alternatively use the setup by D. T. Pegg, L. S. Phillips, and S. M. Barnett, Phys. Rev. Lett. **81**, 1604 (1998), to introduce an amount of identity.

[31] A quadrature eigenstate can have $\langle (P_M^{(\vartheta)})^2 \rangle = 0$; however, this is not a physical state.

[32] M. Dakna, J. Clausen, L. Knöll, and D.-G. Welsch, Phys. Rev. A **59**, 1658 (1999).

[33] We note that our scheme cannot be used to transform a coherent state as quanta subtraction leaves this state unchanged.

[34] J. Fiurášek, R. García-Patrón, and N. J. Cerf, Phys. Rev. A **72**, 033822 (2005).

[35] K. C. Lee, B. J. Sussman, M. R. Sprague, P. Michelberger, K. F. Reim, J. Nunn, N. K. Langford, P. J. Bustard, D. Jaksch, and I. A. Walmsley, Nat. Photonics **6**, 41 (2012).

[36] A. G. Kuhn *et al.*, Appl. Phys. Lett. **99**, 121103 (2011).

[37] K. Børkje and S. M. Girvin, New J. Phys. **14**, 085016 (2012).

[38] G. D. Cole, I. Wilson-Rae, M. R. Vanner, S. Groblacher, J. Pohl, M. Zorn, M. Weyers, A. Peters, and M. Aspelmeyer, Proc. IEEE Micr. Elect., 847 (2010); G. D. Cole, S. Groblacher, K. Gugler, S. Gigan, and M. Aspelmeyer, Appl. Phys. Lett. **92**, 261108 (2008).

[39] Similar filtering arrangements were also considered by U. Akram, N. Kiesel, M. Aspelmeyer, and G. J. Milburn, New J. Phys. **12**, 083030 (2010); K. Børkje, A. Nunnenkamp, and S. M. Girvin, Phys. Rev. Lett. **107**, 123601 (2011).

[40] A ring cavity with a 4 m cavity perimeter can provide this required linewidth with the modest finesse of 2×10^4. Alternatively, two (or more) larger linewidth cavities can be used in series to provide the required filtering.

[41] For a given detection event, however, there is the possibility that a second photon was missed due to optical loss, which was due to a two-phonon operation. This poses no problem to our scheme as the drive fields are chosen here such that the probability of two-photon scattering is negligible.

[42] A. S. Parkins and H. J. Kimble, J. Opt. B **1**, 496 (1999).

[43] See, for example, K. Hammerer, A. S. Sørensen, and E. S. Polzik, Rev. Mod. Phys. **82**, 1041 (2010).

Supplementary Material - Quantum State Orthogonalization and a Toolset for Quantum Optomechanical Phonon Control

M. R. Vanner,[1, 2] M. Aspelmeyer,[1, 2] and M. S. Kim[3]

[1] *Vienna Center for Quantum Science and Technology (VCQ), Boltzmanngasse 5, A-1090 Vienna, Austria*
[2] *Faculty of Physics, University of Vienna, Boltzmanngasse 5, A-1090 Vienna, Austria*
[3] *QOLS, Blackett Laboratory, Imperial College London, SW7 2BW, United Kingdom*

(Dated: August 16, 2012)

A. Determining the Effective Unitary Interaction

Central to our discussion in the main text is the measurement operator Υ_h, which is used to describe the operation to the mechanical resonator via the optomechanical interaction and then single photon detection. $\Upsilon_h = \langle 1,0| U_{\text{eff}} |0,0\rangle$, where the ket is the initial state of light at the cavity resonance for the two orthogonal polarizations used, the bra describes a h-polarization photon detection with no v photon detection, and U_{eff} is the effective optomechanical interaction including the manipulations to the optical field made after interaction with the mechanical resonator. In this supplementary we provide a discussion how U_{eff} is obtained.

The time evolutions described in Eq. (2) of the main text are generated by the beam-splitter and two-mode-squeezing effective interaction Hamiltonians. In the former case a accumulates correlation with b and in the latter case a accumulates correlation with $b^\dagger$. For vacuum on the input of mode a, the expectation of the number operator in the output of mode a for the beam-splitter and two-mode-squeezing interactions are

$$\sin^2\tfrac{\theta}{2}\,\langle b^\dagger b\rangle, \quad \text{and} \quad \sinh^2 r\,\langle b b^\dagger\rangle,$$

respectively, where $\sin^2(\frac{\theta}{2})$ is the (intensity) reflectivity of the beam-splitter and r is the squeezing parameter. In the optomechanical scheme we have considered, the mean photon number scattered by the optomechanical interaction for the beam-splitter and two-mode-squeezing interactions are

$$\langle n_h\rangle = (1-e^{-2G_h\tau})\langle b_0^\dagger b_0\rangle, \text{ and } \langle n_v\rangle = (e^{2G_v\tau}-1)\langle b_0 b_0^\dagger\rangle,$$

respectively. For small $\frac{\theta}{2}$, r, and $G\tau$ we then have

$$\tfrac{\theta}{2} = \sqrt{2G_h\tau}, \quad \text{and} \quad r = \sqrt{2G_v\tau},$$

for the effective optomechanical beam-splitter and two-mode-squeezing parameters, respectively. It is noted here that computing the mean number output in mode b can also be performed to yield these parameters. As both the beam-splitter and two-mode-squeezing processes are driven simultaneously, we expect that the effective optomechanical unitary take the form $U_{\text{eff}} = \exp\left[-\frac{i}{\hbar}(H_{BS}+H_{SQ})\tau\right]$, where $H_{BS} \propto a^\dagger b + a b^\dagger$ and $H_{SQ} \propto ab + a^\dagger b^\dagger$ are the beam-splitter and two-mode-squeezing Hamiltonians respectively. To first order in the beam-splitter and squeezing parameters the effective unitary describing the cavity optomechanical interaction is then

$$U_{\text{eff}} = 1 + (\tfrac{\theta}{2} a_h^\dagger b e^{-i\phi} - r a_v^\dagger b^\dagger e^{i\varphi} - \text{H.c.}).$$

Finally, to obtain the effective unitary used for the measurement operator, the polarization manipulations to the optical fields, as discussed in the main text, must be performed.

B. Arbitrary Quantum State Transformation

In the main text we introduced a scheme for *arbitrary quantum state transformation* that generates a target state from a known input state. Here we further discuss our protocol and provide a specific quantum state transformation example.

The protocol works as follows. For a known initial state

$$|\psi\rangle = \sum_{n=0}^{N} \psi_n |n\rangle\,,$$

which has no excitation beyond N quanta (or has been approximated by truncation at this level), any target state of the form

$$|\phi\rangle = \sum_{n=0}^{N} \phi_n |n\rangle\,,$$

can be generated by applying a controllably weighted superposition of identity and subtraction N times, i.e.

$$\Phi = \prod_{j=1}^{N} (\mu_j + \nu_j b)/\sqrt{2} = \sum_{i=0}^{N} C_i b^i. \tag{B.1}$$

Applying this operation to the initial state we have

$$\Phi|\psi\rangle = \sum_{i=0}^{N}\sum_{k=0}^{N} C_i \psi_k \sqrt{\frac{k!}{(k-i)!}}\,|k-i\rangle\,,$$

where we have used $b|n\rangle = \sqrt{n}\,|n-1\rangle$.

The operation Φ is a non-unitary process and the unnormalized matrix elements of the state after application of Φ are

$$\langle n|\,\Phi\,|\psi\rangle = \sum_{i=0}^{N-n} C_i\,\psi_{i+n}\sqrt{\frac{(i+n)!}{n!}}. \tag{B.2}$$

The target state $|\phi\rangle$ is reached when $\langle n|\,\Phi\,|\psi\rangle = \phi_n$. Provided that $\psi_N \neq 0$ a set of coefficients C_i fulfilling $\langle n|\,\Phi\,|\psi\rangle = \phi_n$ can be determined via matrix inversion. Once a set of coefficients C_i is determined, a set of complex coefficients μ_j and ν_j that satisfy (B.1) can also readily be determined via matrix inversion.

We now provide a specific example of a quantum state transformation. Starting with an initial state $|\psi\rangle = |4\rangle$ we wish to reach the target state $|\phi\rangle = (|1\rangle + |4\rangle)/\sqrt{2}$. This target state can be reached with three applications of identity and subtraction. Solving (B.2) we find that $C_0 = \sqrt{24}C_3$ and $C_1 = C_2 = 0$. As identity has been used with each application we set $\mu = 1$ and obtain

$$\begin{aligned} \nu_1 + \nu_2 + \nu_3 &= 0, \\ \nu_1\nu_2 + \nu_1\nu_3 + \nu_2\nu_3 &= 0, \\ \nu_1\nu_2\nu_3\sqrt{24} &= 1. \end{aligned}$$

These equations can be readily solved exactly to provide the relative amplitudes between identity and subtraction to produce the target state. Numerical approximations to the solutions and the intermediate states during the quantum state transformation process are shown in Fig. B.1.

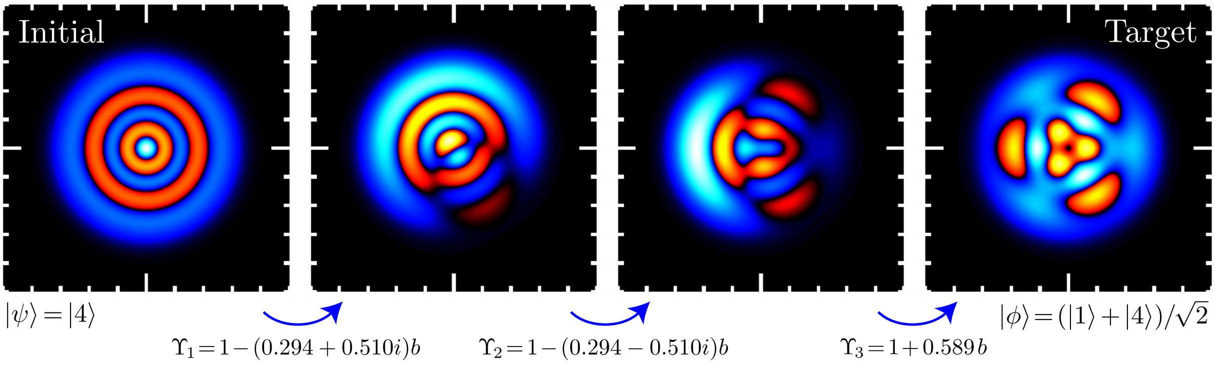

FIG. B.1: An example quantum state transformation. Shown are Wigner functions (blue-cyan: positive, red-yellow: negative, larger ticks mark the origin and they increment by unity) of an initial Fock state (left) to a target state (right). The target state is reached by a sequence of three operations of a controllably weighted superposition of identity and subtraction. The relative amplitude between identity and subtraction for each step is shown.

6 Pulsed Quantum Optomechanics

An important tool in the field of quantum optics is quantum state tomography (QST). When implemented, such a tool provides an experimentalist the ability to completely characterize a quantum state and thus explore the state's coherences and complimentary properties. QST has been utilized to characterize quantum mechanical behaviour in a number of physical systems such as light [32, 79], molecular vibration [80], trapped ions [81], and spin ensembles [82], however is yet to be experimentally realized for mechanical resonators.

In this theoretical work [83] we proposed a method for QST of a mechanical resonator utilizing a pulsed optomechanical interaction with optical pulses much shorter in duration than a mechanical period of motion. During the short interaction the mechanical position is essentially constant and so the back-action associated with the optomechanical interaction, i.e. the momentum transfer to the mechanical oscillator, does not evolve into mechanical position noise thus allowing for a back-action-evading measurement of the mechanical position. Such a measurement is not constrained by the standard quantum limit and so mechanical position features smaller than the ground state width can then be observed, which is vital for quantum state tomography. After mechanical state preparation at a known time, our QST protocol is to perform a pulsed position measurement after a controlled time of mechanical free harmonic evolution to sample that quadrature. This is then repeated numerous times for a large set of mechanical quadratures. Histograms of the measurement outcomes are then constructed and this set of histograms can then be used to determine a phase-space (quasi-)probability distribution by a numerical inversion process such as the inverse Radon transformation.

Performing a pulsed measurement of the mechanical position can significantly reduce the uncertainty of this observable below the width of a mechanical thermal state or even the ground state of motion. The conditional mechanical state, i.e. the state after updating the mechanical probability distribution, is therefore a squeezed state of motion that is an asymmetric Gaussian in phase-space with a narrow position width and large momentum width. The increase in knowledge of the mechanical state also results in a reduction in the entropy, which, as explained in the publication below, can be conveniently expressed in terms of effective thermal occupation. In addition to QST, we considered utilizing the pulsed measurements to conditionally prepare a low entropy squeezed state of motion and then a subsequent pulse can be used for QST, therefore providing a complete framework.

My specific contributions to this project were: in mid 2008 I conceived the research direction; I realised that a pulsed interaction could conditionally prepare a mechanical squeezed state of motion and I conceived the protocol for QST; I performed the calculations together with Igor Pikovski; and refined our ideas together with all co-authors. This was my first theoretical project and I tremendously enjoyed learning many of the mathematical tools of quantum optics.

To the best of our knowledge this work is the first quantum optomechanical protocol that uses a short optical pulses as defined in Fig. 1.2. This theoretical proposal formed the backbone for three further theoretical projects and we also completed a proof-of-principle experiment, which form the following four chapters.

Pulsed quantum optomechanics

M. R. Vanner[a,1], I. Pikovski[a], G. D. Cole[a], M. S. Kim[b], Č. Brukner[a,c], K. Hammerer[c,d], G. J. Milburn[e], and M. Aspelmeyer[a]

[a]Vienna Center for Quantum Science and Technology (VCQ), Faculty of Physics, University of Vienna, Boltzmanngasse 5, A-1090 Vienna, Austria; [b]QOLS (Quantum Optics and Laser Science Group), Blackett Laboratory, Imperial College London, London SW7 2BW, United Kingdom; [c]Institute for Quantum Optics and Quantum Information (IQOQI) of the Austrian Academy of Sciences, A-1090 Vienna and A-6020 Innsbruck, Austria; [d]Institute for Theoretical Physics and Albert Einstein Institute, University of Hannover, Callinstrasse 38, D-30167 Hannover, Germany; and [e]School of Mathematics and Physics, University of Queensland, Saint Lucia 4072, Australia

Edited by Mikhail Lukin, Harvard University, Cambridge, MA, and accepted by the Editorial Board July 21, 2011 (received for review April 1, 2011)

Studying mechanical resonators via radiation pressure offers a rich avenue for the exploration of quantum mechanical behavior in a macroscopic regime. However, quantum state preparation and especially quantum state reconstruction of mechanical oscillators remains a significant challenge. Here we propose a scheme to realize quantum state tomography, squeezing, and state purification of a mechanical resonator using short optical pulses. The scheme presented allows observation of mechanical quantum features despite preparation from a thermal state and is shown to be experimentally feasible using optical microcavities. Our framework thus provides a promising means to explore the quantum nature of massive mechanical oscillators and can be applied to other systems such as trapped ions.

optomechanics | quantum measurement | squeezed states

Coherent quantum mechanical phenomena, such as entanglement and superposition, are not apparent in the macroscopic realm. It is currently held that on large scales quantum mechanical behavior is masked by decoherence (1) or that quantum mechanical laws may even require modification (2–5). Despite substantial experimental advances, see for example ref. 6, probing this regime remains extremely challenging. Recently however, it has been proposed to utilize the precision and control of quantum optical fields in order to investigate the quantum nature of massive mechanical resonators by means of the radiation-pressure interaction (7–13). Quantum state preparation and the ability to probe the dynamics of mechanical oscillators, the most rigorous method being quantum state tomography, are essential for such investigations. These important elements have been experimentally realized for various quantum systems, e.g., light (14, 15), trapped ions (16, 17), atomic ensemble spin (18, 19), and intracavity microwave fields (20). By contrast, an experiment realizing both quantum state preparation and tomography of a mechanical resonator is yet to be achieved. Also, schemes that can probe quantum features without full tomography [e.g., (9, 10, 21)] are similarly challenging. In nanoelectromechanics, cooling of resonator motion and preparation of the ground state have been observed (22, 23) but quantum state reconstruction (24) remains outstanding. In cavity optomechanics significant experimental progress has been made towards quantum state control over mechanical resonators (11–13), which includes classical phase-space monitoring (25, 26), laser cooling close to the ground state (27, 28), and low noise continuous measurement of mechanically induced phase fluctuations (29–31). Still, quantum state preparation is technically difficult primarily due to thermal bath coupling and weak radiation-pressure interaction strength, and quantum state reconstruction remains little explored. Thus far, a common theme in proposals for mechanical state reconstruction is state transfer to and then read-out of an auxillary quantum system (32–35). This technique is a technically demanding approach and remains a challenge.

In this paper we introduce an optomechanical scheme that provides direct access to all the mechanical quadratures in order to obtain full knowledge about the quantum state of mechanical motion. This quadrature access is achieved by observing the distribution of phase noise of strong pulses of light at various times throughout a mechanical period. We show that the same experimental tools used for quantum state tomography can also be used for squeezed state preparation and state purification, which thus provides a complete experimental framework. Our scheme does not require "cooling via damping" (11–13) and can be performed within a single mechanical cycle thus significantly relaxing the technical requirements to minimize thermal contributions from the environment.

Using a pulsed interaction that is very short compared to the period of an oscillator to provide a back-action-evading measurement of position was introduced in the seminal contributions of Braginsky and coworkers (36, 37), where schemes for sensitive force detection were developed. In our work, the quantum nature of a mechanical resonator is itself the central object of investigation. Here, the pulsed interaction is used to provide an experimentally feasible means to generate and fully reconstruct quantum states of mechanical motion. The proposed experimental setup is shown in Fig. 1. A pulse of duration much less than the mechanical period is incident upon an optomechanical Fabry-Pérot cavity which we model as being single sided. Due to the entanglement generated during the radiation-pressure interaction, the optical phase becomes correlated with the mechanical position while the optical intensity imparts momentum to the mechanical oscillator. Time-domain homodyne detection (15) is then used to determine the phase of the field emerging from the cavity, and thus to obtain a measurement of the mechanical position. For each pulse, the measurement outcome P_L is recorded, which for Gaussian optical states has mean and variance

$$\langle P_L\rangle = \chi\langle X_M^{\mathrm{in}}\rangle, \qquad \sigma_{P_L}^2 = \sigma_{P_L^{\mathrm{in}}}^2 + \chi^2\sigma_{X_M^{\mathrm{in}}}^2, \tag{1}$$

respectively. X_M^{in} is the mechanical position quadrature immediately prior to the interaction and P_L^{in} describes the input phase of light. The position measurement strength χ is an important parameter in this work as it quantifies the scaling of the mechanical position information onto the light field. A derivation of Eq. **1** including an optimization of χ by determining the input pulse envelope to gain the largest cavity enhancement is provided in the *Appendix*.

In order to describe and quantify the pulse interaction and measurement we use the nonunitary operator Υ that determines the new mechanical state via $\rho_M^{\mathrm{out}} \propto \Upsilon\rho_M^{\mathrm{in}}\Upsilon^\dagger$. This operator is mechanical state independent and can be determined from the probability density of measurement outcomes

$$\Pr(P_L) = \mathrm{Tr}_M(\Upsilon^\dagger\Upsilon\rho_M^{\mathrm{in}}). \tag{2}$$

For pure optical input, it takes the form

Author contributions: M.R.V., I.P., G.D.C., M.S.K., Č.B., K.H., G.J.M., and M.A. designed research; M.R.V., I.P., G.D.C., M.S.K., Č.B., K.H., G.J.M., and M.A. performed research; and M.R.V., I.P., G.D.C., M.S.K., Č.B., K.H., G.J.M., and M.A. wrote the paper.

The authors declare no conflict of interest.

This article is a PNAS Direct Submission. M.L. is a guest editor invited by the Editorial Board.

Freely available online through the PNAS open access option.

[1]To whom correspondence should be addressed. E-mail: michael.vanner@univie.ac.at.

www.pnas.org/cgi/doi/10.1073/pnas.1105098108

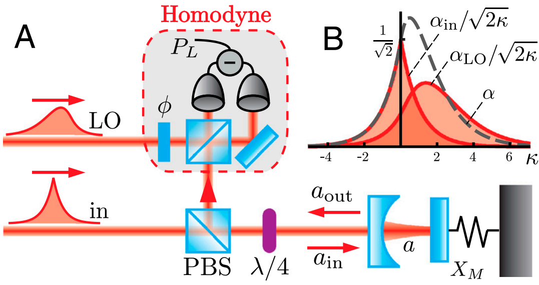

Fig. 1. (*A*) Schematic of the optical setup to achieve measurement based quantum state engineering and quantum state tomography of a mechanical resonator. An incident pulse (in) resonantly drives an optomechanical cavity, where the intracavity field *a* accumulates phase with the position quadrature X_M of a mechanical oscillator. The field emerges from the cavity (out) and balanced homodyne detection is used to measure the optical phase with a local oscillator pulse (LO) shaped to maximize the measurement of the mechanical position. (*B*) Scaled envelopes of the optimal input pulse, its corresponding intracavity field and the optimal local oscillator as computed in the *Appendix*.

$$\Upsilon = (\pi 2\sigma^2_{P_L^{\rm in}})^{-\frac{1}{4}} \exp\left[i\Omega X_M - \frac{(P_L - \chi X_M)^2}{4\sigma^2_{P_L^{\rm in}}}\right], \qquad [3]$$

where Ω quantifies the momentum transfer to the mechanics due to the pulse mean photon number. Υ can be readily understood by considering its action on a mechanical position wavefunction. This operator selectively narrows the wavefunction to a width scaling with χ^{-2} about a position which depends upon the measurement outcome. Moreover, the quantum non-demolition-like nature of Υ allows for back-action-evading measurements of X_M, i.e., the back-action noise imparted by the quantum measurement process occurs in the momentum quadrature only*. Other methods, such as the continuous variational measurement scheme (38), which has recently been considered for gravitational-wave detectors (39, 40), also allow for back-action-evading measurements. However, using short pulses offers a technically simpler route for quantum state tomography and is readily implementable, as will be discussed below.

In the following, we consider coherent drive i.e., $\sigma^2_{P_L^{\rm in}} = 1/2$. We first address the important challenge of how to experimentally determine the motional quantum state of a mechanical resonator. We then discuss how such a measurement can be used for quantum state preparation and finally we provide details for a physical implementation and analyze a thorough list of potential experimental limitations.

Mechanical Quantum State Tomography

Of vital importance to any experiment aiming to explore quantum mechanical phenomena is a means to measure coherences and complementary properties of the quantum system. Such measurement is best achieved by complete quantum state tomography, which despite being an important quantum optical tool has received very little attention for mechanical resonators†. Any measurement made on a single realization of a quantum state cannot yield sufficient information to characterize that quantum state. The essence of quantum state tomography is to make measurements of a specific set of observables over an ensemble of identically prepared realizations. The set is such that the measurement results provide sufficient information for the quantum state to be uniquely determined. One such method is to measure the marginals $\langle X|e^{-i\theta n}\rho e^{i\theta n}|X\rangle$, where n is the number operator, for all phase-space angles θ, see refs. 14, 15, 42 and e.g., ref. 43.

Our scheme provides a means for precision measurement of the mechanical quadrature marginals, thus allowing the mechanical quantum state to be determined. Specifically, given a mechanical state $\rho_M^{\rm in}$, harmonic evolution of angle $\theta = \omega_M t$ provides access to all the quadratures of this mechanical quantum state which can then be measured by a subsequent pulse. Thus, reconstruction of any mechanical quantum state can be performed. The optical phase distribution Eq. **2**, including this harmonic evolution, becomes

$$\Pr(P_L) = \int \frac{\mathrm{d}X_M}{\sqrt{\pi}} e^{-(P_L - \chi X_M)^2} \langle X_M|e^{-i\theta n}\rho_M^{\rm in} e^{i\theta n}|X_M\rangle, \qquad [4]$$

which is a convolution between the mechanical marginal of interest and a kernel that is dependent upon χ and the quantum phase noise of light. The effect of the convolution is to broaden the marginals and to smooth any features present.

Let us consider the specific example of a mechanical resonator in a superposition of two coherent states, i.e., $|\psi_\delta\rangle \propto |i\delta\rangle + |-i\delta\rangle$. The X_M marginal of this mechanical Schrödinger-cat state contains oscillations on a scale smaller than the ground state. The convolution scales the amplitude of these oscillations by $\exp(-\frac{2\delta^2}{\chi^2+1})$ and thus for small χ they become difficult to resolve in the optical phase noise distribution. Shown in Fig. 2 are marginals of the mechanical state $|\psi_\delta\rangle$ and the optical phase distributions that would be observed according to Eq. **4**. Scaling the phase distribution by using the variable P_L/χ provides an approximation to the mechanical marginals, which becomes more accurate with increasing χ and may even show the interference features in a superposition state. Indeed, the limiting case of infinite χ corresponds to a von-Neumann projective measurement of the mechanical position, such that the distribution obtained for P_L/χ becomes identical to the mechanical marginals. However, *the mechanical marginals can be recovered even for small measurement strength* χ. This recovery is achieved as follows: First, by fixing the length of the cavity the optical phase distribution can be observed without contributions from mechanical position fluctuations. This rigidity allows measurement of the convolution kernel for a particular χ (determined by the proper-

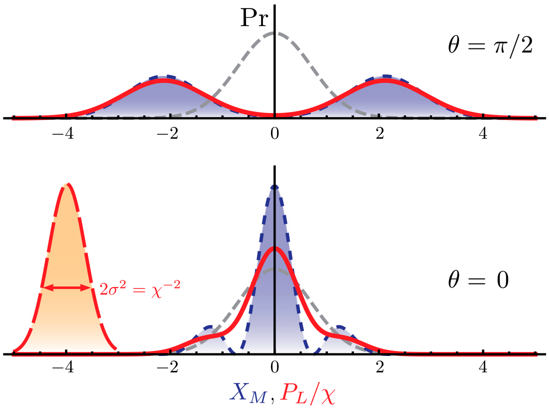

Fig. 2. The scheme presented here provides an experimentally feasible means to obtain direct access to the marginals of a quantum state of a mechanical resonator. Shown are complementary quadrature marginals of the mechanical coherent state superposition $|\psi_\delta\rangle \propto |i\delta\rangle + |-i\delta\rangle$, for $\delta = 1.5$ (blue dashed lines with fill, plotted with X_M). The mechanical ground state is shown for comparison in gray dashed lines. The two population components are seen for the quadrature angle $\theta = \pi/2$ and the quantum interference fringes for $\theta = 0$. A coherent optical pulse is used to probe the mechanical state where its phase quadrature becomes the convolution between the intrinsic phase noise, with variance scaling with χ^{-2}, and the mechanical marginal (red solid lines, plotted with P_L/χ where $\chi = 2$), see Eq. **4**. The convolution kernel can be observed by using a fixed length cavity, shown in the $\theta = 0$ plot (red dashed line with fill, fixed length with $X_M = -4$), which allows for accurate recovery of the mechanical marginals even for a weak measurement strength χ.

---

*No mechanical position noise is added as our measurement operator commutes with the mechanical position. This is because the mechanical evolution can be neglected during the short optomechanical interaction.

†During the submission process of this manuscript a scheme to perform tomography of the motional state of a trapped particle using a time-of-flight expansion was proposed (41).

ties of the mechanical resonator of interest, cavity geometry, and pulse strength, see Eq. **14**). With χ and the kernel known one can then perform deconvolution to determine the mechanical marginals. The performance of such a deconvolution is limited by experimental noise in the calibration of χ and the measurement of $\Pr(P_L)$. However, it is expected that these quantities can be accurately measured as quantum noise limited detection is readily achieved.

Mechanical Quantum State Engineering and Characterization

We now discuss how the measurement affects the mechanical state. First, we consider Υ acting on a mechanical coherent state $|\beta\rangle$. By casting the exponent of Υ in a normal ordered form, one can show that the resulting mechanical state, which is conditioned on measurement outcome P_L, is $\mathcal{N}_\beta\Upsilon|\beta\rangle = S(r)D(\mu_\beta)|0\rangle$. Here, $\mathcal{N}_\beta$ is a β-dependent normalization, D is the displacement operator for $\mu_\beta = (\sqrt{2}\beta + i\Omega + \chi P_L)/\sqrt{2(\chi^2+1)}$, and S is the squeezing operator, which yields the position width $2\sigma_{X_M}^2 = e^{-2r} = (\chi^2+1)^{-1}$.

In most experimental situations, the initial mechanical state is in a thermal state $\rho_{\bar{n}} = \frac{1}{\pi\bar{n}}\int d^2\beta e^{-|\beta|^2/\bar{n}}|\beta\rangle\langle\beta|$, quantified by its average phonon occupation number $\bar{n}$. The marginals of the resulting state after the action of Υ are

$$\langle X_M|e^{-i\theta n}\Upsilon\rho_{\bar{n}}\Upsilon^\dagger e^{i\theta n}|X_M\rangle \propto \exp\left[-\frac{(X_M - \langle X_M^\theta\rangle)^2}{2\sigma_\theta^2}\right], \qquad [5]$$

where

$$\langle X_M^\theta\rangle = \frac{\chi P_L}{\chi^2 + \frac{1}{1+2\bar{n}}}\cos(\theta) - \Omega\sin(\theta),$$

$$\sigma_\theta^2 = \frac{1}{2}\frac{\cos^2(\theta)}{\chi^2 + \frac{1}{1+2\bar{n}}} + \frac{1}{2}(\chi^2 + 1 + 2\bar{n})\sin^2(\theta) \qquad [6]$$

are the mean and variance of the resulting conditional state, respectively. For large initial occupation (provided thermal fluctuations are negligible during the short interaction), the resultant position quadrature of the mechanics has mean $\langle X_M^{\theta=0}\rangle \simeq P_L/\chi$ and width $2\sigma_{\theta=0}^2 \simeq \chi^{-2}$. Thus, squeezing in the X_M quadrature below the ground state is obtained when $\chi > 1$ and is *independent of the initial thermal occupation of the mechanics.* We have thus shown how the remarkable behavior of quantum measurement (also used in refs. 18–20, 44–47) can be experimentally applied to a mechanical resonator for quantum state preparation.

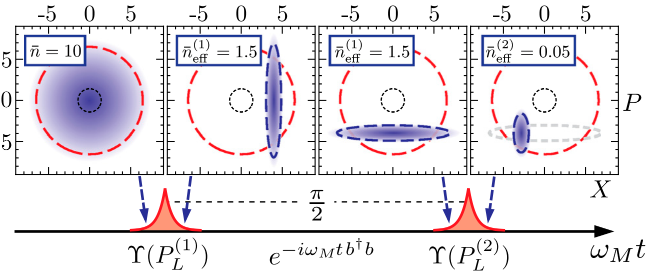
-5
0
5
-5
0
5
-5
0
5
-5
0
5
5
0
-5
$\bar{n} = 10$
$\bar{n}_{\text{eff}}^{(1)} = 1.5$
$\bar{n}_{\text{eff}}^{(1)} = 1.5$
$\bar{n}_{\text{eff}}^{(2)} = 0.05$
P
X
$\frac{\pi}{2}$
$\Upsilon(P_L^{(1)})$
$e^{-i\omega_M t\, b^\dagger b}$
$\Upsilon(P_L^{(2)})$
$\omega_M t$

Fig. 3. Wigner functions of the mechanical state (above) at different times (indicated by arrows) during the experimental protocol (below). From left: Starting with an initial thermal state $\bar{n} = 10$, (this is chosen to ensure the figure dimensions are reasonable,) a pulsed measurement is made with $\chi = 1.5$ and outcome $P_L^{(1)} = 4\chi$ obtained, which yields an X_M quadrature squeezed state. The mechanical state evolves into a P_M quadrature squeezed state following free harmonic evolution of 1/4 of a mechanical period prior to a second pulse with outcome $P_L^{(2)} = -3\chi$ yielding the high-purity mechanical squeezed state. The effective thermal occupation of the mechanical states during the protocol is indicated. The final state's occupation can be reduced below unity even for large initial occupation, see Eq. **7** of the main text. Dashed lines indicate the 2σ-widths and the dotted lines show the ground state ($\bar{n} = 0$) for comparative purposes. The displacement Ω is not shown.

There is currently significant interest in the preparation of low entropy states of mechanical resonators as a starting point for quantum experiments, e.g., refs. 22, 23, 27, 28. The two main methods being pursued in optomechanics (11–13) are "passive cooling" which requires the stable operation of a (usually cryogenically compatible) high-finesse cavity, and "active cooling" which requires precision measurement and feedback. Closer in spirit to the latter, our pulsed measurement scheme provides a third method to realize high-purity states of the mechanical resonator. We quantify the state purity after measurement via an effective mechanical thermal occupation $\bar{n}_{\text{eff}}$, which we define through $1 + 2\bar{n}_{\text{eff}} = \sqrt{4\sigma_{\theta=0}^2\sigma_{\theta=\pi/2}^2}$. When acting on an initial thermal state, the measurement dramatically reduces uncertainty in the X_M quadrature, but leaves the thermal noise in the P_M quadrature unchanged: use of Eq. **6** for $\bar{n} \gg 1$ yields $\bar{n}_{\text{eff}}^{(1)} \simeq \sqrt{\bar{n}/2\chi^2}$. The purity can be further improved by a second pulse, which is maximized for pulse separation $\theta = \omega_M t = \pi/2$, where the initial uncertainty in the momentum becomes the uncertainty in position. Such a sequence of pulses[‡] is represented in Fig. 3, where the resulting state was obtained akin to Eq. **5**. The effective occupation of the final state after two pulses is

$$\bar{n}_{\text{eff}}^{(2)} \simeq \frac{1}{2}\left(\sqrt{1 + \frac{1}{\chi^4}} - 1\right), \qquad [7]$$

which is also independent of initial occupation. For $\chi > 1$, $\bar{n}_{\text{eff}}^{(2)}$ is well below unity and therefore this scheme can be used as an alternative to "cooling via damping" for mechanical state purification.

Following state preparation, one can use a subsequent "read-out" pulse after an angle of mechanical free evolution θ to perform tomography. During state preparation however, the random measurement outcomes will result in random mechanical means Eq. **6**. This randomness can be overcome by recording and utilizing the measurement outcomes. One can achieve unconditional state preparation with use of appropriate displacement prior to the read-out pulse. Or, use postselection to analyze states prepared within a certain window. Alternatively, one may compensate during data analysis by appropriately adjusting each measurement outcome obtained during read-out. We now look at the latter option and consider a Gaussian mechanical state prepared by a prior pulsed measurement. The position distribution has variance σ^2 to be characterized and has a known mean $\langle X_M^{(p)}\rangle$, which is dependent upon the random measurement outcome. The read-out pulse will then have the distribution $\Pr(P_L) \propto \exp[(-(P_L - \chi\langle X_M^{(p)}\rangle)^2)/(1 + \chi^2 2\sigma^2)]$. For each read-out pulse, by taking $P_L|_p = P_L - \chi\langle X_M^{(p)}\rangle$ one can obtain the conditional variance $\sigma_{P_L|_p}^2$ for all θ to characterize the noise of the prepared Gaussian state. We note that this concept of compensating for a random but known mean can also be used to characterize non-Gaussian states.

Experimental Feasibility

We now provide a route for experimental implementation, discussing potential limitations and an experimentally feasible parameter regime. To ensure that the interaction time be much less than mechanical time scales the cavity decay rate κ must be much larger than the mechanical frequency. To this end, we consider the use of optical microcavities operating at $\lambda = 1{,}064$ nm, length 4λ and finesse of 7,000, which have an amplitude decay rate $\kappa/2\pi \simeq 2.5$ GHz. Such short cavity devices incorporating a micromechanical element as one of the cavity mirrors have previously been fabricated for tunable optical filters, vertical-cavity surface-emitting lasers and amplifiers (see for example ref. 50), but are yet to be considered for quantum optomechanical applications. Typically, these devices employ plane-parallel geometries, which places a severe constraint on the minimum lateral dimensions of the suspended mirror structure in order to minimize diffraction losses (51). Geometries using curved mirrors are required to reduce diffraction losses for the practical realization of high-finesse cavities. Presently, all realizations use a curved suspended mirror, see e.g., refs. 52, 53. However, in order to allow for enhanced freedom in the construction of the mechanical resonator, particularly with respect to the development of ultra-low loss mechanical devices (54), a flat suspended mirror is desired. In Fig. 4 our proposed fabrication procedure for such a device is shown. The small-mode-volume cavity considered here provides the bandwidth necessary to accommodate the short optical pulses and additionally offers a large optomechanical coupling rate. One technical challenge associated with these microcavities is fabrication with sufficient tolerance to achieve the desired optical resonance (under the assumption of a limited range of working wavelength), however this can be overcome by incorporating electrically controlled tunability of the cavity length (50, 52, 53).

[‡] We note that strong squeezing of an oscillator can also be achieved by using rapid modifications to the potential at quarter period intervals (48). However, we would like to emphasize that the squeezing we are discussing here does not arise from a parametric process, see e.g., ref. 49, rather it is due to the nonunitary action of measurement.

For a mechanical resonator with eigenfrequency $\omega_M/2\pi =$ 500 kHz and effective mass $m = 10$ ng, the mechanical ground-state size is $x_0 = \sqrt{\hbar/m\omega_M} \simeq 1.8$ fm and optomechanical coupling proceeds at $g_0/2\pi = \omega_c(x_0/\sqrt{2}L)/2\pi \simeq 86$ kHz, where ω_c is the mean cavity frequency and L is the mean cavity length. The primary limitation in measurement strength is the optical intensity that can be homodyned before photodetection begins to saturate. Using pulses of mean photon number $N_p = 10^8$, which can be homodyned, yields $\Omega \simeq 10^4$ for the mean momentum transfer[§] and $\chi \simeq 1.5$. For this χ, the action of a single pulse on a large thermal state reduces the mechanical variance to $\sigma^2_{X_M} \simeq 0.2$, i.e., less than half the width of the ground state. With a second pulse after mechanical evolution the effective occupation [7] is $\bar{n}^{(2)}_{\text{eff}} \simeq 0.05$.

In order to observe mechanical squeezing, i.e., $\sigma^2_{X_M} < 1/2$, the conditional variance must satisfy $\sigma^2_{P_L|_p} < \sigma^2_{P_L^{\text{in}}} + \chi^2/2$, where additional noise sources that do not affect the mechanical state, e.g., detector noise, can be subsumed into $\sigma^2_{P_L^{\text{in}}}$. It is therefore necessary to have an accurate experimental calibration of χ to quantify the mechanical width. (Similarly, Ω must also be accurately known to determine the conditional mean, see Eq. **6**). This calibration can be performed in the laboratory as follows: For a fixed length cavity and a given pulse intensity, the length of the cavity is adjusted by a known amount (by a calibrated piezo for example) and the proportionality between the homodyne measurement outcomes and the cavity length is determined. The pulses are then applied to a mechanical resonator and χ is determined with knowledge of x_0 of the resonator. With χ known Ω can then also be measured by observing the displacement of the mechanical state after one-quarter of a period.

Finally we discuss practical limitations. Firstly, finite mechanical evolution during the interaction decreases the back-action-evading nature of the measurement, which is described in the *Appendix*. Such evolution is not expected to be a severe limitation in the proposed implementation considered here as $\omega_M/\kappa \simeq 10^{-4}$. Secondly, the optical measurement efficiency η, affected by optical loss, inefficient detection, and mode mismatch, yields a reduced measurement strength $\chi \to \sqrt{\eta}\chi$. And thirdly, in many situations coupling to other mechanical vibrational modes is expected. This coupling contributes to the measurement outcomes and yields a spurious broadening of the tomographic results for the mode of interest. In practice however, one can minimize these contributions by engineering mechanical devices with high effective masses for the undesired modes and tailoring the intensity profile of the optical spot to have good overlap with a particular vibrational profile (55).

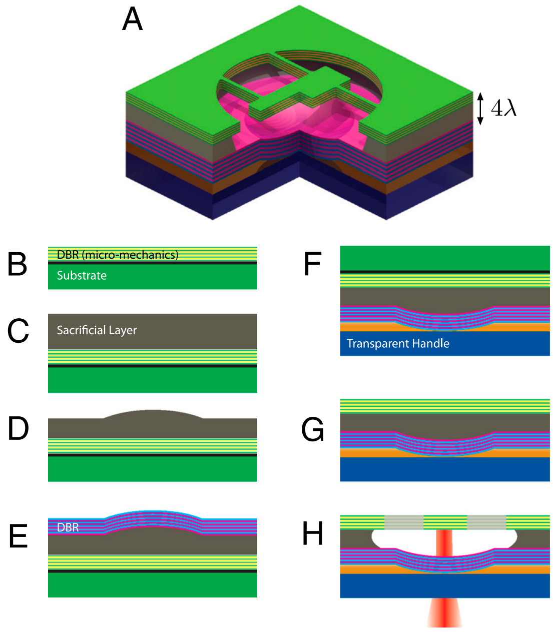

Fig. 4. Our proposed design and fabrication procedure for high-finesse optomechanical microcavities: Using microcavities provides optomechanical coupling rates many orders of magnitude larger than current millimeter or centimeter length scale implementations of optomechanical Fabry-Pérot cavities and can provide sufficient radiation-pressure interaction to resolve the small scale quantum properties of the mechanical resonator. (*A*) Cross-sectional view with a quarter of the device removed. Uppermost (colored green) is the mechanical resonator supported by auxiliary beams as was considered in ref. 54. The optical field is injected into the device from below through a transparent handle (colored blue) and the curved rigid input mirror (colored pink) and then resonates in the vacuum-gap between this and the mechanical device before being retroreflected. The design is a layered structure, fabricated in the following steps: (*B*) The base consists of a high-reflectivity distributed Bragg reflector (DBR) and an etch stop layer deposited on a suitable handle substrate. (*C*) First, a sacrificial film is deposited atop the DBR. (*D*) Next, a microlens pattern is transferred into the sacrificial layer through a reflow and reactive ion etching process. The radius of curvature of this structure is designed to match the phase front of the optical mode to minimize diffraction loss. (*E*) Following the microlens fabrication process a high reflectivity dielectric DBR is deposited over the sample surface. (*F*) The structure is then flipped and bonded to a transparent handle using a suitable low-absorption adhesive (e.g., spin on glass or UV-curable epoxy). (*G*) After mounting, the original growth substrate and etch stop are removed via chemo-mechanical etching. (*H*) Finally, the mechanical resonator is patterned and subsequently released via selective removal of the underlying sacrificial film. We remark that these integrated structures provide a platform for "on-chip" hybridization with other quantum systems.

Coupling to a Thermal Bath

For our tomography scheme the mechanical quantum state must not be significantly perturbed during the time scale ω_M^{-1}. To estimate the effect of the thermal bath following state preparation we consider weak and linear coupling to a Markovian bath of harmonic oscillators. For this model, assuming no initial correlations between the mechanics and the bath, the rethermalization scales with $\bar{n}\gamma_M$, where γ_M is the mechanical damping rate. It follows that an initially squeezed variance $(\chi > 1)$ will increase to $1/2$ on a time scale

$$\tau = \frac{Q}{\bar{n}\omega_M}\frac{1}{2}\left(1 - \frac{1}{\chi^2}\right). \qquad [8]$$

[§] This momentum is comparable to the width of a thermal state, i.e., $\Omega/\sqrt{\bar{n}} < 10$ for room temperature. Thus the mechanical motion remains harmonic.

Thus, for the parameters above and mechanical quality $Q = \omega_M/\gamma_M \simeq 10^5$ a temperature $T \lesssim 1$ K is required for the observation of squeezing during one mechanical period.

The state purification protocol, as shown in Fig. 3, is affected by rethermalization between the two pulsed measurements. This thermal process increases the effective thermal occupation and [**7**] is modified to

$$\bar{n}_{\mathrm{eff}}^{(2)}(T) \simeq \frac{1}{2}\left(\sqrt{1+\frac{1}{\chi^4}+\frac{\pi\bar{n}}{Q\chi^2}}-1\right). \qquad \textbf{[9]}$$

For the above system parameters $\bar{n}_{\mathrm{eff}}^{(2)}(T = 1\ \mathrm{K}) \simeq 0.15$. Thus, mechanical state purification by measurement is readily attainable even at a modest bath temperature.

Moreover, we note that the position measurements of this scheme can be used to probe open system dynamics and thus provide an empirical means to explore decoherence and bath coupling models (56).

Conclusions

We have described a scheme to overcome the current challenge of quantum state reconstruction of a mechanical resonator, which provides a means to explore quantum mechanical phenomena on a macroscopic scale. Our experimental protocol allows for state purification, remote preparation of a mechanical squeezed state, and direct measurements of the mechanical marginals for quantum state reconstruction, thus providing a complete experimental framework. The experimental feasibility has been analyzed and we have shown that with the use of optomechanical microcavities this scheme can be readily implemented. The optomechanical entanglement generated by the pulsed interaction may also be a useful resource for quantum information processing. Moreover, the framework we have introduced can be built upon for further applications in quantum optomechanics and can be generalized to other systems, such as nanoelectromechanics and superconducting resonators, or used with dispersive interaction to study the motional state of mechanical membranes, trapped ions, or particles in a cavity.

Appendix

Model. The intracavity optomechanical Hamiltonian in the rotating frame at the cavity frequency is

$$H = \hbar\omega_M b^\dagger b - \hbar g_0 a^\dagger a(b + b^\dagger), \qquad \textbf{[10]}$$

where a (b) is the optical (mechanical) field operator. The cavity field accumulates phase in proportion to the mechanical position and is driven by resonant radiation via the equation of motion

$$\frac{\mathrm{d}a}{\mathrm{d}t} = ig_0(b + b^\dagger)a - \kappa a + \sqrt{2\kappa}a_{\mathrm{in}}, \qquad \textbf{[11]}$$

where κ is the cavity decay rate and a_{in} describes the optical input including drive and vacuum. During a pulsed interaction of time scale $\kappa^{-1} \ll \omega_M^{-1}$ the mechanical position is approximately constant. This constancy allows decoupling of Eq. **11** from the corresponding mechanical equation of motion and during the short interaction we have $\mathrm{d}b/\mathrm{d}t \simeq ig_0 a^\dagger a$, where we neglect the mechanical harmonic motion, mechanical damping, and noise processes. We write $a_{\mathrm{in}}(t) = \sqrt{N_p}\alpha_{\mathrm{in}}(t) + \tilde{a}_{\mathrm{in}}(t)$, where $\alpha_{\mathrm{in}}(t)$ is the slowly varying envelope of the drive amplitude with $\int \mathrm{d}t\alpha_{\mathrm{in}}^2 = 1$ and N_p is the mean photon number per pulse and similarly $a = \sqrt{N_p}\alpha(t) + \tilde{a}(t)$. Neglecting $ig_0(b + b^\dagger)\tilde{a}$ and approximating α as real, Eq. **11** becomes the pair of linear equations:

$$\frac{\mathrm{d}\alpha}{\mathrm{d}t} = \sqrt{2\kappa}\alpha_{\mathrm{in}} - \kappa\alpha, \qquad \textbf{[12]}$$

$$\frac{\mathrm{d}\tilde{a}}{\mathrm{d}t} = ig_0\sqrt{N_p}(b + b^\dagger)\alpha + \sqrt{2\kappa}\tilde{a}_{\mathrm{in}} - \kappa\tilde{a}. \qquad \textbf{[13]}$$

After solving for $\tilde{a}(t)$, the output field is then found by using the input-output relation $\tilde{a}_{\mathrm{out}} = \sqrt{2\kappa}\tilde{a} - \tilde{a}_{\mathrm{in}}$.

The mechanical position and momentum quadratures are $X_M = (b + b^\dagger)/\sqrt{2}$ and $P_M = i(b^\dagger - b)/\sqrt{2}$, respectively, the cavity (and its input/output) quadratures are similarly defined via $\tilde{a}$ ($\tilde{a}_{\mathrm{in}}/\tilde{a}_{\mathrm{out}}$). The statistics of the optical amplitude quadrature are unaffected by the interaction, however, the phase quadrature contains the phase dependent upon the mechanical position. The output phase quadrature emerging from the cavity is $P_L^{\mathrm{out}}(t) = \frac{g_0}{\kappa}\sqrt{N_p}\varphi(t)X_M^{\mathrm{in}} + 2\kappa e^{-\kappa t}\int_{-\infty}^{t}\mathrm{d}t' e^{\kappa t'}P_L^{\mathrm{in}}(t') - P_L^{\mathrm{in}}(t)$, where $\varphi(t) = (2\kappa)^{\frac{3}{2}}e^{-\kappa t}\int_{-\infty}^{t}\mathrm{d}t' e^{\kappa t'}\alpha(t')$ describes the accumulation of phase, X_M^{in} is the mechanical position prior to the interaction, and the last two terms are the input phase noise contributions. P_L^{out} is measured via homodyne detection, i.e., $P_L = \sqrt{2}\int \mathrm{d}t\alpha_{\mathrm{LO}}(t)P_L^{\mathrm{out}}(t)$. To maximize the measurement of the mechanical position the local oscillator envelope is chosen as $\alpha_{\mathrm{LO}}(t) = \mathcal{N}_\varphi\varphi(t)$, where $\mathcal{N}_\varphi$ ensures normalization. The contribution of X_M^{in} in P_L scales with $\chi = \sqrt{2}\frac{1}{\mathcal{N}_\varphi}\frac{g_0}{\kappa}\sqrt{N_p}$, which quantifies the mechanical position measurement strength. The mean and variance of P_L are given in Eq. **1** for pure Gaussian optical input and together with Ω and Eq. **2** are used to determine Υ, as given in Eq. **3**. We have thus arrived, for our physical setting, at an operator which is known from generalized linear measurement theory (see for example ref. 57). Also, we note that Eq. **3** is equivalent to $\Upsilon = e^{i\Omega X_M}\langle P_L|e^{i\chi X_L X_M}|0\rangle$, though the nonunitary process of cavity filling and decay is not explicit. We also remark that the construction of Υ can be readily generalized to include non-Gaussian operations.

The maximum χ is obtained for the input drive $\alpha_{\mathrm{in}}(t) = \sqrt{\kappa}e^{-\kappa|t|}$. This maximization can be seen by noting that $\mathcal{N}_\varphi^{-2} = \int \mathrm{d}t\varphi^2(t)$, which in Fourier space is $\mathcal{N}_\varphi^{-2} \propto \int \mathrm{d}\omega(\omega^2 + \kappa^2)^{-2}|\alpha_{\mathrm{in}}(\omega)|^2$. Hence, for such cavity-based measurement schemes, the optimal drive has Lorentzian spectrum. This drive, $\alpha(t)$ obtained from Eq. **12** and the local oscillator are shown in Fig. 1*B*. The resulting optimal measurement strength is given by

$$\chi = 2\sqrt{5}\frac{g_0}{\kappa}\sqrt{N_p}, \qquad \textbf{[14]}$$

and the mean momentum transfer due to α^2 is $\Omega = \frac{3}{\sqrt{2}}\frac{g_0}{\kappa}N_p$.

We note that this optimization of the driving field may also be applied to cavity-enhanced pulsed measurement of the spin of an atomic ensemble (18, 19, 58) or the coordinate of a trapped ion/particle (59–61). Particularly in the latter case, this approach will broaden the repertoire of measurement techniques available and may lead to some interesting applications.

Finite Mechanical Evolution During Interaction. In the model used above we have assumed that the mechanical position remains constant during the pulsed optomechanical interaction. Including finite mechanical evolution, the intracavity field dynamics Eq. **13** must be determined simultaneously with the mechanical dynamics. In the mechanical rotating frame with the conjugate quadratures $\overline{X}_M$,$\overline{P}_M$ these dynamics are solved to first order in ω_M/κ resulting in the input-output relations:

$$\overline{P}_M^{\mathrm{out}} = \overline{P}_M^{\mathrm{in}} + \Omega + \mathcal{N}_1\chi X_{C1},$$

$$\overline{X}_M^{\mathrm{out}} = \overline{X}_M^{\mathrm{in}} - \frac{\omega_M}{\kappa}\xi_1\Omega - \frac{\omega_M}{\kappa}\chi\mathcal{N}_2 X_{C2},$$

$$P_L = P_L^{\mathrm{in}} + \chi(\overline{X}_M^{\mathrm{in}} + \frac{\omega_M}{\kappa}\xi_2\overline{P}_M^{\mathrm{in}}) + \chi\frac{\omega_M}{\kappa}\xi_3\Omega + \chi^2\frac{\omega_M}{\kappa}\mathcal{N}_3 X_{C3}, \textbf{[15]}$$

where P_L still represents the measurement outcome, $\mathcal{N}_{1,2,3}$ and $\xi_{1,2,3}$ are input drive-dependent dimensionless parameters of order unity, the former normalizing the nonorthogonal amplitude quadrature temporal modes $X_{C1,2,3}$. The main effects of the finite mechanical evolution can be seen in P_L. (*i*) The mechanical quadrature measured has been rotated, which in terms of the nonrotating quadratures is $\widetilde{X}_M \simeq X_M + \frac{\omega_M}{\kappa}\xi_2 P_M$. Such a rotation poses no principle limitation to our scheme however this must be taken into account for the measurement of a particular mechanical quadrature. (*ii*) Each pulsed measurement now has a nonzero mean proportional to Ω. This mean can be experimentally characterized and appropriately subtracted from the outcomes. (*iii*) P_L now includes a term proportional to the optical amplitude noise. This term decreases the back-action evading quality of the measurement and has arisen due to mechanical momentum noise gained from the optical amplitude quadrature evolving into position noise. The conditional variance of the rotated mechanical quadrature including these effects, for large initial occupation, is

$$\sigma^2_{\tilde{X}_M} \simeq \frac{1}{2}\left[\frac{1}{\chi^2} + \zeta^2\chi^2\left(\frac{\omega_M}{\kappa}\right)^2\right], \qquad [16]$$

where ζ is another drive-dependent parameter of order unity. The two competing terms here give rise to a minimum variance of $\zeta\omega_M/\kappa$ when $\chi^2 = \kappa/(\zeta\omega_M)$. Experimentally reasonable values of χ will lie much below this optimum point, however, as $\kappa \gg \omega_M$ for the parameters we consider, the broadening due to finite evolution is small and strong squeezing can be achieved.

ACKNOWLEDGMENTS. The kind hospitality provided by the University of Gdańsk (I.P.), the University of Queensland (M.R.V.) and the University of Vienna (G.J.M.) is acknowledged. We thank S. Hofer, N. Kiesel and M. Żukowski for useful discussion. We thank the Australian Research Council (ARC) (Grant FF0776191), United Kingdom Engineering and Physical Sciences Research Council (EPSRC) and the Royal Society, European Research Council (ERC) (StG QOM), European Commission (MINOS, Q-ESSENCE), Foundational Questions Institute (FQXi), Fonds zur Förderung der wissenschaftlichen Forschung (FWF) (L426, P19570, SFB FoQuS, START), Centre for Quantum Engineering and Space-Time Research (QUEST), and an ÖAD/MNiSW program for support. M.R.V. and I.P. are members of the FWF Doctoral Programme CoQuS (W 1210). M.R.V. is a recipient of a DOC fellowship of the Austrian Academy of Sciences. G.D.C. is a recipient of a Marie Curie Fellowship of the European Commission.

1. Zurek WH (2003) Decoherence, einselection, and the quantum origins of the classical. *Rev Mod Phys* 75:715–775.
2. Ghirardi GC, Rimini A, Weber T (1986) Unified dynamics for microscopic and macroscopic systems. *Phys Rev D* 34:470–491.
3. Diosi L (1989) Models for universal reduction of macroscopic quantum fluctuations. *Phys Rev A* 40:1165–1174.
4. Pearle P (1989) Combining stochastic dynamical state-vector reduction with spontaneous localization. *Phys Rev A* 39:2277–2289.
5. Penrose R (1996) On gravity's role in quantum state reduction. *Gen Relat Gravit* 28:581–600.
6. Hackermüller L, Hornberger K, Brezger B, Zeilinger A, Arndt M (2004) Decoherence of matter waves by thermal emission of radiation. *Nature (London)* 427:711–714.
7. Bose S, Jacobs K, Knight PL (1997) Preparation of nonclassical states in cavities with a moving mirror. *Phys Rev A* 56:4175–4186.
8. Bose S, Jacobs K, Knight PL (1999) Scheme to probe the decoherence of a macroscopic object. *Phys Rev A* 59:3204–3210.
9. Marshall W, Simon C, Penrose R, Bouwmeester D (2003) Towards quantum superpositions of a mirror. *Phys Rev Lett* 91:130401.
10. Kleckner D, et al. (2008) Creating and verifying a quantum superposition in a micro-optomechanical system. *New J Phys* 10:095020.
11. Kippenberg TJ, Vahala KJ (2008) Cavity optomechanics: back-action at the mesoscale. *Science* 321:1172–1176.
12. Marquardt F, Girvin S (2009) Optomechanics. *Physics* 2:40.
13. Aspelmeyer M, Groeblacher S, Hammerer K, Kiesel N (2010) Quantum optomechanics throwing a glance. *J Opt Soc Am B* 27:A189.
14. Smithey DT, Beck M, Raymer MG, Faridani A (1993) Measurement of the Wigner distribution and the density matrix of a light mode using optical homodyne tomography: application to squeezed states and the vacuum. *Phys Rev Lett* 70:1244–1247.
15. Lvovsky AI, Raymer MG (2009) Continuous-variable optical quantum-state tomography. *Rev Mod Phys* 81:299–332.
16. Leibfried D, et al. (1996) Experimental determination of the motional quantum state of a trapped atom. *Phys Rev Lett* 77:4281–4285.
17. Leibfried D, Blatt R, Monroe C, Wineland D (2003) Quantum dynamics of single trapped ions. *Rev Mod Phys* 75:281–324.
18. Kuzmich A, Mandel L, Bigelow NP (2000) Generation of spin squeezing via continuous quantum nondemolition measurement. *Phys Rev Lett* 85:1594–1597.
19. Appel J, et al. (2009) Mesoscopic atomic entanglement for precision measurements beyond the standard quantum limit. *Proc Natl Acad Sci USA* 106:10960–10965.
20. Deléglise S, et al. (2008) Reconstruction of non-classical cavity field states with snapshots of their decoherence. *Nature (London)* 455:510–514.
21. Armour A, Blencowe M, Schwab K (2002) Entanglement and decoherence of a micromechanical resonator via coupling to a cooper-pair box. *Phys Rev Lett* 88:148301.
22. Rocheleau T, et al. (2010) Preparation and detection of a mechanical resonator near the ground state of motion. *Nature (London)* 463:72–75.
23. O'Connell AD, et al. (2010) Quantum ground state and single-phonon control of a mechanical resonator. *Nature (London)* 464:697–703.
24. Rabl P, Shnirman A, Zoller P (2004) Generation of squeezed states of nanomechanical resonators by reservoir engineering. *Phys Rev B* 70:205304.
25. Tittonen I, et al. (1999) Interferometric measurements of the position of a macroscopic body: towards observation of quantum limits. *Phys Rev A* 59:1038–1044.
26. Briant T, Cohadon PF, Pinard M, Heidmann A (2003) Optical phase-space reconstruction of mirror motion at the attometer level. *Eur Phys J D* 22:131–140.
27. Groeblacher S, et al. (2009) Demonstration of an ultracold micro-optomechanical oscillator in a cryogenic cavity. *Nature Physics* 5:485–488.
28. Schliesser A, Arcizet O, Riviere R, Anetsberger G, Kippenberg TJ (2009) Resolved-sideband cooling and position measurement of a micromechanical oscillator close to the Heisenberg uncertainty limit. *Nature Physics* 5:509–514.
29. Teufel JD, Donner T, Castellanos-Beltran MA, Harlow JW, Lehnert KW (2009) Nanomechanical motion measured with an imprecision below that at the standard quantum limit. *Nat Nanotechnol* 4:820–823.
30. Anetsberger G, et al. (2010) Measuring nanomechanical motion with an imprecision below the standard quantum limit. *Phys Rev A* 82:061804(R).
31. Clerk AA, Girvin SM, Marquardt F, Schoelkopf RJ (2010) Introduction to quantum noise, measurement, and amplification. *Rev Mod Phys* 82:1155–1208.
32. Zhang J, Peng K, Braunstein S (2003) Quantum-state transfer from light to macroscopic oscillators. *Phys Rev A* 68:013808.
33. Woolley M, Doherty A, Milburn G, Schwab K (2008) Nanomechanical squeezing with detection via a microwave cavity. *Phys Rev A* 78:062303.
34. Singh S, Meystre P (2010) Atomic probe Wigner tomography of a nanomechanical system. *Phys Rev A* 81:041804(R).
35. Marek P, Filip R (2010) Noise-resilient quantum interface based on quantum nondemolition interactions. *Phys Rev A* 81:042325.
36. Braginsky VB, Vorontsov YI, Khalili FY (1978) Optimal quantum measurements in detectors of gravitation radiation. *JETP Lett+* 27:276–280.
37. Braginsky VB, Khalili FY (1992) *Quantum Measurement* (Cambridge University Press, United Kingdom).
38. Vyatchanin SP, Matsko AB (1993) Quantum limit on force measurements. *JETP Lett+* 77:218–221.
39. Mueller-Ebhardt H, et al. (2009) Quantum-state preparation and macroscopic entanglement in gravitational-wave detectors. *Phys Rev A* 80:043802.
40. Miao H, et al. (2010) Probing macroscopic quantum states with a sub-Heisenberg accuracy. *Phys Rev A* 81:012114.
41. Romero-Isart O, et al. (2011) Optically levitating dielectrics in the quantum regime: theory and protocols. *Phys Rev A* 83:013803.
42. Vogel K, Risken H (1989) Determination of quasiprobability distributions in terms of probability distributions for the rotated quadrature phase. *Phys Rev A* 40:2847–2849.
43. Dunn TJ, Walmsley IA, Mukamel S (1995) Experimental determination of the quantum-mechanical state of a molecular vibrational mode using fluorescence tomography. *Phys Rev Lett* 74:884–887.
44. Levenson MD, Shelby RM, Reid M, Walls DF (1986) Quantum nondemolition detection of optical quadrature amplitudes. *Phys Rev Lett* 57:24732476.
45. La Porta A, Slusher RE, Yurke B (1989) Back-action evading measurements of an optical field using parametric down conversion. *Phys Rev Lett* 62:28–31.
46. Roch J-F, et al. (1997) Quantum nondemolition measurements using cold trapped atoms. *Phys Rev Lett* 78:634–637.
47. Hammerer K, Aspelmeyer M, Polzik ES, Zoller P (2009) Establishing Einstein-Poldosky-Rosen channels between nanomechanics and atomic ensembles. *Phys Rev Lett* 102:020501.
48. Janszky J, Adam P (1992) Strong squeezing by repeated frequency jumps. *Phys Rev A* 46:6091–6092.
49. Walls DF (1983) Squeezed states of light. *Nature (London)* 306:141–146.
50. Cole GD, Behymer E, Bond TC, Goddard LL (2008) Short-wavelength MEMS-tunable VCSELs. *Opt Express* 16:16093–16103.
51. Riazi A (1981) Resonator equation relating Fresnel number, finesse, and number of beam transits. *Appl Optics* 20:3469–3470.
52. Tayebati P, et al. (1998) Half-symmetric cavity tunable microelectromechanical VCSEL with single spatial mode. *IEEE Photonic Tech L* 10:1679–1681.
53. Riemenschneider F, Aziz M, Halbritter H, Sagnes I, Meissner P (2002) Low-cost electrothermally tunable optical microcavities based on GaAs. *IEEE Photonic Tech L* 14:1566–1568.
54. Cole GD, Wilson-Rae I, Werbach K, Vanner MR, Aspelmeyer M (2010) Phonon-tunnelling dissipation in mechanical resonators. *Nature Communications* 2:231.
55. Pinard M, Hadjar Y, Heidmann A (1999) Effective mass in quantum effects of radiation pressure. *Eur Phys J D* 7:107–116.
56. Breuer H-P, Petruccione F (2002) *The Theory of Open Quantum Systems* (Oxford University Press, United Kingdom).
57. Caves CM, Milburn GJ (1987) Quantum-mechanical model for continuous position measurements. *Phys Rev A* 36:5543–5555.
58. Teper I, Vrijsen G, Lee J, Kasevich MA (2008) Backaction noise produced via cavity-aided nondemolition measurement of an atomic clock state. *Phys Rev A* 78:051803(R).
59. Jost JD, et al. (2009) Entangled mechanical oscillators. *Nature (London)* 459:683–685.
60. Chang DE, et al. (2010) Cavity opto-mechanics using an optically levitated nanosphere. *Proc Natl Acad Sci USA* 107:1005–1010.
61. Romero-Isart O, Juan ML, Quidant R, Cirac JI (2010) Toward quantum superposition of living organisms. *New J Phys* 12:033015.

7 Experimental Pulsed Quantum Optomechanics

Prior to publishing our pulsed quantum optomechanics proposal discussed in the previous chapter we were sufficiently confident of the proposal's feasibility to start an experiment and enter this experimentally unexplored direction. We began a room-temperature cavity-free experiment, where the pulse of light simply reflects from the mechanical resonator. This type of cavity-free interaction is qualitatively identical to the cavity description in section 1.1 above and, for small phase shifts, the input-output to the mechanics and the temporal mode of the pulse is accurately described by an $H_{int} \propto X_L X_M$ interaction.

After approximately two years, including a complete shift and re-setup of the experiment on a second new blank optical table, an experimental implementation of our theoretical proposal was completed in late 2012 [84], albeit at a level where the measurement precision is above the mechanical ground state width. This included state tomography and reconstruction of mechanical motional states prepared by one or two pulses for position variance reduction and entropy reduction, respectively. In addition, we performed state reconstruction on a displaced, phase randomized, mechanical state as an example of a (classical) non-Guassian state of motion.

Details of the experimental setup listing the parts used is shown in Fig. 7.1 and a photograph of the setup is shown in Fig. 7.2. One of the main challenges of the experiment was to minimize classical phase noise in the interferometer output signal so that the quantum noise on the optical pulses could be observed in the time-domain. This is important because if classical noise dominates the statistics of the measurement outcomes then one can no longer decrease the width of the mechanical conditional state by increasing the optical power. This was achieved in our experiment by (i) using appropriate transimpedance amplification of the photocurrent output of the homodyne circuit, see Fig. 7.3 for more detail, (ii) locking the interferometer phase with appropriate low-pass filtering to minimize high frequency classical phase noise, and (iii) hunting down and eliminating the numerous sources of (mainly electronic) noise that contaminated the signal. It should be noted at this point, however, that our protocol itself, which utilizes the correlation between pulses, significantly relaxes the requirements to minimize low-frequency phase noise.

My specific contributions to this project were: I designed and built the fiber based optical interferometer building upon knowledge gained during the experimental component discussed in chapter 4; together with Garrett Cole we put together the 4 K cryogenic compatible vacuum chamber with encoded nanopositioning stages; I designed and built the electrical homodyne circuit; I wrote the LabVIEW code that ran the experiment and babysat the experiment on the late night data runs; together with Joachim Hofer, who joined the project when the setup was completed, we developed the calibration procedure and performed the data analysis; and I played the leading role in writing the manuscript, with valuable input from all co-authors, and working through the peer review process.

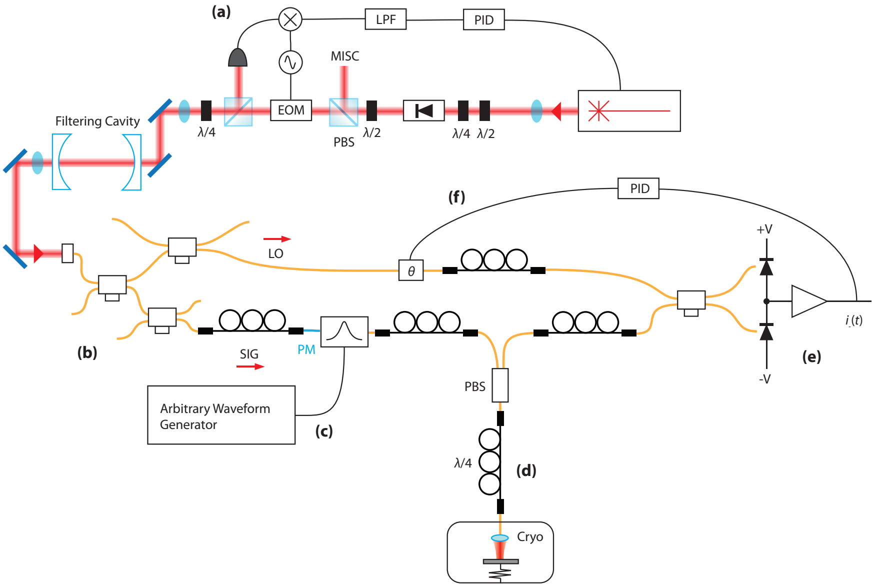

Figure 7.1: Experimental setup. (a) A continuous wave Nd:YAG laser operating at 1,064 nm is collimated and passed through a free space optical isolator. A small and controllable amount of light (MISC) is picked off by a polarizing beam splitter (PBS) for use on other experiments on the table. The light is then phase modulated by an electro-optic modulator (EOM) for Pound-Drever-Hall frequency stabilisation to a filter cavity using a PID controller (Toptica) to reduce laser frequency and amplitude noise. In our pulsed experiment reported in this chapter the filter cavity was not used as only optical phase quadrature measurements were performed. (b) The light is then coupled into optical fibre and split by a tunable beam splitter (Newport) to form the signal (SIG) and local oscillator (LO) paths. In each path another tunable beam splitter is used to independently control the optical powers. (c) The signal field is injected into an optical intensity modulator (JenOptik), which is a polarization dependent device and so the polarization is first adjusted using fiber paddles (ThorLabs). Pulses are generated by driving the modulator with an arbitrary waveform generator (Agilent). (d) The pulses of light are then sent into a 4 K cryogenic compatible vacuum chamber and are focussed onto the micro-mechanical oscillator by a fiber focuser (OzOptics). The field is retroreflected and separated from the incoming light using a fibre-based polarizing beam splitter (Advanced Fiber Resources). (e) The signal and local oscillator are then mixed on another tunable beam-splitter used to perform balanced homodyne detection. (f) The difference photo current is amplified and also used to stabilise the phase in the optical interferometer using a commercial fiber stretcher (Optiphase).

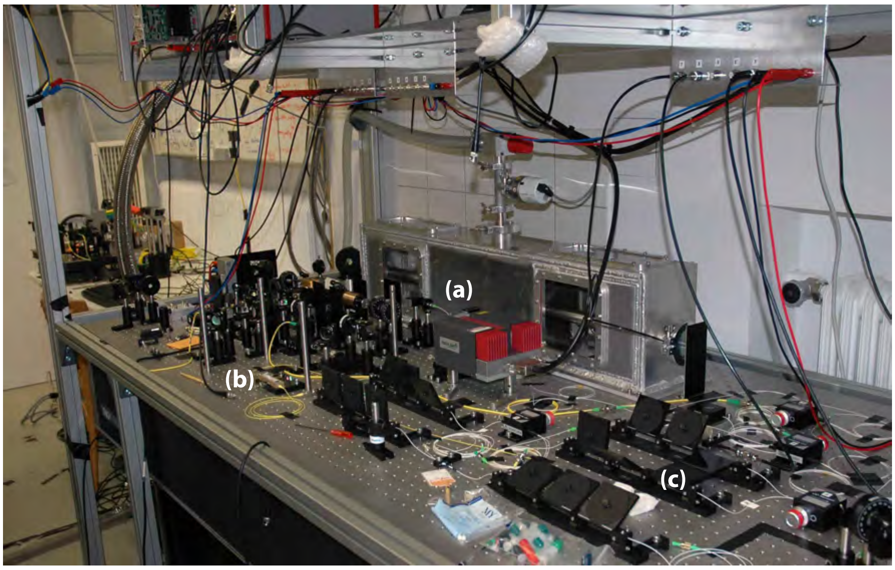

Figure 7.2: Photograph of the experimental setup in the Institute for Quantum Optics and Quantum Information (IQOQI) shortly before we shifted labs to The University of Vienna. (a) The laser and free space optics can be seen on the left of the optical table with a vacuum chamber holding the filter cavity behind. (b) The fiber-based optical amplitude modulator for pulse generation. (c) The optical fiber-based Mach-Zehnder interferometer.

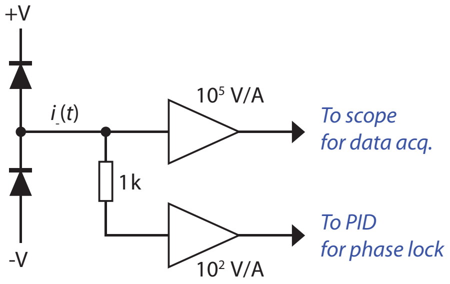

Figure 7.3: Homodyne photocurrent amplification. A 1 kOhm resistor is used to pick off a small amount of the photocurrent that is then passed through a low gain transimpedance amplifier (10^2 V/A). This signal is sent to a PID controller and is used to stabilize the phase of the interferometer. When the lock is stable and the photocurrent is close to zero amps, a high gain transimpedance amplifier (10^5 V/A) is activated that provides a signal containing the optical quantum noise that can be observed in the time domain on an oscilloscope. The amplifiers used are variable-gain high-speed transimpedance amplifiers model DHCPA-100 manufactured by FEMTO.

nature COMMUNICATIONS

ARTICLE

Received 15 May 2013 | Accepted 11 Jul 2013 | Published 15 Aug 2013

DOI: 10.1038/ncomms3295

Cooling-by-measurement and mechanical state tomography via pulsed optomechanics

M.R. Vanner[1], J. Hofer[1], G.D. Cole[1] & M. Aspelmeyer[1]

Observing a physical quantity without disturbing it is a key capability for the control of individual quantum systems. Such back-action-evading or quantum non-demolition measurements were first introduced in the 1970s for gravitational wave detection, and now such techniques are an indispensable tool throughout quantum science. Here we perform measurements of the position of a mechanical oscillator using pulses of light with a duration much shorter than a period of mechanical motion. Utilizing this back-action-evading interaction, we demonstrate state preparation and full state tomography of the mechanical motional state. We have reconstructed states with a position uncertainty reduced to 19 pm, limited by the quantum fluctuations of the optical pulse, and we have performed 'cooling-by-measurement' to reduce the mechanical mode temperature from an initial 1,100 to 16 K. Future improvements to this technique will allow for quantum squeezing of mechanical motion, even from room temperature, and reconstruction of non-classical states exhibiting negative phase-space quasi-probability.

---

[1] University of Vienna, Faculty of Physics, Vienna Center for Quantum Science and Technology (VCQ), Boltzmanngasse 5 A-1090, Vienna, Austria. Correspondence and requests for materials should be addressed to M.R.V. (email: michael.vanner@univie.ac.at).

© 2013 Macmillan Publishers Limited. All rights reserved.

Experiments are now beginning to investigate non-classical motion of massive mechanical devices[1–3]. This opens up new perspectives for quantum-physics-enhanced applications and for tests of the foundations of physics. A versatile approach to manipulate mechanical states of motion is provided by the interaction with electromagnetic radiation, typically confined to microwave or optical cavities. Such cavity-optomechanics experiments[4–8] have thus far largely concentrated on high-sensitivity continuous monitoring of the mechanical position[9-14]. Because of the back-action imparted by the probe onto the measured object, the precision of such a measurement is fundamentally constrained by the standard quantum limit (SQL)[15,16], and therefore only allows for classical phase-space reconstruction[9,17,18]. In order to observe quantum mechanical features that are smaller than the mechanical zero-point motion, back-action-evading measurement techniques that can surpass the SQL[19-22] are required. Following the early insights of Braginsky and Khalili[15], beating the SQL '*can be achieved only in one way: design the probe so it 'sees' only the measured observable'*. Such back-action-evading techniques were first realized for the detection of optical quadratures[23–25] and have now also been used for precision measurement of atomic ensemble spin[26–30] and quantum non-demolition microwave photon counting[31]. In optomechanics, to perform a back-action-evading measurement of the mechanical position, a time-dependent measurement scheme is required. One prominent example is the so-called 'two-tone approach'[22,32], which uses a probe with an intensity that oscillates at twice the mechanical frequency. The field probes the mechanics periodically and the back-action imparted to the mechanical motion by the optical probe does not affect the measurement of the mechanical amplitude. This is closely analogous to a stroboscopic measurement of the mechanical motion[22]. Using the two-tone approach with a microwave probe field, a back-action-evading interaction was recently realized to measure a single quadrature of a nanomechanical resonator[33].

Here we take a different tack to perform position measurements of a mechanical oscillator using single optical pulses. Our experimental approach employs optical pulses that have a duration much shorter than a mechanical period of motion. This provides a back-action-evading interaction for measuring the mechanical position because the interaction leaves the position unchanged, perturbing only the mechanical momentum, and was first suggested by Braginsky *et al.*[34] The precision of this pulsed measurement process is no longer limited by the SQL but is ultimately limited by the quantum optical phase noise. We implement a pulsed protocol[35], where one or two pulses are used to prepare a motional state 'by measurement' and then a subsequent pulse is used for state tomography. Mechanical state preparation 'by measurement' is achieved by utilizing the information gained from the pulsed measurement to update the probability distribution that describes the motional state. The experiments reported here have been performed in the weak interaction regime, where the backaction itself is negligible; however, the pulsed measurements have a dramatic effect on the mechanical thermal state and the measurement precision we achieved was limited by the quantum optical phase noise. We therefore require a quantized description of the optical field; however, it is important to note that at this stage all the mechanical motional states presented here are classical, that is, they can be described by an incoherent mixture of mechanical coherent states. Our protocol can be used to prepare mechanical states independent of the initial mechanical thermal occupation and thus, no initial cooling of the mechanical motion is required. Moreover, by contrast to continuous schemes, our pulsed protocol has considerable resilience against the surrounding mechanical thermal bath, as it can be performed on short time scales[35]. Employing our pulsed approach, mechanical dynamics rather than the steady-state can be conveniently probed and non-equilibrium mechanical behaviour can be characterized. Also note that pulsed quantum optomechanics operates fully in the so-called 'non-resolved sideband regime', in which the cavity decay rate is much larger than the mechanical frequency. Indeed, all results reported here were obtained without the use of an optical cavity.

Results

Experimental protocol. Our experimental setup is shown schematically in Fig. 1a. Optical pulses are injected into a Mach-Zehnder interferometer that has a micromechanical oscillating mirror in one of the two interferometer paths. The pulses are first divided by a beam-splitter that forms one intense beam that acts as a local oscillator (LO) and one weak beam that we will henceforth refer to as the signal. The signal is focussed onto and reflects from a micromechanical oscillator (Fig. 1b). During the reflection of the short optical pulse, changes to the position of the mechanical oscillator are negligible. The coherent optical pulse gains a phase shift in proportion to the mechanical position, which is accurately described by a phase quadrature displacement, as the mechanical position fluctuations are small. Concurrently, the radiation-pressure force of the reflection imparts momentum to the mechanical resonator. This momentum can be decomposed into a classical component due to the mean photon number and a component dependent upon the photon number fluctuations. Quantitatively, this optomechanical interaction is described by the input–output relations:

$$X_L^{\mathrm{out}} = X_L^{\mathrm{in}}, \quad P_L^{\mathrm{out}} = P_L^{\mathrm{in}} + \chi X_M^{\mathrm{in}},$$
$$X_M^{\mathrm{out}} = X_M^{\mathrm{in}}, \quad P_M^{\mathrm{out}} = P_M^{\mathrm{in}} + \chi X_L^{\mathrm{in}} + \Omega \qquad (1)$$

Here, the subscripts label the light (L) and mechanics (M); X and P are the dimensionless amplitude (position) and phase (momentum) quadratures for the light (mechanics); $\chi = 4\pi x_0\sqrt{N}/\lambda$ quantifies the quadrature information exchanged between the light and the mechanics and determines the strength of the mechanical position measurement and $\Omega = 8\pi x_0 N/\lambda$ is the classical momentum transfer to the mechanical oscillator (N, mean photon number per pulse; λ, optical wavelength; $x_0 = (\hbar/2m_{\mathrm{eff}}\omega_M)^{1/2}$, mechanical ground state width; m_{eff}, mechanical effective mass; and ω_M, mechanical angular frequency). After the optomechanical reflection, the signal then overlaps and interferes with the LO pulse on a 50/50 beam-splitter, where the (mean) phase between the LO and signal beams is set to be $\pi/2$. The intensities of both beam-splitter outputs are measured by photodiodes, and the photocurrents are subtracted to implement homodyne detection of the optical phase quadrature. A typical difference current time trace is shown in Fig. 1c, where the measurement outcome P_L is the time integral over the pulse duration of the difference current.

After the pulsed measurement, the mechanical state of motion is changed as our knowledge of the mechanical position has increased. For an initial thermal state of the mechanical resonator with a large thermal occupation, that is, $\chi^2(1+2\bar{n}) > 1$, the means and variances of the mechanical quadratures, upon obtaining the measurement outcome P_L are as follows[35]:

$$\langle X_M^{\mathrm{out}}\rangle \simeq P_L/\chi, \quad \langle P_M^{\mathrm{out}}\rangle = \Omega,$$
$$\sigma^2_{X_M^{\mathrm{out}}} \simeq 1/(2\chi^2), \quad \sigma^2_{P_M^{\mathrm{out}}} = (\chi^2 + 1 + 2\bar{n})/2, \qquad (2)$$

where $\bar{n} \simeq k_B T/\hbar\omega_M$ is the mean occupation of the mechanical mode when in thermal equilibrium with the environment at temperature $T > \hbar\omega_M/k_B$. Notably the information gained from

© 2013 Macmillan Publishers Limited. All rights reserved.

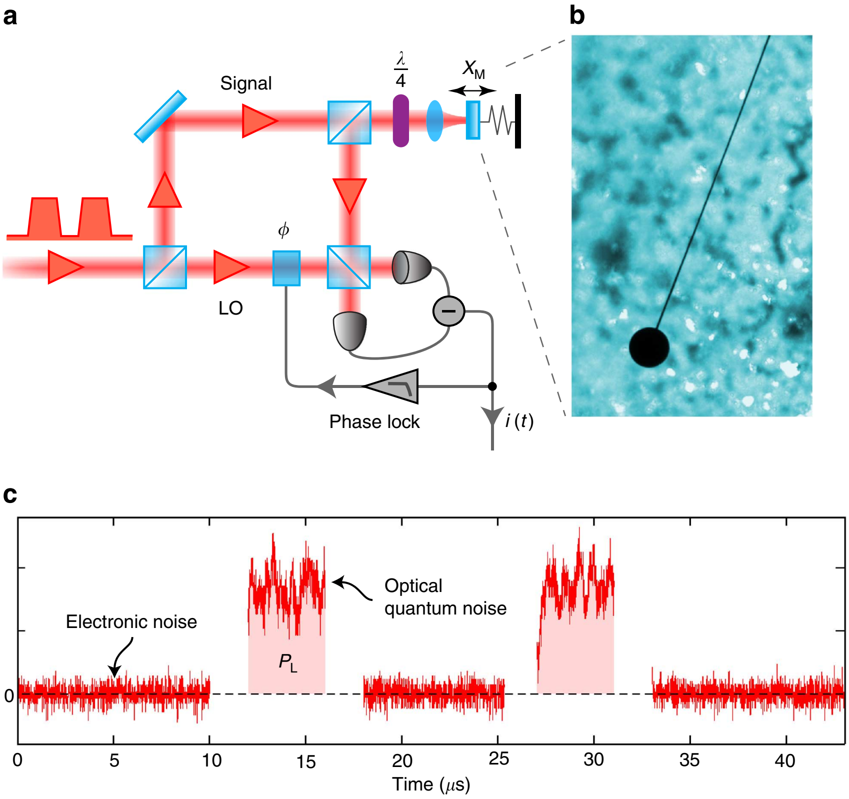

Figure 1 | Experimental setup. (**a**) Schematic of the experimental setup used to perform state tomography and state preparation of the motional state of a mechanical resonator. In addition to the optical pulses, a weak continuous field is used to stabilize the interferometer phase using the homodyne output passed through a low-pass filter with cutoff frequency below the mechanical frequency. (**b**) Colourized optical micrograph of the high-reflectivity micro-mechanical cantilever fabricated for this experiment. The head of the cantilever, where the signal beam is focussed, is 100 μm in diameter. (**c**) Example time trace of the homodyne output for a pair of 4 μs pulses. (For clarity, the pulse rising and falling edges are not shown.) The measurement outcome P_L is the time integral of the homodyne output (indicated by the shaded region). Time resolved optical quantum noise is visible during the pulse.

the measurement reduces the mechanical position variance from $\bar{n}$ to $1/(2\chi^2)$, which does not depend on the initial occupation. The resultant state of mechanical motion, following such a measurement, is no longer in thermal equilibrium with the surrounding environment and has a reduced effective thermal occupation $\bar{n}_{\text{eff}} = (\sigma^2_{X_M}\sigma^2_{P_M})^{1/2} - 1/2 \simeq (\bar{n}/(2\chi^2))^{1/2}$. Moreover, a subsequent pulse performed after one quarter of a period of mechanical harmonic evolution can measure the mechanical momentum at the time of the first pulse to further reduce the effective occupation. This 'cooling-by-measurement' method for entropy reduction, that is, obtaining mechanical position and then momentum information on the initial state, is rapid and has considerable tolerance to both the initial thermal occupation and the surrounding thermal bath[35]. With future experimental improvements, this scheme allows for the generation of high purity and quantum-squeezed states of mechanical motion 'by measurement'. Owing to the resilience against mechanical thermal noise, this scheme may provide a more feasible route to quantum squeezing than parametric modulation[9,17], which can be combined with continuous measurement and feedback[36].

In our experiment, one or two pulses are used to prepare a mechanical state at a known time. Then a read-out pulse is made after time θ/ω_M of mechanical harmonic evolution to sample the mechanical probability distribution of the θ-rotated quadrature, that is, a marginal. Repeating this process many times and obtaining the marginals for a large number of mechanical phase-space angles θ is sufficient to uniquely determine the mechanical quantum state of motion[37]. Quantum state tomography by measurement of the marginals was first realized with optical fields using homodyne interferometry[38] and has now become an indispensable tool in the field of quantum optics[39] being applied to other physical systems such as molecular vibration[40], spin ensembles[41] and microwave fields[42]. Here we implement such mechanical state tomography by utilizing the pulsed measurement outcome probability distribution $\Pr(P_L) = \int dX_M \pi^{-1/2} \exp[-(P_L - \chi X_M)^2] \Pr(X_M, \theta)$ that contains the mechanical marginals $\Pr(X_M, \theta) = \langle X_M | \rho^{\text{in}}_M(\theta) | X_M \rangle$, where $\rho^{\text{in}}_M(\theta)$ is the mechanical input state to be reconstructed after time θ/ω_M of harmonic evolution. In this experiment, we prepare and reconstruct mechanical motional states with features that are not smaller than χ^{-1} and hence, unless otherwise noted, we use the optical measurement outcome distribution as an approximation for the mechanical distribution using the scaled outcome P_L/χ.

Mechanical state preparation and reconstruction. The mechanical resonator used for this experiment is a micro-mirror cantilever constructed from an epitaxial $\text{Al}_x\text{Ga}_{1-x}\text{As}$ crystalline multilayer, see Fig. 1b. The use of such a monocrystalline material structure allows for a significant reduction of the mechanical damping of the resonator when compared with dielectric reflectors[43] and simultaneously provides high optical reflectivity. The crystalline material used here is nominally identical in composition and individual layer thickness to structures used previously[44] and is designed for maximum reflectivity at our

© 2013 Macmillan Publishers Limited. All rights reserved.

optical wavelength of 1,064 nm. The multilayer Bragg mirror comprises 40.5 layer pairs in order to minimize transmission losses. The cantilever was etched from a 6.88-μm thick multilayer and is 1.45 mm in length with a cantilever arm 5 μm in width with a circular head 100 μm in diameter, where the optical signal beam is focussed. For details of the microfabrication procedure see Cole[45]. Note that the resonator is etched directly from the multilayer mirror material and is therefore equally reflective at all points along the structure with an (intensity) reflectivity of 99.982%. This cantilever has a fundamental out-of-plane vibrational mode with frequency $\omega_{\rm M}/2\pi = 984.3$ Hz, effective mass $m_{\rm eff} = 260$ ng (see the methods section), ground state width $x_0 = 5.7 \times 10^{-15}$ m and a mechanical quality of $Q = 3.1 \times 10^4$ in vacuum (10^{-5} mbar) and at room temperature measured via mechanical ringdown.

Our optical setup (Fig. 1a) was constructed from optical-fibre-based components that provides good phase stability and excellent spatial mode matching. Indeed, when the optical powers in the two arms of the interferometer are balanced, we observed an interference visibility exceeding 99.9%. We use a continuous laser source and generate optical pulses of duration 1 μs (excluding the pulse edges) with a fibre-based intensity modulator. The mean photon number in a signal pulse was up to 10^7 and in order to provide a homodyne signal well above the electronic noise, we use a large LO to signal ratio with up to 10^{10} photons per LO pulse. (These photon numbers were determined via optical power measurement during continuous wave operation.) The signal pulses are directed onto the cantilever head using an antireflection-coated fibre focuser and are then retro-reflected. To calibrate the proportionality between the measurement outcomes and the mechanical position, we reflect the signal beam from a rigid mirror adjacent to the mechanical resonator and scan the mirror position using a calibrated piezoelectric actuator, recording both the piezo scan positions and pulse measurement outcomes (see the methods section). For our mechanical resonator ground state width ($x_0 = 5.7 \times 10^{-15}$ m), this photon number per pulse yields a measurement strength χ of order 10^{-4} and a momentum transfer Ω of order unity. The radiation pressure backaction from the reflection of the pulse is smaller than the mechanical thermal noise and is not observed; however, as will be detailed in the following, this measurement strength has a strong effect on the mechanical thermal noise.

After a pulsed measurement is performed to sample a mechanical marginal, the mechanical state is reinitialized by first allowing it to return to equilibrium with the environment and then the mechanical state is reprepared. This process is repeated many times to accumulate sufficient data to characterize the statistical properties of the mechanical motion. The marginal distributions were then obtained by constructing a histogram from the many measurement outcomes recorded for each mechanical phase-space angle θ. As the states studied here are symmetric about the $X_{\rm M}$ and $P_{\rm M}$ axes, we measure a set of many marginals with angles between $\theta = 0$ and $\theta = \pi/2$ to fully characterize the state of motion. The phase-space probability distribution $W(X_{\rm M}, P_{\rm M})$ is then obtained by using the inverse Radon transformation on the set of marginals.

The measurement results we obtained for motional state preparation and reconstruction are summarized in Fig. 2. In Fig. 2a a reconstruction of an initial thermal state that is driven by white noise up to a mode temperature of 1,100 K that has width $\sigma_x = 1.2$ nm is shown. This temperature was obtained using the equipartition theorem $k_{\rm B} T_{\rm eff} = m_{\rm eff}\omega_{\rm M}^2\sigma_x^2$, where the mechanical position variance σ_x^2 was obtained from the calibrated measurement outcome distribution after subtracting the optical noise contribution. A single pulsed measurement made on this initial thermal state generates a motional state that has a reduced position uncertainty (Fig. 2b). The observed momentum distribution of this state, however, is unchanged as the back-action to the mechanical momentum made by the reflection of the optical pulse is much smaller than the mechanical thermal noise. Each pulsed measurement generates a mechanical state with a random but known mean due to the random measurement outcome, see Equation (2). By making the transformation $P_{\rm L}^{(r)} \rightarrow P_{\rm L}^{(r)} - P_{\rm L}^{(p1)}\cos\theta$, where the superscripts (r) and (p_1) indicate read-out and preparation, respectively, this random mean is subtracted and the distribution of the mechanical state can be characterized. We would like to emphasize here that no ‘post selection’ is performed and all measurement outcomes are used in this process. Furthermore, our experimental pulsed technique demonstrates the back-action-evading feature of measurement repeatability, that is, a subsequent measurement is not affected by a prior measurement[19–22]. Specifically, in our case the measurement results of the read-out pulse made a short time after the preparation pulse are the same as the preparation pulse to within the optical quantum noise. The plots for Fig. 2a,b were generated from the same data set, where the statistics of the preparation pulse alone characterizes the unconditional initial thermal state and the read-out pulse characterizes the conditional mechanical state. A 1,100 K thermal state (which has a root-mean-square (RMS) amplitude less than a factor of two larger than a thermal state at 300 K) was used to increase the mechanical contribution to the optical phase noise over the relevant ∼ DC to MHz bandwidth for our pulses to improve the signal-to-noise ratio for mechanical conditional state preparation.

In Fig. 2c the reconstruction of a mechanical state of motion prepared via two pulsed measurements separated by one quarter of a mechanical period is shown. The width of the mechanical phase-space distribution has been significantly reduced in both the position and momentum quadratures compared with the initial thermal state (Fig. 2a) and hence the effective mode temperature has significantly decreased. This method of cooling is rapid as it takes place well within a single mechanical period and is, to the best of our knowledge, yet to be experimentally reported elsewhere. For this pulse sequence the read-out pulse outcome is transformed using $P_{\rm L}^{(r)} \rightarrow P_{\rm L}^{(r)} - P_{\rm L}^{(p2)}\cos\theta + P_{\rm L}^{(p1)}\sin\theta$, where θ is the angle of mechanical evolution made between the second preparation pulse and the read-out pulse. Ideally, for this mechanical state, the width of the mechanical marginals should be constant for all θ; however, in our experiment the phase correlation between the pulses reduces with increasing pulse separation as low frequency noise, due to imperfect phase locking, enters the signal. This results in a broadening of the conditional mechanical marginals as θ increases. The effective temperature $T_{\rm eff} = m_{\rm eff}\omega_{\rm M}^2\sigma_x^{(\theta=0)}\sigma_x^{(\theta=\pi/2)}/k_{\rm B}$ observed for this state is 16 K, which depends on the product of the standard deviations of the position and momentum quadratures. Were the pulses to remain correlated to within the quantum noise, the effective temperature that could be reached for this measurement strength, taking the effects of mechanical rethermalization into account, would be 4.4 K (ref. 35). We would like to highlight here that rethermalization contributes to less than 1% of this value. To summarize the observed effects of single- and two-pulse mechanical state preparation discussed above, Fig. 2e provides a plot of the measured mechanical widths with θ for the initial thermal state and the two mechanical conditional states. In this plot, the mechanical widths were determined from the calibrated pulse outcome distributions after subtracting the optical noise contributions that were measured independently. The data for both of the mechanical conditional states were taken with the same signal pulse powers and for each phase-space angle 300 pulses were recorded to construct the histograms.

© 2013 Macmillan Publishers Limited. All rights reserved.

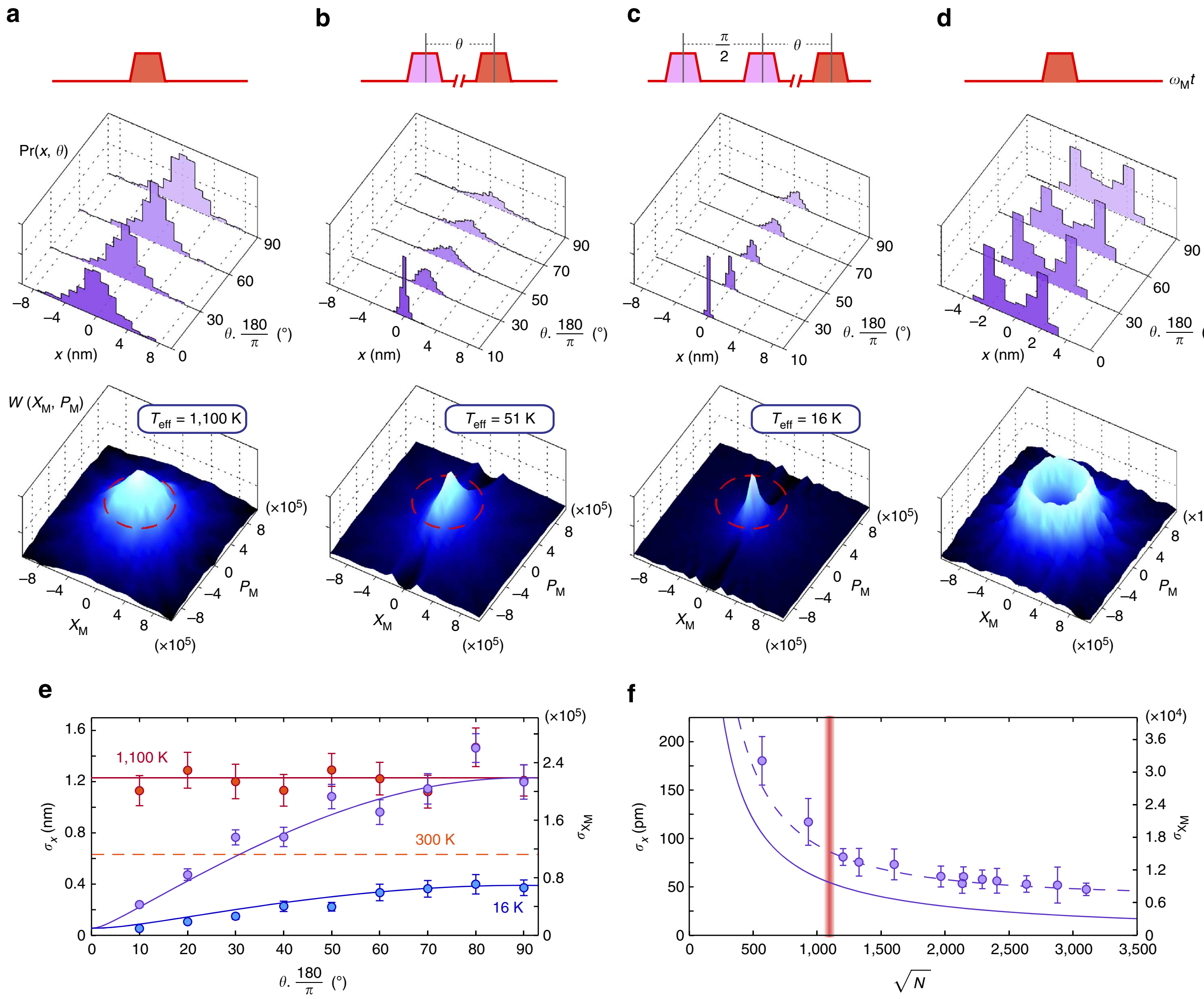

Figure 2 | Mechanical motional state preparation and full state reconstruction using optical pulsed quantum measurement. The uppermost row shows the pulse protocols (pink - preparation, red - tomography). The two rows below show a subset of the measured probability distributions of the mechanical quadratures $Pr(x,\theta)$ and the reconstructed phase-space distributions $W(X_M,P_M)$, respectively. The phase-space distributions were reconstructed using nine marginal angles up to $\theta\cdot\pi/180=90°$ (with a larger number of bins used than that shown for the marginals). For our current measurement strength, that is, $\chi<1$, all the mechanical motional states reconstructed here can be described classically. (**a**) In the first column, tomography and reconstruction of an initial mechanical thermal state driven by white noise up to a mode temperature of 1100 K is shown. The red dashed circle has a radius equal to 2σ of the initial thermal distribution. (**b**) A single pulsed measurement reduces the mechanical position variance, but leaves the momentum distribution unchanged. (**c**) 'Cooling-by-measurement' performed with two pulses separated by one quarter of a mechanical period rapidly reduces the mechanical state's entropy. The effective temperature of the mechanical state reconstructed here has been reduced to 16 K. (**d**) State reconstruction of a non-Gaussian mechanical state of motion generated by resonant sinusoidal drive. (**e**) The (one s.d.) width of the position distribution observed for states (**a**–**c**) with phase-space angle θ. The thermal state (red points) shows a position width approximately twice of that when at room temperature (dashed line). State (**b**) has a reduced position width for small phase-space angles (purple points). The position width of state (**c**) is reduced for all phase-space angles (blue points). The solid lines are theoretical fits obtained using Equation (2) generalized for all θ as well the two-pulse-preparation case. (**f**) Plot of the conditional mechanical width with pulse strength obtained using two pulses separated by 5° of mechanical evolution. The dashed line is a theoretical fit with a model using two units of optical quantum noise and finite mechanical evolution. The solid line is the inferred conditional mechanical width immediately after the preparation pulse. The vertical line indicates the pulse strength used for states (**a**–**c**). The error bars on (**e**) and (**f**) indicate a one s.d. uncertainty.

As an example of a non-Gaussian state of motion, we have reconstructed a driven thermal state (Fig. 2d) that was generated by applying a sinusoidal drive on resonance with the mechanical eigenfrequency. Note that the two peaks in the mechanical marginals are narrower than the broad thermal state in Fig. 2a, as this state was prepared at room temperature without the white noise drive. Even though this state of motion and the thermal state are rotationally invariant in phase space, many marginals are measured for their reconstruction. On the other hand, the conditional mechanical states of motion are not rotationally invariant in phase-space as the time of the preparation pulse(s) sets the time for $\theta=0$. Note that this pulse-based tomography scheme does not measure the angle $\theta=0$ as the read-out pulse is temporally separated from the preparation pulse(s). The lack of this marginal angle causes the rippling near $X_M=0$ in the reconstructed phase-space distributions. By employing shorter pulses and measuring the marginals at smaller angles this rippling can be reduced.

© 2013 Macmillan Publishers Limited. All rights reserved.

To demonstrate the scaling of our measurement strength in Fig. 2f, the conditional mechanical width observed by a read-out pulse made after 5° of mechanical free evolution is plotted with increasing pulse amplitude. For this pulse separation, the two pulses are well correlated and the width of the conditional mechanical state is limited by the optical quantum noise in the measurement (see the methods section for more details). As the signal pulse strength is increased, the standard deviation of the conditional mechanical position distribution decreases with $N^{-1/2}$, which is a result of the optical number-phase uncertainty relation. The dashed line in the plot is a theoretical prediction including the two units of optical shot noise, one each for the preparation and read-out pulses, and the small contribution from the mechanical evolution between the two pulses. The relative amplitudes for the data points were measured precisely and scaled by a free fitting parameter into units of square-root photon number, where the photon number per pulse obtained is consistent with measurements of the optical power made during continuous wave operation. For the largest optical pulse strength used the statistics of the read-out pulse demonstrate a conditional mechanical width (after the preparation pulse) of $\sigma_x = 19$ pm corresponding to a measurement strength of $\chi = 2.1 \times 10^{-4}$.

Discussion

The techniques developed in this work provide the ability to experimentally perform quantum optomechanics in the time domain. This offers significant potential for optomechanics-based quantum information and quantum metrology applications by providing the framework for quantum state preparation of a mechanical resonator via quantum measurement[46]. One may then also envision combining such measurement based state preparation with feedback to implement full quantum control[47]. One exciting example of mechanical dynamics that can be probed by pulsed optomechanics has been recently theoretically discussed by Buchmann *et al.*[48], where pulsed measurements, as now realized in this work, are considered for the observation of quantum tunnelling of a mechanical oscillator in a double-well potential. Another example for quantum state preparation is that, even though the optomechanical interaction used here is linear with the mechanical position, by exploiting the optical non-linearity, X_M^2 measurements with a strength significantly larger than that attainable with dispersive optomechanics can be performed[49]. An X_M^2 measurement can be used to conditionally prepare highly non-Guassian mechanical superposition states and experimentally characterizing the decoherence of such states is important to determine the feasibility of using mechanical elements for coherent quantum applications and can also be used to empirically test collapse models[50–53]. The pulsed measurements performed here may also be utilized for a quantum non-demolition measurement-based light-mechanics quantum interface[54]. Furthermore, a sequence of four pulsed optomechanical interactions can be used to generate non-classical mechanical states of motion via an optomechanical geometric phase[55] and can even be used to experimentally explore potential quantum-gravitational phenomena[56].

For this experiment, to prepare a quantum-squeezed state of mechanical motion, the measurement strength needs to be increased to $\chi > 1$. An effective route to meet this requirement would be to employ an optical cavity to enhance the optomechanical interaction. Using the experimental parameters achieved in this work, a cavity finesse of 10^4 is sufficient. As such a cavity simultaneously requires a high finesse, as well as a large bandwidth to accommodate a short optical pulse, this is best achieved with an optomechanical microcavity[35]. Such improvements to the measurement sensitivity will not only enable Wigner reconstruction with significant negativity but, owing to this pulsed protocol's resilience against mechanical thermal noise, may also allow the generation of non-classical mechanical states in the regime of room temperature quantum optomechanics.

Methods

Verification of optical quantum noise. To verify that the measurement scheme used here is optical quantum noise limited, we measured the phase quadrature conditional variance of a pair of optical pulses with increasing total photon number, that is, the sum of the signal and LO photons per pulse, while keeping the signal to LO ratio fixed, see Fig. 3. As with our calibration procedure, the signal beam is focussed onto a rigid mirror adjacent to the mechanical oscillator to prevent coupling to the mechanical motion. The pulse separation used for this measurement was 14.1 μs, which would correspond to 5° of mechanical free evolution, and is the same as that used for the data set shown in Fig. 2f. With this pulse separation the conditioning is essentially the second pulse outcome minus the first pulse outcome. The quantum noise components of these two temporal modes are uncorrelated; however, the lower frequency classical noise components vary slowly between the two pulses and are thus suppressed by the conditioning. Quantum mechanics predicts a linear dependence for the variance with total photon number; however, had classical phase noise been the dominant contribution, a quadratic dependence with the total photon number per pulse would have been observed. (For a discussion on experimental aspects of observing optical quantum noise, see Bachor and Ralph[57]). During this measurement, we were limited to a total photon number of 10^{10} as the phase lock performance dramatically reduced beyond this point. Were we able to measure beyond this optical power the classical phase noise would have eventually become the dominant noise and the conditional mechanical variance that could have been achieved would have saturated.

The data points for Fig. 3 were obtained from Gaussian fits to histograms of the conditional outcomes. The error bars indicate a one s.d. uncertainty as determined from the fit. The observed conditional variance shows a linear dependence with the total photon number with a 'goodness of fit' parameter $R^2 = 0.97$, taking the error bars into account. This demonstrates that, up to a total photon number of order 10^{10}, the conditional variance is quantum noise limited.

Also included in Fig. 3 is the measured electronic noise, that is, the conditional variance observed using no light. This contribution is 19.5 dB smaller than the observed optical quantum noise at the data point with the highest optical intensity ($N_{\mathrm{TOT}} = 9.5 \times 10^9$).

Effective mass measurement. The optically probed effective mass of a mechanical vibrational mode depends upon the geometry and material properties of the mechanical structure as well as the intensity profile of the incident optical beam. The mass associated with the mechanical displacement mode shape, that is, the modal mass, is in general less than the total mass of the structure; however, the optically probed effective mass can have a strong dependence on the position and profile of the optical beam. We estimate the optically probed effective mass of the cantilever in our experiment using a combination of measurements and finite element analysis. Using the established values for the relevant elastic constants averaged over the crystalline multilayer ($C_{11} = 119.6$, $C_{12} = 55.5$, $C_{44} = 59.1$ GPa) and the average material density 4,476 kg m^{-3}, the lateral geometry of the

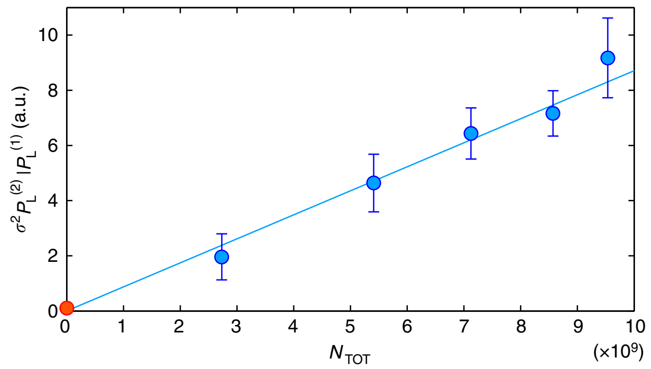

Figure 3 | Verification of optical quantum noise. The measured optical phase quadrature conditional variance $\sigma^2_{P_L^{(2)} | P_L^{(1)}}$ plotted with the total photon number (signal plus LO) per pulse N_{TOT}. The linear dependence observed demonstrates that the measurement scheme is optical quantum noise limited up to $N_{\mathrm{TOT}} \simeq 10^{10}$. Were classical phase noise to be the dominant noise source, a quadratic dependence would be observed. Error bars indicate a one s.d. uncertainty.

© 2013 Macmillan Publishers Limited. All rights reserved.

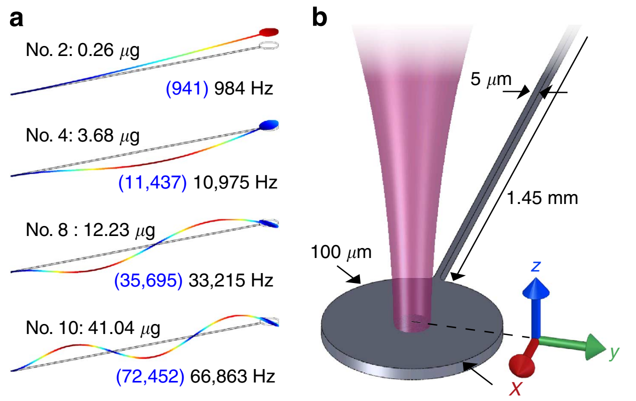

Figure 4 | Optically probed effective mass. (**a**) Finite element simulations of the vibrational modes (no. 2, 4, 8 and 10) that have the four lowest optically probed effective masses. The displacements shown are exaggerated (blue to red indicates increasing displacement) and the outline indicates the cantilever rest position. The optically probed effective mass is given next to each mode number and underneath are the simulated mechanical frequencies in brackets and the measured frequencies. (**b**) Schematic of the cantilever and the focussed signal beam. The coordinate axis used when determining the optically probed effective mass is in the centre of the cantilever head on the mirror surface.

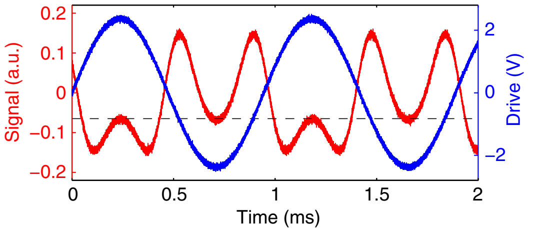

Figure 5 | Piezo calibration. Plot of the homodyne output (red, left axis) during piezo drive (blue, right axis) to calibrate the piezo response. The sinusoidal drive generates a peak-to-peak piezo scan of one half of an optical wavelength that was determined by adjusting the drive amplitude until the turning points in the homodyne output coincide (dashed line).

simulated resonator is adjusted until minimal error is found between the measured and simulated eigenfrequencies for the first four out-of-plane mechanical modes, see Fig.4a. (Note that the lowest frequency vibrational mode for our cantilever is an in-plane mode as the cantilever used is slightly thicker than wide.) A mean discrepancy between the measured and simulated frequencies of 6.1% was obtained by reducing the feature linewidth by 0.875 μm with respect to the lithographic mask. Note that the thickness of the free-standing mirror material was not used as a fitting parameter as it was accurately determined from the reflectance spectrum of the mirror[58] and found to be 6.88 μm. Once the geometry is determined, the effective mass is calculated via the volume integral[59]

$$m_{\mathrm{eff}} = \frac{\rho \int\int\int \mathrm{d}x\mathrm{d}y\mathrm{d}z(u^2 + v^2 + w^2)}{D^2} \tag{3}$$

Here, ρ is the material density; u, v and w are the displacements of the body along the x, y, and z directions, respectively, and the optically probed displacement D is the overlap between the mechanical deflection and the optical Gaussian intensity profile, that is

$$D = \frac{1}{2\pi r_0^2} \int\int \mathrm{d}x\mathrm{d}y w(x, y, z = 0) \exp\left[-\frac{x^2 + y^2}{2r_0^2}\right] \tag{4}$$

where r_0 is the standard deviation of the Gaussian optical intensity profile and the coordinate axis used for x, y and z has its origin in the centre of the cantilever head, see Fig. 4b. The antireflection-coated fibre focuser used in our experiment provides an optical beam diameter ($4r_0$) of 10.6 μm, which is much smaller than the nominal cantilever head diameter of 100 μm (as fabricated diameter of 98.25 μm). Thus, for the fundamental out-of-plane mode, there is only a weak optical beam position and width dependence on the effective mass. (In this case, the effective mass is approximately equal to the intrinsic modal mass.) We have determined that the fundamental out-of-plane mechanical mode utilized in our experiment, which oscillates at 984.3 Hz, has an effective mass of 260 ng and thus a spring constant of 0.01 N m^{-1}. For the higher order modes of the structure; however, lateral displacement of the beam leads to a rapid change in the effective mass. To minimize the contribution from these higher mechanical modes it is necessary to carefully position the optical beam. Assuming careful alignment, the geometry of our mechanical structure is such that the contributions from higher order modes are further suppressed as the effective mass rapidly increases with mode number. Indeed, the unconditional RMS amplitudes of modes no. 4, 8 and 10 are 2.4%, 0.4% and 0.1% that of mode no. 2, respectively.

Calibration procedure. We have used a two-step calibration procedure to determine the proportionality between the pulsed homodyne measurement outcomes and the mechanical displacement. During this procedure the signal beam is focused onto the chip edge, that is, a rigid unpatterned part of mirror material adjacent to the mechanical resonator, to prevent mechanical motion contributing to the signal. First, we calibrate the displacement of a piezoelectric actuator, which our fabricated structure containing the mechanical oscillator is placed upon, in response to a known drive voltage. We then drive the piezo and record the pulse measurement outcomes during the controlled actuation in order to calibrate the pulsed interferometer. Each step is detailed below in the next two subsections, respectively.

Piezo calibration. To calibrate the piezoelectric actuator, we applied a sinusoidal drive voltage and used a continuous signal beam to monitor the piezo motion. The frequency of the drive was chosen such that the piezo mechanical response was either in or out of phase with the drive voltage. (Experimentally, care was needed to find a suitable drive frequency as the piezo does not have a flat spectral response.) During this procedure, the phase between the signal and LO beams does not require locking, and the piezo drive was at a higher frequency than the phase noise components in the interferometer. We then adjusted the drive amplitude such that the peak-to-peak piezo motion was one half of the optical wavelength. This can be done precisely as the difference current output of the interferometer has separate turning points occurring at the same level for this modulation depth and is then proportional to $\cos[\varphi_0 + \pi \sin \omega t]$, see Fig. 5, here φ_0 is the (unlocked) slowly varying phase in the interferometer and ω is the piezo drive angular frequency. As φ_0 slowly changes this merely shifts the level of the turning points. In our experiment, we used a drive frequency of 1.06 kHz and exploited a resonance of the piezo to achieve a peak-to-peak scan of 532 nm using 4.6 Vpp.

Pulse calibration. Using the same piezo drive frequency as above, and using the piezo actuator calibration value (metres per Volt) obtained, the actuator was scanned with a reduced amplitude so that the optical phase shifts are small. (It was verified that the piezo responds linearly with the applied Voltage over our range of interest.) Then, during the piezo scan, pulsed position measurements are performed and both the voltage applied to the piezo at the time of the measurement and the pulsed measurement outcomes are recorded. The proportionality between these recorded values is used to obtain the outcome per metre calibration. This calibration value is optical amplitude dependent and had to be measured for several optical amplitudes for the measurement shown in Fig. 2f.

References

1. O'Connell, A. D. *et al.* Quantum ground state and single-phonon control of a mechanical resonator. *Nature* **464,** 697–703 (2010).
2. Lee, K. C. *et al.* Entangling macroscopic diamonds at room temperature. *Science* **334,** 1253–1256 (2011).
3. Lee, K. C. *et al.* Macroscopic non-classical states and terahertz quantum processing in room-temperature diamond. *Nat. Photonics* **6,** 41–44 (2012).
4. Blencowe, M. Quantum electromechanical systems. *Phys. Rep.* **395,** 159–222 (2004).
5. Schwab, K. C. & Roukes, M. L. Putting mechanics into quantum mechanics. *Phys. Today* **58,** 36–42 (2005).
6. Kippenberg, T. J. & Vahala, K. J. Cavity optomechanics: back-action at the mesoscale. *Science* **321,** 1172–1176 (2008).
7. Marquardt, F. & Girvin, S. M. Optomechanics. *Physics* **2,** 40 (2009).
8. Aspelmeyer, M., Meystre, P. & Schwab, K. C. Quantum optomechanics.. *Phys. Today* **65,** 29–35 (2012).
9. Briant, T., Cohadon, P. F., Pinard, M. & Heidmann, A. Optical phase-space reconstruction of mirror motion at the attometer level. *Eur. Phys. J. D.* **22,** 131–140 (2003).
10. Regal, C. A., Teufel, J. D. & Lehnert, K. W. Measuring nanomechanical motion with a microwave cavity interferometer. *Nat. Phys.* **4,** 555–560 (2008).
11. Abbott, B. P. *et al.* LIGO: the Laser Interferometer Gravitational-Wave Observatory. *Rep. Prog. Phys.* **72,** 076901 (2009).
12. Teufel, J. D. *et al.* Sideband cooling of micromechanical motion to the quantum ground state. *Nature* **475,** 359–363 (2011).
13. Chan, J. *et al.* Laser cooling of a nanomechanical oscillator into its quantum ground state. *Nature* **478,** 89–92 (2011).

© 2013 Macmillan Publishers Limited. All rights reserved.

14. Faust, T., Krenn, P., Manus, S., Kotthaus, J. P. & Weig, E. M. Microwave cavity-enhanced transduction for plug and play nanomechanics at room temperature. *Nat. Comm.* **3,** 728 (2012).
15. Braginsky, V. B. & Khalili, F. Y. *Quantum Measurement* (Cambridge University Press, 1992).
16. LaHaye, M. D., Buu, O., Camarota, B. & Schwab, K. C. Approaching the quantum limit of a nanomechanical resonator. *Science* **304,** 74–77 (2004).
17. Rugar, D. & Grutter, P. Mechanical parametric amplification and thermomechanical noise squeezing. *Phys. Rev. Lett.* **67,** 699–702 (1991).
18. Tittonen, I. *et al.* Interferometric measurements of the position of a macroscopic body: Towards observation of quantum limits. *Phys. Rev. A* **59,** 1038–1044 (1999).
19. Braginsky, V. B. & Vorontsov, Y. I. Quantum-mechanical limitations in macroscopic experiments and modern experimental technique. *Sov. Phys. Usp.* **17,** 644 (1975).
20. Thorne, K. S. *et al.* Quantum nondemolition measurements of harmonic oscillators. *Phys. Rev. Lett.* **40,** 667–671 (1978).
21. Unruh, W. G. Quantum nondemolition and gravity-wave detection. *Phys. Rev. D* **19,** 2888–2896 (1979).
22. Braginsky, V. B., Vorontsov, Y. I. & Thorne, K. S. Quantum nondemolition measurements. *Science* **209,** 547–557 (1980).
23. Levenson, M. D., Shelby, R. M., Reid, M. & Walls, D. F. Quantum nondemolition detection of optical quadrature amplitudes. *Phys. Rev. Lett.* **57,** 2473–2476 (1986).
24. La Porta, A., Slusher, R. E. & Yurke, B. Back-action evading measurements of an optical field using parametric down conversion. *Phys. Rev. Lett.* **62,** 28–31 (1989).
25. Grangier, P., Levenson, J. A. & Poizat, J.-P. Quantum non-demolition measurements in optics. *Nature* **396,** 537–542 (1998).
26. Kuzmich, A., Mandel, L. & Bigelow, N. P. Generation of spin squeezing via continuous quantum nondemolition measurement. *Phys. Rev. Lett.* **85,** 1594–1597 (2000).
27. Teper, I., Vrijsen, G., Lee, J. & Kasevich, M. A. Backaction noise produced via cavity-aided nondemolition measurement of an atomic clock state. *Phys. Rev. A* **78,** 051803(R) (2008).
28. Takano, T., Fuyama, M., Namiki, R. & Takahashi, Y. Spin squeezing of a cold atomic ensemble with the nuclear spin of one-half. *Phys. Rev. Lett.* **102,** 033601 (2009).
29. Appel, J. *et al.* Mesoscopic atomic entanglement for precision measurements beyond the standard quantum limit. *Proc. Natl Acad. Sci. USA* **106,** 10960–10965 (2009).
30. Schleier-Smith, M. H., Leroux, I. D. & Vuletic', V. States of an ensemble of two-level atoms with reduced quantum uncertainty. *Phys. Rev. Lett.* **104,** 073604 (2010).
31. Guerlin, C. *et al.* Progressive field-state collapse and quantum non-demolition photon counting. *Nature* **448,** 889–893 (2007).
32. Clerk, A. A., Marquardt, F. & Jacobs, K. Back-action evasion and squeezing of a mechanical resonator using a cavity detector. *New J. Phys.* **10,** 095010 (2008).
33. Hertzberg, J. B. *et al.* Back-action-evading measurements of nanomechanical motion. *Nat. Phys.* **6,** 213–217 (2010).
34. Braginsky, V. B., Vorontsov, Y. I. & Khalili, F. Y. Optimal quantum measurements in detectors of gravitation radiation. *JETP Lett.* **27,** 276 (1978).
35. Vanner, M. R. *et al.* Pulsed quantum optomechanics. *Proc. Natl Acad. Sci. USA* **108,** 16182–16187 (2011).
36. Szorkovszky, A., Doherty, A. C., Harris, G. I. & Bowen, W. P. Mechanical squeezing via parametric amplification and weak measurement. *Phys. Rev. Lett.* **107,** 213603 (2011).
37. Vogel, K. & Risken, H. Determination of quasiprobability distributions in terms of probability distributions for the rotated quadrature phase. *Phys. Rev. A* **40,** 2847–2849(R) (1989).
38. Smithey, D. T., Beck, M., Raymer, M. G. & Faridani, A. Measurement of the Wigner distribution and the density matrix of a light mode using optical homodyne tomography: application to squeezed states and the vacuum. *Phys. Rev. Lett.* **70,** 1244–1247 (1993).
39. Lvovsky, A. I. & Raymer, M. G. Continuous-variable optical quantum-state tomography. *Rev. Mod. Phys.* **81,** 299–332 (2009).
40. Dunn, T. J., Walmsley, I. A. & Mukamel, S. Experimental determination of the quantum-mechanical state of a molecular vibrational mode using fluorescence tomography. *Phys. Rev. Lett.* **74,** 884–887 (1995).
41. Fernholz, T. *et al.* Spin squeezing of atomic ensembles via nuclear-electronic spin entanglement. *Phys. Rev. Lett.* **101,** 073601 (2008).
42. Mallet, F. *et al.* Quantum state tomography of an itinerant squeezed microwave field. *Phys. Rev. Lett.* **106,** 220502 (2011).
43. Harry, G. M. *et al.* Thermal noise in interferometric gravitational wave detectors due to dielectric optical coatings. *Class. Quantum Grav.* **19,** 897–917 (2002).
44. Cole, G. D. *et al.* Megahertz monocrystalline optomechanical resonators with minimal dissipation. *Proc. IEEE Micr. Elect.* 847–850 (2010).
45. Cole, G. D. Cavity optomechanics with low-noise crystalline mirrors. *Proc. SPIE* 8458–07 (2012).
46. Wiseman, H. M. & Milburn, G. J. *Quantum Measurement and Control* (Cambridge University Press, 2010).
47. Sayrin, C. & Dotsenko, I. *et al.* Real-time quantum feedback prepares and stabilizes photon number states. *Nature* **477,** 73–77 (2011).
48. Buchmann, L. F., Zhang, L., Chiruvelli, A. & Meystre, P. Macroscopic tunneling of a membrane in an optomechanical double-well potential. *Phys. Rev. Lett.* **108,** 210403 (2012).
49. Vanner, M. R. Selective linear or quadratic optomechanical coupling via measurement. *Phys. Rev. X* **1,** 021011 (2011).
50. Bose, S., Jacobs, K. & Knight, P. L. Scheme to probe the decoherence of a macroscopic object. *Phys. Rev. A* **59,** 3204–3210 (1999).
51. Marshall, W., Simon, C., Penrose, R. & Bouwmeester, D. Towards quantum superpositions of a mirror. *Phys. Rev. Lett.* **91,** 130401 (2003).
52. Klecker, D. & Pikovski, I. *et al.* Creating and verifying a quantum superposition in a micro-optomechanical system. *New J. Phys.* **10,** 095020 (2008).
53. Romero-Isart, O. Quantum superposition of massive objects and collapse models. *Phys. Rev. A* **84,** 052121 (2011).
54. Marek, P. & Filip, R. Noise-resilient quantum interface based on quantum nondemolition interactions. *Phys. Rev. A* **81,** 042325 (2010).
55. Khosla, K. E., Vanner, M. R., Bowen, W. P. & Milburn, G. J. Quantum state preparation of a mechanical resonator using an optomechanical geometric phase. *New J. Phys.* **15,** 043025 (2013).
56. Pikovski, I., Vanner, M. R., Aspelmeyer, M., Kim, M. S. & Brukner, Č. Probing Planck-scale physics with quantum optics. *Nat. Phys.* **8,** 393–397 (2012).
57. Bachor, H.-A. & Ralph, T. C. *A Guide to Experiments in Quantum Optics* (Wiley-VCH, 2004).
58. Cole, G. D. *et al.* Phonon-tunnelling dissipation in mechanical resonators. *Nat. Comm.* **2,** 231 (2011).
59. Pinard, M., Hadjar, Y. & Heidmann, A. Effective mass in quantum effects of radiation pressure. *Eur. Phys. J. D* **7,** 107–116 (1999).

Acknowledgements

We thank K. Hammerer, S. G. Hofer, M. S. Kim, G. J. Milburn, I. Pikovski, R. Riedinger and J. Schmöle for useful discussion. M.R.V. is a member of the FWF Doctoral Programme CoQuS (W 1210) and is a recipient of a DOC fellowship of the Austrian Academy of Sciences. Microfabrication was carried out at the Zentrum für Mikro- und Nanostrukturen (ZMNS) of the Technische Universität Wien and the epitaxial multilayer was grown by Markus Weyers' group at the The Ferdinand-Braun-Institut, Leibniz-Institut für Höchstfrequenztechnik (FBH), Berlin (Germany). We thank the European Commission (QESSENCE, CQOM), the European Research Council (ERC QOM), the Vienna Science and Technology Fund (WWTF) and the Austrian Science Fund (FWF) (START, SFB FOQUS) for their support.

Author contributions

All authors contributed to the experiment, the data analysis and writing of the manuscript.

Additional information

Competing financial interests: The authors declare no competing financial interests.

Reprints and permission information is available online at http://npg.nature.com/reprintsandpermissions/

How to cite this article: Vanner, M. R. *et al.* Cooling-by-measurement and mechanical state tomography via pulsed optomechanics. *Nat. Commun.* 4:2295 doi: 10.1038/ncomms3295 (2013).

© 2013 Macmillan Publishers Limited. All rights reserved.

8 Enhanced Strength Displacement Squared Measurement

The generation of non-Gaussian quantum superposition states of a mechanical resonator is one of the primary motivations in quantum optomechanics. Reaching this goal is experimentally challenging as the radiation pressure interaction is linear in the mechanical field operator, see Eq. (1.3), and the radiation pressure coupling to single photon level fields is presently unobservable. An interesting route to reaching this goal is to engineer an optomechanical interaction (and optical field measurement strategy) so that a quantum measurement of the mechanical displacement squared instead of displacement itself is performed. In this case the measurement does not reveal whether the position is positive or negative and a coherent superposition of the two can be prepared. This approach was first theoretically considered for mechanical resonators by Jacobs *et al.* [85], where measurements are performed on a qubit that is quadratically coupled to the position of an electro-mechanical resonator.

In optomechanics an interaction to the mechanical displacement squared, i.e. $H_{int} \propto a^\dagger a X_M^2$, is available in the membrane-in-the-middle geometry [86], where a mechanical element is placed at an intensity maximum in a standing wave inside an optical resonator. Mechanical displacement squared fluctuations have been observed for an optomechanical system realized with a cloud of trapped cold atoms inside a Fabry-Pérot resonator [87], however, as this type of coupling is inherently weak no such observations have been performed for a rigid mechanical oscillator.

This solo author theoretical work [88] overcomes this problem of weak coupling and introduces a method to perform strong X_M^2 measurements. Rather than utilizing the weak X_M^2 coupling offered by the membrane-in-the-middle geometry, the method introduced here exploits the underlying optical non-linearity of ‘reflective’ optomechanics and mechanical X_M^2 measurements are achieved by measuring the changes to the optical amplitude quadrature. It was quite surprising to find that this approach offers a coupling that is, remarkably, a factor of the optical cavity finesse, which can be up to 10^5, times stronger than that available with the membrane-in-the-middle geometry. Furthermore, simply by changing a phase in the optical readout interferometer one can also measure displacement itself. Therefore, by combining the strong X_M^2 measurements with state tomography technique discussed in chapters 6 and 7 one can prepare and reconstruct a non-Gaussian quantum superposition state of a mechanical resonator.

PHYSICAL REVIEW X **1**, 021011 (2011)

Selective Linear or Quadratic Optomechanical Coupling via Measurement

Michael R. Vanner
Vienna Center for Quantum Science and Technology (VCQ), Faculty of Physics, University of Vienna,
Boltzmanngasse 5, Vienna A-1090, Austria

(Received 3 June 2011; published 28 November 2011)

The ability to engineer both linear and nonlinear coupling with a mechanical resonator is an important goal for the preparation and investigation of macroscopic mechanical quantum behavior. In this work, a measurement based scheme is presented where linear or square mechanical-displacement coupling can be achieved using the optomechanical interaction that is linearly proportional to the mechanical position. The resulting square-displacement measurement strength is compared to that attainable in the dispersive case that has a direct interaction with the mechanical-displacement squared. An experimental protocol and parameter set are discussed for the generation and observation of non-Gaussian states of motion of the mechanical element.

DOI: 10.1103/PhysRevX.1.021011 Subject Areas: Optics, Quantum Physics, Quantum Information

I. INTRODUCTION

Currently the main approaches to cavity optomechanics [1] can be divided into two categories—reflective and dispersive. In each approach the mechanical and optical degrees of freedom are coupled via radiation pressure and the dependence of the cavity resonance frequency on the mechanical position. The first approach is depicted in Fig. 1(a), where the optical field is reflected from a mechanical element and the change in cavity frequency and hence interaction Hamiltonian are linearly proportional to the mechanical position. Optomechanical realizations of this approach include deformable Fabry-Perot cavities and optical whispering-gallery-mode resonators, which are discussed in Ref. [1]. The second approach is depicted in Fig. 1(b), where a mechanical element is positioned within an optical field and partial reflection from both sides gives rise to a dispersive interaction. In this arrangement, the cavity frequency varies periodically with mechanical displacement. This can be used to give a linear or quadratic position-dependent change in the cavity frequency if the mechanical element is positioned at an antinode or node of the field, respectively. The flexibility to select between linear or quadratic displacement coupling provides considerable versatility and thus dispersive optomechanics is an exciting candidate to observe and explore quantum-mechanical phenomena of macroscopic resonators. Optomechanical realizations of this approach utilize a dielectric membrane [2] or trapped cold atoms [3], positioned within an optical cavity, and experimental work is underway to realize this with an optically trapped microsphere [4]. The quadratic mechanical-position coupling offered by dispersive optomechanics provides a route to observe quantization in mechanical energy [2]. Moreover, such quadratic coupling can also be used for cooling and squeezing of the mechanical element [5] and it can be enhanced by using additional optical spatial modes, which even allows for quartic interaction [6].

In this paper, a scheme is presented that allows measurement of the mechanical displacement squared using an optomechanical interaction that is linear with the mechanical position. Here, optical pulses that are short compared to a mechanical period are used and the square-displacement coupling is obtained by exploiting the nonlinear optical dependence of the interaction. This interaction has been linearized in much of the present literature, but continuous nonlinear optomechanical interaction has recently been studied resulting in nonclassical states of light [7] and of the mechanical oscillator [8]. Also, working beyond the linear regime has been proposed for non-Gaussian quantum-state preparation of a collective spin variable [9]. The optomechanical setup considered here is shown in Fig. 1(c), where an optical pulse in a coherent state interacts with an optomechanical system and is then measured via homodyne detection. Following the interaction, Wigner reconstruction of the optical subsystem of the optomechanical entangled state, would yield a "scimitar state" shown in Fig. 1(d). The form of this optical state can be understood as the mechanical position fluctuations (including quantum fluctuations) rotate the optical field. For small rotations, one sees from Fig. 1(d) that measurement of the optical phase quadrature allows for a measurement of the mechanical position. However, of particular interest here, measurement of the amplitude quadrature may give outcomes that could have resulted from two distinct mechanical positions. This is due to an effective displacement-squared coupling, which can be used for non-Gaussian state preparation. In Ref. [10] it was discussed how measurement of the optical phase quadrature can be used to perform quantum-state tomography of the motional state of the mechanical resonator and generate conditional squeezed mechanical states.

Published by the American Physical Society under the terms of the Creative Commons Attribution 3.0 License. Further distribution of this work must maintain attribution to the author(s) and the published article's title, journal citation, and DOI.

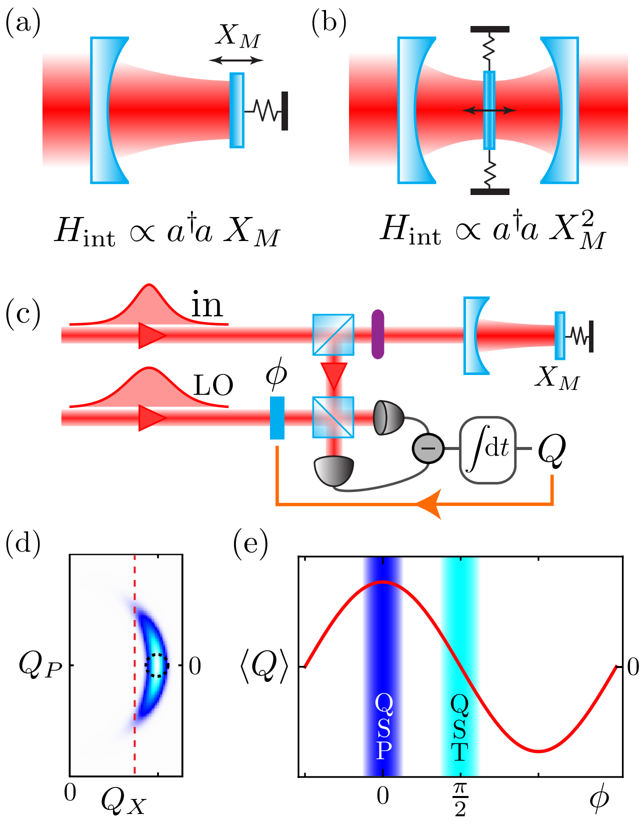

FIG. 1. Cavity optomechanics is currently realized using (a) reflective and (b) dispersive approaches. The interaction in the former is proportional to mechanical displacement X_M, however, in the latter the interaction can be tuned to being proportional to X_M or X_M^2. Pulses of light may be used to probe and manipulate the motional state of the mechanical resonator. The optical setup considered here (c) is a pulse incident upon an optomechanical system with an interaction proportional to X_M and then an optical quadrature measurement performed via homodyne detection. Following the interaction, the Wigner function of the optical field (d) is scimitar shaped due to mechanical-position-induced optical rotations. The distribution of the initial coherent state is indicated by the dashed circle. (The parameters for this plot were chosen to exaggerate the curvature.) For small rotations, the phase quadrature Q_P is proportional to X_M and the amplitude quadrature carries X_M^2 information. The amplitude-quadrature measurement outcome indicated by the red dashed line may have originated from two distinct mechanical positions, which provides a means for superposition preparation. By choosing the phase in (e) homodyne detection one can use the amplitude quadrature for X_M^2 measurements and quantum-state preparation or use the phase quadrature for X_M measurements to perform quantum-state tomography.

Thus, the possibility to select between displacement and displacement-squared measurements provides the tools to generate non-Gaussian quantum states of the mechanical resonator and perform state reconstruction simply by choosing the phase in the homodyne interferometer as is shown in Fig. 1(e).

II. MODEL

The optomechanical Hamiltonian with linear mechanical position coupling in the optical rotating frame at the cavity frequency including a coherent resonant drive is

$$\frac{H_{\rm lin}}{\hbar} = \omega_M b^\dagger b - g_{\rm lin}\sqrt{2}a^\dagger a X_M - i\sqrt{2\kappa N_p}\,\alpha_{\rm in}(a - a^\dagger), \tag{1}$$

where the optomechanical-coupling rate, which is realization dependent, is of the form $g_{\rm lin} = \omega_L x_0/L$. The cavity field's resonance frequency, annihilation operator, and amplitude decay rate are ω_L, a, and κ, respectively, and L is the cavity length. The mechanical zero-point extension is $x_0 = \sqrt{\hbar/2m\omega_M}$, where ω_M, b, m, and $X_M(P_M)$ are the mechanical element's eigenfrequency, annihilation operator, effective mass, and position (momentum) quadrature (operator), respectively, where a single mechanical mode is considered. The input pulse has mean photon number N_p and is described by $\alpha_{\rm in}$, the normalized envelope, i.e., $\int dt\alpha^2_{\rm in}(t) = 1$, which is assumed real.

During the interaction, which is short with respect to a mechanical period, thus requiring $\kappa \gg \omega_M$, the mechanical position is considered constant and the optical and mechanical equations of motion can be solved independently of one another. Immediately after the pulse interaction, the mechanical position is unchanged, i.e., $X_M^{\rm out} = X_M^{\rm in}$; however, optomechanical entanglement is generated and correlations are established between the mechanical momentum and the optical intensity, $P_M^{\rm out} = P_M^{\rm in} + \sqrt{2}g_{\rm lin}\int dt a^\dagger a$.

The intracavity field evolves during the nonlinear optomechanical interaction according to

$$\frac{da}{dt} = \left(ig_{\rm lin}\sqrt{2}X_M - \kappa\right)a + \sqrt{2\kappa}\left(\sqrt{N_p}\alpha_{\rm in} + a_{\rm in}\right), \tag{2}$$

where the field is rotated in proportion to the mechanical position and $a_{\rm in}$ is the optical input noise. This can be immediately solved exactly [11], however, in this work the solution is approximated as the rotation is assumed small and the mean of the field is

$$\frac{\langle a(t)\rangle}{\sqrt{N_p}} \simeq \alpha_0(t) + i\frac{g_{\rm lin}}{\kappa}\alpha_1(t)\langle X_M\rangle - \frac{g^2_{\rm lin}}{\kappa^2}\alpha_2(t)\langle X_M^2\rangle, \tag{3}$$

where the dimensionless temporal mode functions $\alpha_{0,1,2}$ are introduced [12]. The phase quadrature of the intracavity field contains information on the mechanical displacement, and the amplitude quadrature carries information of the mechanical-displacement squared [Fig. 1(e)]. Measurements of these quadratures can be performed by time-domain homodyne detection of the output field $a_{\rm out} = \sqrt{2\kappa}a - a_{\rm in}$. Homodyning the amplitude quadrature is described by $Q_X = \sqrt{2}\int dt\alpha_{\rm LO}(t)X_L^{\rm out}(t)$, where $X_L^{\rm out} = 2^{-1/2}(a_{\rm out} + a^\dagger_{\rm out})$ (similarly Q_P describes phase-quadrature detection). For an optimal measurement of X_M^2, (X_M)

one chooses the local oscillator pulse α_{LO} to have an amplitude directly proportional to α_2, (α_1). The mean of the amplitude-quadrature measurement is $\langle Q_X\rangle = Q_X^{(0)} - \chi_X\langle X_M^2\rangle$, where the first term is the contribution from α_0 and χ_X is the square-displacement measurement strength. For convenience, the outcome of the homodyne measurement is rewritten as $\Delta Q_X = Q_X^{(0)} - Q_X$. The optimal single-pulsed measurement of X_M is achieved with an input drive with a Lorentzian spectrum, which matches the natural decay of the cavity [10]. The square-displacement measurement strength is optimal when $\alpha_{\mathrm{in}}^2(\omega) = (3\pi)^{-1}8\kappa^5/(\kappa^2+\omega^2)^3$, which is not Lorentzian due to the higher-order nature of the interaction considered here. This gives $\chi_X = \sqrt{42N_p}g_{\mathrm{lin}}^2/\kappa^2$.

This kind of pulsed interaction and measurement is well suited to being described with the use of measurement operators as outcome probabilities, and conditional mechanical states can be readily determined [13]. Homodyne detection of the amplitude quadrature has the outcome probability density $\Pr(\Delta Q_X) = \mathrm{Tr}_M(\Upsilon_X^\dagger\Upsilon_X\rho_M^{\mathrm{in}})$, where Υ_X is the corresponding measurement operator. In this pulsed regime ΔQ_X has mechanical dependence only on X_M, which allows $\Upsilon_X^\dagger\Upsilon_X$ to be interpreted as an outcome probability density conditioned on a mechanical position. For the coherent optical drive considered here one obtains

$$\Upsilon_X(X_M, \Delta Q_X) = \pi^{-1/4}e^{i\Omega_{\mathrm{lin}}X_M}\exp[-\tfrac{1}{2}(\Delta Q_X - \chi_X X_M^2)^2], \tag{4}$$

where the mean momentum transfer is $\Omega_{\mathrm{lin}} = (5\sqrt{2}/3)N_p g_{\mathrm{lin}}/\kappa$.

III. COMPARISON TO THE DISPERSIVE QUADRATIC INTERACTION

Before proceeding to a discussion of the mechanical states of motion that can be prepared with Υ_X, the square-displacement measurement scheme introduced above is compared with the dispersive case. The Hamiltonian from Ref. [2] for optomechanical systems with a dispersive element positioned so that the cavity frequency varies quadratically with the position of the element, in the optical rotating frame at resonance, including the drive is

$$\frac{H_{\mathrm{sq}}}{\hbar} = \omega_M b^\dagger b + g_{\mathrm{sq}}a^\dagger a X_M^2 - i\sqrt{2\kappa N_p}\alpha_{\mathrm{in}}(a - a^\dagger), \tag{5}$$

where the quadratic-optomechanical coupling rate is $g_{\mathrm{sq}} = (16\pi^2 c x_0^2/L\lambda^2)\sqrt{2(1-r)}$, r is the (field) reflectivity of the dispersive element, and λ is the optical wavelength. The phase quadrature of an optical pulse incident upon such an optomechanical system will be displaced in proportion to X_M^2, and it is readily shown that for a homodyne measurement of the phase quadrature with outcome Q_P the measurement operator is $\Upsilon_{\mathrm{sq}} = \pi^{-1/4}e^{-i\Omega_{\mathrm{sq}}X_M^{\mathrm{in}}X_M}\times\exp[-\frac{1}{2}(Q_P + \chi_{\mathrm{sq}}X_M^2)^2]$, which has recently been used in Ref. [14]. After pulse-shape optimization, $\Omega_{\mathrm{sq}} = 3N_p g_{\mathrm{sq}}/\kappa$ and $\chi_{\mathrm{sq}} = \sqrt{10N_p}g_{\mathrm{sq}}/\kappa$. Comparing the measurement strengths for the dispersive direct X_M^2 interaction and the effective X_M^2 coupling from the linear interaction for identical N_p and λ gives

$$\frac{\chi_X}{\chi_{\mathrm{sq}}} \simeq \frac{1}{\pi}\frac{\mathcal{F}_{\mathrm{lin}}^2}{\mathcal{F}_{\mathrm{sq}}}\frac{x_{\mathrm{lin}}^2}{x_{\mathrm{sq}}^2}\frac{1}{\sqrt{2(1-r)}}, \tag{6}$$

where the cavity finesses and mechanical zero-point extensions are distinguished by subscripts for the two optomechanical cases. Remarkably, using the optomechanical interaction that is linearly proportional to X_M and optical amplitude-quadrature measurements allows for X_M^2 measurements that are stronger than that available with the direct X_M^2 interaction in dispersive optomechanics by approximately the cavity finesse. This, in combination with the measurement-based selectability between linear or quadratic couplings offered here, is the main result of this work.

IV. EXPERIMENTAL PROTOCOL AND DISCUSSION

Jacobs and colleagues discussed the preparation of superposition of the position of a mechanical resonator via X_M^2 measurements [15]. This work has recently been extended to include feedback control of the superposition separation [16]. Such benchmark quantum states show striking differences between classical and quantum behavior and are thus highly sought experimentally to study the quantum-mechanical properties of macroscopic objects [17–19]. In the following, an experimental protocol and a parameter set are discussed to prepare and observe the spatial superposition of a massive mechanical resonator using the nonlinear interaction and measurement Υ_X. A measurement on a variety of experimentally accessible initial states is considered, and the resulting conditional and unconditional mechanical states of motion are determined.

As the spectrum of measurement outcomes is continuous, it is not experimentally possible to postselect from many experimental runs on a single measurement outcome. Instead, a window must be used. The mechanical state conditioned on outcomes occurring in the window $\Delta Q_X \pm w/2$ (labeled by w) is

$$\rho_M^{(w)} = \frac{1}{\Pr(w)}\int_w d\Delta Q_X'\,\Upsilon_X(\Delta Q_X')\rho_M^{\mathrm{in}}\Upsilon_X^\dagger(\Delta Q_X'), \tag{7}$$

where $\Pr(w) = \int_w d\Delta Q_X \Pr(\Delta Q_X)$ is the probability of obtaining an outcome in the window. The mean measurement outcome for a mechanical thermal state with thermal occupation $\bar{n}$ is $\langle\Delta Q_X\rangle = \chi_X(1/2 + \bar{n})$. As the mean is greater than zero, some insight is gained into the form of

$\Pr(\Delta Q_X)$, which is a non-Gaussian function with a large wing for positive outcomes that increases for a larger mechanical position variance.

In Fig. 2 the action of Υ_X is considered on three mechanical Gaussian states: the ground state, a thermal state, and a momentum-squeezed state. One may suspect that quite a narrow window for conditioning must be used in order to achieve significant coherence between the superposition components, however, conditional mechanical states, prepared from high-purity initial states, show strong quantum coherence even for relatively large conditioning windows. For example, the conditional mechanical state shown in Fig. 2(b) exhibits strong Wigner negativity even for $w = 0.8$, which allows the use of 15% of the measurement outcomes. This plot also reveals the interesting feature that the negative regions are ''curled around'' positive regions, a feature which is not seen in the more commonly studied superposition of coherent states. This arises due to the population components having an asymmetric distribution about their peaks, specifically, there is a broader wing nearer $X_M = 0$ and a sharper edge on the other side. This form of the population components is more clearly seen in Fig. 2(e), which is the conditional mechanical state starting from a low-occupation thermal state. When the population components have a more symmetric X_M distribution about their peak, the interferences no longer curl as strongly, as is seen in Fig. 2(h), the conditional state starting from a squeezed state.

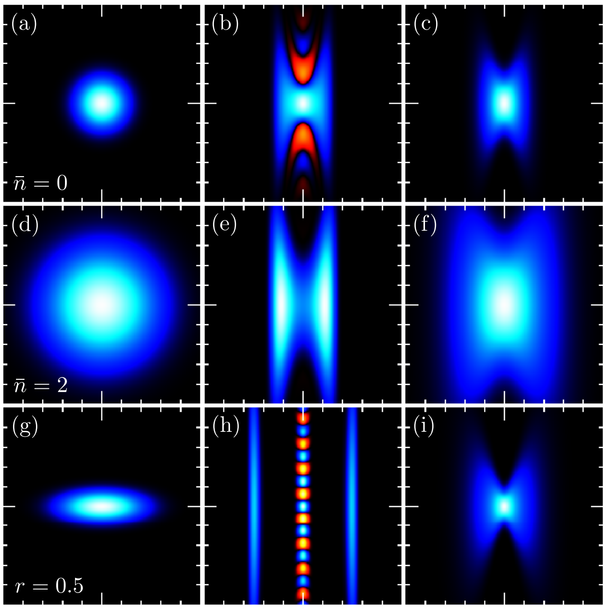

FIG. 2. Mechanical Wigner functions of initial states (left), conditional states (center), and unconditional states (right). (X_M is the horizontal axis, P_M is the vertical axis. The plot range is ±5 for all axes. Color scale: black is for zero magnitude, blue for positive values, and red for negative values.) The initial states are the ground state, $\bar{n} = 0$ (a), a thermal state with $\bar{n} = 2$ (d), and a momentum-squeezed vacuum state with squeezing parameter $r = 0.5$ (g). Conditional states prepared with Υ_X acting on the corresponding initial states with $\chi_X = 1$, $\Delta Q_X = 1.5$, $w = 0.8$ are shown in (b) and (e) and $\Delta Q_X = 6.4$ has been used in (h). The probabilities of obtaining an outcome in the windows used above are: (b) 14.9%, (e) 14.5%, and (h) 1.1%. Note the disappearance of negativity—a quantum-to-classical transition—for initial thermal occupation (e) and if the measurement outcomes are ignored (c), (f), (h).

Since a measurement of the optical amplitude quadrature erases all the linear-displacement information gained during the interaction and $\langle \Delta Q_X \rangle > 0$, the unconditional (i.e., all measurement outcomes are ignored) mechanical state, $\rho_M^{\mathrm{out}} = \int_{-\infty}^{\infty} d\Delta Q_X \Upsilon_X \rho_M^{\mathrm{in}} \Upsilon_X^\dagger$, is also non-Gaussian, however, mixed.

The superposition separation δ is defined as the distance between the maxima of the two population components. This depends on the initial mechanical distribution, the measurement outcome, and the square-displacement measurement strength. For Gaussian initial mechanical states with a standard deviation σ in their position spread, the superposition separation is

$$\delta = \frac{\sqrt{4\Delta Q_X \chi_X - \sigma^{-2}}}{\chi_X}. \tag{8}$$

Experimental progress in optomechanics is steadily approaching the regime where the important parameter g_{lin}/κ, which quantifies the mechanical momentum displacement by a single photon (for $\kappa \gg \omega_M$), approaches unity. In this work χ_X scales with the square of this parameter and the pulsed position-measurement strength for mechanical quantum-state tomography [10] scales linearly with this parameter. In present-day experiments [20], $g_{\mathrm{lin}}/\kappa \ll 1$, which this work overcomes by utilizing large coherent amplitudes in order to achieve sufficient coupling to prepare and observe non-Gaussian mechanical states of motion. To ensure a short interaction, the cavity decay rate is chosen as $\kappa = 10^3 \omega_M$, which for a desired finesse sets the cavity length required. In Table I a list of parameters is provided for a deformable Fabry-Perot optomechanical system with a kHz-scale mechanical resonator.

The protocol for quantum-state preparation and quantum-state tomography comprises three steps: (i) an initialization stage of mechanical precooling and/or squeezing. Since $\kappa \gg \omega_M$ is required here and low-frequency mechanical resonators are considered, active-feedback cooling is most suitable [21,22]. Alternatively, in this regime, squeezing and purification can be achieved with the use of conditional measurements [10]. Additionally, squeezing can be achieved by applying a parametric modulation to the mechanical device [23]. (ii) Following this, an optical pulse is injected into the optomechanical cavity to realize Υ_X and the measurement outcome is recorded. At this point, the mechanical oscillator has gained the momentum Ω_{lin}, which after one quarter of a period of free evolution shifts the cavity

TABLE I. An experimentally accessible set of parameters to achieve unity square-displacement measurement strength.

Optical wavelength:	λ	1064 nm
Mechanical effective mass:	m	40 ng
Mechanical eigenfrequency:	$\omega_M/2\pi$	2 kHz
Cavity finesse:	$\mathcal{F}$	5×10^4
Photon number per pulse:	N_p	1.7×10^9
Cavity length:	L	750 μm
Mechanical ground-state size:	x_0	10 fm
Optomechanical coupling:	$g_{\rm lin}/2\pi$	3.8 kHz
Single-photon strength:	$g_{\rm lin}/\kappa$	1.9×10^{-3}
Separation ($\bar{n} = 0$, $\Delta Q_X = 1.5$):	δ	2.0

resonance frequency by $\Delta\omega_\Omega = g_{\rm lin}\sqrt{2}\Omega_{\rm lin}$. As this can be much larger than κ any subsequent pulse will not resonantly drive the cavity. In order to overcome this, a two-pulse preparation sequence can be used where a second pulse follows after half a mechanical period of free evolution to cancel the mean momentum gained by the resonator. In this case, one applies Υ_X twice where both outcomes are recorded, thus strengthening the measurement of X_M^2. This procedure requires a good degree of optical amplitude stability, which is necessary for Υ_X measurements anyway. During the free evolution, the appropriate master equation is solved to determine the mechanical state immediately prior to the second measurement. However, as discussed below, given the parameters considered here, the coupling to the mechanical bath is not expected to play a strong role during this time scale. (iii) With the resonator state near the origin of phase space, quantum-state tomography, as discussed in Ref. [10], is now performed. This is achieved by later injecting a subsequent pulse with the local oscillator phase switched to measure the optical phase quadrature as in Fig. 1(e). Repeating this protocol many times and post-selecting the measurement outcomes ΔQ_X within the desired window provides a powerful experimental platform to generate and fully reconstruct a non-Gaussian state of motion of a mechanical resonator.

In order to prepare mechanical superposition states with Υ_X there needs to be a sufficient mechanical-displacement-induced optical rotation such that two distinct positions give the same amplitude-quadrature outcome. This is best achieved if the mechanical mean position gives zero rotation. For mechanical states that have a nonzero mean, which could have been conditionally prepared with a prior pulse [10], non-Gaussian state preparation and tomography can be performed by providing a feedback phase shift [indicated by the arrow in Fig. 1(c)] to rotate the optical scimitar to be centered about the Q_X axis, as in Fig. 1(d). Additionally, it is noted that for optical rotation beyond that considered in (3), existing experimental calibration procedures and the interpretation of optical phase measurements will require modification to take the optomechanical nonlinearity into account.

Studying the decoherence of quantum superposition in a mechanical resonator is important to determine the feasibility of optomechanical systems as components for quantum-information applications. Proposals for such applications are numerous and include quantum memory [24], optomechanically mediated qubit-light transduction [25], and coherent optical wavelength conversion [26], to name a few. There is much literature on the topic of environmental coupling and decoherence [27], so no detailed discussion will be provided here. However, in the context of this proposal, what is important is the parameter $\bar{n}/Q$, where Q is the mechanical quality factor. This parameter quantifies the rate of rethermalization normalized to the mechanical frequency and must be much less than unity for studying the evolution of quantum-mechanical phenomena over the time scale ω_M^{-1}. A temperature of 25 mK accessible with dilution refrigeration and a $Q = 5 \times 10^6$ give $\bar{n}/Q = 0.05$ using the mechanical frequency above. With the full quantum-state tomography available here, this scheme allows the dynamics of mechanical superposition states to be measured, which may be used to characterize the couplings responsible for decoherence, thus allowing for improved mechanical device engineering.

Furthermore, the significant mass involved in the spatial superposition offers a parameter regime that allows for an experimental test of collapse models. Very recent proposals in matter-wave interferometry [14,28], which also consider the use of filtering-type operations to generate superposition, may provide the ability to test continuous spontaneous localization [29]. The mechanical resonator parameters considered here are not suitable for testing continuous spontaneous localization predominantly because the superposition separation is small [30]. However, the separation can be larger than the distribution of the mass contained within the nucleus and so this can be used to test gravitational collapse [31]. For example, using the parameters above ($\delta = 2.0$, $x_0 = 10$ fm) the separation is approximately 28 fm and the diameter of a ^{28}Si nucleus is approximately 8 fm. It may be useful in such an investigation to start with an initial squeezed mechanical state, as is considered in Figs. 2(g)–2(i), as one can study a larger range of superposition separations as the probability density of measurement outcomes is broader.

V. CONCLUSION

This work has provided a means to measure the displacement or displacement squared of a mechanical resonator using the optomechanical interaction linearly proportional to the mechanical displacement by simply changing the phase in optical homodyne measurement. Displacement-squared measurements have so far been predominantly considered in dispersive optomechanics; however, the optimal square-displacement measurement strength obtained in the scheme introduced here can be significantly stronger than that available in dispersive optomechanics as it scales more favorably with the cavity finesse. This opens the possibility that optomechanics with an interaction Hamiltonian that is linear with the mechanical position may also provide a route to observe mechanical-energy quantization, as was considered in [2]. Moreover, as was proposed in [15], with an X_M^2 coupling to a mechanical resonator one can prepare a superposition of positions via measurement. This, applied to the X_M^2 coupling achieved here and combined with the ability to perform mechanical state tomography with time [10], provides an alternative to Refs. [17,19] to generate the superposition of a mechanical resonator without the need for large single-photon mechanical displacement g_{lin}/κ. Such mechanical superposition states are important to investigate experimentally in order to determine the feasibility of mechanical resonators as elements in quantum-information applications and to explore decoherence mechanisms arising from environment interaction or, for example, gravitationally induced collapse.

ACKNOWLEDGMENTS

M. R. V. acknowledges support from the FWF Doctoral Programme CoQuS (W 1210), the Austrian Academy of Sciences, and gratefully acknowledges discussion with Markus Aspelmeyer, Gerard J. Milburn, and Igor Pikovski.

[1] T. J. Kippenberg and K. J. Vahala, *Cavity Optomechanics: Back-Action at the Mesoscale*, Science **321**, 1172 (2008); I. Favero and K. Karrai, *Optomechanics of Deformable Optical Cavities*, Nat. Photon. **3**, 201 (2009); F. Marquardt and S. T. Girvin, *Optomechanics*, Physics **2**, 40 (2009); M. Aspelmeyer, S. Groeblacher, K. Hammerer, and N. Kiesel, *Quantum Optomechanics—Throwing a Glance*, JOSA B **27**, A189 (2010).

[2] J. D. Thompson, B. M. Zwickl, A. M. Jayich, F. Marquardt, S. M. Girvin, and J. G. E. Harris, *Strong Dispersive Coupling of a High-Finesse Cavity to a Micromechanical Membrane*, Nature (London) **452**, 72 (2008).

[3] T. P. Purdy, D. W. C. Brooks, T. Botter, N. Brahms, Z.-Y. Ma, and D. M. Stamper-Kurn, *Tunable Cavity Optomechanics with Ultracold Atoms*, Phys. Rev. Lett. **105**, 133602 (2010).

[4] See, for example, T. Li, S. Kheifets, and Mark G. Raizen, *Millikelvin Cooling of an Optically Trapped Microsphere in Vacuum*, Nature Phys. **7**, 527 (2011).

[5] A. Nunnenkamp, K. Borkje, J. G. E. Harris, and S. M. Girvin, *Cooling and Squeezing via Quadratic Optomechanical Coupling*, Phys. Rev. A **82**, 021806(R) (2010).

[6] J. C. Sankey, C. Yang, B. M. Zwickl, A. M. Jayich, and J. G. E. Harris, *Strong and Tunable Nonlinear Optomechanical Coupling in a Low-Loss System*, Nature Phys. **6**, 707 (2010).

[7] P. Rabl, *Photon Blockade Effect in Optomechanical Systems*, Phys. Rev. Lett. **107**, 063601 (2011).

[8] A. Nunnenkamp, K. Borkje, and S. M. Girvin, *Single-Photon Optomechanics*, Phys. Rev. Lett. **107**, 063602 (2011).

[9] S. Massar and E. S. Polzik, *Generating a Superposition of Spin States in an Atomic Ensemble*, Phys. Rev. Lett. **91**, 060401 (2003).

[10] M. R. Vanner, I. Pikovski, G. D. Cole, M. S. Kim, C. Brukner, K. Hammerer, G. J. Milburn, and M. Aspelmeyer, *Pulsed Quantum Optomechanics*, Proc. Natl. Acad. Sci. U.S.A. **108**, 16182 (2011).

[11] This Hamiltonian has been previously used to model wave-mixing processes, which allow for the quantum nondemolition measurement of the number squared, see G. J. Milburn and D. F. Walls, *Quantum Nondemolition Measurements via Quantum Counting*, Phys. Rev. A **28**, 2646 (1983).

[12] The cavity integrates the input drive and phase accumulates proportional to X_M and X_M^2 with the dimensionless envelopes: $\alpha_0(t) = \sqrt{2\kappa}\int_{-\infty}^{t} dt' e^{-\kappa(t-t')}\alpha_{\mathrm{in}}(t')$, $\alpha_1(t) = \sqrt{2\kappa}\int_{-\infty}^{t} dt' e^{-\kappa(t-t')}\kappa\sqrt{2}(t-t')\alpha_{\mathrm{in}}(t')$, $\alpha_2(t) = \sqrt{2\kappa}\int_{-\infty}^{t} dt' e^{-\kappa(t-t')}\kappa^2(t-t')^2\alpha_{\mathrm{in}}(t')$, respectively.

[13] For a recent discussion on generalized quantum measurement see, for example, H. M. Wiseman and G. J. Milburn, *Quantum Measurement and Control* (Cambridge University Press, Cambridge, 2010).

[14] O. Romero-Isart, A. C. Pflanzer, F. Blaser, R. Kaltenbaek, N. Kiesel, M. Aspelmeyer, and J. I. Cirac, *Large Quantum Superpositions and Interference of Massive Nanometer-Sized Objects*, Phys. Rev. Lett. **107**, 020405 (2011).

[15] K. Jacobs, L. Tian, and J. Finn, *Engineering Superposition States and Tailored Probes for Nanoresonators via Open-Loop Control*, Phys. Rev. Lett. **102**, 057208 (2009).

[16] K. Jacobs, J. Finn, and S. Vinjanampathy, *Real-Time Feedback Control of a Mesoscopic Superposition*, Phys. Rev. A **83**, 041801(R) (2011).

[17] S. Bose, K. Jacobs, and P. Knight, *Scheme to Probe the Decoherence of a Macroscopic Object*, Phys. Rev. A **59**, 3204 (1999).

[18] A. D. Armour, M. P. Blencowe, and K. C. Schwab, *Entanglement and Decoherence of a Micromechanical Resonator via Coupling to a Cooper-Pair Box*, Phys. Rev. Lett. **88**, 148301 (2002).

[19] W. Marshall, C. Simon, R. Penrose, and D. Bouwmeester, *Towards Quantum Superpositions of a Mirror*, Phys. Rev. Lett. **91**, 130401 (2003).

[20] Examples of experiments with comparatively large g_{lin}/κ can be found in the following: A. H. Safavi-Naeini, T. P. Mayer Alegre, M. Winger, and O. Painter, *Optomechanics in an Ultrahigh-Q Two-Dimensional Photonic Crystal Cavity*, Appl. Phys. Lett. **97**, 181106 (2010); J. D. Teufel, Dale Li, M. S. Allman, K. Cicak, A. J. Sirois, J. D. Whittaker, and R. W. Simmonds, *Circuit Cavity Electromechanics in the Strong-Coupling Regime*, Nature (London) **471**, 204 (2011).

[21] C. Genes, D. Vitali, P. Tombesi, S. Gigan, and M. Aspelmeyer, *Ground-State Cooling of a Micromechanical Oscillator: Comparing Cold Damping and Cavity-Assisted Cooling Schemes*, Phys. Rev. A **77**, 033804 (2008).

[22] J. Zhang, Y.-x. Liu, and F. Nori, *Cooling and Squeezing the Fluctuations of a Nanomechanical Beam by Indirect Quantum Feedback Control*, Phys. Rev. A **79**, 052102 (2009).

[23] See, for example, A. Mari and J. Eisert, *Gently Modulating Optomechanical Systems*, Phys. Rev. Lett. **103**, 213603 (2009).

[24] J. Zhang, K. Peng, and S. L. Braunstein, *Quantum-State Transfer from Light to Macroscopic Oscillators*, Phys. Rev. A **68**, 013808 (2003).

[25] K. Stannigel, P. Rabl, A. S. Sorensen, P. Zoller, and M. D. Lukin, *Optomechanical Transducers for Long-Distance Quantum Communication*, Phys. Rev. Lett. **105**, 220501 (2010).

[26] L. Tian and H. Wang, *Optical Wavelength Conversion of Quantum States with Optomechanics*, Phys. Rev. A **82**, 053806 (2010).

[27] See M. Schlosshauer, *Decoherence and the Quantum-to-Classical Transition* (Springer, New York, 2007) for a recent discussion.

[28] S. Nimmrichter, P. Haslinger, K. Hornberger, and M. Arndt, *Concept of an Ionizing Time-Domain Matter-Wave Interferometer*, New J. Phys. **13**, 075002 (2011); S. Nimmrichter, K. Hornberger, P. Haslinger, and M. Arndt, *Testing Spontaneous Localization Theories with Matter-Wave Interferometry*, Phys. Rev. A **83**, 043621 (2011).

[29] See, for example, S. L. Adler and A. Bassi, *Is Quantum Theory Exact?*, Science **325**, 275 (2009) and references therein.

[30] A. Bassi, E. Ippoliti, and S. L. Adler, *Towards Quantum Superpositions of a Mirror: An Exact Open Systems Analysis*, Phys. Rev. Lett. **94**, 030401 (2005).

[31] L. Diósi, *Models for Universal Reduction of Macroscopic Quantum Fluctuations*, Phys. Rev. A **40**, 1165 (1989); R. Penrose, *On Gravity's Role in Quantum State Reduction*, Gen. Relativ. Gravit. **28**, 581 (1996).

9 A Scheme to Probe Planck-Scale Modifications to the Canonical Commutation Relation

For several decades now modern physics has been unable to unify general relativity with quantum mechanics. The challenge of this endeavour is made more difficult by the lack of experimental observations of quantum gravitational phenomena that would provide important road signs to a theory of quantum gravity - as was of paramount importance for the development of quantum theory itself. While the Planck energy ($E_{\mathrm{P}} = 1.2 \times 10^{19}$ GeV), Planck length ($L_{\mathrm{P}} = 1.6 \times 10^{35}$ m), and Planck time ($t_{\mathrm{P}} = 10^{-44}$ s) are at present out of reach to experimentally explore directly, while a great challenge, it is not unreasonable to expect to be able to probe quantum mechanical phenomena at the scale of the Planck mass ($m_{\mathrm{P}} = 22$ μg). Cavity quantum optomechanics may provide such a route to do this as mechanical oscillators with vibrational modes of masses of order m_{P} are readily fabricated and early signs of quantum mechanical behaviour are now being observed.

A common feature of many current models of quantum gravity is the existence of a minimum length scale in the universe. Excitingly, such a quantity yields experimentally testable phenomena. Such a minimum length may be described theoretically by a modification to the quantum mechanical Heisenberg uncertainty relation [89] and thus a deformation to the commutation relation between position and momentum. There are a variety of such deformations currently under consideration that yield a minimum length scale, see e.g. Refs [90, 91], and also deformations that also yield a maximum momentum [92, 93].

This theoretical project [94] proposed a method, using quantum optomechanics and the pulsed interaction studied in chapter 6, to probe for such commutator deformations. The key result of our scheme is a sequence of four pulsed optomechanical interactions that allows for a highly sensitive inference of mechanical commutator with a precision many orders of magnitude better than any existing scheme.

This project emerged from discussion, with very clever input from Myungshik Kim and Igor Pikovski, how to generate optomechanical phases of a geometric nature and how to infer the commutator between the position and momentum of a mechanical oscillator at a quantum mechanical level. It was well within the project's development that we realized that the quantum gravitational commutator deformations could be tested. In addition to participating in the project's early discussions, my specific contributions to this project were to conceive the optical setup that allows for the four pulsed optomechanical interactions followed by a measurement of the optical phase shift, and to, together with all co-authors, determine the parameter sets to test three different commutator deformations and analyze the experimental feasibility.

nature physics

ARTICLES

PUBLISHED ONLINE: 18 MARCH 2012 | DOI: 10.1038/NPHYS2262

Probing Planck-scale physics with quantum optics

Igor Pikovski[1,2]*, Michael R. Vanner[1,2], Markus Aspelmeyer[1,2], M. S. Kim[3]* and Časlav Brukner[2,4]

One of the main challenges in physics today is to merge quantum theory and the theory of general relativity into a unified framework. Researchers are developing various approaches towards such a theory of quantum gravity, but a major hindrance is the lack of experimental evidence of quantum gravitational effects. Yet, the quantization of spacetime itself can have experimental implications: the existence of a minimal length scale is widely expected to result in a modification of the Heisenberg uncertainty relation. Here we introduce a scheme to experimentally test this conjecture by probing directly the canonical commutation relation of the centre-of-mass mode of a mechanical oscillator with a mass close to the Planck mass. Our protocol uses quantum optical control and readout of the mechanical system to probe possible deviations from the quantum commutation relation even at the Planck scale. We show that the scheme is within reach of current technology. It thus opens a feasible route for table-top experiments to explore possible quantum gravitational phenomena.

It is at present an open question whether our underlying concepts of space–time are fully compatible with those of quantum mechanics. The ongoing search for a quantum theory of gravity is therefore one of the main challenges in modern physics. A major difficulty in the development of such theories is the lack of experimentally accessible phenomena that could shed light on the possible route for quantum gravity. Such phenomena are expected to become relevant near the Planck scale, that is, at energies on the order of the Planck energy $E_P = 1.2 \times 10^{19}$ GeV or at length scales near the Planck length $L_P = 1.6 \times 10^{-35}$ m, where space–time itself is assumed to be quantized. However, such a minimal length scale is not a feature of quantum theory. The Heisenberg uncertainty relation, one of the cornerstones of quantum mechanics[1], states that the position x and the momentum p of an object cannot be simultaneously known to arbitrary precision. Specifically, the indeterminacies of a joint measurement of these canonical observables are always bound by $\Delta x \Delta p \geq \hbar/2$. Yet, the uncertainty principle still allows for an arbitrarily precise measurement of only one of the two observables, say position, at the cost of our knowledge about the other (momentum). In stark contrast, in many proposals for quantum gravity the Planck length constitutes a fundamental bound below which position cannot be defined. It has therefore been suggested that the uncertainty relation should be modified to take into account such quantum gravitational effects[2]. In fact, the concept of a generalized uncertainty principle is found in many approaches to quantum gravity, for example in string theory[3,4], in the theory of doubly special relativity[5,6], within the principle of relative locality[7] and in studies of black holes[8–10]. A generalized uncertainty relation also follows from a deformation of the underlying canonical commutator $[x,p] \equiv xp - px$ (refs 11–15), as they are related via $\Delta x \Delta p \geq (1/2)|\langle [x,p]\rangle|$.

Preparing and probing quantum states at the Planck scale is beyond today's experimental possibilities. Current approaches to test quantum gravitational effects mainly focus on high-energy scattering experiments, which operate still 15 orders of magnitude away from the Planck energy E_P, or on astronomical observations[16,17], which have not found any evidence of quantum gravitational effects as of yet[18,19]. Another route would be to perform high-sensitivity measurements of the uncertainty relation, as any deviations from standard quantum mechanics are, at least in principle, experimentally testable[13–15]. However, with the best position measurements being of order $\Delta x/L_p \sim 10^{17}$ (refs 20,21), at present sensitivities are still insufficient and quantum gravitational corrections remain unexplored.

Here we propose a scheme that circumvents these limitations. Our scheme allows one to test quantum gravitational modifications of the canonical commutator in a novel parameter regime, thereby reaching a hitherto unprecedented sensitivity in measuring Planck-scale deformations. The main idea is to use a quantum optical ancillary system that provides a direct measurement of the canonical commutator of the centre of mass of a massive object. In this way Planck-scale accuracy of position measurements is not required. Specifically, the commutator of a very massive quantum oscillator is probed by a sequence of interactions with a strong optical field in an optomechanical setting, which uses radiation pressure inside an optical cavity[22,23]. The sequence of optomechanical interactions is used to map the commutator of the mechanical resonator onto the optical pulse. The optical field experiences a measurable change that depends on the commutator of the mechanical system and that is nonlinearly enhanced by the optical intensity. Observing possible commutator deformations thus reduces to a measurement of the mean of the optical field, which can be performed with very high accuracy by optical interferometric techniques. We show that, already with state-of-the art technology, tests of Planck-scale deformations of the commutator are within experimental reach.

Modified commutation relations

A common modification of the Heisenberg uncertainty relation that appears in a vast range of approaches to quantum gravity[2–4,24,25] is $\Delta x \Delta p \geq \hbar(1+\beta_0(\Delta p/(M_P c))^2)/2$. Here, β_0 is a numerical parameter that quantifies the modification strength, c is the speed of light and $M_P \simeq 22\,\mu\text{g}$ is the Planck mass. The minimal measurable length scale appears as a natural consequence with $\Delta x_{\min} = L_P\sqrt{\beta_0}$ (Fig. 1). Such a modification alters the allowed state-space and can

---

[1]Vienna Center for Quantum Science and Technology (VCQ), Boltzmanngasse 5, A-1090 Vienna, Austria, [2]Faculty of Physics, University of Vienna, Boltzmanngasse 5, A-1090 Vienna, Austria, [3]Quantum Optics and Laser Science (QOLS) group, Blackett Laboratory, Imperial College London, SW7 2BW, UK, [4]Institute for Quantum Optics and Quantum Information (IQOQI), Austrian Academy of Sciences, Boltzmanngasse 3, A-1090 Vienna, Austria. *e-mail: igor.pikovski@univie.ac.at; m.kim@imperial.ac.uk.

© 2012 Macmillan Publishers Limited. All rights reserved.

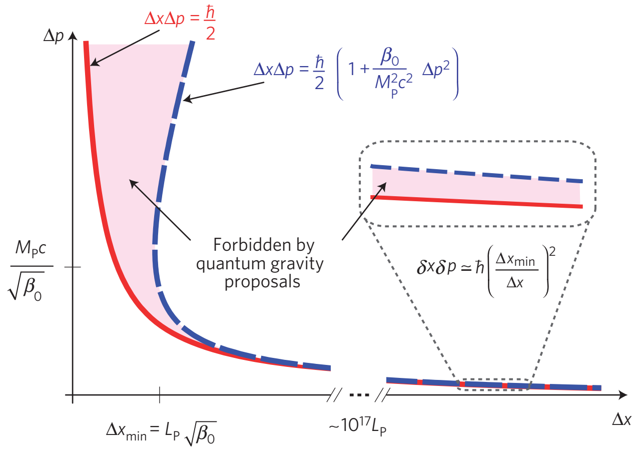

Figure 1 | The quantum uncertainty relation and a quantum gravitational modification. The minimum Heisenberg uncertainty (red curve) is plotted together with a modified uncertainty relation (dashed blue curve) with modification strength β_0. M_P and L_P are the Planck mass and Planck length, respectively. The shaded region represents states that are allowed in regular quantum mechanics but are forbidden in theories of quantum gravity that modify the uncertainty relation. The inset shows the two curves far from the Planck scale at typical experimental position uncertainties $\Delta x \gg \Delta x_{min}$. An experimental precision of $\delta x \delta p$ is required to distinguish the two curves, which is beyond experimental possibilities at present. However, this can be overcome by our scheme, which allows one to probe the underlying commutation relation in massive mechanical oscillators and its quantum gravitational modifications.

be seen as a manifestation of a deformed canonical commutator, for example of the form[12]

$$[x,p]_{\beta_0} = i\hbar\left(1+\beta_0\left(\frac{p}{M_P c}\right)^2\right) \tag{1}$$

So far, no effect of a modified canonical commutator has been observed in experiments. At present the best available measurement precision (Table 1) allows one to put an upper bound on the magnitude of the deformation of $\beta_0 < 10^{33}$ (ref. 13). For theories that modify the commutator this rules out the existence of an intermediate fundamental length scale on the order of $x \sim 10^{-19}$ m. Note that the Planck-scale modifications correspond to $\beta_0 \sim 1$ and are therefore untested. Furthermore, the above modification of the commutator is not unique and experiments can, in principle, distinguish between the various theories. In particular, a generalized version of the commutator deformation is[11]

$$[x,p]_{\mu_0} = i\hbar\sqrt{1+2\mu_0\frac{(p/c)^2+m^2}{M_P^2}} \tag{2}$$

Here, m is the rest mass of the particle and μ_0 is again a free numerical parameter. For small masses $m \ll p/c \lesssim M_P$, and for $\mu_0 = \beta_0$, the above modified commutator reduces to equation (1). However, an important difference is that the commutation relation in equation (2) depends directly on the rest mass of the particle. In the limit $p/c \ll m \lesssim M_P$, the commutator reduces to $[x,p]_{\mu_0} \approx i\hbar(1+\mu_0 m^2/M_P^2)$, which can be seen as a mass-dependent rescaling of $\hbar$. It is worth noting that a modified, mass-dependent Planck constant $\hbar = \hbar(m)$ also appears in other theories, some of which predict that the value of Planck's constant can decrease with increasing mass ($\hbar \to 0$ for $m \gg M_P$), in contrast to the prediction above. Such a reduction would also account for a transition to classicality in massive systems or at energies close to the Planck energy[6,10].

Table 1 | Current experimental bounds on quantum gravitational commutator deformations.

System/experiment	$\beta_{0,\max}$	$\gamma_{0,\max}$	References
Position measurement	10^{34}	10^{17}	20,21
Hydrogen Lamb shift	10^{36}	10^{10}	13,15
Electron tunnelling	10^{33}	10^{11}	13,15

The parameters β_0 and γ_0 quantify the deformation strengths of the modification given in equation (1) and of the modification given in equation (3), respectively. For electron tunnelling an electric current measurement precision of $\delta I \sim 1$ fA was taken.

Among the various proposals for different commutator deformations, we choose as a last example the recently proposed commutator[14] which also accounts for a maximum momentum that is present in several approaches to quantum gravity[5,6]

$$[x,p]_{\gamma_0} = i\hbar\left(1-\gamma_0\frac{p}{M_P c}+\gamma_0^2\left(\frac{p}{M_P c}\right)^2\right) \tag{3}$$

Here, γ_0 is again a free numerical parameter that characterizes the strength of the modification. Experimental bounds on γ_0 are more stringent than in the case of equation (1) and were considered in ref. 15. The best bound at present can be obtained from Lamb shift measurements in hydrogen, which yield $\gamma_0 \lesssim 10^{10}$ (Table 1).

The strength of the modifications in all the discussed examples depends on the mass of the system. For a harmonic oscillator in its ground state the minimum momentum uncertainty is given by $p_0 = \sqrt{\hbar m \omega_m}$, where m is the mass of the oscillator and ω_m is its angular frequency. The deformations are therefore enhanced in massive quantum systems. We note that theories of deformed commutators have an intrinsic ambiguity as to which degrees of freedom it should apply to for composite systems (see Supplementary Information). For the centre of mass mode, the mass dependence of the deformations suggests that using massive quantum systems allows easier experimental access to the possible deformations of the commutator, provided that precise quantum control can be attained. Optomechanical systems, where the oscillator mass can be around the Planck mass and even larger, therefore offer a natural test-bed for probing commutator deformations of its centre of mass mode.

Scheme to measure the deformations

In the following we will outline a quantum optical scheme that allows one to measure deformations of the canonical commutator of a mechanical oscillator with unprecedented precision. For simplicity we use dimensionless quadrature operators X_m and P_m. They are related to the position and momentum operators via $x = x_0 X_m$ and $p = p_0 P_m$, where $x_0 = \sqrt{\hbar/(m\omega_m)}$ and $p_0 = \sqrt{\hbar m \omega_m}$.

The scheme relies on displacements of the massive mechanical oscillator in phase space, where the displacement operator is given by[26] $D(z/\sqrt{2}) = e^{i(\mathrm{Re}[z]X_m - \mathrm{Im}[z]P_m)}$. The action of this operator displaces the mean position and momentum of any state by $\mathrm{Im}[z]$ and $\mathrm{Re}[z]$, respectively. In quantum mechanics, two subsequent displacements provide an additional phase to the state, which can be used to engineer quantum gates[27–29]. Here we consider displacements of the mechanical resonator that are induced by an ancillary quantum system, the optical field, with an interaction strength λ. A sequence of four optomechanical interactions is chosen such that the mechanical state is displaced around a loop in phase space, described by the four-displacement operator

$$\xi = e^{i\lambda n_L P_m} e^{-i\lambda n_L X_m} e^{-i\lambda n_L P_m} e^{i\lambda n_L X_m} \tag{4}$$

© 2012 Macmillan Publishers Limited. All rights reserved.

In classical physics, after the whole sequence, neither of the two systems would be affected because the four operations cancel each other. However, for non-commuting X_m and P_m there is a change in the optical field depending on the commutator $[X_\mathrm{m}, P_\mathrm{m}] = iC_1$. We can rewrite equation (4) using the well-known relation[30] $\mathrm{e}^{aX_\mathrm{m}} P_\mathrm{m} \mathrm{e}^{-aX_\mathrm{m}} = \sum_{k=0}^{\infty} (i^k a^k / k!) C_k$, where $iC_k = [X_\mathrm{m}, C_{k-1}]$ and $C_0 = P_\mathrm{m}$. This yields $\xi = \exp(-i\lambda n_\mathrm{L} \sum_k (\lambda n_\mathrm{L})^k C_k / k!)$, which depends explicitly on the commutation relation for the oscillator, but not on the commutator of the optical field. For the quantum mechanical commutator, that is $C_1 = 1$, we obtain $\xi = \mathrm{e}^{-i\lambda^2 n_\mathrm{L}^2}$. In this case, the optical field experiences a self-Kerr nonlinearity, that is an n_L^2 operation, and the mechanical state remains unaffected. However, any deformations of the commutator would show in ξ, resulting in an observable effect in the optical field.

As an example we consider the modification given by equation (1). To first order in $\beta \equiv \beta_0 \hbar \omega_\mathrm{m} m / (M_\mathrm{P} c)^2 \ll 1$ one obtains $C_1 = 1 + \beta P_\mathrm{m}^2$, $C_2 \approx \beta 2 P_\mathrm{m}$, $C_3 \approx 2\beta$ and $C_k \approx 0$ for $k \geq 4$. Equation (4) thus becomes $\xi_\beta = \mathrm{e}^{-i\lambda^2 n_\mathrm{L}^2} \mathrm{e}^{-i\beta(\lambda^2 n_\mathrm{L}^2 P_\mathrm{m}^2 + \lambda^3 n_\mathrm{L}^3 P_\mathrm{m} + (1/3)\lambda^4 n_\mathrm{L}^4)}$ (this approximation has the physical meaning that one can neglect contributions which are higher order in β for the observables considered below). As one can see immediately, a deformed commutator affects the optical field differently owing to non-vanishing nested commutators C_k, $k > 1$. In addition to a Kerr-type nonlinearity the optical field experiences highly non-Gaussian n_L^3 and n_L^4 operations. The additional effect scales with β and therefore allows a direct measure of the deformations of the canonical commutator of the mechanical system via the optical field. To see that explicitly, let us denote the optical field by a_L, with the real and imaginary parts representing its measurable amplitude and phase quadratures, respectively. Also, for simplicity, we restrict the discussion to coherent states $|\alpha\rangle$ with real amplitudes of the optical input field and we neglect possible deformations in the commutator of the optical field during read-out[31,32] as those are expected to be negligible compared with the deformations of the massive mechanical oscillator (see refs 33,34 for schemes that can probe the non-commutativity of the optical field). For a large average photon number $N_\mathrm{p} \gg 1$, and for a mechanical thermal state with mean phonon occupation $\bar{n} \ll \lambda N_\mathrm{p}$, the mean of the optical field becomes (for $|\Theta| \ll 1$):

$$\langle a_\mathrm{L} \rangle \simeq \langle a_\mathrm{L} \rangle_\mathrm{qm} \mathrm{e}^{-i\Theta} \tag{5}$$

where $\langle a_\mathrm{L} \rangle_\mathrm{qm} = \alpha \mathrm{e}^{-i\lambda^2 - N_\mathrm{p}(1 - \mathrm{e}^{-i2\lambda^2})}$ is the quantum mechanical value for the unmodified dynamics. The β-induced contribution causes an additional displacement in phase space by

$$\Theta(\beta) \simeq \frac{4}{3} \beta N_\mathrm{p}^3 \lambda^4 \mathrm{e}^{-i6\lambda^2} \tag{6}$$

The resulting optical state is represented in Fig. 2. We note that the magnitude of the effect is enhanced by the optical intensity and the interaction strength. For the μ- and the γ-deformation of the commutator, referring to equations (2) and (3), respectively, the effect on the optical field is similar, but shows a different scaling with the system parameters (see Table 2 and Supplementary Information for the derivation). Probing deviations from the quantum mechanical commutator of the massive oscillator thus boils down to a precision measurement of the mean of the optical field, which can be achieved with very high accuracy via interferometric means, such as homodyne detection.

Experimental implementation

We now discuss a realistic experimental scenario that can attain sufficient sensitivity to resolve the deformation-induced change in the optical field even for small values of β_0, μ_0 and γ_0, that is in a regime that can be relevant for quantum gravity. The optomechanical scheme proposed here can achieve such a regime: it combines the ability to coherently control large masses with strong optical fields. From a more general perspective, optomechanical systems provide a promising avenue for preparing and investigating quantum states of massive objects ranging from a few picograms up to several kilograms[22,23]. Significant experimental progress has been recently made towards this goal, including laser cooling of nano- and micromechanical devices into their quantum ground state[35,36], operation in the strong-coupling regime[37–39] and coherent interactions[39,40]. Owing to their high mass they have also been proposed for tests of so-called collapse models[41,42], which predict a breakdown of the quantum mechanical superposition principle for macroscopic objects. For our purpose here, which is the high-precision measurement of the canonical commutator of a massive oscillator, we focus on the pulsed regime of quantum optomechanics[43].

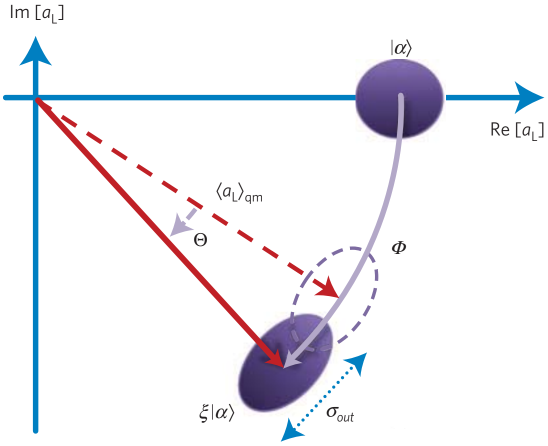

Figure 2 | Changes to the optical field following the pulsed optomechanical interactions. The effect of the four-displacement operation ξ onto an optical state for the experimentally relevant case $\lambda \ll 1$. In this case, an initial optical coherent state $|\alpha\rangle$ is rotated in phase-space through an angle Φ. A part Θ of the rotation is due to a possible quantum gravitational deformation of the canonical commutator of the mechanical resonator (see equation (6)). Measuring the mean of the optical field $\langle a_\mathrm{L} \rangle$ and extracting the Θ-contribution allows one to probe deformations of the canonical commutator. Optical interferometric schemes can provide a measurement of the overall mean rotation with a fundamental imprecision $\delta\langle\Phi\rangle = \sigma_\mathrm{out}/\sqrt{N_\mathrm{p} N_\mathrm{r}}$, ($N_\mathrm{r}$: number of measurement runs, N_p: number of photons, σ_out: quadrature width of the optical state, which remains very close to the coherent state value 1/2). To resolve the Θ-contribution, the measurement imprecision must fulfill $\delta\langle\Phi\rangle < \Theta$, which we show can be achieved in quantum optomechanical systems even for deformations on the Planck scale.

We consider the set-up depicted in Fig. 3, where a mechanical oscillator is coupled to the optical input pulse via radiation pressure inside a high-finesse optical cavity. This is described by the intra-cavity Hamiltonian[44] $H = \hbar \omega_\mathrm{m} n_\mathrm{m} - \hbar g_0 n_\mathrm{L} X_\mathrm{m}$, where n_m is the mechanical number operator and $g_0 = \omega_\mathrm{c}(x_0/L)$ is the optomechanical coupling rate with the mean cavity frequency ω_c and mean cavity length L. For sufficiently short optical pulses the mechanical harmonic evolution can be neglected and the intracavity dynamics can be approximated by the unitary operation $U = \mathrm{e}^{i\lambda n_\mathrm{L} X_\mathrm{m}}$ (ref. 43). Here, the effective interaction strength is (see Supplementary Information) $\lambda \simeq g_0/\kappa = 4\mathcal{F} x_0/\lambda_\mathrm{L}$, where κ is the optical amplitude decay rate, $\mathcal{F}$ is the cavity finesse and λ_L is the optical wavelength. To realize the desired displacement operation in phase-space it is also required to achieve a direct optomechanical coupling, with the same optical pulse, to the mechanical momentum (equation (4)). Such a momentum

© 2012 Macmillan Publishers Limited. All rights reserved.

NATURE PHYSICS DOI: 10.1038/NPHYS2262

Table 2 | Experimental parameters to measure quantum gravitational deformations of the canonical commutator.

$[X_\mathrm{m}, P_\mathrm{m}]$	Equation (2)	Equation (3)	Equation (1)
$\lvert\Theta\rvert$	$\mu_0 \frac{32\hbar\mathcal{F}^2 m N_\mathrm{p}}{M_\mathrm{P}^2\lambda_\mathrm{L}^2\omega_\mathrm{m}}$	$\gamma_0 \frac{96\hbar^2\mathcal{F}^3 N_\mathrm{p}^2}{M_\mathrm{P} c\lambda_\mathrm{L}^3 m\omega_\mathrm{m}}$	$\beta_0 \frac{1024\hbar^3\mathcal{F}^4 N_\mathrm{p}^3}{3M_\mathrm{P}^2 c^2\lambda_\mathrm{L}^4 m\omega_\mathrm{m}}$
$\mathcal{F}$	10^5	2×10^5	4×10^5
m	10^{-11} kg	10^{-9} kg	10^{-7} kg
$\omega_\mathrm{m}/2\pi$	10^5 Hz	10^5 Hz	10^5 Hz
λ_L	1,064 nm	1,064 nm	532 nm
N_p	10^8	5×10^{10}	10^{14}
N_r	1	10^5	10^6
$\delta\langle\Phi\rangle$	10^{-4}	10^{-8}	10^{-10}

The parameters are chosen such that a precision of $\delta\mu_0\sim1$, $\delta\gamma_0\sim1$ and $\delta\beta_0\sim1$ can be achieved, which amounts to measuring Planck-scale deformations.

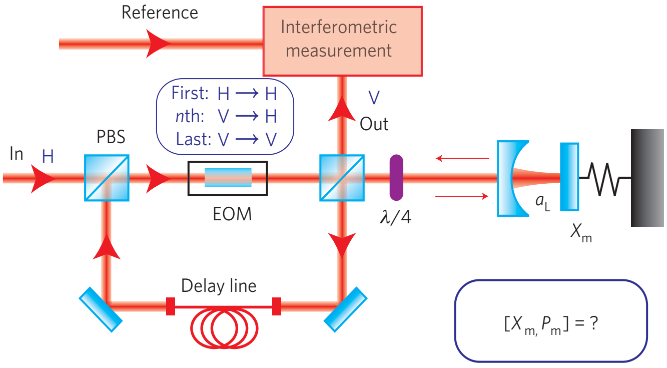

Figure 3 | Proposed experimental set-up to probe deformations of the canonical commutator of a macroscopic mechanical resonator. An incident pulse 'In' is transmitted through a polarizing beam splitter (PBS) and an electro-optic modulator (EOM) and then interacts with a mechanical resonator with position X_m via a cavity field a_L. The optical field is retro-reflected from the optomechanical system and then enters a delay line, during which time the mechanical resonator evolves for one quarter of a mechanical period. The optical pulse, now vertically polarized, is rotated by the EOM to be horizontally polarized and interacts again with the mechanical resonator. This is repeated for a total of four interactions, such that the canonical commutator of the resonator is mapped onto the optical field. Finally, the EOM does not rotate the polarization and the pulse exits in the mode labelled 'Out', where it is then measured interferometrically with respect to a reference field such that the commutator deformations can be determined with very high accuracy.

coupling could be achieved for example via the Doppler effect by using mirrors with a strongly wavelength-dependent optical reflectivity[45]. A more straightforward route is to use the harmonic evolution of the mechanical resonator between pulse round-trips (for example, ref. 43), which effectively allows X_m and P_m to be interchanged after a quarter of the oscillator period. In this case, the contribution from the commutator deformation has a different pre-factor, but remains of the same form (see Supplementary Information), and part of the phase-space rotation in the optical field is of classical nature. This has no effect on the ability to distinguish and observe the rotation due to the deformed commutator. After the four-pulse interaction has taken place the optical field can be analysed in an interferometric measurement, which yields the phase information of the light with very high precision.

As in previous approaches to measure possible modifications of the canonical commutator[13,15], the relevant question is which ultimate resolution $\delta\beta_0$, $\delta\mu_0$, $\delta\gamma_0$ the experiments can provide. In the case of a null result, these numbers would set an experimental bound for β_0, μ_0, γ_0 and hence provide an important empirical feedback for theories of quantum gravity. We restrict our analysis to the experimentally relevant case $\lambda < 1$, for which the effect of a deformed commutator resembles a pure phase-space rotation of the optical output state by angle Φ (Fig. 2). The inaccuracy $\delta\Phi$ of the measurement outcome depends on the quantum noise σ_out of the outgoing pulse along the relevant generalized quadrature and can be further reduced by quantum estimation protocols[46]. For our purposes we only require to measure the mean optical field, equation (5). The precision of this measurement is not fundamentally limited and is enhanced by the strength of the field and the number of experimental runs N_r via $\delta\langle\Phi\rangle = \sigma_\mathrm{out}/\sqrt{N_\mathrm{p}N_\mathrm{r}}$, from which one directly obtains the fundamental resolutions $\delta\beta_0$, $\delta\mu_0$, $\delta\gamma_0$. For each of the discussed deformations it is possible to find a realistic parameter regime (Table 2) with markedly improved performance compared with existing bounds. In particular, we assume a mechanical oscillator of frequency $\omega_\mathrm{m}/2\pi = 10^5$ Hz and mass $m = 10^{-11}$ kg, and an optical cavity of finesse $\mathcal{F} = 10^5$ at a wavelength of $\lambda_\mathrm{L} = 1{,}064$ nm, which is in the range of current experiments[37,47–50]. To test a μ-modified commutator (equation (2)), a pulse sequence of mean photon-number $N_\mathrm{p} = 10^8$ is sufficient to obtain a resolution $\delta\mu_0 \sim 1$ already in a single measurement run ($N_\mathrm{r} = 1$). For the case of a γ-modified commutator (equation (3)), the same sequence would result in $\delta\gamma_0 \sim 10^9$. By increasing the photon-number to $N_\mathrm{p} = 5\times10^{10}$, the finesse to $\mathcal{F} = 2\times10^5$ and the number of measurement runs to $N_\mathrm{r} = 10^5$ (this would require stabilizing the experiment on a timescale of the order of seconds) one obtains $\delta\gamma_0 \sim 1$. Note that this would improve the existing bounds for γ_0 (ref. 15) by ten orders of magnitude. To obtain similar bounds for a β-modification is more challenging. The pulse sequence with the previous parameters yields $\delta\beta_0 \sim 10^{12}$, which already constitutes an improvement by about 20 orders of magnitude compared with the current bound for β_0 (ref. 13). This can provide experimental access to a possible intermediate length-scale or a meaningful feedback to theories of quantum gravity in the case of a null result. By further pushing the parameters to $N_\mathrm{p} = 10^{14}$, $N_\mathrm{r} = 10^6$, $\mathcal{F} = 4\times10^5$, $m = 10^{-7}$ kg and $\lambda_\mathrm{L} = 532$ nm it is even possible to reach $\delta\beta_0 \sim 1$, that is, a regime where Planck-scale deformations are relevant and 33 orders of magnitude beyond current experiments. To achieve such experimental parameters is challenging, but is well within the reach of current technology.

The above considerations refer to the ideal case in which experimental noise sources can be neglected. Effects such as mechanical damping and distortions of the effective interaction strength impose additional requirements on the experimental parameters, which are discussed in detail in the Supplementary Information. In summary, being able to neglect the effects of pulse shape distortion and optical loss requires that the mechanical mode is optically cooled close to a thermal occupation of about $\bar{n} < 30$. Similarly, decoherence effects are negligible when the whole mechanical system is in a bath of temperature $T < 100$ mK for resonators with a quality factor of $Q > 10^6$, which can be achieved with dilution refrigeration. In general, the scheme is very robust against many noise sources, as it relies on the measurement of the mean of the optical field and the noise sources can be isolated by independent measurements. We also note that contributions from a modified commutator scale in a different way with the system parameters as compared with deleterious effects. It is therefore possible to distinguish these by varying the relevant parameters, such as optical intensity and the oscillator mass. The proposed scheme thus offers a feasible route to probe the possible effects of quantum gravity in a table-top quantum optics experiment and hence to provide important empirical feedback for theories of quantum gravity.

© 2012 Macmillan Publishers Limited. All rights reserved.

Received 4 November 2011; accepted 13 February 2012;
published online 18 March 2012; corrected online
26 March 2012 and 10 April 2012

References

1. Heisenberg, W. Über den anschaulichen Inhalt der quantentheoretischen Kinematik und Mechanik. *Z. Phys.* **43,** 172–198 (1927).
2. Garay, L. G. Quantum gravity and minimum length. *Int. J. Mod. Phys.* **A10,** 145–165 (1995).
3. Amati, D., Ciafaloni, M. & Veneziano, G. Superstring collisions at planckian energies. *Phys. Lett. B* **197,** 81–88 (1987).
4. Gross, D. J. & Mende, P. F. String theory beyond the Planck scale. *Nucl. Phys. B* **303,** 407–454 (1988).
5. Amelino-Camelia, G. Doubly special relativity: First results and key open problems. *Int. J. Mod. Phys. D* **11,** 1643–1669 (2002).
6. Magueijo, J. & Smolin, L. Generalized Lorentz invariance with an invariant energy scale. *Phys. Rev. D* **67,** 044017 (2003).
7. Amelino-Camelia, G., Freidel, L., Kowalski-Glikman, J. & Smolin, L. Principle of relative locality. *Phys. Rev. D* **84,** 084010 (2011).
8. Maggiore, M. A generalized uncertainty principle in quantum gravity. *Phys. Lett. B* **304,** 65–69 (1993).
9. Scardigli, F. Generalized uncertainty principle in quantum gravity from micro-black hole gedanken experiment. *Phys. Lett. B* **452,** 39–44 (1999).
10. Jizba, P., Kleinert, H. & Scardigli, F. Uncertainty relation on a world crystal and its applications to micro black holes. *Phys. Rev. D* **81,** 084030 (2010).
11. Maggiore, M. The algebraic structure of the generalized uncertainty principle. *Phys. Lett. B* **319,** 83–86 (1993).
12. Kempf, A., Mangano, G. & Mann, R. B. Hilbert space representation of the minimal length uncertainty relation. *Phys. Rev. D* **52,** 1108–1118 (1995).
13. Das, S. & Vagenas, E. C. Universality of quantum gravity corrections. *Phys. Rev. Lett.* **101,** 221301 (2008).
14. Ali, A. F., Das, S. & Vagenas, E. C. Discreteness of space from the generalized uncertainty principle. *Phys. Lett. B* **678,** 497–499 (2009).
15. Ali, A. F., Das, S. & Vagenas, E. C. A proposal for testing quantum gravity in the lab. *Phys. Rev. D* **84,** 044013 (2011).
16. Amelino-Camelia, G., Ellis, J., Mavromatos, N. E., Nanopoulos, D. V. & Sarkar, S. Tests of quantum gravity from observations of gamma-ray bursts. *Nature* **393,** 763–765 (1998).
17. Jacob, U. & Piran, T. Neutrinos from gamma-ray bursts as a tool to explore quantum-gravity-induced Lorentz violation. *Nature Phys.* **7,** 87–90 (2007).
18. Abdo, A. A. *et al.* A limit on the variation of the speed of light arising from quantum gravity effects. *Nature* **462,** 331–334 (2009).
19. Tamburini, F., Cuofano, C., Della Valle, M. & Gilmozzi, R. No quantum gravity signature from the farthest quasars. *Astron. Astrophys.* **533,** A71 (2011).
20. Grote, H. & the LIGO Scientific Collaboration. The status of GEO 600. *Class. Quantum Grav.***25,** 114043 (2008).
21. Abbott, B. P. *et al.* LIGO: The Laser Interferometer Gravitational-wave Observatory. *Rep. Prog. Phys.* **72,** 076901 (2009).
22. Kippenberg, T. J. & Vahala, K. J. Cavity optomechanics: Back-action at the mesoscale. *Science* **321,** 1172–1176 (2008).
23. Aspelmeyer, M., Groeblacher, S., Hammerer, K. & Kiesel, N. Quantum optomechanics—throwing a glance. *J. Opt. Soc. Am. B* **27,** A189–A197 (2010).
24. Milburn, G. J. Lorentz invariant intrinsic decoherence. *New J. Phys.* **8,** 96 (2006).
25. Kempf, A. Information-theoretic natural ultraviolet cutoff for spacetime. *Phys. Rev. Lett.* **103,** 231301 (2009).
26. Barnett, S. M. & Radmore, P. M. *Methods in Theoretical Quantum Optics* (Oxford Univ. Press, 2002).
27. Milburn, G. J., Schneider, S. & James, D. F. V. Ion trap quantum computing with warm ions. *Fortschr. Phys.* **48,** 801–810 (2000).
28. Sørensen, A. & Mølmer, K. Entanglement and quantum computation with ions in thermal motion. *Phys. Rev. A* **62,** 022311 (2000).
29. Leibfried, D. *et al.* Experimental demonstration of a robust, high-fidelity geometric two ion-qubit phase gate. *Nature* **422,** 412–415 (2003).
30. Wilcox, R. M. Exponential operators and parameter differentiation in quantum physics. *J. Math. Phys.* **8,** 962–982 (1967).
31. Nozari, K. Some aspects of Planck scale quantum optics. *Phys. Lett. B.* **629,** 41–52 (2005).
32. Ghosh, S. & Roy, P. "Stringy" coherent states inspired by generalized uncertainty principle. Preprint at http://arxiv.org/hep-ph/11105136 (2011).
33. Parigi, V., Zavatta, A., Kim, M. S. & Bellini, M. Probing quantum commutation rules by addition and subtraction of single photons to/from a light field. *Science* **317,** 1890–1893 (2007).
34. Kim, M. S., Jeong, H., Zavatta, A., Parigi, V. & Bellini, M. Scheme for proving the bosonic commutation relation using single-photon interference. *Phys. Rev. Lett.* **101,** 260401 (2008).
35. Teufel, J. D. *et al.* Sideband cooling of micromechanical motion to the quantum ground state. *Nature* **475,** 359–363 (2010).
36. Chan, J. *et al.* Laser cooling of a nanomechanical oscillator into its quantum ground state. *Nature* **478,** 89–92 (2011).
37. Gröblacher, S., Hammerer, K., Vanner, M. R. & Aspelmeyer, M. Observation of strong coupling between a micromechanical resonator and an optical cavity field. *Nature* **460,** 724–727 (2009).
38. Teufel, J. D. *et al.* Circuit cavity electromechanics in the strong-coupling regime. *Nature* **471,** 204–208 (2011).
39. O'Connell, A. D. *et al.* Quantum ground state and single-phonon control of a mechanical resonator. *Nature* **464,** 697–703 (2010).
40. Verhagen, E., Deléglise, S., Weis, S., Schliesser, A. & Kippenberg, T. J. Quantum-coherent coupling of a mechanical oscillator to an optical cavity mode. *Nature* **482,** 63–67 (2012).
41. Marshall, W., Simon, C., Penrose, R. & Bouwmeester, D. Towards quantum superpositions of a mirror. *Phys. Rev. Lett.* **91,** 130401 (2003).
42. Romero-Isart, O. *et al.* Large quantum superpositions and interference of massive nanometer-sized objects. *Phys. Rev. Lett.* **107,** 020405 (2011).
43. Vanner, M. R. *et al.* Pulsed quantum optomechanics. *Proc. Natl Acad. Sci. USA* **108,** 16182–16187 (2011).
44. Law, C. K. Interaction between a moving mirror and radiation pressure: A Hamiltonian formulation. *Phys. Rev. A* **51,** 2537–2541 (1995).
45. Karrai, K., Favero, I. & Metzger, C. Doppler optomechanics of a photonic crystal. *Phys. Rev. Lett.* **100,** 240801 (2008).
46. Boixo, S. *et al.* Quantum-limited metrology and Bose–Einstein condensates. *Phys. Rev. A* **80,** 032103 (2009).
47. Corbitt, T. *et al.* Optical dilution and feedback cooling of a gram-scale oscillator to 6.9 mK. *Phys. Rev. Lett.* **99,** 160801 (2007).
48. Thompson, J. D. *et al.* Strong dispersive coupling of a high-finesse cavity to a micromechanical membrane. *Nature* **452,** 72–76 (2008).
49. Verlot, P., Tavernarakis, A., Briant, T., Cohadon, P-F. & Heidmann, A. Scheme to probe optomechanical correlations between two optical beams down to the quantum level. *Phys. Rev. Lett.* **102,** 103601 (2008).
50. Kleckner, D. *et al.* Optomechanical trampoline resonators. *Opt. Express* **19,** 19708–19716 (2011).

Acknowledgements

This work was supported by the Royal Society, by the Engineering and Physical Sciences Research Council, by the European Comission (Quantum InterfacES, SENSors, and Communication based on Entanglement (Q-ESSENCE)), by the European Research Council Quantum optomechanics: quantum foundations and quantum information on the micro- and nanoscale (QOM), by the Austrian Science Fund (FWF) (Complex Quantum Systems (CoQuS), START program, Special Research Programs (SFB) Foundations and Applications of Quantum Science (FoQuS)), by the Foundational Questions Institute and by the John Templeton Foundation. M.R.V. is a recipient of a DOC fellowship of the Austrian Academy of Sciences. I.P. and M.R.V are members of the FWF Doctoral Programme CoQuS and they are grateful for the kind hospitality provided by Imperial College London. The authors thank S. Das, S. Gielen, H. Grosse, A. Kempf, W. T. Kim and J. Lee for discussions.

Author contributions

I.P. and M.S.K. conceived the research, which was further developed by Č.B. and all co-authors. M.R.V. conceived the experimental scheme. M.A. analysed the feasibility of the scheme with input from all co-authors. All authors performed the research under the supervision of Č.B. and all authors wrote the manuscript.

Additional information

The authors declare no competing financial interests. Supplementary information accompanies this paper on www.nature.com/naturephysics. Reprints and permissions information is available online at www.nature.com/reprints. Correspondence and requests for materials should be addressed to I.P. or M.S.K.

© 2012 Macmillan Publishers Limited. All rights reserved.

nature physics
SUPPLEMENTARY INFORMATION
DOI: 10.1038/NPHYS2262

Probing Planck-scale physics with quantum optics

A Alternative Commutator deformations

In this section we compute the change in the optical field for the two alternative commutator deformation theories considered in the main text, i.e. for the μ- and the γ-deformation given by Eqs. 2 and 3, respectively. For the case $[x,p]_{\mu_0} \approx i\hbar\left(1+\mu_0 m^2/M_P^2\right)$ the four-displacement operator becomes $\xi_\mu = e^{-i\lambda^2 n_L^2(1+\mu)}$, where we defined $\mu \equiv \mu_0 m^2/M_P^2$. The resulting mean of the optical field is thus $\langle a_L\rangle = \alpha e^{-i\lambda^2(1+\mu)}\, e^{-N_P\left(1-e^{-i2\lambda^2(1+\mu)}\right)}$. In the limit $\mu \lesssim 1$ and $N_P \gg 1$, it reduces to $\langle a_L\rangle \simeq \langle a_L\rangle_{qm}\, e^{-i\Theta}$ with the deformation-induced contribution $\Theta(\mu)$ given by

$$\Theta(\mu) \simeq 2\mu N_p \lambda^2 e^{-i2\lambda^2}\,. \tag{A.1}$$

For a γ-deformation of the commutator we define $\gamma \equiv \gamma_0\sqrt{\hbar m\omega_m}/M_P c \ll 1$ and the four-displacement operator becomes $\xi_\gamma = e^{-i\lambda^2 n_L^2}\, e^{i\gamma\left(\lambda^2 n_L^2 P_m + \frac{1}{2}\lambda^3 n_L^3\right)}$ to first order in γ. In the limit $N_P \gg 1$, this results in the additional contribution to the quantum mechanical mean of the optical field given by

$$\Theta(\gamma) \simeq \frac{3}{2}\gamma N_p^2 \lambda^3\, e^{-i4\lambda^2}\,. \tag{A.2}$$

Finally, we note that theories with a modified commutator have an intrinsic ambiguity as to which particles or degrees of freedom of a composite system the deformations should apply to. For example, a system consisting of N particles with identical mass and each with position x_i and momentum p_i has the center of mass degrees of freedom given by $x_{cm} = \sum_i^N x_i/N$ and $p_{cm} = \sum_i^N p_i$. If the β-modified commutation relation as given by Eq. 1 is applied to each single particle individually (rather than to the center of mass itself), the commutator of the center of mass becomes $[x_{cm}, p_{cm}] = i\hbar\left(1+\beta_0\sum_i^N p_i^2/(M_P^2 c^2 N)\right) = i\hbar\left(1+\frac{\beta_0}{M_P^2 c^2 N}\left(p_{cm}^2 - \sum_{i\neq j}^N p_i p_j\right)\right)$. This result differs from a direct deformation of the center of mass mode. Depending on the state of the system, in particular on the pairwise correlations between the constituent particles, the difference in the commutator deformation can be approximated by the substitution $\beta_0 \to \chi\beta_0$ where χ lies between $1/N$ (for vanishing pairwise correlations) and $1/N^2$ (for all pairs being equally correlated).

B Modified harmonic evolution

For the implementation utilizing free harmonic evolution between the pulsed interactions, it is necessary to take a deformed evolution due to a deformation of the commutator into account. Here we consider the β-deformation as given by Eq. 1. Keeping the quantum mechanical canonical commutation relation and modifying the momentum operator to $P_m \to P_m\left(1+\frac{1}{3}\beta P_m^2\right)$ incorporates the deformation to first order in β [13]. It is therefore necessary to solve for $X_m(t)$ for a modified evolution governed by the effective Hamiltonian $H = \frac{1}{2}\hbar\omega_m\left(X_m^2+P_m^2\right) + \frac{1}{3}\hbar\omega_m\beta P_m^4 \equiv H_0 + H'$. These correspond to the unitary evolutions U_0 and U', respectively. In a frame rotating at frequency ω_m, the time evolution of the operators $X_m' = U_0 X_m U_0^\dagger$ and $P_m' = U_0 P_m U_0^\dagger$ is generated by $H'(P_m')$. This yields $P_m'(t) = P_m'(0)$

© 2012 Macmillan Publishers Limited. All rights reserved.

and $X'_m(t) = X'_m(0) + \frac{4}{3}\beta\omega_m t P'^3_m$. In the original frame, the result is thus

$$X_m(t) = X_m(0)\cos(\omega_m t) - P_m(0)\sin(\omega_m t) + \frac{4}{3}\beta\omega_m t\left(P_m(0)\cos(\omega_m t) + X_m(0)\sin(\omega_m t)\right)^3 . \tag{B.1}$$

Using four interactions separated by a quarter mechanical period, the four-displacement operator becomes $\xi = e^{i\lambda n_L(P_m - 2\beta\pi X_m^3)} e^{i\lambda n_L(-X_m - 4\beta\pi P_m^3/3)} e^{i\lambda n_L(-P_m + 2\beta\pi X_m^3/3)} e^{i\lambda n_L X_m}$. This expression can be simplified using the Zassenhaus formula [30] $\exp(X+Y) = \exp(X)\exp(Y)\prod_{i=1}^{\infty}\exp(Z_i)$, where $Z_1 = -[A,B]/2$, $Z_2 = [A,[A,B]]/6 + [B,[A,B]]/3$, $Z_3 = -([B,[A,[A,B]]] + [B,[B,[A,B]]])/8 - [A,[A,[A,B]]]/24$ and Z_k, $k > 3$ are functions of higher nested commutators. To leading order in n_L, the four-displacement operator becomes

$$\xi \simeq e^{-i\lambda^2 n_L^2}\, e^{i\beta\pi\frac{5}{3}\lambda^4 n_L^4}. \tag{B.3}$$

The optical field due to this operation is of the same form as in Eq. 5 with a modified numerical strength. The modified dynamics therefore does not alter the main conclusions.

C Additional requirements due to deleterious effects

In the following we analyze the experimental parameters necessary to overcome some additional deleterious effects in the opto-mechanical system. We analyze the cavity dynamics and its influence on the effective interaction, the effect of varying interaction strengths for each pulse round trip and the influence of mechanical decoherence. We neglect additional contributions from a modified commutator since these will be less prominent than that considered in the ideal case.

The Hamiltonian $H = \hbar\omega_m n_m - \hbar g_0 n_L X_m$ refers to the interaction between the optical field and the mechanics within the cavity [44]. To quantify the effects of cavity filling and decay for a short pulse we solve the optical Langevin equation

$$\frac{da_L}{dt} = (ig_0 X_m - \kappa)a_L + \sqrt{2\kappa}\left(a_L^{(in)} + \sqrt{N_p}\alpha_{\text{in}}\right) \tag{7}$$

with the boundary condition $a_L^{(in)} + a_L^{(out)} = \sqrt{2\kappa}a_L$ for the input and output optical fields and the incident cavity drive α_{in} that is normalized to the mean photon number per pulse, i.e. $\int \mathrm{d}t\, \alpha_{\text{in}}^2 = 1$. Since the mechanical motion can be neglected in the short pulse regime the overall effect on both the optical field and the mechanical oscillator can be described by the effective unitary operator $U = e^{i\lambda n_L X_m}$. The coupling strength λ depends on the intra-cavity field envelope and can be determined via the total momentum transfer onto the mechanics by the optical pulse $\langle P_m\rangle = g_0\int dt\,\langle n_L(t)\rangle$, where $n_L(t)$ is obtained from Eq. 7. This yields $\lambda = \zeta\, g_0/\kappa$ with $\zeta = \int \mathrm{d}t e^{-2\kappa t}\kappa^2\left[\int_{-\infty}^{t}\mathrm{d}t'\, e^{\kappa t'}\alpha_{\text{in}}(t')\right]^2$ for the effective unitary operator.

In general, the pulse shape of the output optical field is altered by the cavity. When such a distorted pulse is directed back for the i-th time into the cavity, the effective interaction time within the cavity will be different and will give rise to a modified opto-mechanical interaction strength λ_i. To minimize the distortion, one requires that the pulse duration τ is much longer than the intra-cavity lifetime, i.e. $\omega_m \ll \tau^{-1} \ll \kappa$, where κ is the cavity bandwidth. This ensures that the optical pulses are short

© 2012 Macmillan Publishers Limited. All rights reserved.

compared to the mechanical period and that the cavity is empty in between the pulsed interactions. In this regime we have $\zeta \simeq 1$ such that $\lambda \simeq g_0/\kappa$.

An additional effect that distorts the interaction strength λ from pulse to pulse is the loss of light. To include both loss and pulse shape change in the effective interaction, we define an overall distortion parameter η. With this parameter, the opto-mechanical interaction strength λ_i for the i-th interaction is approximately given by $\lambda_{i+1} = \eta\lambda_i$. We note that in the regime considered here the loss of light will be dominant and we assume a value of $\eta \sim 0.9$.

The effect of varying interaction strengths modifies the four-displacement operator to $\xi_\eta = e^{i\lambda_4 n_L P_m} \times e^{-i\lambda_3 n_L X_m} e^{-i\lambda_2 n_L P_m} e^{i\lambda_1 n_L X_m}$. Using $\lambda = \lambda_1$, it can be written as

$$\xi_\eta = \xi_0' \, e^{i\eta\lambda(1-\eta^2)n_L P_m} \, e^{i\lambda(1-\eta^2)n_L X_m} \,, \tag{8}$$

where ξ_0' is the four-displacement operator as considered previously, but with modified interaction strengths: For the β-, γ- and μ-deformations, the interaction strength is reduced to $\lambda^4 \to \eta^7\lambda$, $\lambda^3 \to \eta^5\lambda$ and $\lambda^2 \to \eta^3\lambda$, respectively. For $\eta \sim 0.9$ the $\Theta-$contribution to the optical mean by the β-modified commutator would therefore be reduced by a factor ~ 0.5, the contribution by the γ-modified commutator would be reduced by ~ 0.6 and the contribution by a μ-modified commutator would be reduced by ~ 0.7. Additionally, Eq. 8 contains a strong dependence of the outgoing optical field on the mechanical state. Given a thermal distribution of the mechanical center-of-mass mode with mean phonon occupation $\bar{n}$, the optical mean is reduced by $e^{-\bar{n}\lambda^2(1-\eta^2)(1-\eta^4)/2}$. For $\eta \sim 0.9$ and $\lambda \sim 1$, the mechanics therefore needs to be damped to $\bar{n} \lesssim 30$. This can be achieved by optical cooling of the mechanical mode, which has recently been demonstrated in Refs. [35, 36].

Finally, we discuss mechanical decoherence in between pulse interactions due to coupling of the mechanical mode to other degrees of freedom in the oscillator. We consider a linear coupling to an infinite bath of harmonic oscillators, which can be described by the interaction Hamiltonian

$$H_{int} = \sum_i \nu_i \left(b_i \, e^{-i\omega_i t} + b_i^\dagger \, e^{i\omega_i t} \right) X_m \,, \tag{9}$$

where b_i are operators for the i-th bath mode with frequency ω_i that interact with the mode of interest with interaction strength ν_i. Using the notation $B(t) = \sum_i \nu_i \left(b_i \, e^{-i\omega_i t} + b_i^\dagger \, e^{i\omega_i t} \right)$, the solutions for the position and momentum operators become

$$\begin{aligned} X_m(t) &= X_m^{(0)}(t, t_0) - \int_{t_0}^{t} \mathrm{d}t' B(t') \sin(\omega_m(t - t')) \\ P_m(t) &= P_m^{(0)}(t, t_0) + \int_{t_0}^{t} \mathrm{d}t' B(t') \cos(\omega_m(t - t')) \,, \end{aligned} \tag{10}$$

where $X_m^{(0)}(t, t_0) = \mathrm{Re}[A(t_0)e^{i\omega_m(t-t_0)}]$ and $P_m^{(0)}(t, t_0) = \mathrm{Im}[A(t_0)e^{i\omega_m(t-t_0)}]$ are the position and momentum operators without decoherence, respectively, with the initial value $A(t_0) = X_m(t_0) + iP_m(t_0)$. For a bath that is initially uncorrelated with the mechanical mode of interest, the ξ-operator changes to

$$\xi_B = \xi_0 \, e^{i\lambda n_L B_3} \, e^{i\lambda n_L B_2} \, e^{i\lambda n_L B_1} \tag{11}$$

where ξ_0 is the operator without decoherence as given in Eq. 4 and the bath degrees of freedom enter through the operators $B_1 = \int_0^{\pi/2\omega_m} dt B(t') \cos(\omega_m t)$, $B_2 = \int_0^{\pi/\omega_m} dt B(t') \sin(\omega_m t)$ and

© 2012 Macmillan Publishers Limited. All rights reserved.

$B_3 = -\int_0^{3\pi/2\omega_m} dt B(t') \cos(\omega_m t)$. We consider a Markovian bath with negligible bath correlation times such that $\langle B(t) \rangle = 0$ and $\langle B(t)B(t') \rangle = \gamma_m \coth(\hbar\omega_m/2k_B T)\delta(t-t')$, where the mechanical damping can be written in terms of the mechanical quality factor as $\gamma_m = \omega_m/Q$. To first order in T/Q the mean of the optical field becomes

$$\langle a_L \rangle_B \simeq \langle a_L \rangle_0 \,(1 - \lambda^2 \frac{k_B T}{\hbar\omega_m Q})\,, \tag{12}$$

where $\langle a_L \rangle_0$ is the mean of the optical field without decoherence. For $Q = 10^6$ one therefore requires $T \lesssim 100$ mK to keep the decoherence sufficiently weak. Such parameters can be achieved for kHz-resonators with dilution refrigeration.

© 2012 Macmillan Publishers Limited. All rights reserved.

10 Optically Induced Mechanical Non-Linearity

A challenge faced throughout quantum optics is how to engineer quantum systems that that have significant non-linearity at the single quanta level. As an example, such non-linearity is important for photonic quantum science to allow deterministic quantum logic operations between photonic qubits. Within quantum optomechanics, generating mechanical non-linearity, i.e. mechanical state dependent dynamics, will open a vast experimental research avenue for the deterministic generation of non-classical motional states but is yet to be experimentally attained.

In this work [95], we theoretically proposed a technique how to produce significant non-linearities in the motion of a mechanical resonator by exploiting a geometric phase generated by a sequence of four pulsed optomechanical interactions. Building upon the work in chapter 6, the pulse sequence takes place over a time-scale much shorter than a mechanical period of motion and the position of the oscillator is a constant of motion. Simply put, the non-linearity generated by our scheme arises from the mechanical position information acquired by the early pulses coherently interfering with the latter pulses, yielding a mechanical position dependent change to the mechanical momentum. Using the optomechanical interaction $H_{int} \propto a^{\dagger}aX_M$ one obtains a time evolution operator of the form $U = \exp[-i\chi_1^2 X_M^2]$, which can be used for deterministic motional squeezed state preparation. Here, $\chi_1^2 X_M^2$ is the enclosed area made in optical phase space during the protocol. We also considered the interaction $H_{int} \propto a^{\dagger}aX_M^2$, which is available in membrane-in-the-middle geometry [86], and the resultant time evolution operator is of the form $U = \exp[-i\chi_2^2 X_M^4]$. This type of non-linearity causes a mechanical position cubed dependent change to the mechanical momentum and when applied to a low temperature mechanical thermal state will generate a non-Gaussian quantum state exhibiting Wigner negativity.

Although this work is quite similar in spirit to the four pulsed protocol used in chapter 9 it was conceived quite independently. The leading creative contributor to this project was Gerard Milburn who adapted his prior work on geometric phase based ion trap quantum computing [96, 97]. My specific contribution to this project was to refine Gerard's optomechanical scheme by considering short optical pulses instead of the sideband based scheme Gerard initially had in mind. Using this interaction regime allowed us to achieve the X_M^4 evolution and, owing to its speed, provides resilience against mechanical decoherence thus improving experimental feasibility. In addition to this creative contribution, I guided Kiran Khosla, at that time an honours student, during a visit he made to Vienna in the summer of 2011, and together we completed the bulk of the calculations for this project.

New Journal of Physics
The open access journal for physics

Quantum state preparation of a mechanical resonator using an optomechanical geometric phase

K E Khosla[1,3], **M R Vanner**[1,2], **W P Bowen**[1] **and G J Milburn**[1]
[1] Center for Engineered Quantum Systems, University of Queensland,
St Lucia 4072, Australia
[2] Vienna Center for Quantum Science and Technology (VCQ) and Faculty of
Physics, University of Vienna, Boltzmanngasse 5, A-1090 Vienna, Austria
E-mail: k.khosla@uq.edu.au

New Journal of Physics **15** (2013) 043025 (11pp)
Received 27 September 2012
Published 17 April 2013
Online at http://www.njp.org/
doi:10.1088/1367-2630/15/4/043025

Abstract. We theoretically show that a geometric phase, generated by a sequence of four optomechanical interactions can be used to generate or increase nonlinearities in the evolution of a mechanical resonator. Interactions of this form lead to new mechanisms for preparing mechanical squeezed states of motion, and the preparation of non-classical states with significant Wigner negativity.

Contents

1. Introduction 2
2. Model 2
3. Experimental scheme 4
4. Experimental parameters 5
5. Conclusion 9
Acknowledgments 10
References 10

---

[3] Author to whom any correspondence should be addressed.

Content from this work may be used under the terms of the Creative Commons Attribution-NonCommercial-ShareAlike 3.0 licence. Any further distribution of this work must maintain attribution to the author(s) and the title of the work, journal citation and DOI.

1367-2630/13/043025+11$33.00
© IOP Publishing Ltd and Deutsche Physikalische Gesellschaft

1. Introduction

The geometric phase is a phase imparted on the wavefunction of a quantum state by driving a system about a circuit [1]. Within quantum optics this phase has been widely used to create logic gates for quantum computing [2–4], but has received little attention in optomechanics. Some notable exceptions come from recent proposals that have considered the effect of a geometric phase involving mechanical oscillators coupled to a qubit [5] or light [6], however not for mechanical state engineering. In this paper we consider an optomechanical system [7–12] with a time dependent optical drive [9, 12, 13] that, via the optomechanical interactions, traverses a closed loop in phase space thus imparting a geometric phase onto the mechanical element.

In an optomechanical system, the radiation pressure force due to light in an optical resonator can be used to accelerate a mechanical resonator. Driving the optical resonator with a suitable sequence of laser pulses can be used to manipulate the motion of the mechanics. In our scheme, strong mechanical nonlinearity is generated with a sequence of four pulsed optomechanical interactions in a measurement free process. During this sequence the optical field makes a circuit in phase space and the mechanical oscillator obtains a phase proportional to the area enclosed within the loop [1], i.e. a Berry phase. It is shown how this phase produces an effective nonlinear potential for the mechanical resonator from the otherwise linear optomechanical radiation pressure interaction. We then discuss how this mechanical nonlinearity can be used for quantum state preparation of the mechanical oscillator. Our full protocol takes place within a small fraction of one period of the mechanical oscillator, and is hence robust against rethermalization and decoherence (similar to [12]).

2. Model

We model the optomechanical system as an optical cavity coupled linearly to the position of a mechanical element. The interaction Hamiltonian for such a system is given by $H_\mathrm{I} = \hbar g_0 a^\dagger a \sqrt{2} X_\mathrm{M}$, where g_0 is the interaction rate, $\hbar$ is the reduced Planck's constant, a, $(a^\dagger)$ and b, $(b^\dagger)$ are the annihilation (creation) operators of the optical and mechanical field respectively. The $\sqrt{2}$ arises from our definition of $X_\mathrm{M} = (b + b^\dagger)/\sqrt{2}$.

The Langevin equation of motion for a is given by $\dot{a}(t) = -\mathrm{i}g_0 a(t) X_\mathrm{M} - \kappa a(t) + \sqrt{2\kappa} a_\mathrm{in}(t)$ where a_in is the field entering the cavity and κ is the cavity decay rate. For the following the intracavity field is taken to be on resonance and κ is taken to be large compared to the mechanical frequency. The optical field is written as a noise operator $\bar{a}$ about a coherent amplitude $\alpha(t) = \langle a(t) \rangle$, such that $a(t) = \alpha(t) + \bar{a}(t)$. The coherent amplitude follows the classical equation of motion for a field in a cavity with input $\alpha_\mathrm{in}(t)$, $\dot{\alpha} = -\kappa\alpha(t) + \sqrt{2\kappa}\alpha_\mathrm{in}(t)$.[4] The mechanical period T_M is assumed much larger than the pulse envelope $\alpha(t)$, so the dynamics of the mechanical oscillator may be neglected, i.e. $X_\mathrm{M}(t) = X_\mathrm{M}$. The noise operator follows the equation of motion

$$\dot{\bar{a}}(t) = -\mathrm{i}g_0[\alpha(t) + \bar{a}(t)]X_\mathrm{M} - \kappa\bar{a}(t) + \sqrt{2\kappa}\bar{a}_\mathrm{in}(t). \tag{1}$$

For the rest of this work, the optomechanical system is taken to be in the weak coupling regime, $g_0 \ll \kappa$. In this limit coupling between the mechanical element and optical vacuum field

---

[4] If the pulse were detuned from the cavity resonance, the coherent amplitude inside the cavity would be smaller, reducing the optomechanical interaction.

(the $\bar{a}(t)X_{\mathrm{M}}$ term) is negligibly weak and is dropped. The Hamiltonian that gives the simplified equation of motion is given by

$$H_{\mathrm{I}}/\hbar = g_0|\alpha(t)|^2 X_{\mathrm{M}} + g_0|\alpha(t)|(\mathrm{e}^{\mathrm{i}\theta}\bar{a}^{\dagger} + \mathrm{e}^{-\mathrm{i}\theta}\bar{a})\sqrt{2}X_{\mathrm{M}}, \tag{2}$$

where θ is the phase angle of the coherent amplitude. For a single pulse θ may be taken to be arbitrary but it is kept here as it will become important when considering multiple pulses. The first term generates a classical momentum imparted to the oscillator, $P_{\mathrm{M}} \to P_{\mathrm{M}} - g_0 \int \mathrm{d}t|\alpha(t)|^2$, where the integral is over the duration of the pulse and therefore proportional to the input pulse intensity. The unitary operator for the quantum interaction in equation (2) is given by

$$U(X_{\mathrm{L}}^{\theta}) = \exp\left[-\mathrm{i}\chi X_{\mathrm{M}} X_{\mathrm{L}}^{\theta} - \mathrm{i}g_0 \int \mathrm{d}t|\alpha(t)|^2 X_{\mathrm{M}}\right], \tag{3}$$

where $\chi = \sqrt{2}g_0 \int \mathrm{d}t|\alpha(t)|$ and $X_{\mathrm{L}}^{\theta} = (\bar{a}\,\mathrm{e}^{-\mathrm{i}\theta} + \bar{a}^{\dagger}\,\mathrm{e}^{\mathrm{i}\theta})/\sqrt{2}$ is an arbitrary optical quadrature. In calculating this unitary operator we have used the assumption that the mechanical period T_{M} is large compared to the temporal width (σ) of the pulse.

We now consider a sequence of four pulsed optomechanical interactions. The same pulse is recycled and undergoes four separate interactions. After each interaction the pulse is displaced in optical phase space such that each interaction has a different phase angle X_{L}^{θ}. Let the four optical quadratures used be $\{X_{\mathrm{L}}, P_{\mathrm{L}}, -X_{\mathrm{L}}, -P_{\mathrm{L}}\}$, with $X_{\mathrm{L}} = (\bar{a} + \bar{a}^{\dagger})/\sqrt{2}$, $P_{\mathrm{L}} = (\bar{a} - \bar{a}^{\dagger})/(\sqrt{2}\mathrm{i})$. For each interaction the pulse has been taken to have the same temporal profile. This is valid as long as the pulse width is much larger than the cavity decay rate $\sigma \gg \kappa^{-1}$. Under this assumption the cavity filed follows the input pulse, $\alpha(t) = \alpha_{\mathrm{in}}(t)\sqrt{2/\kappa}$. The Baker–Campbell–Hausdorff formula [14] is used to calculate the effective unitary operator for the four interactions

$$\begin{aligned} U_{\mathrm{eff}} &= U(-P_{\mathrm{L}})U(-X_{\mathrm{L}})U(P_{\mathrm{L}})U(X_{\mathrm{L}}) \\ &= \exp[-\mathrm{i}\chi^2 X_{\mathrm{M}}^2] \exp\left[-4\mathrm{i}g_0 \int \mathrm{d}t|\alpha(t)|^2 X_{\mathrm{M}}\right]. \end{aligned} \tag{4}$$

The first exponential in U_{eff} is a geometric phase dependent on the position quadrature of the mechanical oscillator. The second exponential is the dynamical phase [15] which would be present in the corresponding classical system. The dynamical phase is simply a sum of the momentum displacements the mechanical oscillator receives from each pulsed interaction. The geometric phase can be seen as a momentum displacement proportional to the mechanical position, $U_{\mathrm{eff}}^{\dagger} P_{\mathrm{M}} U_{\mathrm{eff}} = P_{\mathrm{M}} - \chi^2 X_{\mathrm{M}} - 4g_0 \int |\alpha(t)|^2 \mathrm{d}t$. The momentum of the oscillator is displaced and becomes correlated with the position, resulting in a squeezed quadrature in the final mechanical state.

One may show more generally that the area of an arbitrary closed circuit will appear in this exponential. The proof (also discussed in [5]) goes as follows: consider an arbitrary closed curve in phase space made by a sequence of optomechanical interactions. One may break this sequence into a series of small but finite phase space displacements and then write the overall unitary operator as a product of each displacement. Converting the product of displacements to a single operator will generate a phase depending on each successive displacement. Taking the continuum limit where the number of displacements becomes infinite, one may convert the phase term into an integral and then use Stokes theorem to show the integral to be the area enclosed by the path.

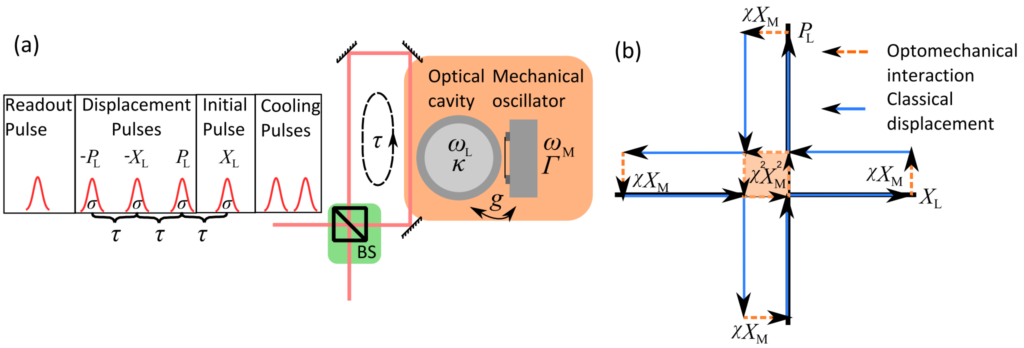

Figure 1. (a) A schematic for an experimental protocol to realize mechanical nonlinearity via an optomechanical geometric phase. The required pulse sequence is shown entering the beamsplitter. The first two pulses cool the mechanical oscillator close to the ground state. The initial pulse enters the large fiber cavity via the highly reflective beamsplitter. The following three displacement pulses only displace the coherent amplitude of the pulse inside the large fiber cavity, leaving the noise operator unchanged, effectively meaning the noise operator of the first pulse interacts with the mechanics four times. (b) The evolution of the optical field in phase space. The solid lines show the coherent drive, with the dashed lines (each of length χX_M) representing the optomechanical interaction. The geometric phase arises due to a sequence of four optomechanical interactions, hence it is the area enclosed by these mechanical position dependent optical phase shifts (dashed lines) that generate the geometric phase. The coherent optical amplitude drives the optomechanical system and gives rise to the dynamical phase, i.e. the momentum transfer to the mechanical resonator from each optical pulse.

3. Experimental scheme

Figure 1(a) shows a schematic of one possible experiment to realize the geometric phase. Two pulses separated by one quarter of a mechanical period are used to cool the mechanical element (as outlined in [12]), leaving it in a thermal state with a mean phonon occupation lower than that of the bath. Following the cooling pulses, a coherent laser pulse of temporal width σ enters a large fiber cavity with round trip time τ via a highly reflective beamsplitter. The pulse interacts with the mechanical oscillator via evanescent coupling from a toroidal cavity [16] with decay rate κ before exiting the toroidal cavity back into the large fiber cavity. As the pulse passes the highly reflective beamsplitter, its coherent amplitude is displaced in optical phase space leaving the noise operator fixed. The optical displacement is performed at the highly reflective beamsplitter using a second, phase controlled laser pulse to displace away the coherent amplitude, and displace up in an orthogonal quadrature. The pulse then repeats the optomechanical interactions and displacement three more times to give the four pulses sequence. Figure 1(b) shows the field inside the toroidal cavity over the experimental protocol.

The first pulse correlates the phase quadrature of the light, P_L, with the position of the mechanics, X_M. The first optical displacement changes the coherent amplitude of the pulse from the X_M to the P_L quadrature, before the second optomechanical interaction. For the second interaction, X_L is correlated with the mechanical position as it used to be P_L before the

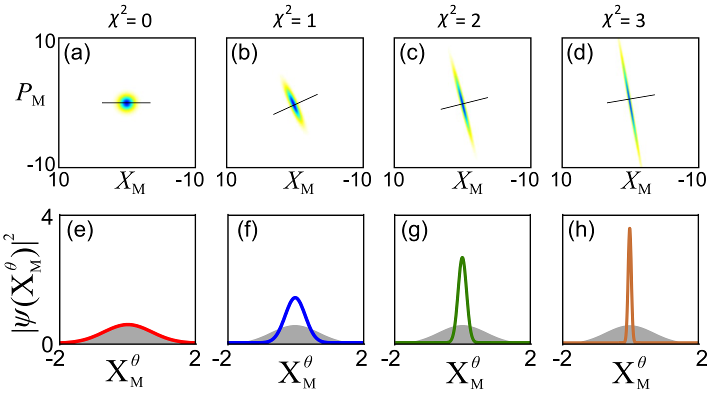

Figure 2. (a)–(d) Effect of a sequence of four optomechanical interactions on the Wigner function of the mechanical oscillator, initially prepared in the ground state. The squeezed quadrature (X_M^θ) is marked by a line in each graph. This quadrature is maximally squeezed at an angle $\tan\theta = \sqrt{\chi^4+1} - \chi^2$ to the X_M quadrature. (e)–(h) The probability amplitude for the squeezed quadrature compared to the ground state value (shown in gray).

displacement. During the second interaction the back action of X_L on the mechanical resonator effectively correlates the momentum of the oscillator with its position. As the position does not change over these interactions, correlating the momentum with the position produces a mechanical squeezed state. At this point the optical field is still correlated with the mechanical state, however, after the following two pulsed interactions, the correlation is undone such that the final optical pulse is uncorrelated with the mechanical state, leaving the final state disentangled. A readout pulse can now be sent into the cavity to measure the mechanical element and verify the mechanical state.

To generate the geometric phase we require $\kappa^{-1} < 4\sigma < \tau \ll T_M$. Setting $\kappa^{-1} < 4\sigma$ ensures the field inside the toroid follows input field. Constraining $4\sigma < \tau$ ensures that each successive pulse decays out of the cavity prior to the next pulse entering. Consequently interference between successive pulses can be neglected. Finally requiring $\tau \ll T_M$ means the mechanics remains near motionless during the four pulse protocol. The mechanical Q must be high enough such that on average much less than 1 phonon is exchanged with the bath over the time scale of the protocol.

Figure 2 shows the effect of the four pulse sequence on a mechanical oscillator initially prepared in the ground state, demonstrating how correlating X_M and P_M leads to a squeezed mechanical state of motion. Increasing the coupling strength χ benefits the protocol in two ways. Firstly it increases the effect of squeezing in the oscillator. Secondly it rotates the state so the squeezed quadrature aligns closer with the position quadrature, so that less time is required before the state can be verified (see section 4), and therefore the degradation in the squeezing due to thermalization will be reduced.

4. Experimental parameters

The previous section showed that under ideal conditions the geometric phase can be used to produce squeezed mechanical states. In this section we will consider experimental technicalities such as thermalization of the mechanical oscillator, optical losses and possible non-closing of the optical phase space loop. Each of these effects will have a detrimental effect on the squeezing of the mechanical oscillator.

Optical losses effect this protocol in two ways. Firstly, classical attenuation from the beamsplitter will result in the phase space loop remaining unclosed after the four pulse sequence. This can be corrected by changing either the amplitude or phase of each subsequent displacement to counteract the attenuation. Secondly, optical losses will also add amplitude-noise back action on the momentum of the mechanics. In the absence of vacuum noise entering each cycle, any back action on the momentum in the X_{L} (P_{L}) pulse will be reversed by the $-X_{\mathrm{M}}$ ($-P_{\mathrm{M}}$) pulse. However when vacuum noise is introduced at the beamsplitters, the amplitude noise in the $-X_{\mathrm{M}}$ pulse will no longer perfectly cancel the amplitude noise from the X_{M} pulse. Unlike the attenuation of the classical amplitude this mechanism cannot be easily corrected for in the protocol.

For a beamsplitter with 99:1 reflectivity for the optical displacement, we expect $1 - 0.99^2 \approx 2\%$ vacuum noise to be imparted onto the oscillator from each of the $X_{\mathrm{L}}, -X_{\mathrm{L}}$ and $P_{\mathrm{L}}, -P_{\mathrm{L}}$ pulse pairs. Quantifying the total loss over a single cycle (beamsplitter, fiber loss, input–output coupling etc—modeled as an effective beamsplitter with vacuum input) by η, then $1 - \eta^2$ vacuum noise would be introduced to the oscillator. The square arises from the fact the pulse must circulate twice before it cancels the noise, e.g. the noise imparted from the X_{M} pulse will only be canceled two cycles later from the $-X_{\mathrm{M}}$ pulse. Even after correcting for the effect of losses, classical fluctuations in the pulse intensities could result in non-closure of the phase space loop. If the loop is not closed after the four pulse sequence, the effective geometric phase[5] unitary operator is given by $U = \exp[-\mathrm{i}X_{\mathrm{M}} \sum_j \chi_j X_{\mathrm{L}}^{\phi_j} - \mathrm{i}\chi^2 X_{\mathrm{M}}^2]$, where here $\chi^2 = \sum_{j=1,j<k\leq 4}^{j=4} \chi_j \chi_k [X_{\mathrm{M}}^{\phi_k}, X_{\mathrm{M}}^{\phi_j}]/(2\mathrm{i})$ and $\chi_i = 4g_0\sqrt{N_i \sigma_i \sqrt{\pi/2}/\kappa}$ for a Gaussian pulse with temporal width σ_i and N_i photons. The second term in the above operator is the geometric phase. The first term leaves the mechanical element in an entangled state with the light after the interaction. This can be viewed as a momentum displacement on the mechanics that depends on the optical field, $D(-\mathrm{i}\chi^{\mathrm{fin}} X_{\mathrm{L}}^{\phi^{\mathrm{fin}}})$, where χ^{fin} is the displacement in the $X_{\mathrm{L}}^{\phi^{\mathrm{fin}}}$ quadrature that defines the final optical state. If χ^{fin} and ϕ^{fin} are unknown, the final state must be averaged over possible values, reducing the squeezing. A homodyne measurement of the light lost from the beamsplitter will give an estimate of χ^{fin} and ϕ^{fin}, meaning this error can be accounted for retrospectively. Note laser phase noise will change the direction of each displacement pulse which may result in non-closure of the optical phase space loop. Figure 3 shows how $\chi^{\mathrm{fin}} \neq 0$ changes the squeezed state. Note for when χ^{fin} is small, the squeezing is only slightly affected.

Even if classical drifts in the optical displacements are corrected for, vacuum noise introduced by losses in the feedback loop can cause non-closure resulting in a mixed mechanical state. For a single pass efficiency in the fiber loop η, the cancellation of noise between pairs of displacement measurements (e.g. X_{M} and $-X_{\mathrm{M}}$) will be degraded by a factor $1 - \eta^2$, leading to a loop non-closure of $2 - 2\eta$. For realistic inefficiencies in the range of 10% (corresponding to $2 - 2 \times 1.8 = 0.2$—i.e. 20% vacuum noise) the loop non-closure due to non-cancellation of noise is negligible, i.e. $\chi^{\mathrm{fin}} = 4g_0\sqrt{0.2\sigma\sqrt{\pi/2}/\kappa} \ll 1$. Hence the squeezing is not significantly affected by the addition of vacuum noise.

The following considers the effect of thermalization on the mechanical squeezed state. Thermalization can have two detrimental effects. Firstly, phonon exchange with the bath during

---

[5] I.e. ignoring the dynamical phase.

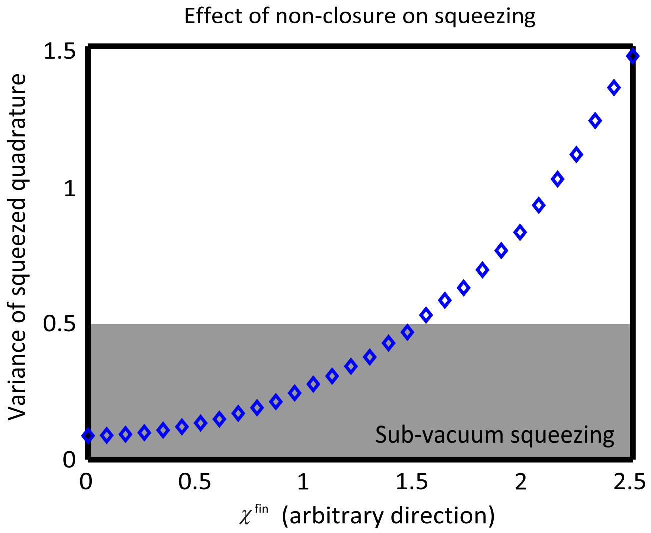

Figure 3. Effect of non-closure of the loop on the squeezed state for a fixed $\chi^2 = 1$. χ^{loss} is the magnitude of non-closure in an unknown quadrature $X_L^{\phi\text{loss}}$. Once the variance of the squeezed state goes above one, squeezing becomes impossible as the amount of noise added from the non-closure of the loop is larger than the ground state variance.

the four pulse sequence will render the dynamics over the pulse sequence non-unitary and change the final mechanical state. Secondly phonons that enter during the time scale required for the squeezed quadrature to rotate into the measurable position quadrature will degrade the squeezing. The first of these effects can be neglected since the four pulses can be very closely spaced with only a short delay between them. For example, for a mechanical oscillator with resonance frequency $\omega_M = 24\,\text{kHz}$, and quality factor $Q = 10^5$, the pulse duration should be $\sigma \simeq 10^{-8}$ s, such that the time for four pulses (on the order of 10^{-7} s), is much smaller than the time scale for one phonon to enter the oscillator, $1/(\Gamma\bar{N}) \approx 10^{-5}$ s at 1 K. Consequently, only thermal phonon exchange after the state has been prepared will be considered. The mechanical oscillator was modeled as an oscillator with noised added only on the momentum quadrature. For small times $t \ll \omega_m^{-1}$ one may neglect the oscillator decay. The equation of motion was then solved to find the variance $\langle \Delta^2 X_M \rangle = \langle X_M^2 \rangle - \langle X_M \rangle^2$ of the position as a function of time

$$\begin{aligned}\langle \Delta^2 X_M \rangle = {} & [\langle X_M^2(0) \rangle \cos^2(\omega t) + \langle {P_M}^2(0) \rangle \sin^2(\omega t)] \\ & + \langle X_M(0) P_M(0) + P_M(0) X_M(0) \rangle \sin(\omega t) \cos(\omega t) \\ & + \Gamma \left(\bar{N} + \frac{1}{2} \right) \left[\frac{t}{2} - \frac{\sin(2\omega t)}{4\omega} \right],\end{aligned} \tag{5}$$

where $\langle X_M^2(0) \rangle = \bar{N} + \frac{1}{2}$, $\langle P_M^2(0) \rangle = (\bar{N} + \frac{1}{2})(1 + 4\chi^4)$ and $\langle X_M(t) P_M(0) + P_M(0) X_M(0) \rangle = -4\chi^2$ $(\bar{N} + \frac{1}{2})$ are the expectation values after the geometric phase has been applied.

To minimize the initial phonon number before the four pulse sequence we envisage cooling via pulsed measurement as outlined in [12]. In this protocol, two pulses separated by 1/4 of the mechanical period are used to measure the oscillator in two orthogonal quadratures, leading to a low entropy state. The result in [12] shows an effective thermal phonon number of

$$\bar{N}_{\mathrm{eff}} \simeq \frac{1}{2}\left(\sqrt{1+\frac{1}{\chi^4}+\frac{\pi\bar{N}}{Q\chi^2}}-1\right), \tag{6}$$

where $\chi = 4g_0\sqrt{N_p\sigma\sqrt{\frac{\pi}{2}}/\kappa}$ (the same χ used elsewhere). This gives $\bar{N}_{\mathrm{eff}} \simeq 10$ for a 1 mm, 24 kHz SiN resonator with $Q \approx 10^5$ and photon number $N_p = |\alpha|^2 \approx 10^6$. Using the SiN string mechanical oscillators considered in this paper, the effective phonon number is achievable for resonance frequencies of $\omega_M < 70\,\mathrm{kHz}$ and length $L < 5\,\mathrm{mm}$ with a maximum incident photon flux of $\dot{N}_p = 10^{16}\,\mathrm{Hz}$ ($\approx$2 mW at 630 nm). Although this is the initial phonon occupation, the bath occupation remains at $\bar{N} \approx 10^5$.

SiN strings present a particularly attractive mechanical oscillator, high mechanical quality factors of up to 7×10^6 have been observed, and the mechanical resonance frequency may be tuned via tensioning [17, 18]. The protocol requires the mechanical period to be large compared to all other characteristic time scales. From this constraint we will limit the following analysis to low frequency, $\omega_m = 1$–$70\,\mathrm{kHz}$, SiN strings. From [18], the expected Q factor of a stressed SiN string of dimensions $L\times h\times w$ is

$$Q = \left[\frac{(n\pi)^2Eh^2}{12SL^2}+1.0887\sqrt{\frac{E}{S}}\frac{h}{L}\right]^{-1} Q_{\mathrm{Bending}} \tag{7}$$

with $E = 241\pm4\,\mathrm{GPa}$ the Young's modulus of SiN, $Q_{\mathrm{Bending}} = 17\,000$ the quality factor related to bending damping mechanisms and $S = 4\omega_m^2L^2\rho_{\mathrm{SiN}}$ the tensile stress of SiN (with density ρ_{SiN}) in the high stress limit.

The optomechanical coupling rate g_0 is calculated from evanescently coupled SiN string coupling rate $G = 200\,\mathrm{MHz\,nm^{-1}}$ [19] and the oscillators zero point motion: $g_0 = Gx_0 = G\sqrt{\hbar/(2m\omega_M)}$ with m the effective mass of the mode. The pulse width and optical cavity decay rate are defined by $T_m = 10^{-3}\sigma = 5/\kappa$ to satisfy the experimental requirements.

After preparing the mechanical quantum state with the four pulse sequence, it may be characterized with a measurement pulse. Figures 4(a) and (b) show the temporal progression of the variance over various time scales after the four pulse sequence. Figure 4(c) shows a plot of $\langle\Delta^2X_M\rangle$ as a function of length and resonance frequency of a SiN string at 1 K with cross section 157 nm × 3 μm. These two parameters may be chosen independently by tensioning the string to the desired frequency. The dashed line of $Q = 7\times10^6$ is just larger than the highest observed Q in a SiN string [18]. This figure shows it is experimentally feasible to achieve quantum squeezing for a wide range of geometries with the best squeezing of $\Delta^2X_M \approx 10^{-2}$ predicted for a 3.5 mm long oscillator with 20 kHz resonance frequency and $Q = 5\times10^6$. For all points in this figure, the initial state had an effective phonon number of $N_{\mathrm{eff}} = 10$ phonons; the maximum intracavity photon number to achieve such cooling was 10^6 photons which is readily achieved.

The X_M^2 appearing in the unitary operator is a result of the geometric phase changing a linear optomechanical interaction into an effective quadratic potential. If the mechanics was instead quadratically coupled to the light field [10, 16, 20, 21] ($H_I = g_0\hbar a^\dagger aX_M^2$), the result would be a factor X_M^4 in the unitary operator—increasing the nonlinearity present in the Hamiltonian to fourth order. In this case we may view the interaction as a position-cubed dependent displacement, $U = \exp[-\mathrm{i}\chi^2X_M^4] = D(-\mathrm{i}\chi^2x^3)$ correlating the momentum of the oscillator with the cube of its position. With large enough quadratic coupling, this

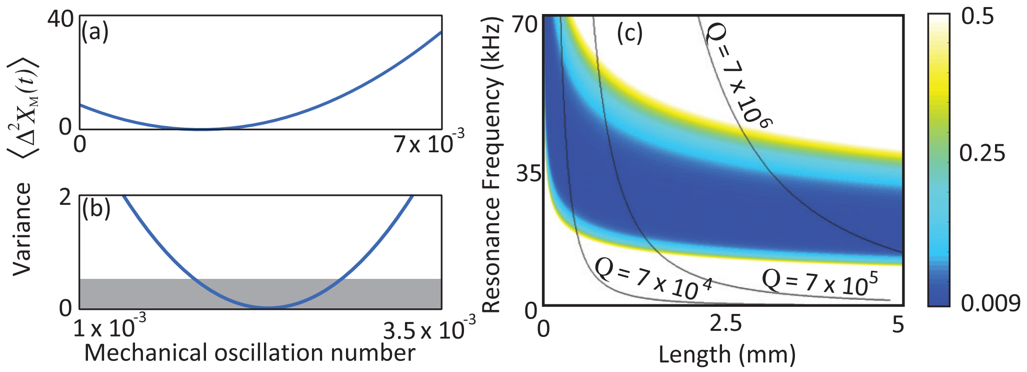

Figure 4. Progression of the variance of the mechanical oscillator over two time scales: (a) free evolution immediately after the four pulse sequence, (b) explicitly showing the squeezed region and (c) experimentally observable squeezing generated via a geometric phase of an oscillator initially cooled to $N_{\mathrm{eff}} = 10$. The color scale gives the variance in the position quadrature over one decay time of the oscillator. A value less than 0.5 indicates squeezing below the ground state variance. The plot color axis is truncated at 0.5.

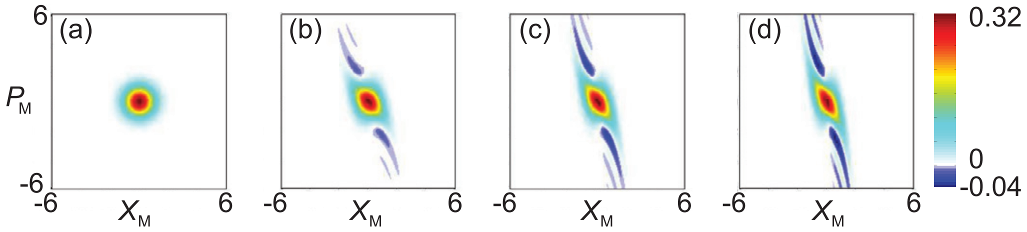

Figure 5. Wigner functions of the mechanical state after a geometric phase interaction on the mechanical ground state of motion with a quadratically coupled mechanical oscillator for values of (a) $\chi^2 = 0$, (b) $\chi^2 = 0.066$, (c) $\chi^2 = 0.133$, (d) $\chi^2 = 0.2$. The momentum becomes correlated with the cube of the position—this can be seen in the Wigner function follows a profile proportional to $-x^3$ with negativity arising in the concave sections of the curve.

provides an avenue to generate quantum states of the oscillator involving significant Wigner negativity, see figure 5. Wigner negativity is an unambiguous and sufficient indicator of non-classicality [22, 23]. Exploring such states experimentally is of vital importance to determine the feasibility of mechanical oscillators as elements in quantum applications and to gain a deeper empirical understanding of the quantum-to-classical transition.

5. Conclusion

In summary, we have proposed an experiment that uses a geometric phase to generate nonlinearity and non-classical motional states of a mechanical resonator. This provides a new tool in optomechanics for quantum state engineering of mechanical oscillators. We have shown our method to be both experimentally feasible and robust to optical and mechanical noise sources.

Acknowledgments

This research was funded by the Australian Research Council Center of Excellence CE110001013.

References

[1] Berry M V 1987 The adiabatic phase and Pancharatnam's phase for polarized light *J. Mod. Opt.* **34** 1401–7

[2] Sørensen A and Mølmer K 2000 Entanglement and quantum computation with ions in thermal motion *Phys. Rev.* A **62** 022311

[3] Milburn G J, Schneider S and James D F V 2000 Ion trap quantum computing with warm atoms *Fortschr. Phys.* **48** 801–10

[4] Leibfried D *et al* 2003 Experimental demonstration of a robust, high-fidelity geometric two ion-qubit phase gate *Nature* **422** 412–5

[5] Vacanti G, Fazio R, Kim M S, Palma G M, Paternostro M and Vedral V 2012 Geometric phase kickback in a mesoscopic qubit-oscillator system *Phys. Rev.* A **85** 022129

[6] Pikovski I, Vanner M R, Aspelmeyer M, Kim M S and Brukner Č 2012 Probing Planck-scale physics with quantum optics *Nature Phys.* **8** 393–7

[7] Bose S, Jacobs K and Knight P L 1999 Scheme to probe the decoherence of a macroscopic object *Phys. Rev.* A **59** 3204–10

[8] Mancini S, Giovannetti V, Vitali D and Tombesi P 2002 Entangling macroscopic oscillators exploiting radiation pressure *Phys. Rev. Lett.* **88** 120401

[9] Marshall W, Simon C, Penrose R and Bouwmeester D 2003 Towards quantum superpositions of a mirror *Phys. Rev. Lett.* **91** 130401

[10] Thompson J D, Zwickl B M, Jayich A M, Marquardt F, Girvin S M and Harris J G E 2008 Strong dispersive coupling of a high-finesse cavity to a micromechanical membrane *Nature* **452** 72–5

[11] Eichenfield M, Chan J, Camacho R M, Vahala K J and Painter O 2009 Optomechanical crystals *Nature* **462** 78–82

[12] Vanner M R, Pikovski I, Cole G D, Kim M S, Brukner Č, Hammerer K, Milburn G J and Aspelmeyer M 2011 Pulsed quantum optomechanics *Proc. Natl Acad. Sci. USA* **108** 16182–7

[13] Jacobs K 2007 Engineering quantum states of a nanoresonator via a simple auxiliary system *Phys. Rev. Lett.* **99** 117203

[14] Dynkin E B 1947 Calculation of the coefficients in the Campbell–Hausdorff formula *Dokl. Akad. Nauk. SSSR (N.S.)* **57** 323–6

[15] Berry M V 1984 Quantal phase factors accompanying adiabatic changes *Proc. R. Soc. Lond.* **392** 45–57

[16] Anetsberger G, Arcizet O, Unterreithmeier Q P, Rivière R, Schliesser A, Weig E M, Kotthaus J P and Kippenberg T J 2009 Near-field cavity optomechanics with nanomechanical oscillators *Nature Phys.* **5** 909–14

[17] Verbridge S S, Shapiro D F, Craighead H G and Parpia J M 2007 Macroscopic tuning of nanomechanics: substrate bending for reversible control of frequency and quality factor of nanostring resonators *Nano Lett.* **7** 1728–35

[18] Schmid S, Jensen K D, Nielsen K H and Boisen A 2011 Damping mechanisms in high-Q micro and nanomechanical string resonators *Phys. Rev.* B **84** 165307

[19] Anetsberger G, Weig E M, Kotthaus J P and Kippenberg T J 2011 Cavity optomechanics and cooling nanomechanical oscillators using microresonator enhanced evanescent near-field coupling *C. R. Phys.* **12** 800–16

[20] Jayich A M, Sankey J C, Zwickl B M, Yang C, Thompson J D, Girvin S M, Clerk A A, Marquardt F and Harris J G E 2008 Dispersive optomechanics: a membrane inside a cavity *New J. Phys.* **10** 095008

[21] Purdy T P, Brooks D W C, Botter T, Brahms N, Ma Z-Y and Stamper-Kurn D M D M 2010 Tunable cavity optomechanics with ultracold atoms *Phys. Rev. Lett.* **105** 133602

[22] Bužek V and Knight P L 1995 Quantum interference, superposition states of light and nonclassical effects *Prog. Opt.* **34** 1–158

[23] Kenfack A and Zyczkowski K 2004 Negativity of the Wigner function as an indicator of non-classicality *J. Opt. B: Quantum Semiclass. Opt.* **6** 396–404

Conclusions

The research conducted during this thesis advanced the field of quantum optomechanics by making both conceptual and technical contributions. Foremost, building upon the seminal work of V. B. Braginsky, this research introduced and pioneered the regime of *pulsed* quantum optomechanics. This pulsed regime provides an experimentally feasible route to conditionally prepare quantum states of motion, and protocols to prepare squeezed and quantum superposition states of motion have been introduced here. Furthermore, pulsed quantum optomechanics provides an answer to the important question of how to perform state tomography of the motion of a mechanical resonator that would allow the reconstruction of non-Gaussian quantum features such as Wigner negativity. Conditional thermal noise squeezing was demonstrated by a back-action-evading cavity-free experiment that reduced the mechanical position uncertainty to less than 20 pm. Full state tomography for motional state reconstruction was also performed.

A pulsed interaction also opens a research avenue for protocols that utilise a sequence of multiple pulses. In this direction, this thesis introduced a scheme how to deterministically introduce mechanical non-linearity by exploiting an optomechanical geometric phase generated by a sequence of four pulsed optomechanical interactions. In addition, we proposed an experiment that also used a sequence of four pulsed optomechanical interactions to infer the canonical commutation relation between the mechanical position and momentum. Primarily, this proposal aims to probe consequences of Planck-scale phenomena by observing potential deformations to the quantum mechanical commutation relation due to a minimum length scale in the universe. Excitingly, the outcomes of our analysis indicate that an experiment implementing our protocol can probe the commutator deformation parameter space by several orders of magnitude deeper than the current experimental best.

Using a continuous interaction between the optical cavity field and the motion of the mechanical system we achieved sufficiently strong coupling to be the first to observe optomechanical normal mode splitting. Achieving this level of coupling is crucial to implement a unitary state-swap operation between the optical and mechanical states. In addition, we made improvements to cooling the mechanical motion by a combination of cryogenic and laser cooling techniques. We also studied both theoretically and experimentally the dependence between the mechanical quality factor and the shape of the mechanical resonator due to phonon tunneling. This study will be of vital importance to minimize mechanical clamping losses that reduce the mechanical quality factor and thus increase quantum decoherence that can hinder and limit efforts to generate a non-classical mechanical motional state.

Bridging the pulsed and continuous interaction regimes, this research introduced a technique how to perform an arbitrary superposition of phonon addition, phonon subtraction and the identity operation. This tool offers considerable potential for quantum state engineering of the mechanical motional state and by using a superposition of the addition and subtraction components we introduced the concept of a quantum state orthogonalizer that can be used to generate a new type of continuous-variable qubit.

Acknowledgments

It is a great pleasure to reflect upon the past five years of my academic life to list and thank those people that supported me throughout this period.

I have been very fortunate to have had several academic father figures and I benefited greatly from the wisdom they shared with me. Foremost, I would like to thank my primary supervisor Prof. Markus Aspelmeyer. Markus has built a fantastic research group that is dedicated to asking questions that probe the foundations of physics and I enjoyed tremendously working in this environment and participating in our group discussions. I've come to realize that Markus was the ideal supervisor for me. Markus' ceaseless energy never failed to inspire and he allowed and encouraged me to pursue my own research questions and dive into unexplored territory in both theory and in the laboratory.

I would like to thank next my external thesis advisor Prof. Gerard J. Milburn. In the beginning of my thesis I was a devoted experimentalist, but I wanted to author a theoretical publication during my PhD. During his visits to Vienna, Gerard patiently taught me much about theoretical quantum optics, in particular quantum stochastic differential equations, and I discovered the thrill of doing theoretical research. I will always be an experimentalist at heart, but now theory is a vitally important part of my research that I will continue throughout my career. I would also like to thank Gerard for his kind hospitality during my "annual migration" to Brisbane each summer.

My third official supervisor was Prof. Anton Zeilinger. For the three years before we shifted laboratory it was a great pleasure to be part of the Institute for Quantum Optics and Quantum Information (IQOQI) and take part in the numerous discussions on the foundations of quantum physics and the associated interpretational questions. I was always very impressed by Anton's breadth of knowledge and I certainly feel that being a part of the "Vienna quantum group" has strongly influenced my research.

Unofficially I had a fourth supervisor, Prof. Myungshik Kim. I had the pleasure of working with Myungshik on three theoretical projects and Myungshik repeatedly impressed me with his creativity and clarity. I certainly feel that Myungshik and I "clicked" due to our common appreciation of continuous variable quantum optics and I sincerely hope that our current collaboration will continue throughout my career. Many thanks Myungshik.

My warmest thanks are extended to my friend and colleague Igor Pikovski. Igor

and I worked closely on the main theoretical work of this thesis and I tremendously enjoyed our numerous discussions at the black-board in the kitchen, which was certainly our most productive place for doing physics. Looking back now, what I enjoyed most about our discussions was how we refined our intuition and bridged these thoughts with the mathematical model we developed. Developing such connections between intuition and mathematics is perhaps one of the most enjoyable aspects of physics and it was a great pleasure to experience this with Igor.

It was a pleasure to work together in the lab with Garrett D. Cole and Joachim Hofer. Thanks guys for all the time we spent solving the technical problems we faced and discussing the data.

Completing a PhD in physics is as much an exploration and development of one's self as it is an exploration of physics. Sharing this route with me was my office neighbour Jonas Schmöle who I thank for our discussions and time together that I'm sure helped keep me sane.

When I began my PhD I was one of just a few people working on optomechanics in Vienna. It was very exciting to be part of a growing team and so I would like to thank Florian Blaser, Uros Delic, David Grass, Simon Gröblacher, Jason Hoelscher-Obermaier, Sebastian Hofer, Rainer Kaltenbaek, Nikolai Kiesel, Philipp Köhler, Stephen Minter, Ralf Riedinger, Alexandra Seiringer, Karoline Siquans, Alexey Trubarov, and Witlef Wieczorek, for making the group such a friendly place to work. Also I'd like to thank our close collaborators Caslav Brukner, Claudiu Genes, Klemens Hammerer, and Ignacio Wilson-Rae.

Other people from whom I had enjoyable discussions that influenced the work outlined here include Markus Arndt, Hans Bachor, Oliver Benson, Reinhold Bertlmann, from whom I learnt much about open quantum systems during his lectures, Warwick Bowen, Carl Caves, Andrew Doherty, Danny Greenberger, Michael Horne, Peter Knight, Johannes Kofler, Anthony Leggett, Ulf Leonhardt, Tim Ralph, Joerg Schmiedmayer, Marlan O. Scully, and Mandip Singh.

Several people beyond physics helped to 'humanise' me on weekends and evenings. I'd like to express my warmest thanks to William R. Naylor for our semi-regular walks in the Wienerwald on those Austrian summer afternoons and Andrea for our wonderful weekends together.

Bibliography

[1] E. F. Nichols and G. F. Hull. A preliminary communication on the pressure of heat and light radiation. *Physical Review (Series I)*, 13(5):307–320, November 1901.

[2] E. F. Nichols and G. F. Hull. The pressure due to radiation. (second paper.). *Physical Review (Series I)*, 17(1):26–50, July 1903.

[3] P. N. Lebedev. Experimental examination of light pressure. *Annalen der Physik*, 6:433, 1901.

[4] A. Ashkin. Acceleration and trapping of particles by radiation pressure. *Physical Review Letters*, 24(4):156–159, January 1970.

[5] Stig Stenholm. The semiclassical theory of laser cooling. *Reviews of Modern Physics*, 58(3):699–739, July 1986.

[6] E. L. Raab, M. Prentiss, Alex Cable, Steven Chu, and D. E. Pritchard. Trapping of neutral sodium atoms with radiation pressure. *Physical Review Letters*, 59(23):2631–2634, December 1987.

[7] T. J. Kippenberg and K. J. Vahala. Cavity optomechanics: Back-action at the mesoscale. *Science*, 321(5893):1172–1176, August 2008.

[8] Florian Marquardt and Steven M. Girvin. Optomechanics. *Physics*, 2:40, May 2009.

[9] G. J. Milburn and M. Woolley. An introduction to quantum optomechanics. *Acta Physica Slovaca. Reviews and Tutorials*, 61(5):483–601, October 2011.

[10] Markus Aspelmeyer, Pierre Meystre, and Keith Schwab. Quantum optomechanics. *Physics Today*, 65(7):29–35, 2012.

[11] Pierre Meystre. A short walk through quantum optomechanics. *Annalen der Physik*, 525(3):215–233, 2013.

[12] Markus Aspelmeyer, Tobias J. Kippenberg, and Florian Marquardt. Cavity optomechanics. arXiv e-print 1303.0733, March 2013.

[13] Alex Abramovici, William E. Althouse, Ronald W. P. Drever, Yekta Gürsel, Seiji Kawamura, Frederick J. Raab, David Shoemaker, Lisa Sievers, Robert E. Spero, Kip S. Thorne, Rochus E. Vogt, Rainer Weiss, Stanley E. Whitcomb, and Michael E. Zucker. LIGO: the laser interferometer gravitational-wave observatory. *Science*, 256(5055):325–333, April 1992.

[14] The LIGO Scientific Collaboration. LIGO: the laser interferometer gravitational-wave observatory. *Reports on Progress in Physics*, 72(7):076901, July 2009.

[15] Carlton M. Caves. Quantum-mechanical noise in an interferometer. *Physical Review D*, 23(8):1693–1708, April 1981.

[16] P. Meystre and M. O. Scully. *Quantum Optics, Experimental Gravity, and Measurement Theory.* Springer, NATO ASI Series, 1983.

[17] V. B. Braginsky and F. Ya. Khalili. Quantum nondemolition measurements: the route from toys to tools. *Reviews of Modern Physics*, 68(1):1–11, January 1996.

[18] Aleksandr F Andreev, Sergei N Bagaev, Fedor V Bunkin, Sergei P Vyatchanin, Yurii V Gulyaev, Vladimir S Imshennik, Nikolai S Kardashev, Viktor A Matveev, Oleg V Rudenko, Ol'ga G Ryazhskaya, Alexei R Khokhlov, and Anatolii M Cherepashchuk. Vladimir borisovich braginsky (on his 80th birthday). *Physics-Uspekhi*, 55(1):109–110, January 2012.

[19] V. B. Braginsky and F. Y. Khalili. *Quantum Measurement.* Cambridge University Press, 1995.

[20] A. Dorsel, J. D. McCullen, P. Meystre, E. Vignes, and H. Walther. Optical bistability and mirror confinement induced by radiation pressure. *Physical Review Letters*, 51(17):1550–1553, October 1983.

[21] S. Mancini and P. Tombesi. Quantum noise reduction by radiation pressure. *Physical Review A*, 49(5):4055–4065, May 1994.

[22] C. Fabre, M. Pinard, S. Bourzeix, A. Heidmann, E. Giacobino, and S. Reynaud. Quantum-noise reduction using a cavity with a movable mirror. *Physical Review A*, 49(2):1337–1343, February 1994.

[23] Daniel W. C. Brooks, Thierry Botter, Sydney Schreppler, Thomas P. Purdy, Nathan Brahms, and Dan M. Stamper-Kurn. Non-classical light generated by quantum-noise-driven cavity optomechanics. *Nature*, 488(7412):476–480, August 2012.

[24] Amir H. Safavi-Naeini, Simon Groblacher, Jeff T. Hill, Jasper Chan, Markus Aspelmeyer, and Oskar Painter. Squeezed light from a silicon micromechanical resonator. *Nature*, 500(7461):185–189, August 2013.

[25] T. P. Purdy, P.-L. Yu, R. W. Peterson, N. S. Kampel, and C. A. Regal. Strong optomechanical squeezing of light. *Physical Review X*, 3(3):031012, September 2013.

[26] Thomas Corbitt, Yanbei Chen, Farid Khalili, David Ottaway, Sergey Vyatchanin, Stan Whitcomb, and Nergis Mavalvala. Squeezed-state source using radiation-pressure-induced rigidity. *Physical Review A*, 73(2):023801, February 2006.

[27] Thomas Corbitt. *Quantum Noise and Radiation Pressure Effects in High Power Optical Interferometers.* PhD thesis, Massachusetts Institute Of Technology, 2008.

[28] The LIGO Scientific Collaboration. A gravitational wave observatory operating beyond the quantum shot-noise limit. *Nature Physics*, 7(12):962–965, September 2011.

[29] Samuel Deleglise, Igor Dotsenko, Clement Sayrin, Julien Bernu, Michel Brune, Jean-Michel Raimond, and Serge Haroche. Reconstruction of non-classical cavity field states with snapshots of their decoherence. *Nature*, 455(7212):510–514, September 2008.

[30] Brian Julsgaard, Alexander Kozhekin, and Eugene S. Polzik. Experimental long-lived entanglement of two macroscopic objects. *Nature*, 413(6854):400–403, September 2001.

[31] C. Monroe, D. M. Meekhof, B. E. King, and D. J. Wineland. A Schroedinger cat superposition state of an atom. *Science*, 272(5265):1131–1136, May 1996. PMID: 8662445.

[32] D. T. Smithey, M. Beck, M. G. Raymer, and A. Faridani. Measurement of the wigner distribution and the density matrix of a light mode using optical homodyne tomography: Application to squeezed states and the vacuum. *Physical Review Letters*, 70(9):1244–1247, March 1993.

[33] S. Bose, K. Jacobs, and P. L. Knight. Preparation of nonclassical states in cavities with a moving mirror. *Physical Review A*, 56(5):4175–4186, November 1997.

[34] S. Bose, K. Jacobs, and P. L. Knight. Scheme to probe the decoherence of a macroscopic object. *Physical Review A*, 59(5):3204–3210, May 1999.

[35] S. Mancini, V. I. Man'ko, and P. Tombesi. Ponderomotive control of quantum macroscopic coherence. *Physical Review A*, 55(4):3042–3050, April 1997.

[36] William Marshall, Christoph Simon, Roger Penrose, and Dik Bouwmeester. Towards quantum superpositions of a mirror. *Physical Review Letters*, 91(13):130401, 2003.

[37] A. D. Armour, M. P. Blencowe, and K. C. Schwab. Entanglement and decoherence of a micromechanical resonator via coupling to a cooper-pair box. *Physical Review Letters*, 88(14):148301, March 2002.

[38] G. C. Ghirardi, A. Rimini, and T. Weber. Unified dynamics for microscopic and macroscopic systems. *Physical Review D*, 34(2):470–491, July 1986.

[39] L. Diósi. Models for universal reduction of macroscopic quantum fluctuations. *Physical Review A*, 40(3):1165–1174, August 1989.

[40] Philip Pearle. Combining stochastic dynamical state-vector reduction with spontaneous localization. *Physical Review A*, 39(5):2277–2289, March 1989.

[41] Roger Penrose. On gravity's role in quantum state reduction. *General Relativity and Gravitation*, 28(5):581–600, May 1996.

[42] Stefano Mancini, David Vitali, and Paolo Tombesi. Scheme for teleportation of quantum states onto a mechanical resonator. *Physical Review Letters*, 90(13):137901, April 2003.

[43] Stefano Mancini, Vittorio Giovannetti, David Vitali, and Paolo Tombesi. Entangling macroscopic oscillators exploiting radiation pressure. *Physical Review Letters*, 88(12):120401, March 2002.

[44] M Pinard, A Dantan, D Vitali, O Arcizet, T Briant, and A Heidmann. Entangling movable mirrors in a double-cavity system. *Europhysics Letters (EPL)*, 72(5):747–753, December 2005.

[45] Helge Mueller-Ebhardt, Henning Rehbein, Roman Schnabel, Karsten Danzmann, and Yanbei Chen. Entanglement of macroscopic test masses and the standard quantum limit in laser interferometry. *Physical Review Letters*, 100(1):013601, January 2008.

[46] M. R. Vanner, M. Aspelmeyer, and M. S. Kim. Quantum state orthogonalization and a toolset for quantum optomechanical phonon control. *Physical Review Letters*, 110(1):010504, January 2013.

[47] A. D. OConnell, M. Hofheinz, M. Ansmann, Radoslaw C. Bialczak, M. Lenander, Erik Lucero, M. Neeley, D. Sank, H. Wang, M. Weides, J. Wenner, John M. Martinis, and A. N. Cleland. Quantum ground state and single-phonon control of a mechanical resonator. *Nature*, 464(7289):697–703, April 2010.

[48] K. C. Lee, M. R. Sprague, B. J. Sussman, J. Nunn, N. K. Langford, X.-M. Jin, T. Champion, P. Michelberger, K. F. Reim, D. England, D. Jaksch, and I. A. Walmsley. Entangling macroscopic diamonds at room temperature. *Science*, 334(6060):1253–1256, December 2011.

[49] K. C. Lee, B. J. Sussman, M. R. Sprague, P. Michelberger, K. F. Reim, J. Nunn, N. K. Langford, P. J. Bustard, D. Jaksch, and I. A. Walmsley. Macroscopic non-classical states and terahertz quantum processing in room-temperature diamond. *Nature Photonics*, 6(1):41–44, 2012.

[50] A. F. Pace, M. J. Collett, and D. F. Walls. Quantum limits in interferometric detection of gravitational radiation. *Physical Review A*, 47(4):3173–3189, April 1993.

[51] C. K. Law. Interaction between a moving mirror and radiation pressure: A hamiltonian formulation. *Physical Review A*, 51(3):2537–2541, March 1995.

[52] C. W. Gardiner and P. Zoller. *Quantum Noise.* Springer, 3 edition, 2004.

[53] Jing Zhang, Kunchi Peng, and Samuel L. Braunstein. Quantum-state transfer from light to macroscopic oscillators. *Physical Review A*, 68(1):013808, July 2003.

[54] A S Parkins and H J Kimble. Quantum state transfer between motion and light. *Journal of Optics B: Quantum and Semiclassical Optics*, 1(4):496–504, August 1999.

[55] S. Gigan, H. R. Böhm, M. Paternostro, F. Blaser, G. Langer, J. B. Hertzberg, K. C. Schwab, D. Bäuerle, M. Aspelmeyer, and A. Zeilinger. Self-cooling of a micromirror by radiation pressure. *Nature*, 444(7115):67–70, November 2006.

[56] H. R. Bohm. *Radiation-Pressure Cooling of a Mechanical Oscillator.* PhD thesis, University of Vienna, 2007.

[57] S. Groblacher. *Quantum opto-mechanics with micromirrors: combining nanomechanics with quantum optics.* PhD thesis, University of Vienna, 2010.

[58] V. B. Braginsky, Y. I. Vorontsov, and F. Y. Khalili. Optimal quantum measurements in detectors of gravitation radiation. *JETP Lett.*, 27:276–280, March 1978.

[59] V. B. Braginsky, A. B. Manukin, and M. Yu Tikhonov. Investigation of dissipative ponderomotive effects of electromagnetic radiation. *JETP Lett.*, 31:829, 1970.

[60] F. Diedrich, J. C. Bergquist, Wayne M. Itano, and D. J. Wineland. Laser cooling to the zero-point energy of motion. *Physical Review Letters*, 62(4):403–406, January 1989.

[61] Constanze Hohberger Metzger and Khaled Karrai. Cavity cooling of a microlever. *Nature*, 432(7020):1002–1005, December 2004.

[62] O. Arcizet, P.-F. Cohadon, T. Briant, M. Pinard, and A. Heidmann. Radiation-pressure cooling and optomechanical instability of a micromirror. *Nature*, 444(7115):71–74, November 2006.

[63] Simon Groblacher, Jared B. Hertzberg, Michael R. Vanner, Garrett D. Cole, Sylvain Gigan, K. C. Schwab, and Markus Aspelmeyer. Demonstration of an ultracold micro-optomechanical oscillator in a cryogenic cavity. *Nature Physics*, 5(7):485–488, 2009.

[64] J. D. Teufel, T. Donner, Dale Li, J. W. Harlow, M. S. Allman, K. Cicak, A. J. Sirois, J. D. Whittaker, K. W. Lehnert, and R. W. Simmonds. Sideband cooling of micromechanical motion to the quantum ground state. *Nature*, 475(7356):359–363, July 2011.

[65] Jasper Chan, T. P. Mayer Alegre, Amir H. Safavi-Naeini, Jeff T. Hill, Alex Krause, Simon Groblacher, Markus Aspelmeyer, and Oskar Painter. Laser cooling of a nanomechanical oscillator into its quantum ground state. *Nature*, 478(7367):89–92, October 2011.

[66] Alexander I. Lvovsky, Barry C. Sanders, and Wolfgang Tittel. Optical quantum memory. *Nature Photonics*, 3(12):706–714, December 2009.

[67] Y. Kaluzny, P. Goy, M. Gross, J. M. Raimond, and S. Haroche. Observation of self-induced rabi oscillations in two-level atoms excited inside a resonant cavity: The ringing regime of superradiance. *Physical Review Letters*, 51(13):1175–1178, September 1983.

[68] M. G. Raizen, R. J. Thompson, R. J. Brecha, H. J. Kimble, and H. J. Carmichael. Normal-mode splitting and linewidth averaging for two-state atoms in an optical cavity. *Physical Review Letters*, 63(3):240–243, July 1989.

[69] Florian Marquardt, Joe P. Chen, A. A. Clerk, and S. M. Girvin. Quantum theory of cavity-assisted sideband cooling of mechanical motion. *Physical Review Letters*, 99(9):093902, August 2007.

[70] J. M. Dobrindt, I. Wilson-Rae, and T. J. Kippenberg. Parametric normal-mode splitting in cavity optomechanics. *Physical Review Letters*, 101(26):263602, December 2008.

[71] Simon Groblacher, Klemens Hammerer, Michael R. Vanner, and Markus Aspelmeyer. Observation of strong coupling between a micromechanical resonator and an optical cavity field. *Nature*, 460(7256):724–727, August 2009.

[72] J. D. Teufel, Dale Li, M. S. Allman, K. Cicak, A. J. Sirois, J. D. Whittaker, and R. W. Simmonds. Circuit cavity electromechanics in the strong-coupling regime. *Nature*, 471(7337):204–208, March 2011.

[73] E. Verhagen, S. Deléglise, S. Weis, A. Schliesser, and T. J. Kippenberg. Quantum-coherent coupling of a mechanical oscillator to an optical cavity mode. *Nature*, 482(7383):63–67, February 2012.

[74] Garrett D. Cole, Ignacio Wilson-Rae, Katharina Werbach, Michael R. Vanner, and Markus Aspelmeyer. Phonon-tunnelling dissipation in mechanical resonators. *Nature Communications*, 2:231, March 2011.

[75] I. Wilson-Rae. Intrinsic dissipation in nanomechanical resonators due to phonon tunneling. *Physical Review B*, 77(24):245418, June 2008.

[76] Alexei Ourjoumtsev, Rosa Tualle-Brouri, Julien Laurat, and Philippe Grangier. Generating optical schrodinger kittens for quantum information processing. *Science*, 312(5770):83–86, April 2006.

[77] J. S. Neergaard-Nielsen, B. Melholt Nielsen, C. Hettich, K. Molmer, and E. S. Polzik. Generation of a superposition of odd photon number states for quantum information networks. *Physical Review Letters*, 97(8):083604, August 2006.

[78] Alessandro Zavatta, Silvia Viciani, and Marco Bellini. Quantum-to-classical transition with single-photon-added coherent states of light. *Science*, 306(5696):660–662, October 2004. PMID: 15499013.

[79] A. I. Lvovsky and M. G. Raymer. Continuous-variable optical quantum-state tomography. *Reviews of Modern Physics*, 81(1):299–332, March 2009.

[80] T. J. Dunn, I. A. Walmsley, and S. Mukamel. Experimental determination of the quantum-mechanical state of a molecular vibrational mode using fluorescence tomography. *Physical Review Letters*, 74(6):884–887, February 1995.

[81] D. Leibfried, D. M. Meekhof, B. E. King, C. Monroe, W. M. Itano, and D. J. Wineland. Experimental determination of the motional quantum state of a trapped atom. *Physical Review Letters*, 77(21):4281–4285, November 1996.

[82] T. Fernholz, H. Krauter, K. Jensen, J. F. Sherson, A. S. Sorensen, and E. S. Polzik. Spin squeezing of atomic ensembles via nuclear-electronic spin entanglement. *Physical Review Letters*, 101(7):073601, August 2008.

[83] M. R Vanner, I. Pikovski, G. D Cole, M. S Kim, Č Brukner, K. Hammerer, G. J Milburn, and M. Aspelmeyer. Pulsed quantum optomechanics. *Proceedings of the National Academy of Sciences*, 108(39):16182–16187, September 2011.

[84] M. R. Vanner, J. Hofer, G. D. Cole, and M. Aspelmeyer. Cooling-by-measurement and mechanical state tomography via pulsed optomechanics. *Nature Communications*, 4, August 2013.

[85] Kurt Jacobs, Lin Tian, and Justin Finn. Engineering superposition states and tailored probes for nanoresonators via open-loop control. *Physical Review Letters*, 102(5):057208, February 2009.

[86] J. D. Thompson, B. M. Zwickl, A. M. Jayich, Florian Marquardt, S. M. Girvin, and J. G. E. Harris. Strong dispersive coupling of a high-finesse cavity to a micromechanical membrane. *Nature*, 452(7183):72–75, March 2008.

[87] T. P. Purdy, D. W. C. Brooks, T. Botter, N. Brahms, Z.-Y. Ma, and D. M. Stamper-Kurn. Tunable cavity optomechanics with ultracold atoms. *Physical Review Letters*, 105(13):133602, September 2010.

[88] Michael R. Vanner. Selective linear or quadratic optomechanical coupling via measurement. *Physical Review X*, 1(2):021011, November 2011.

[89] Luis J. Garay. Quantum gravity and minimum length. *International Journal of Modern Physics A*, 10(02):145–165, January 1995.

[90] Michele Maggiore. The algebraic structure of the generalized uncertainty principle. *Physics Letters B*, 319:83–86, December 1993.

[91] Achim Kempf, Gianpiero Mangano, and Robert B. Mann. Hilbert space representation of the minimal length uncertainty relation. *Physical Review D*, 52(2):1108–1118, July 1995.

[92] Giovanni Amelino-Camelia. Doubly special relativity first results and key open problems. *International Journal of Modern Physics D*, 11(10):1643–1669, December 2002.

[93] João Magueijo and Lee Smolin. Generalized lorentz invariance with an invariant energy scale. *Physical Review D*, 67(4):044017, February 2003.

[94] Igor Pikovski, Michael R. Vanner, Markus Aspelmeyer, M. S. Kim, and Časlav Brukner. Probing planck-scale physics with quantum optics. *Nature Physics*, 8(5):393–397, March 2012.

[95] K. E. Khosla, M. R. Vanner, W. P. Bowen, and G. J. Milburn. Quantum state preparation of a mechanical resonator using an optomechanical geometric phase. *New Journal of Physics*, 15(4):043025, April 2013.

[96] G.J. Milburn, S. Schneider, and D.F.V. James. Ion trap quantum computing with warm ions. *Fortschritte der Physik*, 48(9-11):801–810, 2000.

[97] D. Leibfried, B. DeMarco, V. Meyer, D. Lucas, M. Barrett, J. Britton, W. M. Itano, B. Jelenković, C. Langer, T. Rosenband, and D. J. Wineland. Experimental demonstration of a robust, high-fidelity geometric two ion-qubit phase gate. *Nature*, 422(6930):412–415, March 2003.

Curriculum Vitae

Michael R. Vanner

PERSONAL DETAILS

Dr Michael Ross Vanner
Nationality: Australian
Date of Birth: 17th March, 1985

EDUCATION

Swinburne University of Technology, Melbourne, Victoria, AUSTRALIA

BSc(Research and Development(Physics))/BEng(Electronics and Computer Systems).
Honours 1st class

Warragul Regional College, Warragul, Victoria, AUSTRALIA

Victorian Certificate of Education, 2002
DUX (awarded to the highest scoring student), ENTER 97.25 (Top 2.75% in Australia)

PUBLICATIONS

1. **Cooling-by-measurement and mechanical state tomography via pulsed optomechanics**
   M. R. Vanner, J. Hofer, G. D. Cole, and M. Aspelmeyer
   Nature Communications **4**, 2295 (2013)
2. **Quantum state preparation of a mechanical resonator using an optomechanical geometric phase**
   K. E. Khosla, M. R. Vanner, W. P. Bowen, G. J. Milburn
   New Journal of Physics **15**, 043025 (2013)
3. **Quantum State Orthogonalization and a Toolset for Quantum Optomechanical Phonon Control**
   M. R. Vanner, M. Aspelmeyer, M. S. Kim
   Phys. Rev. Lett. **110**, 010504 (2013)
4. **Probing Planck-scale physics with quantum optics**
   Igor Pikovski, Michael R. Vanner, Markus Aspelmeyer, Myungshik Kim, Caslav Brukner
   Nature Physics **8**, 393 (2012)
5. **Selective linear or quadratic optomechanical coupling via measurement**
   M. R. Vanner
   Phys. Rev. X **1**, 021011 (2011)
6. **Pulsed Quantum Optomechanics**
   M. R. Vanner, I. Pikovski, G. D. Cole, M. S. Kim, C. Brukner, K. Hammerer, G. J. Milburn and M. Aspelmeyer
   Proc Natl Acad Sci USA 108, 16182 (2011)
7. **Phonon-tunnelling dissipation in mechanical resonators**
   Garrett D. Cole, Ignacio Wilson-Rae, Katharina Werbach, Michael R. Vanner, Markus Aspelmeyer
   Nature Communications **2**, 231 (2011)
8. **Observation of strong coupling between a micromechanical resonator and an optical cavity field**
   Simon Gröblacher, Klemens Hammerer, Michael R. Vanner, Markus Aspelmeyer
   Nature **460**, 724 (2009).
9. **Demonstration of an ultracold micro-optomechanical oscillator in a cryogenic cavity**
   Simon Gröblacher, Jared B. Hertzberg, Michael R. Vanner, Garrett D. Cole, Sylvain Gigan,

Keith C. Schwab, Markus Aspelmeyer
Nature Physics **5**, 485 (2009).

10. **Broadband Optical Delay with Large Dynamic Range Using Atomic Dispersion**
M.R. Vanner, R.J. McLean, P. Hannaford and A.M. Akulshin
J. Phys. B: At. Mol. Opt. Phys. **41**, 051004 (2008).

11. **High-fidelity transmission of polarization encoded qubits from an entangled source over 100 km of fiber**
Hannes Hübel, Michael R. Vanner, Thomas Lederer, Bibiane Blauensteiner, Thomas Lorünser, Andreas Poppe and Anton Zeilinger
Optics Express **15**, 7853 (2007).

12. **Fabrication and characterization of face-centered-cubic void dots photonic crystals in a solid polymer material**
G. Zhou, M.J. Ventura, M.R. Vanner and M. Gu
Applied Physics Letters **86**, 011108 (2005).

13. **Use of ultrafast-laser-driven microexplosion for fabricating three-dimensional void-based diamond-lattice photonic crystals in a solid polymer material**
G. Zhou, M.J. Ventura, M.R. Vanner and M. Gu
Optics Letters **29**, 2240 (2004).

Proceedings

1. **Megahertz monocrystalline optomechnaical resonators with minimal dissipation**
G. D. Cole, I. Wilson-Rae, M. R. Vanner, S. Gröblacher, J. Pohl, M. Zorn. M. Weyers, A. Peters, and M. Aspelmeyer
23rd IEEE International Conference on Microelectromechanical Systems, Hong Kong SAR, China, 2428 January 2010, TP133

2. **Fabrication of three-dimensional void photonic crystals using ultrafast-laser-driven microexplosion in a solid polymer material**
Guangyong Zhou, Michael J. Ventura, Michael R. Vanner and M. Gu
Proc. SPIE **5635**, 129 (2005).

Conference Contributions

1. 2nd Gordon Research Conference on Mechanical Systems in the Quantum Regime, 21-26 March 2010, Galveston, TX, USA
Experimental study of phonon tunneling dissipation in micromechanical resonators (Poster Presentation)
G. D. Cole, I. Wilson-Rae, Katharina Werbach, Michael R. Vanner, and M. Aspelmeyer

2. Spring Meeting of the German Physical Society (DPG), 8-12 March 2010, Hannover, Germany
Quantum state tomography and squeezed state preparation of a mechanical oscillator (Talk)
Michael R. Vanner, Igor Pikovski, M. S. Kim, Nikolai Kiesel, Klemens Hammerer, Caslav Brukner, Gerard J. Milburn, and Markus Aspelmeyer
Minimizing phonon tunneling losses in optomechanical resonators (Talk)
G. D. Cole, I. Wilson-Rae, M. R. Vanner, S. Gröblacher, J. Pohl, M. Zorn. M. Weyers, A. Peters, and M. Aspelmeyer

3. Joint Annual Meeting of the Austrian and Swiss Physical Societies (OePG/SPS), 2 September 2009, Innsbruck, Austria
Optomechanical resonators with minimal acoustic dissipation (Talk)
G. D. Cole, I. Wilson-Rae, M. R. Vanner, S. Gröblacher and M. Aspelmeyer

4. Quantum Optics of Nano- and Micromechanical Systems, July 2009 WE-Heraeus-Seminar, Physikzentrum, Bad Honnef
Demonstration of an ultracold micro-optomechanical oscillator in a cryogenic cavity (Poster Presentation)

Simon Gröblacher, Klemens Hammerer, Michael R. Vanner, Markus Aspelmeyer
Observation of strong coupling between a micromechanical resonator and an optical cavity field (Poster Presentation)
Simon Gröblacher, Jared B. Hertzberg, Michael R. Vanner, Garrett D. Cole, Sylvain Gigan, Keith C. Schwab, Markus Aspelmeyer

5. European Conference on Lasers and Electro-Optics (CLEO) and XIth European Quantum Electronics Conference (EQEC), 14th June 2009, Munich Germany
Quantum optical control of micro-mechanical resonators (Postdeadline Talk)
S. Gröblacher, M. R. Vanner, A. Trubarov, G. D. Cole, N. Kiesel, and M. Aspelmeyer

6. Quantum-Atom Optics Workshop Downunder, 3rd December 2007
Broadband Optical Delay with Large Dynamic Range Using Atomic Dispersion (Poster Presentation)
M.R. Vanner, R.J. McLean, A.I. Sidorov, P. Hannford & A.M. Akulshin
Polarization entanglement over 100 km optical fibre for quantum key distribution (Poster Presentation)
M.R. Vanner, H. Hübel, A. Poppe & A. Zeilinger

7. CLEO/Europe 2007 - IQEC Joint Symposium
Robustness of polarization entanglement for long distance QKD (Invited Talk)
H. Hübel, B. Blauensteiner, M. Hentschel, M.R. Vanner, T. Lorünser, A. Poppe, A. Zeilinger.

8. International Workshop on Quantum Noise, 14th May 2007
Atomic media with controllable dispersion (Poster Presentation)
M.R. Vanner, R.J. McLean, A.I. Sidorov, P. Hannaford & A.M. Akulshin.

TECHNICAL ARTICLES

1. **Fabricating 3D Microstructures and High-Resolution Imaging Using NI LabVIEW**
M.R. Vanner, M. Straub and M. Gu
Invited National Instruments customer solutions article (2005)
Online version available at: http://sine.ni.com/csol/cds/item/vw/p/id/663/nid/124100

PRIZES / FELLOWSHIPS

1. **UQ Postodoctoral Fellowship** This competitive fellowship valued at AUD$234,000 provides my post-doctoral salary to conduct independent research at The University of Queensland for three years beginning 2013. Three applicants across the entire faculty of science were selected.
2. **DOC Fellowship of the Austrian Academy of Sciences** This competitive fellowship valued at AUD$92,000 provided my PhD salary during the last half of my doctoral studies.
3. **Bank Austria preis zur förderung innovativer forschungsprojekte: Hauptpreis**
(Bank Austria prize for young researches: Main prize €5,000) March, 2010
Together with S. Gröblacher and K. Hammerer, this was awarded in recognition of our experimental work published in Nature, *Observation of strong coupling between a micromechanical resonator and an optical cavity field.*
4. **Vice-Chancellor's Scholarship**, Swinburne University of Technology, 2003-2007
This scholarship is valued at over AUD$30,000. It covers university fees for the entire course (5 years) and is awarded to the top engineering and science applicants.

EXPERIENCE

Centre for Quantum Computer Technology, University of Queensland
Theoretical Quantum Optics Feb, 2010
Conducted theoretical investigation with Prof. Gerard J. Milburn on the preparation of squeezed states of a mechanical oscillator via measurement.

Institut für Experimentalphysik, Universität Wien

Experimental Quantum Optics Jan-Jul, 2006
Developed source of polarization entangled photon pairs at the telecom wavelength for long distance quantum key distribution in optical fiber.

Centre for Micro-Photonics, Swinburne University of Technology
Control System Development Dec, 2005
Developed LabVIEW control software and electronics for control of a Microelectromechanical (MEMS) mirror used for endoscopic imaging using two-photon fluorescence for early cancer detection.

Jiujang No. 2 Middle School, Jiujang, CHINA
English Teaching July, 2004
Taught English to classes of high school students aged between 10 & 18.

Modra Technology and Eli Innovataion, Waragul, Victoria, AUSTRALIA
Electronics Technician Dec, 2002 - Feb, 2003
Manufacture, testing and installation of electronics used in automated dairy milking facilities.

OTHER INTERESTS Cross-country mountain biking. I also enjoy classical and contemporary music.

REFEREES
Prof. Markus Aspelmeyer, markus.aspelmeyer@univie.ac.at
Prof. Gerard J. Milburn, g.milburn@uq.edu.au
Prof. Anton Zeilinger, anton.zeilinger@quantum.at